THESIS IN COTUTELLE
Presented at

UNIVERSITY OF BORDEAUX
DOCTORAL SCHOOL OF CHEMICAL SCIENCES
Nanostructures Organiques Research Group-NEO

UNIVERSIDAD NACIONAL DE COLOMBIA
DEPARTAMENTO DE QUIMICA
NanoInorganic Research Group

BY
FREDY GIOVANY ORTIZ CALDERON
TO OBTAIN THE DEGREE OF
DOCTOR

SPECIALTY : CIENCIAS-QUIMICA UN
ANALYTICAL AND ENVIRONMENTAL CHEMISTRY UB

EFFECT OF MERCURY IONS ON THE OPTICAL AND STRUCTURAL PROPERTIES OF QUANTUM DOTS WITH AROMATIC DITHIOCARBAMATES LIGANDS

Defense: 22th November 2023

Supervisor : Dr. Nathan McClenaghan-Université de Bordeaux
Dr. Gilma Granados-Universidad Nacional de Colombia

In front of a jury composed of:

Mme. Laura RODRIGUEZ	Professor at University of Barcelona-Spain	Reporter
Mme. Bridgeen CALLAN	Professor at University of Ulster-UK	Reporter
M. Gediminas JONUSAUSKAS	Directeur de Recherche CNRS-Univ.Bordeaux	Examiner
Mme. Andrea RAMOS	Professor at Universidad del Atlántico-Colombia	Examiner
M. Edwin BAQUERO	Professor at Universidad Nacional de Colombia	Examiner

Acknowledgments

Firstly I would like to thank my parents for their unconditional support during this process.

To my supervisors, Dr. Gilma Granados and Dr. Nathan D. McClenaghan, for allowing me to undertake this project and for their support and guidance.

During this thesis, I was pleased to collaborate with the NanoInorganic Research Group at Universidad Nacional de Colombia and the NEO group at the University of Bordeaux. I want to thank all collaboration partners for their contribution and the fruitful discussion concerning the work with them. Their patience and kindness in answering my questions are greatly appreciated.

My deep gratitude goes in particular to the Ph.D. scholarship program from Ministerio de Ciencias of Colombia for financing this research and Universidad Nacional de Colombia and Université de Bordeaux for providing good working conditions.

Thanks to all my friends in Colombia and France. A special thank you to Elio Rico, Maria Joao, Odille Waselynck, Jorge Meijide, Sebastian Castro, Juan Duque, Brian Gomez, and Yudy Silva, who kept me going through the trickiest of times.

EFFECT OF MERCURY IONS ON THE OPTICAL AND STRUCTURAL PROPERTIES OF QUANTUM DOTS WITH AROMATIC DITHIOCARBAMATES LIGANDS

ABSTRACT

Quantum dots (QDs) are luminescent nanocrystals with sizes around 2-10 nm. These nanomaterials have unique characteristics due to the quantum confinement effect. These features include broad excitation spectra, versatile surfaces, narrow emission spectra, and high quantum yield. Their optical and structural properties depend on the size and surface modification with metal ions or ligands. These properties make their application possible in fluorescence sensing, wherein QDs such as CdSe, CdTe, and CdS are used.

This thesis shows the influence of S and Zn treatments used in the synthesis of three CdSe-ZnS core-shell QDs on the optical properties and the functionalization of CdSe-ZnS with two ligands: an aryl dithiocarbamate (DTC) and aromatic Dye to probe the effect of Hg^{2+} ion sensing on the photoluminescence of QDs. All the core-shell QDs and QDs-L were characterized by X-ray diffractometry to measure the crystallinity, high-resolution electron microscopy (HR TEM) to determine the size and crystallinity, X-ray photoelectron spectroscopy and FT-IR spectroscopy were used to analyze the coordination of ligands on the surface of CdSe-ZnS QDs; the optical properties such as absorption, emission, quantum yield (QY) and time-resolved photoluminescence were determined.

Chapter 2 shows the influence of S and Zn treatments during the synthesis of three CdSe-ZnS core-shell QDs on the structural and optical properties. For example, in the structural characterization, the XRD patterns analysis showed three peaks at 25.5, 42.7, and 50.2 2θ degrees, corresponding to the (111), (220), and (311) lattice planes of cubic zinc blend CdSe. The diffraction peaks of the core-shell show a shift to higher 2θ degrees due to the formation of the ZnS shell around the CdSe core. The HRTEM analysis showed particles non-aggregated with distribution sizes around 2.7 nm, 3.2 nm, and 3.3 nm. The XPS measurements showed changes in the Zn2p, and Cd3d regions, indicating the existence of different species of these elements on the surface of CdSe-ZnS QDs with different S and Zn treatments used during synthesis. The FT-IR results showed the oleic acid and TOP-capped CdSe-ZnS QDs.

The optical properties of QDs with different Zn:S ratios were developed using UV-Vis, fluorescence, and time-resolved photoluminescence spectroscopies. The S-excess used in the synthesis of CdSe-ZnS QD (QD-0.3 ML) produces a lower QY than other QDs studied. The S acts as a hole trap, favoring the decrease in photoluminescence, and nonradiative recombination is favored. However, the increase in the amount of Zn removes/eliminates the hole traps produced by S-excess, the photoluminescence is regenerated, and QY increases, as in QD-0.9 ML (QY: 0.54). The Zn treatment produces a passivation effect of this trap on the surface of QDs to improve photoluminescence. On the other hand, when the Zn-treatment is the highest (QD-1.0 ML), the quantum yield (QY) of corresponding core/shell QDs will decrease due to the traps at the CdSe-ZnS.

The analysis of three CdSe-ZnS core-shell QDs (QD-0.3 ML, QD-0.9 ML, and QD-1.0 ML) as Hg^{2+} ion sensors was performed using a solution of QDs in a mixture $CHCl_3$/ethanol (1/1, v/v) and aqueous solution with different concentrations of Hg^{2+} using UV-Vis, fluorescence, and time-resolved photoluminescence spectroscopies. The addition of Hg^{2+} produces different changes in the photoluminescence of QDs. For example, in QD-0.3 ML, a quenching of photoluminescence is produced due to the formation of HgSe particles on the CdSe core of QD; these HgSe particles are produced by a cation exchange reaction between Cd from core and Hg, the Ksp of HgSe is lower than CdSe, and this reaction is favored. The S-excess from $(TMS)_2S$ used in the synthesis of QD-0.3 ML produces HgS due to the high affinity from S and Hg in concordance with the HSAB theory.

On the other hand, adding Hg^{2+} ions in CdSe-ZnS QDs with thicker shells (QD-0.9 ML and QD-1.0 ML) showed the opposite effect, i.e., an enhancement in the photoluminescence is produced. In these QDs, the Hg^{2+} produces HgS particles on the shell surface, forming a pseudo-shell that passivates the surface traps and improves the photoluminescence. A cation exchange reaction forms these HgS particles from Zn-to-Hg on the ZnS shell because the Ksp of HgS is lower than ZnS, so the reaction is favored.

In addition, the detection limit (LOD) of Hg^{2+} ions was determined with the response obtained in the QD-emission spectra as a function of Hg^{2+} concentrations (0.5-5.0 μM). The LOD for QD-0.3 ML was determined using the Stern-Volmer equation; the LOD calculated was 11.2 nM. The LOD for QDs with thicker shells was 8.98 nM and 10.7 nM for QD-0.9 ML and QD-1.0 ML, respectively. These values of LOD are lower than other QDs reported.

Finally, the analysis with other transition metal ions was developed using aqueous solutions of Zn^{2+}, Mn^{2+}, Cd^{2+}, Pb^{2+}, Co^{2+}, Ni^{2+}, and Hg^{2+} chloride salts and QDs in a solution of $CHCl_3$/ethanol (1/1, v/v). This analysis showed a photoluminescence quenching with all the metal ions evaluated in QD-0.3 ML; however, the most significant quenching observed was produced by Hg^{2+} ions due to the formation of HgSe particles on the core because the Ksp of HgSe is lower than other metal ions evaluated. While in the case of QD-0.9 ML and QD-1.0 ML, photoluminescence is enhanced due to the passivation of surface traps formed during the synthesis of QDs.

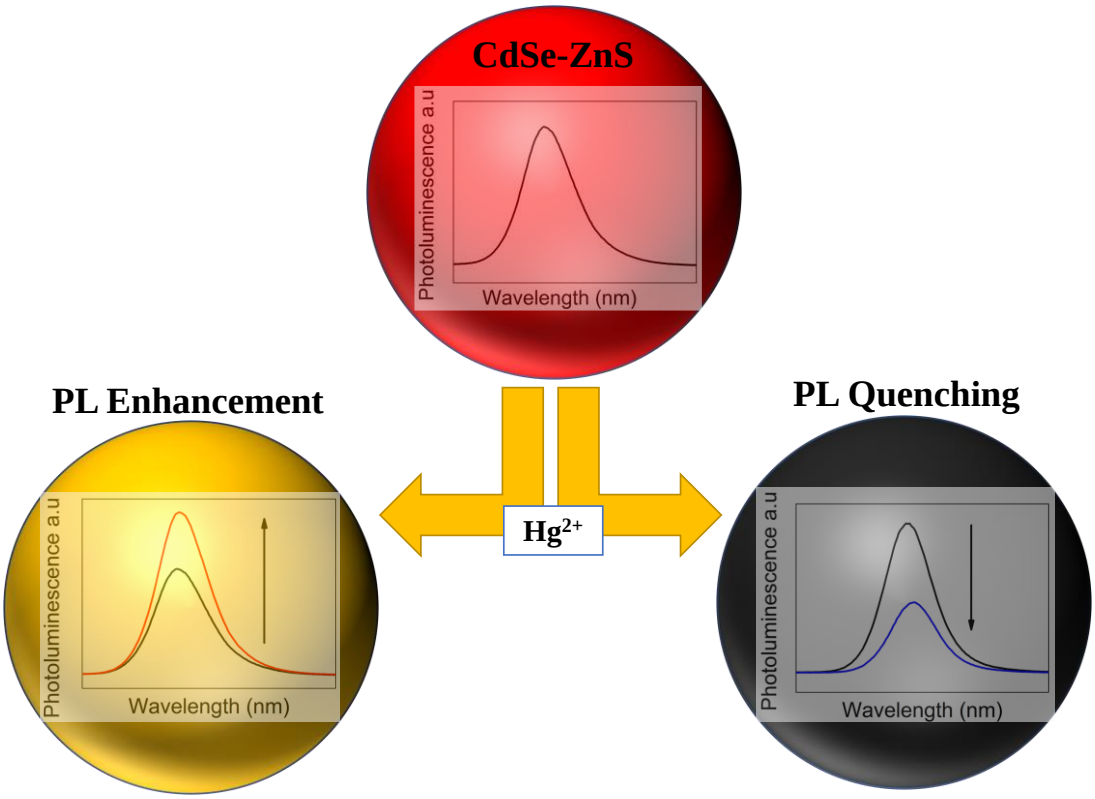

Figure 1. Graphical abstract of the behavior of CdSe-ZnS QDs with the addition of Hg^{2+}.

The versatile character of the surface of QDs is an interesting and advantageous property. Thus, different ligands can coordinate with the surface to modulate the structural and optical properties to improve th scope of their possible application. The ligands capped on the surface of QDs can improve the physical properties, such as solubility in aqueous media, and produce changes in the optical properties, such as QY, absorption, and photoluminescence spectra.

However, the energy levels of capping ligands can affect the optical properties of QDs such as photoluminescence. For example, the literature has shown that the thiolated ligands generally act as hole traps due to the HOMO levels from the ligand being near the valence band (VB), producing overlapped orbitals; when the QD is photoexcited, the ligand trapping the hole photogenerated and delocalization of exciton is produced favoring the formation of new nonradiative centers and the photoluminescence is quenched.

Chapter 3 shows the influence of two surface ligands on the structural and optical properties of CdSe-ZnS core-shell QD (QD-0.9 ML): 1) an aromatic dithiocarbamate (DTC) and 2) an aromatic dye ligand (Dye) capped to the surface of this QD. The QD-0.9 ML was selected because this QD has the highest

determined QY (Chapter 2). Both ligands were capped to the QD with a ligand exchange process, using a saturated solution of ligands (DTC and Dye) in methanol and a solution of QD in hexane at 60°C for 1 h (QD/DTC, 1/3 (mass/mass)). The ligand exchange produced a red-shift in the maximum absorption and emission bands of new QDs: QDTC and QDTCDye, a new emission band appeared in the fluorescence spectra of QDTCDye, which is from the Dye ligand.

The effect of two ligands on the structural properties of QDs was analyzed. The XRD patterns do not show significant changes in the diffraction peaks of QD; the ligand exchange process did not affect the crystallinity. The HRTEM analysis showed an increase in the size of QDs from 3.2 nm (QD-0.9 ML) to 3.4 nm and 3.7 nm for QDTC and QDTCDye, respectively, with no significant changes in the d-spacing factor. The crystallinity is conserved, confirming the XRD analysis observed. The FT-IR analysis showed the coordination of DTC by the CSS^- headgroup due to the band at 1000 cm^{-1} of this functional group disappearing and the Dye ligand being coordinated by both carboxylates in their structure because the band at 1707 cm^{-1} corresponding to the C=O bonds in carboxylic acids is not observed confirming the capping. XPS measurements showed new peaks in C1s and O1s due to the apparition of new bonds such as C-N and C-OH. Furthermore, in Zn2p and Cd3d, the peaks were deconvoluted in several components, indicating the presence of different species of Zn and Cd coordinated with the capped ligands. This characterization showed the influence of the coordination of the ligand on the structural properties of QDs.

Consequently, the effect of capped ligands on QDs and their optical properties, such as absorption, emission, and time-resolved photoluminescence, were studied. The coordination of DTC ligands produces a decrease in photoluminescence (quenching). The HOMO orbital of DTC is overlapped with the valence band (VB), trapping the hole photogenerated, delocalizing the excitonic recombination, and photoluminescence is quenched. The DTC ligand acts as a hole trap affecting the photoluminescence properties of QD, such as QY.

The Hg^{2+} ion sensing analysis was developed using a solution of QDTC and QDTCDye in ethanol as solvent and aqueous solutions with different concentrations of Hg^{2+} ions in 0.5-5.0 μM range. The absorption and emission changes were analyzed with UV-Vis, fluorescence, and time-resolved photoluminescence spectroscopies. The Hg^{2+} ions enhance the fluorescence intensity of QDTC and QDTCDye due to the formation of HgS particles on the ZnS shell of QDs passivating the traps produced by the DTC ligand. These HgS particles are produced on the ZnS surface due to the cation exchange reaction because the Ksp of HgS is lower than the Ksp of ZnS, favoring this reaction.[12] The behavior of QDTCDye with the addition of different concentrations of Hg^{2+} ions is ratiometric. The detection limit (LOD) of QDTC and QDTCDye was determined using fluorescence intensity response as a function of different concentrations of Hg^{2+} ions. The LOD was calculated as 3.7 nM and 4.4 nm for QDTC and

QDTCDye, respectively. These LOD obtained are lower than other similar QDs systems compared including the value reported by EPA and WHO institutions.

Finally, the analysis with other transition metal ions was developed in the same way as in Chapter 2. All the transition metal ions evaluated enhance the photoluminescence in QDTC and QDTCDye. However, Hg^{2+} produces the highest increase in fluorescence intensity in QDTC. Photoluminescence enhancement indicates the passivation of traps on the surface of QD. The enhancement phenomenon, sensitivity (low LOD), and selectivity demonstrated that these materials are promising to apply in Hg^{2+} ions sensing.

Keywords: quantum dots, mercury, capping, ligand, sensitivity, selectivity, surface.

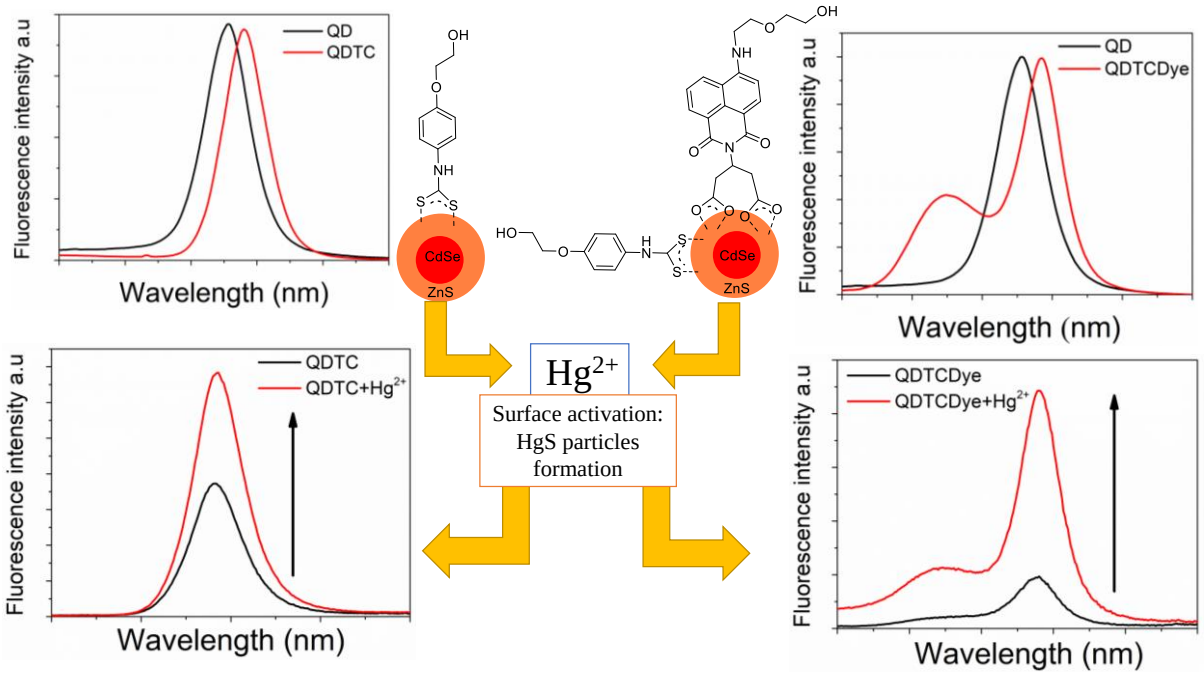

Figure 2. Graphical abstract showing effect of Hg^{2+} on QDTC and QDTCDye photoluminescence.

Institut des Sciences Moléculaires

Bâtiment A12-351 Cours de la Libération

33405 TALENCE cedex

EFFET DES IONS MERCURE SUR LES PROPRIÉTÉS OPTIQUES ET STRUCTURELLES DES POINTS QUANTIQUES À LIGANDS DITHIOCARBAMATES AROMATIQUES

RÉSUMÉ

Les points quantiques (QD) sont des nanocristaux luminescents dont la taille est comprise entre 2 et 10 nm. Ces nanomatériaux présentent des caractéristiques uniques dues à l'effet de confinement quantique. Ces caractéristiques comprennent des spectres d'excitation larges, des surfaces polyvalentes, des spectres d'émission étroits et un rendement quantique élevé. Leurs propriétés optiques et structurelles dépendent de la taille et de la modification de la surface avec des ions métalliques ou des ligands. Ces propriétés rendent possible leur application dans la détection de fluorescence, où des QDs tels que CdSe, CdTe, et CdS sont utilisés.

Cette thèse montre l'influence des traitements S et Zn utilisés dans la synthèse de trois QDs CdSe-ZnS core-shell sur les propriétés optiques et la fonctionnalisation de CdSe-ZnS avec deux ligands : un dithiocarbamate d'aryle (DTC) et un colorant aromatique pour sonder l'effet de la détection de l'ion Hg^{2+} sur la photoluminescence des QDs. Tous les QDs core-shell et QDs-L ont été caractérisés par diffractométrie des rayons X pour mesurer la cristallinité, par microscopie électronique à haute résolution (HR TEM) pour déterminer la taille et la cristallinité, par spectroscopie photoélectronique à rayons X et par spectroscopie FT-IR pour analyser la coordination des ligands à la surface des QDs CdSe-ZnS ; les propriétés optiques telles que l'absorption, l'émission, le rendement quantique (QY) et la photoluminescence résolue dans le temps ont été déterminées.

Le chapitre 2 montre l'influence des traitements S et Zn pendant la synthèse de trois QDs CdSe-ZnS core-shell sur les propriétés structurelles et optiques. Par exemple, dans la caractérisation structurelle, l'analyse des diagrammes XRD a montré trois pics à 25.5, 42.7 et 50.2 2θ degrés, correspondant aux plans de réseau (111), (220) et (311) du mélange cubique de zinc CdSe. Les pics de diffraction du noyau-coquille montrent un déplacement vers des degrés 2θ plus élevés en raison de la formation de la coquille de ZnS autour du noyau de CdSe. L'analyse HRTEM a montré des particules non agrégées avec des tailles de distribution autour de 2.7 nm, 3.2 nm et 3.3 nm. Les mesures XPS ont montré des changements dans les régions Zn2p et Cd3d, indiquant l'existence de différentes espèces de ces éléments à la surface des QDs CdSe-ZnS avec différents traitements S et Zn utilisés pendant la synthèse. Les résultats FT-IR ont montré que les QDs CdSe-ZnS recouverts d'acide oléique et de TOP.

Les propriétés optiques des QDs avec différents rapports Zn:S ont été développées en utilisant des spectroscopies UV-Vis, de fluorescence et de photoluminescence résolue dans le temps. L'excès de S utilisé dans la synthèse des QDs CdSe-ZnS (QD-0.3 ML) produit un QY plus faible que les autres QDs étudiés. Le S agit comme un piège à trous, favorisant la diminution de la photoluminescence, et la recombinaison non radiative est favorisée. Cependant, l'augmentation de la quantité de Zn

enlève/élimine les pièges à trous produits par l'excès de S, la photoluminescence est régénérée et le QY augmente, comme dans le QD-0.9 ML (QY : 0.54). Le traitement au Zn produit un effet de passivation de ce piège à la surface des QDs pour améliorer la photoluminescence. D'autre part, lorsque le traitement au Zn est le plus élevé (QD-1.0 ML), le rendement quantique (QY) des QDs cœur/coquille correspondants diminue en raison des pièges à l'interface CdSe-ZnS.

L'analyse de trois QDs CdSe-ZnS core-shell (QD-0.3 ML, QD-0.9 ML, et QD-1.0 ML) en tant que capteurs d'ions Hg^{2+} a été développée en phase homogène en utilisant une solution de QDs dans un mélange $CHCl_3$/éthanol (1/1, v/v) et une solution aqueuse avec différentes concentrations de Hg^{2+} en utilisant des spectroscopies UV-Vis, de fluorescence, et la photoluminescence résolue dans le temps. L'ajout de Hg^{2+} produit différents changements dans la photoluminescence des QDs. Par exemple, dans le QD-0.3 ML, une extinction de la photoluminescence est produite en raison de la formation de particules de HgSe sur le cœur de CdSe du QD ; ces particules de HgSe sont produites par une réaction d'échange de cations entre le Cd du cœur et le Hg, le Ksp de HgSe est plus faible que celui de CdSe, et cette réaction est favorisée. L'excès de S de $(TMS)_2S$ utilisé dans la synthèse du QD-0.3 ML produit du HgS en raison de la forte affinité entre S et Hg, conformément à la théorie HSAB.

D'autre part, l'ajout d'ions Hg^{2+} dans des QDs CdSe-ZnS avec des coquilles plus épaisses (QD-0.9 ML et QD-1.0 ML) a montré l'effet opposé, c'est-à-dire qu'une augmentation de la photoluminescence est produite. Dans ces QDs, le Hg^{2+} produit des particules de HgS à la surface de la coquille, formant une pseudo-coquille qui passive les pièges de surface et améliore la photoluminescence. Une réaction d'échange de cations forme ces particules de HgS de Zn à Hg sur la coquille de ZnS, car le Ksp de HgS est inférieur à celui de ZnS, et la réaction est donc favorisée.

D'autre part, l'ajout d'ions Hg^{2+} dans des QDs CdSe-ZnS avec des coquilles plus épaisses (QD-0.9 ML et QD-1.0 ML) a montré l'effet opposé, c'est-à-dire qu'une amélioration de la photoluminescence est produite. Dans ces QDs, le Hg^{2+} produit des particules de HgS à la surface de la coquille, formant une pseudo-coquille qui passive les pièges de surface et améliore la photoluminescence. Une réaction d'échange de cations forme ces particules de HgS de Zn à Hg sur la coquille de ZnS car le Ksp de HgS est plus faible que celui de ZnS, et la réaction est donc favorisée.

Le limite de détection (LOD) des ions Hg^{2+} a été déterminée à l'aide de la réponse obtenue dans les spectres d'émission des QD en fonction des concentrations de Hg^{2+} (0.5-5.0 μM). Le limite de détection calculée était de 11.2 nM. La LOD pour les QDs avec des coquilles plus épaisses était de 8.98 nM et 10.7 nM pour QD-0.9 ML et QD-1.0 ML, respectivement. Ces valeurs de LOD sont inférieures à celles d'autres QDs rapportés.

Enfin, l'analyse avec d'autres ions de métaux de transition a été développée en utilisant des solutions aqueuses de sels de chlorure de Zn^{2+}, Mn^{2+}, Cd^{2+}, Pb^{2+}, Co^{2+}, Ni^{2+}, et Hg^{2+} et des QDs dans une solution de $CHCl_3$/éthanol (1/1, v/v). Cette analyse a montré une extinction de la photoluminescence avec tous

les ions métalliques évalués dans les QD-0.3 ML ; cependant, l'extinction la plus significative observée a été produite par les ions Hg^{2+} en raison de la formation de particules de HgSe sur le noyau, car le Ksp de HgSe est plus faible que celui des autres ions métalliques évalués. Dans le cas des QD-0.9 ML et QD-1.0 ML, la photoluminescence est améliorée en raison de la passivation des pièges de surface formés pendant la synthèse des QD.

Le caractère polyvalent de la surface des QDs est une propriété intéressante et avantageuse. Ainsi, différents ligands peuvent se coordonner avec la surface pour moduler les propriétés structurelles et optiques afin d'améliorer les possibilités d'application. Les ligands fixés à la surface des QDs peuvent améliorer les propriétés physiques, telles que la solubilité dans les milieux aqueux, et produire des changements dans les propriétés optiques, telles que le QY, l'absorption et les spectres de photoluminescence.

Cependant, les ligands de fermeture peuvent introduire des niveaux d'énergie favorables ou défavorables dans les QDs et affecter les propriétés optiques telles que la photoluminescence. Par exemple, la littérature a montré que les ligands thiolés agissent généralement comme des pièges à trous en raison des niveaux HOMO du ligand qui sont proches de la bande de valence (VB), produisant des orbitales superposées; lorsque le QD est photoexcité, le ligand piégeant le trou photogénéré et la délocalisation de l'exciton est produite, favorisant la formation de nouveaux centres non radiatifs et la photoluminescence est éteinte.

Le chapitre 3 montre l'influence de deux ligands de surface sur les propriétés structurelles et optiques du QD cœur-coquille CdSe-ZnS (QD-0.9 ML) : 1) un dithiocarbamate aromatique (DTC) et 2) un ligand de colorant aromatique (Dye) fixé à la surface de ce QD. Le QD-0.9 ML a été choisi parce que ce QD a le QY le plus élevé calculé (Chapitre 2). Les deux ligands ont été fixés au QD par un processus d'échange de ligands, en utilisant une solution saturée de ligands (DTC et Dye) dans du méthanol et une solution de QD dans de l'hexane à 60°C pendant 1 heure (QD/DTC, 1/3). L'échange de ligands a produit un décalage vers le rouge des bandes maximales d'absorption et d'émission des nouveaux QDs : QDTC et QDTCDye, une nouvelle bande d'émission est apparue dans les spectres de fluorescence de QDTCDye, qui provient du ligand Dye.

L'effet de deux ligands sur les propriétés structurelles des QDs a été analysé. Les diagrammes XRD ne montrent pas de changements significatifs dans les pics de diffraction des QDs ; le processus d'échange de ligands n'a pas affecté la cristallinité. L'analyse HRTEM a montré une augmentation de la taille des QDs de 3.0 nm (QD-0.9 ML) à 3.4 nm et 3.7 nm pour le QDTC et le QDTCDye, respectivement. Il n'y a pas de changements significatifs dans le facteur d'espacement. La cristallinité est conservée, ce qui confirme l'analyse XRD observée. L'analyse FT-IR a montré la coordination du DTC par le groupe de tête CSS- grâce à la disparition de la bande à 1000 cm^{-1} de ce groupe fonctionnel et la coordination du ligand Dye par les deux carboxylates dans leur structure car la bande à 1707 cm^{-1} correspondant aux

liaisons C=O dans les acides carboxyliques n'est pas observée, ce qui confirme l'encapsulation. Les mesures XPS ont montré de nouveaux pics dans C1s et O1s en raison de l'apparition de nouvelles liaisons telles que C-N et C-OH. En outre, pour Zn2p et Cd3d, les pics ont été déconvolués en plusieurs composantes, ce qui indique la présence de différentes espèces de Zn et de Cd coordonnées avec les ligands. Cette caractérisation a montré l'influence de la coordination du ligand sur les propriétés structurelles des QDs.

Par conséquent, l'effet des ligands sur les QDs et leurs propriétés optiques, telles que l'absorption, l'émission et la photoluminescence résolue dans le temps, ont été étudiés. La coordination des ligands DTC produit une diminution de la photoluminescence (quenching). L'orbitale HOMO du DTC se superpose à la bande de valence (VB), piégeant le trou photogénéré, délocalisant la recombinaison excitonique, et la photoluminescence est atténuée. Le ligand DTC agit comme un piège à trous qui affecte les propriétés de photoluminescence des QD, comme le QY. Toutefois, le ligand Dye améliore légèrement cette propriété optique et la photoluminescence augmente avec la coordination du ligand Dye en raison de son action en tant que composé donneur d'électrons qui produit une repopulation d'électrons dans la bande de conduction (CB) pour régénérer la recombinaison excitonique et neutraliser le piège à trous produit par le ligand DTC. Le QY s'améliore avec la coordination du ligand Dye.

L'analyse de la détection des ions Hg^{2+} a été développée en utilisant une solution de QDTC et de QDTCDye dans l'éthanol comme solvant et des solutions aqueuses avec différentes concentrations d'ions Hg^{2+} dans une gamme linéaire de 0.5-5.0 μM. Les changements d'absorption et d'émission ont été analysés par spectroscopie UV-Vis, fluorescence et photoluminescence résolue dans le temps. Les ions Hg^{2+} augmentent l'intensité de la fluorescence du QDTC et du QDTCDye en raison de la formation de particules HgS sur la coquille ZnS des QDs qui neutralisent les pièges produits par le ligand DTC. Ces particules de HgS sont produites à la surface du ZnS par la réaction d'échange de cations, car le Ksp du HgS est inférieur au Ksp du ZnS, ce qui favorise cette réaction.[12] Le comportement du colorant QDTC avec l'ajout de différentes concentrations d'ions Hg^{2+} est ratiométrique. La limite de détection (LOD) du QDTC et du QDTCDye a été déterminée en utilisant la réponse de l'intensité de fluorescence en fonction de différentes concentrations d'ions Hg^{2+}. La limite de détection a été calculée comme étant de 3.7 nM et 4.4 nm pour le QDTC et le QDTCDye, respectivement. Ces limites de détection obtenues sont inférieures à celles d'autres systèmes similaires de QDs comparés et des institutions comme l'EPA et l'OMS.

Enfin, l'analyse avec d'autres ions de métaux de transition a été développée avec la même forme que celle développée au Chapitre 2. Tous les ions de métaux de transition évalués augmentent la photoluminescence dans le QDTC et le QDTCDye. Cependant, Hg^{2+} produit la plus forte augmentation de l'intensité de fluorescence dans le QDTC. L'augmentation de la photoluminescence indique la

passivation des pièges à la surface des QD. Le phénomène d'augmentation, la sensibilité (faible LOD) et la sélectivité ont démontré que ces matériaux sont prometteurs pour la détection des ions Hg^{2+}.

Mots-clés: points quantiques, mercure, revêtement, sensibilité, sélectivité, surface.

EFECTO DE LOS IONES DE MERCURIO SOBRE LAS PROPIEDADES ÓPTICAS Y ESTRUCTURALES DE PUNTOS CUÁNTICOS CON LIGANDOS DE DITIOCARBAMATOS AROMÁTICOS

RESUMEN

Los puntos cuánticos (QD) son nanocristales luminiscentes con tamaños en torno a 2-10 nm. Estos nanomateriales presentan características únicas debidas al efecto de confinamiento cuántico. Entre estas características se incluyen espectros de excitación amplios, superficies versátiles, espectros de emisión estrechos y un alto rendimiento cuántico. Sus propiedades ópticas y estructurales dependen del tamaño y de la modificación de la superficie con iones metálicos o ligandos. Estas propiedades hacen posible su aplicación en la detección por fluorescencia, en la que se utilizan QDs como CdSe, CdTe y CdS.

Esta tesis muestra la influencia de los tratamientos con S y Zn utilizados en la síntesis de tres QDs core-shell CdSe-ZnS sobre las propiedades ópticas y la funcionalización de CdSe-ZnS con dos ligandos: un ditiocarbamato de arilo (DTC) y un colorante aromático para sondear el efecto del sensado de iones Hg^{2+} sobre la fotoluminiscencia de los QDs. Todos los QDs core-shell y QDs-L se caracterizaron por difractometría de rayos X para medir la cristalinidad, microscopía electrónica de alta resolución (HR TEM) para determinar el tamaño y la cristalinidad, espectroscopía fotoelectrónica de rayos X y espectroscopía FT-IR se utilizaron para analizar la coordinación de ligandos en la superficie de CdSe-ZnS QDs; se determinaron las propiedades ópticas tales como absorción, emisión, rendimiento cuántico (QY) y fotoluminiscencia resuelta en el tiempo.

El capítulo 2 muestra la influencia de los tratamientos con S y Zn durante la síntesis de tres CdSe-ZnS core-shell QDs en las propiedades estructurales y ópticas. Por ejemplo, en la caracterización estructural, el análisis de los patrones de DRX mostró tres picos a 25.5, 42,7 y 50.2 2θ grados, correspondientes a los planos de red (111), (220) y (311) de la mezcla cúbica de zinc CdSe. Los picos de difracción del núcleo-cáscara muestran un desplazamiento hacia grados 2θ superiores debido a la formación de la cáscara de ZnS alrededor del núcleo de CdSe. El análisis HRTEM mostró partículas no agregadas con tamaños de distribución en torno a 2.7 nm, 3.2 nm y 3.3 nm. Las medidas XPS mostraron cambios en las regiones Zn2p, y Cd3d, indicando la existencia de diferentes especies de estos elementos en la superficie de CdSe-ZnS QDs con diferentes tratamientos de S y Zn utilizados durante la síntesis. Los resultados de FT-IR mostraron la existencia de QDs CdSe-ZnS con ácido oleico y recubrimiento TOP.

Las propiedades ópticas de los QDs con diferentes proporciones de Zn:S se desarrollaron mediante espectroscopias UV-Vis, de fluorescencia y de fotoluminiscencia resuelta en el tiempo. El exceso de S utilizado en la síntesis de CdSe-ZnS QD (QD-0.3 ML) produce un QY inferior al de otros QDs estudiados. El S actúa como una trampa de huecos, favoreciendo la disminución de la fotoluminiscencia, y se favorece la recombinación no radiativa. Sin embargo, el aumento de la cantidad de Zn

elimina/elimina las trampas de huecos producidas por el exceso de S, se regenera la fotoluminiscencia y aumenta el QY, como en el QD-0.9 ML (QY: 0.54). El tratamiento con Zn produce un efecto de pasivación de esta trampa en la superficie de los QDs para mejorar la fotoluminiscencia. Por otro lado, cuando el tratamiento con Zn es el más alto (QD-1.0 ML), el rendimiento cuántico (QY) de los QDs núcleo/capa correspondientes disminuirá debido a las trampas en la interfaz CdSe-ZnS.

El análisis de tres CdSe-ZnS core-shell QDs (QD-0.3 ML, QD-0.9 ML, y QD-1.0 ML) como sensores de iones Hg^{2+} se desarrolló en fase homogénea utilizando una solución de QDs en una mezcla $CHCl_3$/Etanol (1/1) y solución acuosa con diferentes concentraciones de Hg^{2+} utilizando espectroscopias UV-Vis, de fluorescencia y de fotoluminiscencia resuelta en el tiempo. La adición de Hg^{2+} produce diferentes cambios en la fotoluminiscencia de los QDs. Por ejemplo, en QD-0.3 ML, se produce un apagamiento de la fotoluminiscencia debido a la formación de partículas de HgSe sobre el núcleo de CdSe del QD; estas partículas de HgSe se producen por una reacción de intercambio catiónico entre el Cd del núcleo y el Hg, el Ksp de HgSe es menor que el de CdSe, y esta reacción se ve favorecida.[12] El exceso de S del $(TMS)_2S$ utilizado en la síntesis de QD-0.3 ML produce HgS debido a la alta afinidad del S y el Hg en concordancia con la teoría HSAB.

Por otro lado, la adición de iones Hg^{2+} en QDs CdSe-ZnS con cáscaras más gruesas (QD-0.9 ML y QD-1.0 ML) mostró el efecto contrario, es decir, se produce una mejora en la fotoluminiscencia. En estos QDs, el Hg^{2+} produce partículas de HgS en la superficie de la cáscara, formando una pseudocáscara que pasiva las trampas superficiales y mejora la fotoluminiscencia. Una reacción de intercambio catiónico forma estas partículas de HgS de Zn a Hg en la cáscara de ZnS porque el Ksp del HgS es menor que el del ZnS,[12] por lo que la reacción se ve favorecida.

Además, se determinó el límite de detección (LOD) de los iones Hg^{2+} con la respuesta obtenida en los espectros de emisión del QD en función de las concentraciones de Hg^{2+} (0.5-5.0 μM). El LOD para QD-0.3 ML fue de 11.2 nM. El LOD para QDs con cáscaras más gruesas fue de 8.98 nM y 10.7 nM para QD-0.9 ML y QD-1.0 ML, respectivamente. Estos valores de LOD son inferiores a los de otros QDs reportados.

Finalmente, se desarrolló el análisis con otros iones de metales de transición utilizando soluciones acuosas de sales de cloruro de Zn^{2+}, Mn^{2+}, Cd^{2+}, Pb^{2+}, Co^{2+}, Ni^{2+}, y Hg^{2+} y QDs en una solución de $CHCl_3$/Etanol (1/1). Este análisis mostró disminución de fotoluminiscencia con todos los iones metálicos evaluados en QD-0.3 ML; sin embargo, el *quenching* más significativo observado fue el producido por los iones Hg^{2+} debido a la formación de partículas de HgSe en el núcleo ya que el Ksp del HgSe es menor que el de otros iones metálicos evaluados. Mientras que en el caso de QD-0.9 ML y QD-1.0 ML, la fotoluminiscencia se ve potenciada debido a la pasivación de las trampas superficiales formadas durante la síntesis de los QDs.

El carácter versátil de la superficie de los QDs es una propiedad interesante y ventajosa. Así, diferentes ligandos pueden coordinarse con la superficie para modular las propiedades estructurales y ópticas con el fin de mejorar su posible aplicación. Los ligandos capados en la superficie de los QDs pueden mejorar las propiedades físicas, como la solubilidad en medios acuosos, y producir cambios en las propiedades ópticas, como los espectros QY, de absorción y de fotoluminiscencia.

Sin embargo, los ligandos pueden introducir niveles de energía favorables o desfavorables (HOMO-LUMO) en los QDs y afectar a las propiedades ópticas, como la fotoluminiscencia. Por ejemplo, la literatura ha demostrado que los ligandos tiolados generalmente actúan como trampas de huecos debido a que los niveles HOMO del ligando están cerca de la banda de valencia (VB), produciendo orbitales solapados; cuando el QD es fotoexcitado, el ligando atrapa el hueco fotogenerado y la deslocalización del excitón se produce favoreciendo la formación de nuevos centros no radiativos y la fotoluminiscencia disminuye.

El capítulo 3 muestra la influencia de dos ligandos superficiales en las propiedades estructurales y ópticas del QD con núcleo de CdSe-ZnS (QD-0.9 ML): 1) un ditiocarbamato aromático (DTC) y 2) un ligando colorante aromático (Dye) capado en la superficie de este QD. Se seleccionó el QD-0.9 ML porque este QD tiene el QY más alto calculado (Capítulo 2). Ambos ligandos se fijaron al QD mediante un proceso de intercambio de ligandos, utilizando una solución saturada de ligandos (DTC y Dye) en metanol y una solución de QD en hexano a 60°C durante 1 h (QD/DTC, 1/3). El intercambio de ligandos produjo un desplazamiento al rojo de las bandas máximas de absorción y emisión de los nuevos QDs: QDTC y QDTCDye, apareciendo una nueva banda de emisión en los espectros de fluorescencia de QDTCDye, que procede del ligando Dye.

Se analizó el efecto de dos ligandos sobre las propiedades estructurales de los QDs. Los patrones de DRX no muestran cambios significativos en los picos de difracción de los QD; el proceso de intercambio de ligandos no afectó a la cristalinidad. El análisis HRTEM mostró un aumento del tamaño de los QDs de 3.0 nm (QD-0.9 ML) a 3.4 nm y 3.7 nm para QDTC y QDTCDye, respectivamente. No hay cambios significativos en el factor d-spacing. La cristalinidad se conserva, confirmando lo observado en el análisis DRX. El análisis FT-IR mostró la coordinación del DTC por el grupo $-CSS^-$ debido a que desaparece la banda a 1000 cm^{-1} de este grupo funcional y el ligando Dye está coordinado por ambos carboxilatos en su estructura ya que no se observa la banda a 1707 cm^{-1} correspondiente a los enlaces C=O en ácidos carboxílicos confirmando su coordinación. Las medidas XPS mostraron nuevos picos en C1s y O1s debido a la aparición de nuevos enlaces como C-N y C-OH. Además, en Zn2p y Cd3d, los picos se deconvolucionaron en varios componentes, indicando la presencia de diferentes especies de Zn y Cd coordinadas con los ligandos capados. Esta caracterización mostró la influencia de la coordinación del ligando en las propiedades estructurales de los QDs.

En consecuencia, se estudió el efecto de los ligandos sobre los QDs y sus propiedades ópticas, como la absorción, la emisión y la fotoluminiscencia resuelta en el tiempo. La coordinación de ligandos DTC produce una disminución de la fotoluminiscencia (quenching). El orbital HOMO del DTC se solapa con la banda de valencia (VB), atrapando el hueco fotogenerado, deslocalizando la recombinación excitónica, y la fotoluminiscencia disminuye drásticamente. El ligando DTC actúa como una trampa de huecos que afecta las propiedades de fotoluminiscencia de los QD, como el QY. Sin embargo, el ligando Dye produce una ligera mejora en esta propiedad óptica, y la fotoluminiscencia aumenta con la coordinación del ligando Dye debido a su acción como compuesto electrón-donador que produce una repoblación de electrones en la banda de conducción (CB) para regenerar la recombinación excitónica y pasivar las trampas de huecos producida por el ligando DTC. El QY mejora con la coordinación del ligando Dye.

El análisis de detección de iones Hg^{2+} se desarrolló utilizando una solución de QDTC y QDTCDye en etanol como disolvente y soluciones acuosas con diferentes concentraciones de iones Hg^{2+} en un rango lineal de 0.5-5.0 μM. Los cambios de absorción y emisión se analizaron con espectroscopias UV-Vis, de fluorescencia y de fotoluminiscencia resuelta en el tiempo. Los iones Hg^{2+} aumentan la intensidad de fluorescencia de QDTC y QDTCDye debido a la formación de partículas de HgS en la capa de ZnS de los QDs pasivando las trampas producidas por el ligando DTC. Estas partículas de HgS se producen en la superficie del ZnS debido a la reacción de intercambio catiónico ya que el Ksp del HgS es menor que el Ksp del ZnS, favoreciendo esta reacción. El comportamiento del QDTCDye con la adición de diferentes concentraciones de iones Hg^{2+} es ratiométrico. El límite de detección (LOD) de QDTC y QDTCDye se determinó utilizando la respuesta de intensidad de fluorescencia en función de diferentes concentraciones de iones Hg^{2+}. El LOD se calculó como 3.7 nM y 4.4 nm para QDTC y QDTCDye, respectivamente. Estos LOD obtenidos son inferiores a los de otros sistemas de QDs similares comparados e incluso a los establecidos por la EPA y la OMS.

Finalmente, el análisis con otros iones de metales de transición se desarrolló con la misma forma desarrollada en el Capítulo 2. Todos los iones metálicos de transición evaluados aumentan la fotoluminiscencia en QDTC y QDTCDye. Sin embargo, el Hg^{2+} produce el mayor incremento en la intensidad de fluorescencia en QDTC. El aumento de la fotoluminiscencia indica la pasivación de trampas en la superficie del QD. Este fenómeno mejora la sensibilidad (bajo LOD) y la selectividad demostrando que estos materiales son prometedores para su aplicación en la detección de iones Hg^{2+}.

Palabras clave: puntos cuánticos, mercurio, capa, sensibilidad, selectividad, superficie.

Abbreviations List

Solvents and reagents:

AcOEt : Ethyl acetate

DMSO : Dimethylsulfoxide

EtOH : Ethanol

MeOH : Methanol

DIPEA : N,N-Diisopropylethylamine

THF : Tetrahydrofuran

Abbreviations and symbols:

δ: Chemical shift in ppm

J : Coupling Constant in Hz

τ Lifetime in ns

Φ Fluorescence quantum yield

λ_{exc} Excitation wavelength in nm

λ_{ems} Emission wavelength in nm

Ksp Solubility constant product

m/z Mass charge ratio

QY Fluorescence quantum yield

Eg : Band-gap energy in eV

VB : Valence band

CB : Conduction band

HOMO : High occupied molecular orbital

LUMO : Low unoccupied molecular orbital

LOD: Limit of detection

EPA : Environmental Protection Agency

WHO : World Health Organization

TLC : Thin layer chromatography

OA : Oleic acid

QD: Quantum dot

DTC: (4-(2-Hydroxyethoxy)phenyl)carbamodithioate triethylammonium ligand

Dye: 3-(6-((2-(2-Hydroxyethoxy)ethyl)amino)-1,3-dioxo-1H-benzo[de]isoquinolin-2(3H)-yl)pentanedioic acid ligand

QDTC: Dithiocarbamate capped quantum dot system

QDTCDye: Dithiocarbamate and dye capped quantum dot system

TOP : Tri-n-octylphosphine

ODE : 1-Octadecene

Characterization techniques :

HR TEM : High Resolution Transmition Electronic Microscopy

HR-MS : High Resolution Mass Spectroscopy

ESI-MS : Electronspray ion mass spectroscopy

FT-IR : Fourier-transform Infrared

NMR : Nuclear Magnetic Resonance

UV-Vis : Ultraviolet-visible

XRD : X-ray Diffraction

XPS : X-photoelectron spectroscopy

PL : Photoluminescence

Units:

°C : Celsius degree

L : Litre ($1L = 10^{-3}\ m^3$)

a.u : Arbitrary Unit

M : Molarity (1M = 1 $mol.L^{-1}$)

µM: Micromolar

nM: Nanomolar

g : Gram

ppm : Part-per-million

ppb : Part-per-billion

Hz : Hertz

K : Kelvin

Table of contents

Chapter 1 Introduction…… 21

1.1 Fluorescent Nanocrystals…… 25

1.2 Quantum confinement and optical properties of semiconductor QDs…… 26

1.3 Synthesis of quantum dots (QDs)……... 29

1.4 Preparation of quantum dots…….. 30

1.5 Characterization of quantum dots…… 31

1.6 Surface modification of quantum dots…….. 32

1.6.1 Organic capped quantum dots…… 33

1.6.2 Inorganically capped QDs: Core/shell QDs……... 34

1.6.2.1 Organic ligands with sulfur group capped CdSe-ZnS QDs……. 35

1.7 Applications of quantum dots…… 38

1.7.1 Effect of ions in quantum dots…… 38

1.7.1.2 Effect of Hg^{+2} on CdSe and CdSe-ZnS Quantum Dots…… 39

1.8 References…… 41

Chapter 2 Influence of mercury ions (Hg^{2+}) on optical and structural properties of quantum dots CdSe-ZnS/OA with different shell thickness…… 58

Abstract…….. 59

2.1 Introduction…… 61

2.2 Methodology…… 63

2.2.1 Synthesis of CdSe-ZnS/OA QDs…… 63

2.2.1 Characterization of CdSe-ZnS/OA QDs……. 63

2.2.2.1 Structural…….. 63

2.2.2.2 Optical…….. 64

2.3 Structural properties…….. 64

2.3.1 XRD analysis…….. 64

2.3.2 HR TEM analysis……... 65

2.3.3 FT-IR analysis…… 67

2.3.4 XPS Analysis…… 68

2.4 Optical properties……... 72

2.4.1 Absorption and fluorescence analysis…… 72

2.4.2 Optical band-gap analysis…….. 73

2.4.3 Photoluminescence decay analysis……. 75

2.4.4 Effect of Hg^{2+} ions on the optical properties of CdSe-ZnS QDs with different shell thickness 80

2.4.4.1 Absorption and fluorescence analysis…….. 80
2.4.4.2 Photoluminescence decay analysis of CdSe-ZnS QDs with different shell thicknesses after interaction with Hg^{2+} ions…….. 84
2.4.5 Effect of metal ions on absorption and fluorescence of CdSe-ZnS QDs…….. 87
2.5 Conclusions……. 90
2.6 References…… 91
Chapter 3 Effect of mercury ions (Hg^{2+}) on optical and structural properties of CdSe/ZnS quantum dots with surface dithiocarbamate and dye ligands…….. 103
Abstract…….. 104
3.1 Introduction…… 106
3.2 Methodology…… 108
3.2.1 Ligand exchange reaction…….. 108
3.2.2 Characterization…… 108
3.2.2.1 Structural…… 108
3.2.2.2 Optical…… 108
3.3 QD ligand exchange with DTC and Dye ligands…….. 109
3.4 Structural properties…….. 112
3.4.1 XRD patterns…… 112
3.4.2 HRTEM analysis…….. 112
3.4.3 FT-IR analysis…….. 113
3.4.4 XPS analysis…… 114
3.5 Optical properties……..... 117
3.5.1 Absorption and fluorescence analysis…….. 117
3.5.2 Optical band-gap analysis…… 118
3.5.3 Photoluminescence decay analysis……..... 119
3.5.4 Effect of different Hg^{2+} concentrations on the optical properties of QDs after the ligand exchange process…….. 122
3.5.4.1 Absorption and emission analysis 122
3.5.4.2 Photoluminescence decay analysis of QDTC and QDTCDye after interaction with Hg^{2+} ions……..... 127
3.5.5 Effect of metal ions on the absorption and emission of the QDs after ligand exchange……. 129
3.6 Conclusions…… 132
3.7 References…….. 133
Chapter 4 Final Conclusion and perspectives…… 144
Chapter 5 Experimental section…… 148

6.1 Solvents…….. 149
6.2 Thin layer chromatography, silica, and alumina columns…… 149
6.3 Nuclear magnetic resonance spectroscopy (NMR)…… 149
6.4 Mass spectrometry…… 149
6.5 Electronic absorption (UV-Vis) and fluorescence Spectroscopy……... 150
6.6 Fluorescence quantum yield……. 150
6.7 Optical change induced by Hg^{2+} ……. 150
6.7.1 UV-Vis and Fluorescence Analysis…….. 150
6.7.2 Effect with other cations…….. 151
6.8 FT-IR spectroscopy …….. 151
6.9 X-ray diffraction (XRD) analysis…… 151
6.10 High-Resolution Transmission Emission Microscopy (HR-TEM)……. 151
6.11 X-ray Photoelectron Spectroscopy (XPS)……. 152
6.12 Time-resolved luminescence……... 152
6.13 Synthesis……... 152
6.13.1 Quantum dots CdSe/ZnS/OA……. 152
6.13.2 Ligands……. 153
6.13.2.1 Dithiocarbamate……... 153
6.13.2.2 Dye……... 155
6.13.3 Ligand Exchange…… 159
6.14 References……. 160
Annexes……. 162

CHAPTER 1
INTRODUCTION

Semiconductor quantum dots are nanomaterials with sizes between 1 and 10 nm. They have been employed as fluorescent probes to detect and quantify Hg^{2+} ions.[1–4] These nanomaterials exhibit a strong quantum confinement effect, and this effect causes the appearance of size-dependent optical properties.[5] The QDs have broad absorption, narrow and size-tunable emission, and high PL quantum yield.[6–8] This has attracted significant attention for applying QDs in different fields, including biological labeling, light-emitting diodes, sensing, and photovoltaic devices.[9–13]

The success of these applications critically depends on the properties of the QD surface, and the surface has been shown to modulate optical properties such as fluorescence efficiency and lifetime.[14–17] The QDs are a lot of amount of atoms on the surface. The control of these surface atoms is critical because their distinct electronic energy states can trap electrons, quench fluorescence emission, and reduce charge transfer rates.[18] These surface atoms must be bonded to coordinate ligands for nearly all applications. The ligands further dictate how the QD interacts with the surrounding medium and influence their application.[19–21]

CdSe is one of the QDs more used due to its flexibility in tuning optical properties, easily modifying the sizes and morphology of nanocrystals.[22] However, core QDs are susceptible to the photo-oxidation and degradation, the growth of a shell composed of a wide-band-gap semiconductor with the functionality of reducing and preventing defects and trap states of the surface to improve the photoluminescence and chemical stability.[6,23,24] CdSe/ZnS core-shell systems are non-toxic since the shell prevents the lixiviation of the Cd^{2+} ions into the surrounding medium.[25,26] However, their photoluminescence QY decreased as the shell coverage grew further.[27]

The capping ligands can modulate the physical and structural properties in QDs, such as solubility, absorption, QY, and photoluminescence.[28] For example, oleic acid (OA) and trioctylphosphine (TOP) are used to synthesize QDs; these ligands prevent nanocrystals' aggregation and maintenance of their union.[29,30] However, as these ligands are hydrophobic, their solubility in water is minimal, and their application in aqueous media is complicated in fields like sensing and biomedical. In this context, the versatile surface permit the ligand exchange to modify the structural and optical properties to improve the application. For example, thiolated ligands are widespread to improve the solubility of QDs in aqueous media.[29]However, these ligands can drastically modify the optical properties such as PL QY, a clear example is the use of aromatic thiolated ligands quenched the photoluminescence and QY; these ligands act as hole trap producing a delocalization of exciton recombination and the photoluminescence decrease in the QDs.[31–33] The structural and optical properties of QDs can be affected by the addition of precursors and ligands used during their synthesis, and thus their application also is affected.

On the other hand, applying QDs in metal ion sensing is fascinating because many metal ions produce health and environmental problems, such as Pb, Cd, As, and Hg.[10,34] Similarly, metal ion sensing can produce different mechanisms; for example, the metal ion can produce small particles in the surface of

QDs by cation exchange reaction and produce the quenching,[30] or enhancement of photoluminescence.[35] In the case of ligands capped QDs, the ligand can desorb from the surface of QD to form a coordination complex producing a quenching of photoluminescence.[30,36] In other studies, the interaction between metal ion only occur with the surface of QD producing small particles by cation exchange reaction to produce a pseudo-shell, and the photoluminescence increase.[37] This mechanism is uncommon in metal ion sensing because the metal transition ions generally act as quenchers of photoluminescence. [10,38–40]

Determining heavy metals in the aquatic environment is very interesting due to the ecosystem and human health, depending on the dose and the toxicity. Many conventional analysis techniques have low detection limits and require specialized conditions, including labs, equipment, and people,[41–46] which are complicated for detecting heavy metal ions directly in the affected location. Developing and designing simple materials with high selectivity and low detection limits for heavy metal ions is necessary due to the difficulties of detecting them in the location affected. This thesis abords this environmental and health problem with the design and analysis of structural and optical properties of CdSe-ZnS QDs with different surface modifications and their application as a fluorescence probe for Hg^{2+} ions.

1.1 Fluorescent Nanocrystals

The study of nanoparticles is a major field in nanotechnology. Nanocrystals are particles with a diameter between 1 and 10 nm, comprising hundreds to thousands of atoms.[47] In the case of semiconductors, they are composed of elements of groups IV, II-VI, III-V, or IV-VI of the periodic table, with semiconductors II-VI (ZnO, ZnS, ZnSe, CdSe, CdS) being the materials that have better luminescent characteristics, of which CdSe and ZnS offer have excellent electronic and optical properties. The optical properties of nanocrystals are size dependent due to the confinement quantum effect.[47,48] In general terms, nanocrystals present a broad absorption spectrum, which extends from the UV to the visible and intense multicolor emission, dependent on crystal size.[47,49]

The surface of nanocrystals is chemically heterogeneous, composed of atoms of a crystalline solid and ligands coordinated to the surface of these atoms.[47,48] The synthesis of the nanocrystals defines the types of face, the crystalline phase, and the ligands that bind to surface atoms.[50] Ligands can be chemisorbed and interchanged to adjust the properties to an application type.[51] The crystalline structure of semiconductors can influence the optical properties of quantum dots.[50,52] For example, the binary semiconductors ZnS and CdSe can exist in thZB and WZ phases, which have the same anion-cation bond length, and their bond geometry is identical to the nearest neighbor (**Figure 3**). The difference is in the second nearest neighbor, which is in a "staggered" (ZB) or eclipsed (WZ) conformation with lattice addresses specified by the Miller indices [111] ZB or [0001] WZ, respectively.[52]

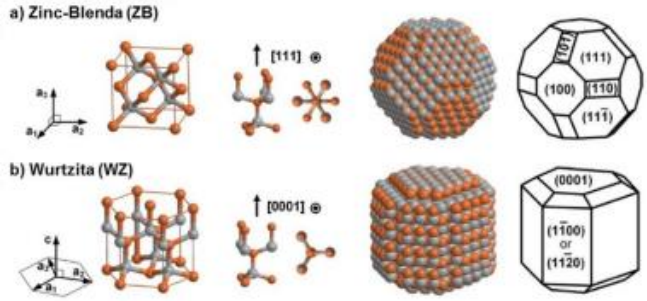

Figure 3. Phases of zinc blende (ZB) or wurtzite (WZ) type CdSe nanocrystals. From left to right: unit vectors of the crystalline phase, unit cell, two views of the internal geometry parallel and perpendicular to the direction [111] for ZB and [0001] for WZ, and schematics of the nanocrystals indicating atoms and identification of the faces. In grey, Cd^{2+} ions; in orange, Se^{2-} ions.[53]

Differences in the crystalline phases give rise to variations in the energy gap (Eg). For example, for the ZB and WZ phases of ZnS, the value of Eg is 3.68 and 3.8 eV, respectively.[47,52] CdSe is one of the semiconductors with the lowest band gap energy *Eg* (1.7 eV) and is mainly characterized by its

multicolor emission dependent on the size of the crystal,[54] for which it is one of the semiconductors with more studies and applications in the optical field;[55] however, the toxicity of cadmium has restricted its use in different applications such as medical and environment.[56] Various modifications on the surface of CdSe nanocrystals have been made to stabilize cadmium ions, making them less toxic and biocompatible.[55,56]

In this context, core/shell type semiconductors, such as CdSe/ZnS, are more stable and friendly to the environment; the ZnS layer prevents the release of cadmium ions in solution and restricts the formation of surface states that function as pair traps electron/hole (formed in typical photo-excitation processes) resulting in materials striking from the optoelectronic field given its fluorescent efficiency (~ 30 - 60%).[47,57,58]

1.2 Quantum confinement and optical properties of semiconductor QDs

The valence and conduction bands are separated in semiconductors by a band gap. The energy gap between the top of the valence band (VB) and the bottom of the conduction band (CB), is called a bandgap. The electrons can excite the BC and create holes in the BV. The distance between the electron in the band of conduction BC and the hole in the valence band BV is called the exciton Bohr radius,[51] a_B^{exc}

$$a_B^{exc} = \frac{\hbar^2 \varepsilon}{e^2}\left(\frac{1}{m_e^* m_0} + \frac{1}{m_h^* m_0}\right) \quad (1)$$

Where $\mathcal{E}$ is the dielectric constant, *h* the Planck constant, a_B^{exc} exciton Bohr radius, *e* mass of electron, $m_e{}^* m_0$ and $m_h{}^* m_0$ are effective masses of electron and hole, respectively.

In bulk semiconductors, the energy gap is constant for a given material. However, in the case of semiconductor QDs with a size comparable to the $a_B{}^{exc}$ of the bulk material, they show a size-dependent energy gap (**Figure 4**). This range in size corresponds to the quantum confinement regime, for which the spatial extent of the electronic wave function is comparable to the QD size. As a result of these geometric constraints, the electrons are affected by the particles boundaries and respond to particle size changes by adjusting their energy.[47,59,60] This phenomenon is known as the quantum size effect, and it plays a significant role in QDs.

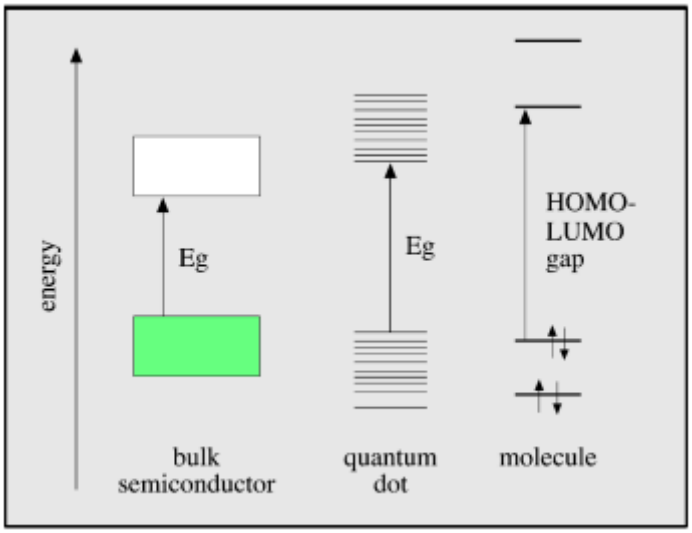

Figure 4. Differences in energy levels between a bulk semiconductor, a QDs nanocrystal, and a molecule.[53]

The decrease in QDs size leads to an increase in band gap and a shift of photon absorption and emission maxima toward shorter wavelengths, compared to the bulk semiconductor material, **Figure 5**. Quantum dots are sometimes referred to as "artificial atoms" because of the analogy of their quantized electronic states with atomic electronic states.

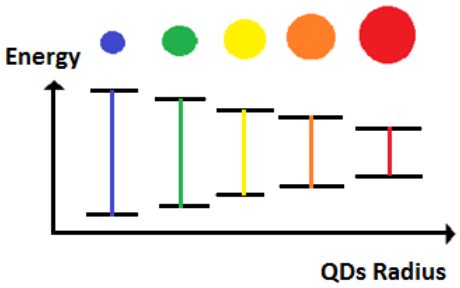

Figure 5. Dependence of the size of the nanocrystals with the value of band gap energy *Eg*.[61]

As a result, nanocrystals can emit a wide range of colors just by changing their size. **Figure 6** shows the displacement of the maximum absorption band for nanocrystals of different sizes. The smaller nanocrystals absorb in the blue and have a sharper absorption band than the larger ones.[62] The emission band is very close to the absorption band, intense and acute for high-quality nanocrystals, such as those formed without surface defects. [63–65]

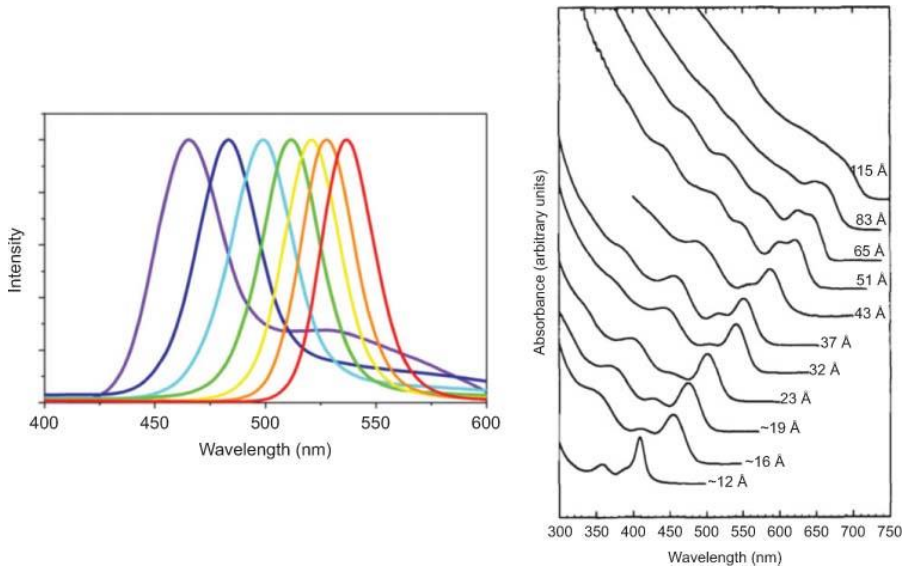

Figure 6. The emission spectra of CdSe QDs (left) and the absorption spectra of CdSe QDs show size-dependent features (suitable). [66]

The shape of the emission spectra of nanocrystals is a characteristic measure of nanocrystal location and size distribution. Sharp and intense emission typically denotes quality and monodispersity, with fluorescence quantum yields as high as 1.00. On many occasions, the quality of the crystals is affected by defects in the nanocrystals (for example, vacancies, impurities, or adsorbates on the surface) that result from the process synthesis, producing wide and low-intensity emissions, decreasing the performance quantum of nanocrystals. Surface defects generate energetic states/ intermediates that can trap electron/hole pairs generated after the excitation of the nanocrystals (**Figure 7**). For example, in the case of obtaining nanocrystals of a diameter of 5 nm, 40% of their atoms are on the surface, which implies the formation of many surface imperfections that trap the electron/hole pairs that form following excitation.[67]

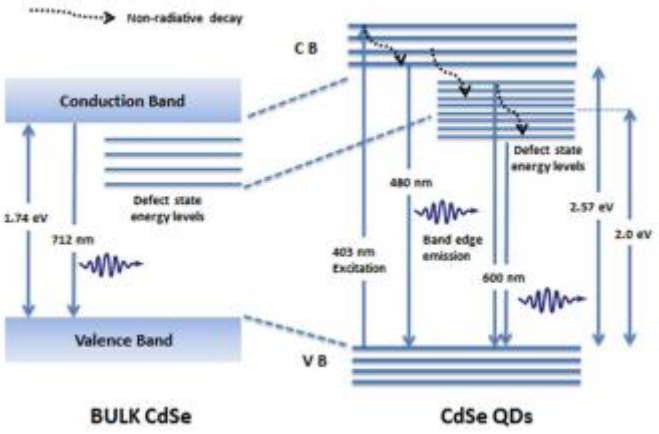

Figure 7. Surface defects (e^-/h^+ traps) of quantum dots.[12]

To increase the quality of nanocrystals, optimize their optical properties, and create new heterostructures with unique photophysical properties, core/shell-type quantum dots were synthesized. These heterostructures result from the encapsulation of the core (for example, CdSe or CdTe) with a second semiconductor of the most significant Eg, known as the shell. Its function is to prevent the formation of surface states that behave as electron/hole traps; it also protects the core from the environment, achieving excellent stability and better luminescence.[68]

In this regard, there have been quantum dots of semiconductors of groups III-V (GaN, GaP, GaAs, InP, and InAs) and of the groups II-VI (ZnO, ZnS, CdS, CdSe, and CdTe). To stabilize the core and improve its luminescence properties, semiconductors with lower Eg (groups II-VI) have been encapsulated with those which have higher Eg (**Figure 8**). A wide variety of heterostructures have resulted from the combination of different semiconductors. For example, the InAs nucleus, with a low value of Eg, has been protected with layers of InP, GaAs, CdSe, ZnSe, and ZnS, resulting in materials with unique photophysical properties and excellent fluorescence yields.[47]

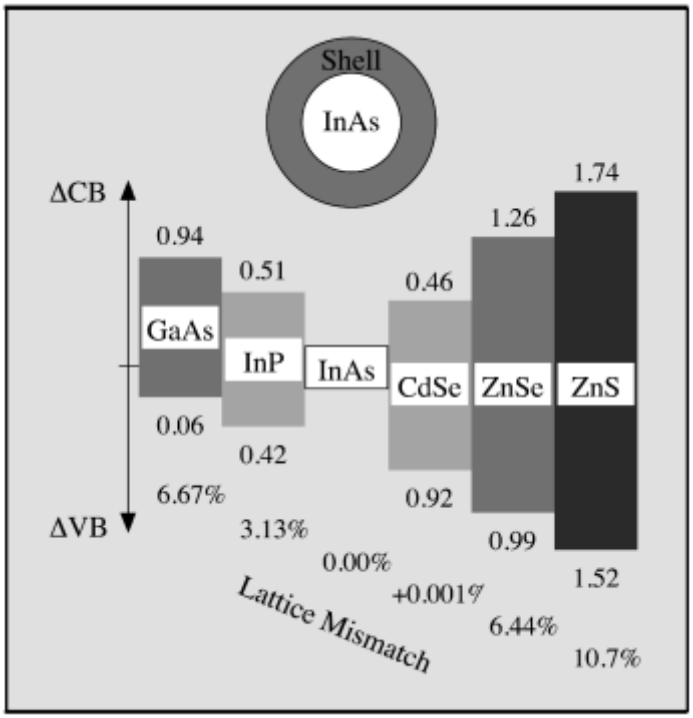

Figure 8. Values (in eV) of the valence band (VB) and the conduction band (CB) of different semiconductors.[53]

1.3 Synthesis of quantum dots (QDs)

Since their discovery in 1981 by Alexey Ekimov,[69] quantum dots have been particularly interesting due to their extraordinary optical properties. In 1993 Bawendi and co-workers modified the synthesis route

to obtain quantum dots with better characteristics, such as higher quantum yield, stability, and fluorescence-tunable size.[70]

The main feature of the quantum dot synthesis is the direct injection of precursors at high temperatures to control the size of the nanoparticle, taking into account the time used for the growth.[5] This method has been the most widely used method of quantum dot synthesis since then and up to the present day.

On the other hand, quantum dots can also be synthesized in the aqueous phase,[71] however, this type of method requires longer synthesis time, which generates aggregation of the nanoparticle, higher hydrodynamic radius,[71,72] and thus a decrease in its optical properties, such as fluorescence, absorption and quantum yield.[71]

Previously, in the colloidal method, dimethyl cadmium ($CdMe_2$) was used as a source of cadmium. However, this compound is highly toxic and pyrophoric, so research was conducted by replacing this cadmium derivative with more stable and less harmful cadmium compounds, such as cadmium oxide (CdO),[73] thus monodisperse and high-quality quantum dots such as CdSe, CdTe and CdSe were obtained. Similarly, using long-chain phosphines was also problematic, so fatty acids such as oleic acid (OA) were tested,[74] which proved easier to handle and environmentally friendly, and thus good results were obtained in the synthesis of quantum dots.

Additionally, the use of oleic acid and octadecyl amine in quantum dot synthesis has been investigated, which showed decreased surface defects, 0.2-0.5 fluorescence quantum yields, and high stability over time.[75] Also, yeasts, fungi, and bacteria have been used to synthesize quantum dots; however, their properties have not been reported.[76–80]

The solvent also plays a crucial role in the synthesis; solvents such as octadecene and olive oil have been investigated, which allows for more excellent stability and controlled growth of the quantum dots.[81] Finally, it is essential to remember that some physical parameters, such as temperature, influence the synthesis.[82,83]

1.4 Preparation of quantum dots

Currently, there are several different methods for the synthesis of quantum dots; some of them are :

1. *Pyrolysis method*: this is the most common method to prepare quantum dots. This technique is based on the pyrolysis of materials at elevated temperatures in an inert atmosphere. For example, the QDs used in this work were obtained by injecting a Se-TOP (organometallic compound) solution into a cadmium oxide (CdO) solution with oleic acid at 225°C to produce a homogeneous nucleation. Oleic acid protects the CdSe QD against oxidation and aggregation, while trioctylphosphine (TOP) protects the QDs from agglomeration. Some reports say this method produces stable quantum dots under ambient temperature for about three months.[84] This

method's advantage is producing quantum dots with optical properties such as high photoluminescence quantum yield and high chemical and photostability.

2. *Microwave assisted-method:* this technique has received particular attention in recent years due to the possibility of eliminating the use of high reaction temperature. It is environmentally friendly and provides a fast, reproducible quantum dots synthesis. The disadvantage is the poor control over size.[5,85]
3. *Sol-gel technique:* here, the materials are in a solution and grow at low temperatures to form a gel. This technique is simple and produces quantum dots of small size.[5]
4. *Solvothermal method:* uses different solvents, and the reaction temperature depends on the solvent's boiling point. It is similar to the pyrolysis method in that it permits size and shape distribution control, and the quantum dots obtained have good crystallinity. These features can change if some parameters of the reaction are varied, such as reaction temperature, reaction time, solvent type, surfactant type, and precursor type.[86,87]

1.5 Characterization of quantum dots

Many techniques are used in the characterization of quantum dots; these techniques offer diverse information about the size, ligands, structure, surface, and optical properties (**Table 1**).[24,47,60,65,88–93]

Table 1. Characterization techniques of quantum dots.

Type of technique	Name	Property
Optical	*Fluorescence spectroscopy*	Optical properties – relation to structural features such as defects, excited-state lifetime
	UV-Visible spectroscopy	Optical properties, size
Structural	*FT-IR*	Surface composition, ligand binding
	Nuclear Magnetic Resonance	The influence of ligands on the surface. Hydrodynamic size.
	Atomic force microscopy	Size and shape in 3D mode, quick examination–elemental composition
	Transmision electron microscopy	Crystal structure of single particles. Distinguish monocrystalline, polycrystalline, and amorphous nanoparticles. Study defects. Size.
	Scanning electron microscopy	Surface composition and shape.

	Laser Light Scattering	Shape. Hydrodynamic size
	X-ray diffraction	Crystal structure, composition, size
	XPS	Electronic structure, elemental composition, oxidation states, ligand binding
	EDX and EDS	Elemental composition (amount)

1.6 Surface modification of quantum dots

Quantum dots, being nanometric, have a high surface/volume ratio; that is, they have hundreds or thousands of atoms on the surface. As such, surface properties are essential, and modification at the surface can lend versatility to properties. Equally, they may possess surface traps, which makes them susceptible to photodegradation and extinction of luminescence. However, this can be corrected by anchoring ligands to the surface according to the desired application.

These surface ligands affect the selectivity and sensitivity of the quantum dots in interacting with various analytes, modifying their fluorescence response when this interaction occurs, and the latter, in turn, can be modified with a capping layer. This control of surface chemistry is essential for their application in sensors, which can help decrease their toxicity.[94–97]

The use of bifunctional ligands helps to improve the solubility and optical properties of the quantum dots, usually using ligands with a hydrophilic end that allows interaction in aqueous media and a hydrophobic part that interacts with the hydrophobic surface of the quantum dot core or shell.[98]

The ligand exchange reaction is used to modify the ligands on the surface of QDs, which consists of reacting a solution of quantum dots with a solution of a coordinating ligand under different conditions. It can use agitation, temperature, radiation for a specific time, thus obtaining quantum dots with new characteristics and which are more friendly to the environment and organisms. Some of the most commonly used ligands include amino acids such as cysteine, glutathione, tyrosine, etc., polymers, biomolecules, silica coatings, and amphiphilic polymers. Some reported research has focused on the sensing capabilities of quantum dots organic or inorganic capped, e.g., core-shell type QDs.[9,99–103]

Surface ligands allow control over QD-dispersion stability in polar or nonpolar solvents through steric and electrostatic mechanisms. The oleophilic ligands with a hydrocarbon tail (**Figure 9-10**) can provide QDs with superior spectroscopic characteristics and solubility in nonpolar solvents. These ligands are commonly organic molecules, e.g., trioctylphosphine/trioctylphosphine oxide (**Figure 9-10**), long-chain alkylamines, and alkyl thiols.[104] For applications involving aqueous or biological media, the water dispersibility of QDs should be considered. Organic molecules with hydrophilic tails, for example,

alcohols, thiol-acids, and siloxane-thiol acids (**Figure 9**), are adopted as ligands to produce quantum dots that can be used in aqueous media, either in chemical synthesis,[105,106] or post-chemical exchange.[107]

The ligands are assumed to guarantee phase transfer and phase transfer efficiency and change the structural and optical properties, such as PLQY. In this context, ligands possessing more than one coordinating unit can provide QDs with extraordinary stability at varying pH mediums and during prolonged storage time.[108]

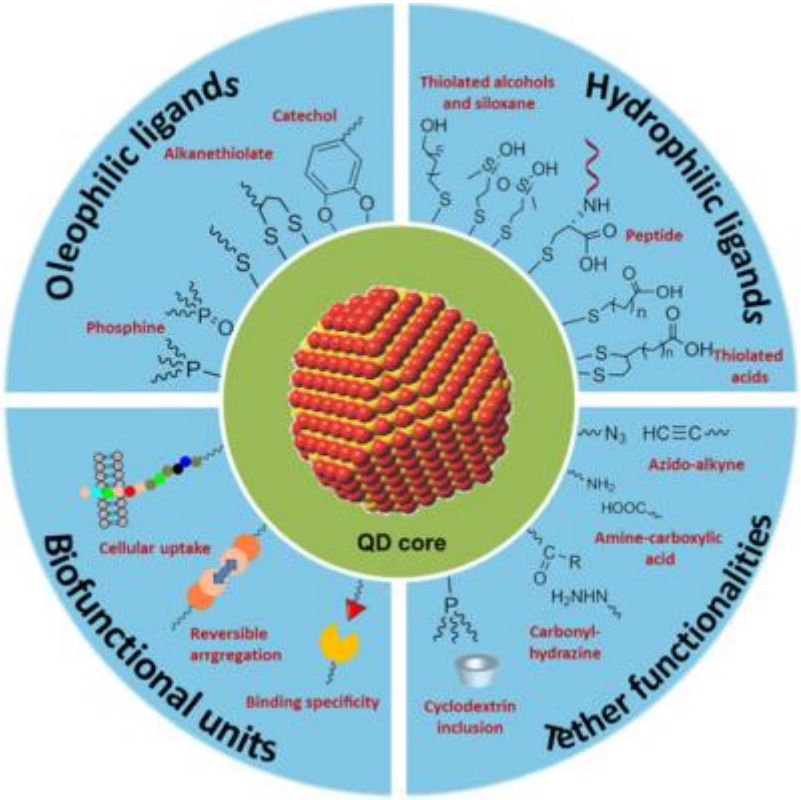

Figure 9. Quantum dots are functionalized with different ligands according to their application.[28]

1.6.1 Organic capped quantum dots:

The use of organic ligands allows the achievement of a colloidal suspension. Some of the most commonly used ligands are phosphines (e.g., tri-n-octylphosphine and tri-n-octylphosphine oxide-TOPO) and mercaptans (-SH) such as propionic acid; the latter is widely used to achieve better solubility in aqueous media (**Figure 10**). However, QDs passivated only with organic ligands are highly toxic, non-photostable, and have surface traps due to their weak binding to surface atoms.[48,85,109–111]

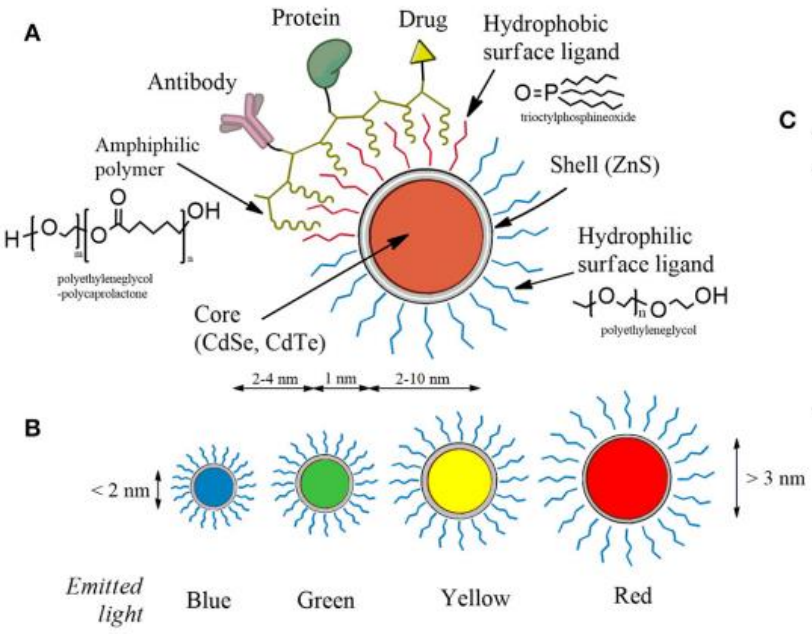

C *Fluorescence lifetimes*

Flurophore	Lifetime (ns)
Tyrosine	2.5
eGFP	2.71
Alexa 488	4
Tissue autofluoresence	1 – 10
Quantum dots	10 – 30
PEG-LPSiNPs	1.2×10^4

Figure 10. The anatomy of quantum dots. (**A**) QDs contain a semiconducting core-shell. The surface can be coated with hydrophilic, hydrophobic, and amphiphilic ligands (common coating molecules are shown), which can be further linked with proteins, drugs, antibodies, and other compounds. (**B**) The emission spectra of QDs can be tuned by adjusting the size. (**C**) Fluorescence lifetimes of QD in comparison with other flurophores.[112,113]

1.6.2 Inorganically capped QDs: Core/shell QDs

An efficient and widely used method for quantum dot passivation is adding peripheral inorganic layers in a shell. Generally, the component of the shell is a material with a band gap higher than the core. The shell passivates surface defects and improves the optical properties maintaining the luminescent properties of the heavy metal core,[68] stability, photoluminescence efficiency, and solubility, and decreases the cytotoxicity.[85] However, the thickness of the shell plays a significant role due to its high quantity and can cause decreases in the optical properties of the nanoparticles.[114,115]

Dabbousi and co-workers reported the effect of the ZnS shell effect on the optical properties of CdSe quantum dots; the fluorescence quantum yield increased from 0.30 to 0.50 (**Figure 11**).[24] Some reports showed the shell (*e.g.*, ZnS) protects the core from oxidation and increases the quantum yield.[116] Other examples include CdS on CdSe and CdSe on CdS,[117] ZnS grown on CdS,[118] ZnS on CdSe and the inverse structure,[119] ZnSe overcoated CdSe.[120]

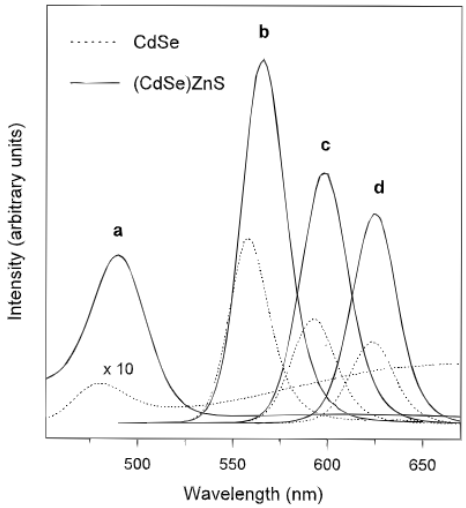

Figure 11. Photoluminescence (PL) spectra for bare CdSe (dashed lines) and CdSe/ZnS core-shell QDs (solid lines) with the following core sizes: (a) 23, (b) 42, (c) 48, and (d) 55 Å in diameter.[24]

1.6.2.1 Organic ligands with sulfur group capped CdSe-ZnS QDs

The organic ligands with sulfur groups had been used to improve CdSe-ZnS QDs properties, such as solubility, optical properties, selectivity, etc. Some representative ligands are DHLA, L-cysteine, dithiocarbamates, thiols, and mercapto acids, such as mercaptopropionic acid. In a study by La Rosa and co-workers,[121] developed an efficient ligand exchange to improve the solubility of QDs in water using the DHLA (Dihydrolipoic acid) capped CdSe-ZnS QDs using methanol/hexane as the solvent and stirring at room temperature; the ligand exchange was a success due to the QDs change from the hexane phase to methanol phase confirming the ligand exchange and improve the solubility of QDs, the optical properties changed also.

Thioalkyl acids such as mercaptoacetic acid (MAA), mercaptosuccinic acid (MSA), and Dihydrolipoic acid (DHLA) were capped CdSe-ZnS QDs to improve the solubility in water,[122] these ligands differ structurally in the number and acidity of carboxyl groups, as well as the number of thiol groups for attachment to the QD surface. Due to these differences, MAA, MSA, and DHLA QDs showed different stabilities against aggregation at low pH. The stability at low pH correlates with the pKa of the ligand, where MSA is the most acidic and stable. During the aggregation process, the emission maxima of the QDs shift towards the red due to changes in the local dielectric constant surrounding each QD.

Zheng and his team used some thiol ligands such as glutathione, N-acetylcysteine, thioctic acid, tiopronin, cysteamine hydrochloride, mercaptosuccinic acid, and 1,4- dithiothreitol capped CdSe-ZnS QDs to evaluate the antioxidant power of these QDs functionalized,[123] these QDs exhibit the optimum properties of high stability, high QY, and low cytotoxicity after ligand exchange. Duran and co-workers

used L-cysteine, cysteamine, and 3-mercaptopropionic acid were capped CdSe-ZnS QDs to improve the solubility in water.[124]

Zhu et al.,[125] used 1,4-benzenedimethanethiol, biphenyl-4,4'-dithiol, 1,16-hexadecanedithiol, 1,11-undecanedithiol and 11-mercapto-1-undecanol capped CdSe-ZnS to improve the optical properties of QDs, after the thiol functionalization, the CdSe-ZnS QDs exhibited significantly enhanced fluorescence efficiency (QY) and storage stability.

Samsulida and co-workers [126] prepared CdSe-ZnS QDs with six organic ligands, L-cysteine, L-histidine, thioglycolic acid (TGA or mercapto-acetic acid, MAA), mercapto-propionic acid, mercapto-succinic acid, and mercapto-undecanoic acid to apply in the detection of glucose. The results showed that the CdSe-ZnS-TGA exhibited the highest fluorescence emission compared to others; the CdSe-ZnS-TGA QDs can be a suitable platform for the fluorescence-based determination of glucose in the current samples.

In a study developed by Montaseri et al.,[127] used L-cysteine, N-acetyl-L-cysteine, and glutathione-capped CdSe-ZnS as sensors for acetaminophen. CdSe-ZnS-L-cysteine QDs were selected due to their enhanced sensitivity as a fluorescence sensor for determining acetaminophen in water. The mechanism was based on the fluorescence *'turn-on'* mode, with the addition of acetaminophen to QDs in aqueous solution, the original fluorescence intensity was enhanced due to fluorescence resonance energy transfer from analytes to QDs, the detection and quantification limits of 1.6 and 5.3 nmol L^{-1}, respectively.

Mercaptopropionic acid-capped CdSe-ZnS QDs were applied as a fluorescent probe for sensitive detection of Pb^{2+} in water. The functionalized QDs showed a high quantum yield, good stability, high solubility in water, and excellent fluorescence properties in a water solution at various pH values. The cation exchange of Zn with Pb led to the linear quenching of fluorescence with the concentration of Pb^{2+} with a detection limit of 3.3 μM.[128]

Zhang and co-workers investigated the suitability of dithiocarbamate (DTC) species as capping ligands for colloidal CdSe-ZnS QDs. DTC ligands are generated by reacting carbon disulfide (CS_2) with primary or secondary amines on appropriate precursor molecules. A biphasic exchange procedure efficiently replaces the existing hydrophobic capping ligands on the QD surface with the newly formed DTCs. The ligand exchange was monitored by UV-vis absorption spectroscopy. The performance of DTC ligands, as evaluated by the preservation of luminescence and colloidal stability, varied widely among amino precursors. The accessibility of the QD surface was evaluated by self-assembly of His-tagged dye-labeled proteins and peptides using fluorescence resonance energy transfer. DTC-capped QDs were also exposed to cell cultures to evaluate their stability and potential use for biological applications.[129]

A series of glucose dithiocarbamates derivatives, such as 1-thio-d-glucose (DG-SH), D-glucosamine dithiocarbamate (DG-DTC), and N-methyl-D-glucamine dithiocarbamate (NMDG-DTC) were capped

to CdSe-ZnS QDs via ligand exchange. The main objective was the optimization of DTC synthesis in aqueous media. Due to the facility of DTCs preparation, colloidal stability, and good optical properties of obtained hydrophilic QDs, DTC derivatives are an alternative to the most commonly used thiolated ligands. Examination of the biological activity of DTC-modified showed negligible intrinsic cytotoxicity, high hydrophilicity, and uncharged surface, indicating the potential of so-modified QDs for cellular imaging and biosensing.[130]

An alkyl-dithiocarbamate (2-hydroxyethyl dithiocarbamate, HDTC) was capped to CdSe-ZnS QDs to apply as a mercury sensor in water. The fluorescent HDTC-QDs were selectively and efficiently quenched by Hg^{2+} through a surface chelating reaction between HDTC and Hg^{2+} due to the desorption of ligand from the surface due to the high affinity with Hg^{2+}, and the detection limit was measured to be 1 ppb. The orange fluorescence of the HDTC-QDs gradually changes to red upon the increasing amount of Hg^{2+} added besides the decreasing fluorescence intensity. Considering this optical phenomenon, a paper-based sensor for aqueous Hg^{2+} detection has been developed by immobilizing the HDTC-QDs on cellulose acetate paper. When Hg^{2+} was dropped onto the paper sensor, the fluorescence color changed from orange to red; this change can be observed depending on the concentration of Hg^{2+}. The limit of detection of the paper sensor was found as 0.2 ppm.[36]

CdSe QDs capped with aromatic thiol ligands, such as α-toluenethiol, thiophenol, and *p*-hydroxythiophenol showed a decrease in the photoluminescence (quenching) of QDs. CdSe QDs functionalized were prepared through ligand exchange. XPS and elemental analysis verified the success of ligand exchange. XRD and HRTEM-SAED studies indicate the crystalline structure of CdSe-thiols QDs is not changing but is improved after ligand exchange with thiol molecules. Time-resolved photoluminescence decay measurements showed that thiophenol and *p*-hydroxythiophenol produce a quenching of the emission and have much shorter photoluminescence lifetimes than other QDs. Thus, both ligands act as effective acceptors for photogenerated holes through aromatic p-electrons (hole traps).[131]

Frederick and co-workers reported that coordinating phenyldithiocarbamate (PDTC) ligands to CdSe QDs decrease photoluminescence. Density functional theory (DFT) calculations suggest that this relaxation occurs through delocalization of the photoexcited hole of the QD into the PDTC ligand shell, i.e., the PDTC is acting as a hole acceptors decreasing the population of the holes in the valence band (VB) and thus decreasing the photoluminescence and optical properties.[31,32,132,133]

The sulfur-containing ligands like thiols and dithiocarbamates can affect the structural and optical properties of QDs; the literature has shown that the alkyl thiols and alkyl dithiocarbamates improve the solubility and optical properties.[131] However, the aromatic thiols and aromatic dithiocarbamates can strongly affect the optical properties due to these ligands acting as hole traps producing a delocalization of exciton and decreasing the photoluminescence and optical properties in general. [31,32,132,133]

1.7 Applications of quantum dots

The properties of quantum dots (QDs), such as size-dependent absorption and emission properties, narrow size distribution, and high luminescence efficiency, are desirable for different applications, including light-emitting diodes (LEDs), solar cells, nanolasers, and sensors.[26,134,135]

Replacing dyes with QDs is possible due to the various advantages of QDs over many organic dyes in terms of photostability, high molar extinction coefficients, size-dependent optical properties, and low cost. QDs are also used in fluorescence labeling to replace molecular dyes for bioimaging, diagnostics, drug delivery, and therapeutic applications. Multicolor optical coding for biological assays has been achieved by using different QDs sizes in which multiple colors and intensities are combined to encode genes, proteins, and intensities to encode genes, proteins and small molecule libraries.[136–143]

The potential applications of QDs depend highly on the structure and properties of nanoscale interfaces. Surface ligands possess an anchoring head group (binding site) and end functionalities, which are an essential component for the synthesis essential component for QDs synthesis, processing, and applications. The binding behavior and functional tail of the ligands can adjust the dispersibility in solution and be inherent to the size-dependent emission.[17] Ligands can act as efficient moderators for exciton relaxation by affecting phonon-assisted intraband relaxation, Auger recombination, or energy transfer to ligand vibrations in QDs.[144]

The competitiveness of radiative recombination of band-edge excitons with electron or electron trap processes largely determines the fluorescence quantum yield (PL-QY) of QDs. The use of σ-donor ligands (e.g., alkylamines) can improve this property in CdSe QDs by around 50% due to the effective passivation of hole traps, resulting in weakened non-radiative exciton recombination of excitons.[145] In this way, compounds such as thiolates are fascinating; these compounds are σ- and π-donor ligands that can effectively passivate electron traps. However, they can introduce hole traps and, as a result, can increase or decrease the PL-QY of QDs.[51,146] Therefore, surface ligands must be carefully selected to control the fluorescence emission.

1.7.1 Effect of ions in quantum dots

Quantum dots have been studied as new fluorescent materials in ion sensors; they can be widely used in chemical analysis. Analyte-generated changes in the optical characteristics of the QDs can accomplish ion detection using quantum dots.[147] These can be classified into luminescence, which shows changes in the fluorescence properties and spectra, and absorbance, which involves changes in the absorption spectra.

There are few reports on the detection of ions with QDs. Some reports are, for example, Chen and Rosenzweig showed for the first time the use of luminescent quantum dots in detecting copper and zinc ions using CdS quantum dots functionalized with different organic ligands in aqueous media.[148] Asfura and Leblanc reported a CdS with a peptide as a sensor for Ag^{+} and Cu^{2+} in aqueous media.[149] Jin and colleagues synthesized functionalized CdSe for the detection of CN^{-}.[150] Several research groups have synthesized different types of functionalized QDs as sensors for Cu^{2+},[117] and Pb^{2+} sensors.[152] These investigations have concluded that during the interaction of analyte and QDs, the photophysical and photochemical properties of QDs are altered. Generally, the design principle in optical sensors for ionic species, either in solution or solid media, is mainly based on the substitution or direct interaction of the surface ligands.[10,28,34,153]

Quantum dots have also been used for the detection of many metal ions, such as K^{+},[154] Ag^{+},[155] Cd^{2+},[156,157] Cu^{2+},[158–164] Hg^{2+},[36,165–170] Pb^{2+},[171] Cr^{3+},[172,173] Fe^{3+},[174] Sb^{3+},[175] Co^{2+},[176] Ba^{2+},[177] Ca^{2+},[178] and Ni^{2+}.[176]

1.7.1.2 Effect of Hg^{2+} on CdSe and CdSe-ZnS Quantum Dots

Different investigations of quantum dots of CdSe (core) and CdSe-ZnS (core-shell) have been developed due to the importance of this metal ion that has led to severe environmental and public health problems worldwide.

- **CdSe**

Chen and co-workers studied the effect of Hg^{2+} ions with water-soluble and highly fluorescent L-cysteine CdSe QDs. This system has a limit of detection (LOD) of 6.0×10^{-9} mol L^{-1} and the effect of this ion produces a fluorescence quenching of the modified CdSe QDs.[179] Shang and co-workers developed a luminescent CdSe QDs modified with triethanolamine in the surface for the detection of Hg^{2+} and I^{-} ions, this nanoparticle showed fluorescence quenching with both ions, while this behavior is not present with individual ions, the LOD was 1.9×10^{-7} mol L^{-1} for Hg^{2+} and 2.8×10^{-7} mol L^{-1} for the I^{-} ion. The electron transfer mechanism from QDs to Hg^{2+} ions can explain the fluorescence quenching.[180]

A water-soluble CdSe QDs, surface modified with β-cyclodextrin (β-CD-QDs), produce fluorescence quenching of QDs in different anions and cations. Anions produced a quenching, but the luminescence could be restored by exposing the QDs to sunlight. Fluorescence quenching was also produced by Ag^{+}, $Hg^{2+,}$ and Co^{2+}.[181]

- **CdSe-ZnS**

In this core-shell type, QDs have been reported some studies about the effect of Hg^{2+}, such as sulfur calixarene capped on CdSe/ZnS QDs by fluorescence quenching.[182] Other research was reported using L-carnitine capped CdSe/ZnS core/shell QDs; this system was luminescent and stable, which showed fluorescence quenching when the mercury ions interacted with the modified QDs, and the LOD reported was 1.8×10^{-7} M.[183]

Freeman and co-workers developed quantum dots CdSe/ZnS functionalized with a nucleic acid; these QDs were studied with Hg^{2+} and Ag^{+} ions, this system showed a multiplexed analysis, and the QDs were modified with thymine-rich nucleic acid for analysis of Hg^{2+} and cytosine-rich nucleic acid for analysis of Ag^{+}, in both cases the CdSe/ZnS QDs showed a fluorescence quenching.[184]

Page and co-workers have developed a ratiometric system using CdSe-ZnS with rhodamine B for Hg^{2+} ions; the behavior in this interaction can explain in terms of an energy-transfer donor coupled to a mercury-sensitive *"turn-on"* dye acceptor.[169]

Yuan and co-workers studied the effect of Hg^{2+} with a water-soluble, CdSe-ZnS QDs functionalized with 2-hydroxyethyldithiocarbamate (HDTC); this system showed a fluorescence quenching by Hg^{2+} through a surface chelating reaction between HDTC and Hg^{2+}, and the LOD was 1 ppb. The orange fluorescence of the HDTC-QDs gradually changes to red with the increasing amount of Hg^{2+} added while the fluorescence intensity decreases. Furthermore, these QDs were immobilized in a paper, and this nanoparticle showed visual changes when interacting with Hg^{2+}. The LOD, in this case, was 0.2 ppm. [36]

Finally, this thesis showed the design, synthesis, and analysis of CdSe-ZnS core-shell QDs with different modifications on their surface: 1) variation in the amount of ZnS shell and 2) surface capped with two aromatic ligands: DTC and Dye and their application as Hg^{2+} ion sensing. These modifications change the structural and optical properties of QDs, such as size, crystallinity, absorption, emission, and QY. The Hg^{2+} ion sensing produces two optical mechanisms: quenching and photoluminescence enhancement. Furthermore, the QDs showed lower LOD than similar nanomaterials and the value established by WHO and EPA. These characteristics showed a CdSe-ZnS QDs studied as promising luminescent nanomaterials to apply in Hg^{2+} sensing.

1.8 **REFERENCES**

(1) Choudhary, Y. S.; Nageswaran, G. Branched Mercapto Acid Capped CdTe Quantum Dots as Fluorescence Probes for Hg 2+ Detection. *Sens Biosensing Res* **2019**, *23*, 100278. https://doi.org/10.1016/j.sbsr.2019.100278.

(2) Zhang, K.; Yu, Y.; Sun, S. Facile Synthesis L-Cysteine Capped CdS:Eu Quantum Dots and Their Hg 2+ Sensitive Properties. *Appl Surf Sci* **2013**, *276*, 333–339. https://doi.org/10.1016/j.apsusc.2013.03.093.

(3) Sharma, E.; Vashisht, D.; Vashisht, A.; Vats, V. K.; Mehta, S. K.; Singh, K. Facile Synthesis of Sulfur and Nitrogen Codoped Graphene Quantum Dots for Optical Sensing of Hg and Ag Ions. *Chem Phys Lett* **2019**, *730* (June), 436–444. https://doi.org/10.1016/j.cplett.2019.06.040.

(4) Pendyala, N. B.; Koteswara Rao, K. S. R. Efficient Hg and Ag Ion Detection with Luminescent PbS Quantum Dots Grown in Poly Vinyl Alcohol and Capped with Mercaptoethanol. *Colloids Surf A Physicochem Eng Asp* **2009**, *339* (1–3), 43–47. https://doi.org/10.1016/j.colsurfa.2009.01.013.

(5) Gidwani, B.; Sahu, V.; Shukla, S. S.; Pandey, R.; Joshi, V.; Jain, V. K.; Vyas, A. Quantum Dots: Prospectives, Toxicity, Advances and Applications. *Journal of Drug Delivery Science and Technology*. Editions de Sante February 1, 2021. https://doi.org/10.1016/j.jddst.2020.102308.

(6) Talapin, D. V; Rogach, A. L.; Kornowski, A.; Haase, M.; Weller, H. Highly Luminescent Monodisperse CdSe and CdSe / ZnS Nanocrystals Synthesized in a Hexadecylamine − Trioctylphosphine Oxide − Trioctylphospine Mixture. *Nano Lett* **2001**, *1* (4), 207–211. https://doi.org/10.1021/nl0155126.

(7) Boatman, E. M.; Lisensky, G. C.; Nordell, K. J. *A Safer, Easier, Faster Synthesis for CdSe Quantum Dot Nanocrystals*; 2005. www.JCE.DivCHED.org.

(8) Zhao, H.; Chaker, M.; Wu, N.; Ma, D. Towards Controlled Synthesis and Better Understanding of Highly Luminescent PbS/CdS Core/Shell Quantum Dots. *J Mater Chem* **2011**, *21* (24), 8898–8904. https://doi.org/10.1039/c1jm11205h.

(9) Medintz, I. L.; Tetsuo Uyeda, H.; Goldman, E. R.; Mattoussi, H. *Quantum Dot Bioconjugates for Imaging, Labelling and Sensing*; 2005. www.nature.com/naturematerials.

(10) Lou, Y.; Zhu, J. Metal Ions Optical Sensing by Semiconductor Quantum Dots. *J Mater Chem C Mater* **2014**, *2* (4), 585–772. https://doi.org/10.1039/c3tc31937g.

(11) Lin, H. J.; Vedraine, S.; Le-Rouzo, J.; Flory, F.; Lin, H. J.; Chen, S. H.; Lee, C. C.; Flory, F. Optical Properties of Quantum Dots Layers: Application to Photovoltaic Solar Cells. *Solar Energy Materials and Solar Cells* **2013**, *117*, 652–656. https://doi.org/10.1016/j.solmat.2012.12.005.

(12) Samuel, B.; Mathew, S.; Anand, V. R.; Correya, A. A.; Nampoori, V. P. N.; Mujeeb, A. Surface Defect Assisted Broad Spectra Emission from CdSe Quantum Dots for White LED Application. *Mater Res Express* **2018**, *5* (2). https://doi.org/10.1088/2053-1591/aaaa83.

(13) Hao, J.; Liu, H.; Miao, J.; Lu, R.; Zhou, Z.; Zhao, B.; Xie, B. A Facile Route to Synthesize CdSe / ZnS Thick-Shell Quantum Dots with Precisely Controlled Green Emission Properties : Towards QDs Based LED Applications. *Sci Rep* **2019**, No. August, 1–8. https://doi.org/10.1038/s41598-019-48469-7.

(14) Graetzel, M.; Janssen, R. A. J.; Mitzi, D. B.; Sargent, E. H. Materials Interface Engineering for Solution-Processed Photovoltaics. *Nature*. August 16, 2012, pp 304–312. https://doi.org/10.1038/nature11476.

(15) Hines, M. A.; Guyot-Sionnest, P. *Synthesis and Characterization of Strongly Luminescing ZnS-Capped CdSe Nanocrystals*; 1996.

(16) Farías, O. J.; Latune, C. L.; Walborn, S. P.; Davidovich, L.; Ribeiro, P. H. S. Determining the Dynamics of Entanglement. *Science (1979)* **2009**, *324* (5933), 1414–1417. https://doi.org/10.1126/science.1171544.

(17) Boles, M. A.; Ling, D.; Hyeon, T.; Talapin, D. V. Erratum : The Surface Science of Nanocrystals. *Nature Publishing Group* **2016**, *15* (3), 364. https://doi.org/10.1038/nmat4578.

(18) Lim, S. J.; Ma, L.; Schleife, A.; Smith, A. M. Quantum Dot Surface Engineering: Toward Inert Fluorophores with Compact Size and Bright, Stable Emission. *Coordination Chemistry Reviews*. Elsevier B.V. August 1, 2016, pp 216–237. https://doi.org/10.1016/j.ccr.2016.03.012.

(19) McBride, J. R.; Pennycook, T. J.; Pennycook, S. J.; Rosenthal, S. J. The Possibility and Implications of Dynamic Nanoparticle Surfaces. *ACS Nano*. October 22, 2013, pp 8358–8365. https://doi.org/10.1021/nn403478h.

(20) Peterson, M. D.; Cass, L. C.; Harris, R. D.; Edme, K.; Sung, K.; Weiss, E. A. The Role of Ligands in Determining the Exciton Relaxation Dynamics in Semiconductor Quantum Dots. *Annu Rev Phys Chem* **2014**, *65*, 317–339. https://doi.org/10.1146/annurev-physchem-040513-103649.

(21) Bozyigit, D.; Volk, S.; Yarema, O.; Wood, V. Quantification of Deep Traps in Nanocrystal Solids, Their Electronic Properties, and Their Influence on Device Behavior. *Nano Lett* **2013**, *13* (11), 5284–5288. https://doi.org/10.1021/nl402803h.

(22) Rathee, N.; Jaggi, N. Time Controlled Growth of CdSe QDs for Applications in White Light Emitting Diodes. *Vacuum* **2019**, *169*. https://doi.org/10.1016/j.vacuum.2019.108910.

(23) Nguyen, H. Q. Synthesis and Optical Properties of CdSe Nanocrystals and CdSe/ZnS Core/Shell Nanostructures in Non-Coordinating Solvents. *Advances in Natural Sciences: Nanoscience and Nanotechnology* **2010**, *1* (2). https://doi.org/10.1088/2043-6254/1/2/025004.

(24) Dabbousi, B. O.; Rodriguez-Viejo, J.; Mikulec, F. V.; Heine, J. R.; Mattoussi, H.; Ober, R.; Jensen, K. F.; Bawendi, M. G. (CdSe)ZnS Core−Shell Quantum Dots: Synthesis and Characterization of a Size Series of Highly Luminescent Nanocrystallites. *J Phys Chem B* **1997**, *101* (46), 9463–9475. https://doi.org/10.1021/jp971091y.

(25) Samanta, A.; Deng, Z.; Liu, Y. Aqueous Synthesis of Glutathione-Capped CdTe/CdS/ZnS and CdTe/CdSe/ZnS Core/Shell/Shell Nanocrystal Heterostructures. *Langmuir* **2012**, *28* (21), 8205–8215. https://doi.org/10.1021/la300515a.

(26) Reiss, P.; Protière, M.; Li, L. Core/Shell Semiconductor Nanocrystals. *Small* **2009**, *5* (2), 154–168. https://doi.org/10.1002/smll.200800841.

(27) Ren, C.; Hao, J.; Chen, H.; Wang, K.; Wu, D. Prepare Core-Multishell CdSe/ZnS Nanocrystals with Pure Color and Controlled Emission by Tri-n-Octylphosphine-Assisted Method. *Appl Surf Sci* **2015**, *353*, 480–488. https://doi.org/10.1016/j.apsusc.2015.06.149.

(28) Zhou, J.; Liu, Y.; Tang, J.; Tang, W. Surface Ligands Engineering of Semiconductor Quantum Dots for Chemosensory and Biological Applications. *Biochem Pharmacol* **2017**, *20* (7), 360–376. https://doi.org/10.1016/j.mattod.2017.02.006.

(29) Dos Santos, J. A. L.; Baum, F.; Kohlrausch, E. C.; Tavares, F. C.; Pretto, T.; Dos Santos, F. P.; Leite Santos, J. F.; Khan, S.; Leite Santos, M. J. 3-Mercaptopropionic, 4-Mercaptobenzoic, and Oleic Acid-Capped CdSe Quantum Dots: Interparticle Distance, Anchoring Groups, and Surface Passivation. *J Nanomater* **2019**, *2019*. https://doi.org/10.1155/2019/2796746.

(30) Granados-Oliveros, G.; Pineros, B. S. G.; Calderon, F. G. O. CdSe/ZnS Quantum Dots Capped with Oleic Acid and L-Glutathione: Structural Properties and Application in Detection of Hg2+. *J Mol Struct* **2022**, *1254*. https://doi.org/10.1016/j.molstruc.2021.132293.

(31) Frederick, M. T.; Weiss, E. A. Relaxation of Exciton Confinement in CdSe Quantum Dots by Modification with a Conjugated Dithiocarbamate Ligand. *ACS Nano* **2010**, *4* (6), 3195–3200. https://doi.org/10.1021/nn1007435.

(32) Frederick, M. T.; Amin, V. A.; Cass, L. C.; Weiss, E. A. A Molecule to Detect and Perturb the Confinement of Charge Carriers in Quantum Dots. *Nano Lett* **2011**, *11* (12), 5455–5460. https://doi.org/10.1021/nl203222m.

(33) Liu, I. S.; Lo, H. H.; Chien, C. T.; Lin, Y. Y.; Chen, C. W.; Chen, Y. F.; Su, W. F.; Liou, S. C. Enhancing Photoluminescence Quenching and Photoelectric Properties of CdSe Quantum Dots with Hole Accepting Ligands. *J Mater Chem* **2008**, *18* (6), 675–682. https://doi.org/10.1039/b715253a.

(34) Zhang, J.; Cheng, F.; Li, J.; Zhu, J.; Lu, Y. Fluorescent Nanoprobes for Sensing and Imaging of Metal Ions: Recent Advances and Future Perspectives. *NanoToday* **2016**, *11* (3), 309–329. https://doi.org/10.1016/j.nantod.2016.05.010.

(35) Wang, H.; Song, D.; Zhou, Y.; Liu, J.; Zhu, A.; Long, F. Fluorescence Enhancement of CdSe/ZnS Quantum Dots Induced by Mercury Ions and Its Applications to the on-Site Sensitive Detection of Mercury Ions. https://doi.org/10.1007/s00604-021-04871-5/Published.

(36) Yuan, C.; Zhang, K.; Zhang, Z.; Wang, S. Highly Selective and Sensitive Detection of Mercuric Ion Based on a Visual Fluorescence Method. *Anal Chem* **2012**, *84* (22), 9792–9801. https://doi.org/10.1021/ac302822c.

(37) Zhu, C.; Li, L.; Fang, F.; Chen, J.; Wu, Y. Functional InP Nanocrystals as Novel Near-Infrared Fluorescent Sensors for Mercury Ions. *Chem Lett* **2005**, *34* (7), 898–899. https://doi.org/10.1246/cl.2005.898.

(38) Wang, B.; Anslyn, E. V. *Chemosensors: Principles, Strategies, and Applications*; 2011. https://doi.org/10.1002/9781118019580.

(39) Jeong, Y.; Yoon, J. Recent Progress on Fluorescent Chemosensors for Metal Ions. *Inorganica Chim Acta* **2012**, *381* (1), 2–14. https://doi.org/10.1016/j.ica.2011.09.011.

(40) Formica, M.; Fusi, V.; Giorgi, L.; Micheloni, M. New Fluorescent Chemosensors for Metal Ions in Solution. *Coord Chem Rev* **2012**, *256* (1–2), 170–192. https://doi.org/10.1016/j.ccr.2011.09.010.

(41) Lin, Y.; Yang, Y.; Li, Y.; Yang, L.; Hou, X.; Feng, X.; Zheng, C. Ultrasensitive Speciation Analysis of Mercury in Rice by Headspace Solid Phase Microextraction Using Porous Carbons and Gas Chromatography-Dielectric Barrier Discharge Optical Emission Spectrometry. *Environ Sci Technol* **2016**, *50* (5), 2468–2476. https://doi.org/10.1021/acs.est.5b04328.

(42) Fang, Y.; Pan, Y.; Li, P.; Xue, M.; Pei, F.; Yang, W.; Ma, N.; Hu, Q. Simultaneous Determination of Arsenic and Mercury Species in Rice by Ion-Pairing Reversed Phase Chromatography with Inductively Coupled Plasma Mass Spectrometry. *Food Chem* **2016**, *213*, 609–615. https://doi.org/10.1016/j.foodchem.2016.07.003.

(43) Harrington, C. F. *The Speciation of Mercury and Organomercury Compounds by Using High-Performance Liquid Chromatography*.

(44) Aranda, P. R.; Colombo, L.; Perino, E.; De Vito, I. E.; Raba, J. Solid-Phase Preconcentration and Determination of Mercury(II) Using Activated Carbon in Drinking Water by X-Ray Fluorescence Spectrometry. *X-Ray Spectrometry* **2013**, *42* (2), 100–104. https://doi.org/10.1002/xrs.2440.

(45) Ioannidou, M. D.; Zachariadis, G. A.; Anthemidis, A. N.; Stratis, J. A. Direct Determination of Toxic Trace Metals in Honey and Sugars Using Inductively Coupled Plasma Atomic Emission Spectrometry. *Talanta* **2005**, *65* (1), 92–97. https://doi.org/10.1016/j.talanta.2004.05.018.

(46) Wu, L.; Long, Z.; Liu, L.; Zhou, Q.; Lee, Y. I.; Zheng, C. Microwave-Enhanced Cold Vapor Generation for Speciation Analysis of Mercury by Atomic Fluorescence Spectrometry. *Talanta* **2012**, *94*, 146–151. https://doi.org/10.1016/j.talanta.2012.03.009.

(47) Vasudevan, D.; Gaddam, R. R.; Trinchi, A.; Cole, I. Core-Shell Quantum Dots: Properties and Applications. *J Alloys Compd* **2015**, No. February. https://doi.org/10.1016/j.jallcom.2015.02.102.

(48) Bera, D.; Qian, L.; Tseng, T. K.; Holloway, P. H. Quantum Dots and Their Multimodal Applications: A Review. *Materials*. MDPI AG 2010, pp 2260–2345. https://doi.org/10.3390/ma3042260.

(49) Lacroix, L.-M.; Delpech, F.; Nayral, C.; Lachaize, S. New Generation of Magnetic and Luminescent Nanoparticles for In-Vivo Real-Time Imaging. **2013**, *3* (3). https://doi.org/10.1098/rsfs.2012.0103ï.

(50) Hartley, C. L.; Kessler, M. L.; Dempsey, J. L. Molecular-Level Insight into Semiconductor Nanocrystal Surfaces. *J Am Chem Soc* **2021**, *143* (3), 1251–1266. https://doi.org/10.1021/jacs.0c10658.

(51) Alivisatos, A. P. Perspectives on the Physical Chemistry of Semiconductor Nanocrystals. *J Phys Chem* **1996**, *100* (31), 13226–13239. https://doi.org/10.1021/jp9535506.

(52) Xia, X.; Liu, Z.; Du, G.; Li, Y.; Ma, M. Wurtzite and Zinc-Blende CdSe Based Core/Shell Semiconductor Nanocrystals: Structure, Morphology and Photoluminescence. *J Lumin* **2010**, *130* (7), 1285–1291. https://doi.org/10.1016/j.jlumin.2010.02.040.

(53) Murphy, C. J.; Coffer, J. L. *Quantum Dots: APrimer*; SOUTH CAROLINA, 2002; Vol. 56.

(54) Ma, C.; Liu, X.; Zhou, M.; Feng, M.; Wu, Y.; Huo, P.; Pan, J.; Shi, W.; Yan, Y. Metal Ion Doped CdSe Quantum Dots Prepared by Hydrothermal Synthesis: Enhanced Photocatalytic Activity and Stability under Visible Light. *Desalination Water Treat* **2015**, *56* (11), 2896–2905. https://doi.org/10.1080/19443994.2014.963152.

(55) Malik, P.; Singh, J.; Kakkar, R. A Review on CdSe Quantum Dots in Sensing. *Advanced Materials Letters*. VBRI Press 2014, pp 612–628. https://doi.org/10.5185/amlett.2014.4562.

(56) Bottrill, M.; Green, M.; Green, M. ChemComm Some Aspects of Quantum Dot Toxicity. **2011**, 7039–7050. https://doi.org/10.1039/c1cc10692a.

(57) Murcia, M. J.; Shaw, D. L.; Woodruff, H.; Naumann, C. A.; Young, B. A.; Long, E. C.; Street, N. B.; March, R. v; Re, V.; Recei, M.; March, V. Facile Sonochemical Synthesis of Highly Luminescent ZnS - Shelled CdSe Quantum Dots. **2006**, No. 6, 2219–2225.

(58) Park, J. J.; de Paoli Lacerda, S. H.; Stanley, S. K.; Vogel, B. M.; Kim, S.; Douglas, J. F.; Raghavan, D.; Karim, A. Langmuir Adsorption Study of the Interaction of CdSe/ZnS Quantum Dots with Model Substrates: Influence of Substrate Surface Chemistry and PH. *Langmuir* **2009**, *25* (1), 443–450. https://doi.org/10.1021/la802324c.

(59) R. W. Knoss. *Quantum Dots: Research, Technology and Applications*; 2008.

(60) Dorfs, D.; Krahne, R.; Falqui, A.; Manna, L.; Giannini, C.; Zanchet, D. *Quantum Dots: Synthesis and Characterization*; Elsevier Ltd., 2011; Vol. 1. https://doi.org/10.1016/B978-0-12-812295-2.00028-3.

(61) Amini, P.; Rostami, G.; Eissa, A. R. E.-M. M. High Throughput Quantum Dot Based LEDs. In *Energy Efficiency Improvements in Smart Grid Components*; Dolatyari, M., Ed.; IntechOpen: Rijeka, 2015; p Ch. 11. https://doi.org/10.5772/59092.

(62) Bera, D.; Qian, L.; Tseng, T.; Holloway, P. H. Quantum Dots and Their Multimodal Applications: A Review. **2010**, 2260–2345. https://doi.org/10.3390/ma3042260.

(63) Hines, M. A.; Guyot-Sionnest, P. Synthesis and Characterization of Strongly Luminescing ZnS-Capped CdSe Nanocrystals. *J Phys Chem* **1996**, *100* (2), 468–471. https://doi.org/10.1021/jp9530562.

(64) Rakovich, Y. P.; Donegan, J. F.; Filonovich, S. A.; Gomes, M. J. M.; Talapin, D. v. Up-Conversion Luminescence via a below-Gap State in CdSe / ZnS Quantum Dots. **2003**, *17*, 99–100. https://doi.org/10.1016/S1386-9477(02)00712-9.

(65) Dzhagan, V. M.; Valakh, M. Y.; Raevskaya, A. E.; Stroyuk, A. L.; Kuchmiy, S. Y.; Zahn, D. R. T. Applied Surface Science Characterization of Semiconductor Core – Shell Nanoparticles by Resonant Raman Scattering and Photoluminescence Spectroscopy. **2008**, *255*, 725–727. https://doi.org/10.1016/j.apsusc.2008.07.018.

(66) Gaponik, N.; Hickey, S. G.; Dorfs, D.; Rogach, A. L.; Eychmüller, A. Progress in the Light Emission of Colloidal Semiconductor Nanocrystals. *Small*. Wiley-VCH Verlag July 5, 2010, pp 1364–1378. https://doi.org/10.1002/smll.200902006.

(67) Peng, X.; Schlamp, M. C.; Kadavanich, A. v; Alivisatos, A. P. Epitaxial Growth of Highly Luminescent CdSe/CdS Core/Shell Nanocrystals with Photostability and Electronic Accessibility. *J Am Chem Soc* **1997**, *119* (30), 7019–7029. https://doi.org/10.1021/ja970754m.

(68) Nirmal, M.; Brus, L. Luminescence Photophysics in Semiconductor Nanocrystals. **1999**, *32* (5), 407–414.

(69) Ekimov, A. I.; A.A.Onushchenko. Quantum Size Effect in Three-Dimensional Micorscopic Semiconductor Crystals. *Jetp Letters*. 1981, pp 345–349. https://doi.org/0021-3640/81/18345-05.

(70) Murray, C. B.; Norris, D. J.; Bawendi, M. G. Synthesis and Characterization of Nearly Monodisperse CdE (E = S, Se, Te) Semiconductor Nanocrystallites. *J Am Chem Soc* **1993**, *115* (19), 8706–8715. https://doi.org/10.1021/ja00072a025.

(71) Poderys, V.; Matulionyte, M.; Selskis, A.; Rotomskis, R. Interaction of Water-Soluble CdTe Quantum Dots with Bovine Serum Albumin. *Nanoscale Res Lett* **2011**, *6* (1), 1–6. https://doi.org/10.1007/s11671-010-9740-9.

(72) Medintz, I. L.; Tetsuo Uyeda, H.; Goldman, E. R.; Mattoussi, H. *Quantum Dot Bioconjugates for Imaging, Labelling and Sensing*; 2005. www.nature.com/naturematerials.

(73) Peng, Z. A.; Peng, X. Formation of High-Quality CdTe, CdSe, and CdS Nanocrystals Using CdO as Precursor [6]. *Journal of the American Chemical Society*. January 10, 2001, pp 183–184. https://doi.org/10.1021/ja003633m.

(74) Jasieniak, J.; Bullen, C.; van Embden, J.; Mulvaney, P. Phosphine-Free Synthesis of CdSe Nanocrystals. *Journal of Physical Chemistry B* **2005**, *109* (44), 20665–20668. https://doi.org/10.1021/jp054289o.

(75) Chandan, H. R.; Saravanan, V.; Pai, R. K.; Geetha Balakrishnaa, R. Synergistic Effect of Binary Ligands on Nucleation and Growth/Size Effect of Nanocrystals: Studies on Reusability of the Solvent. *J Mater Res* **2014**, *29* (14), 1556–1564. https://doi.org/10.1557/jmr.2014.180.

(76) Syed, A.; Ahmad, A. Extracellular Biosynthesis of CdTe Quantum Dots by the Fungus Fusarium Oxysporum and Their Anti-Bacterial Activity. *Spectrochim Acta A Mol Biomol Spectrosc* **2013**, *106*, 41–47. https://doi.org/10.1016/j.saa.2013.01.002.

(77) Yan, Z.; Qian, J.; Gu, Y.; Su, Y.; Ai, X.; Wu, S. Green Biosynthesis of Biocompatible CdSe Quantum Dots in Living Escherichia Coli Cells. *Mater Res Express* **2014**, *1* (1). https://doi.org/10.1088/2053-1591/1/1/015401.

(78) Borovaya, M.; Pirko, Y.; Krupodorova, T.; Naumenko, A.; Blume, Y.; Yemets, A. Biosynthesis of Cadmium Sulphide Quantum Dots by Using Pleurotus Ostreatus (Jacq.) P. Kumm. *Biotechnology and Biotechnological Equipment* **2015**, *29* (6), 1156–1163. https://doi.org/10.1080/13102818.2015.1064264.

(79) Stürzenbaum, S. R.; Höckner, M.; Panneerselvam, A.; Levitt, J.; Bouillard, J. S.; Taniguchi, S.; Dailey, L. A.; Khanbeigi, R. A.; Rosca, E. v.; Thanou, M.; Suhling, K.; Zayats, A. v.; Green, M. Biosynthesis of Luminescent Quantum Dots in an Earthworm. *Nat Nanotechnol* **2013**, *8* (1), 57–60. https://doi.org/10.1038/nnano.2012.232.

(80) Bao, H.; Hao, N.; Yang, Y.; Zhao, D. Biosynthesis of Biocompatible Cadmium Telluride Quantum Dots Using Yeast Cells. *Nano Res* **2010**, *3* (7), 481–489. https://doi.org/10.1007/s12274-010-0008-6.

(81) Sapra, S.; Rogach, A. L.; Feldmann, J. Phosphine-Free Synthesis of Monodisperse CdSe Nanocrystals in Olive Oil. *J Mater Chem* **2006**, *16* (33), 3391–3395. https://doi.org/10.1039/b607022a.

(82) Biju, V.; Makita, Y.; Sonoda, A.; Yokoyama, H.; Baba, Y.; Ishikawa, M. Temperature-Sensitive Photoluminescence of CdSe Quantum Dot Clusters. *Journal of Physical Chemistry B* **2005**, *109* (29), 13899–13905. https://doi.org/10.1021/jp050424l.

(83) Valerini, D.; Cretí, A.; Lomascolo, M.; Manna, L.; Cingolani, R.; Anni, M. Temperature Dependence of the Photoluminescence Properties of Colloidal CdSeZnS Core/Shell Quantum Dots Embedded in a Polystyrene Matrix. *Phys Rev B Condens Matter Mater Phys* **2005**, *71* (23). https://doi.org/10.1103/PhysRevB.71.235409.

(84) Ahamefula, C.; Baa, N.; Ibrahim, yah; Ahamefula Ubani, C.; Sulaiman, M. Y.; Ibarahim, Z.; Ibrahim, N. B.; Othman, M. Y.; Pengajian Fizik Gunaan, P.; Sains dan Teknologi, F. *Synthesis and Characterization of CdSe Quantum Dot Via Pyrolysis OfOrganometalic Reagent*; 2011; Vol. 1. http://ssrn.com/abstract=1963222.

(85) Farzin, M. A.; Abdoos, H. A Critical Review on Quantum Dots: From Synthesis toward Applications in Electrochemical Biosensors for Determination of Disease-Related Biomolecules. *Talanta*. Elsevier B.V. March 1, 2021. https://doi.org/10.1016/j.talanta.2020.121828.

(86) Rafienia, M.; Bigham, A.; Hassanzadeh-Tabrizi, S. A. Solvothermal Synthesis of Magnetic Spinel Ferrites. *J Med Signals Sens* **2018**, *8* (2), 108–118. https://doi.org/10.4103/2228-7477.232087.

(87) Byranvand, M. M.; Kharat, A. N.; Fatholahi, L.; Beiranvand, Z. M. A Review on Synthesis of Nano-TiO2 via Different Methods. *JNS* **2013**, *3* (1), 1–9.

(88) Subila, K. B.; Kumar, G. K.; Shivaprasad, S. M.; Thomas, K. G. Luminescence Properties of CdSe Quantum Dots: Role of Crystal Structure and Surface Composition. **2013**.

(89) Shi, D.; Guo, Z.; Bedford, N. Characterization and Analysis of Nanomaterials. *Nanomaterials and Devices* **2015**, *26*, 25–47. https://doi.org/10.1016/B978-1-4557-7754-9.00002-0.

(90) Gadalla, A.; Abd El-Sadek, M. S.; Hamood, R. Characterization of CdSe Core and CdSe/ZnS Core/Shell Quantum Dots Synthesized Using a Modified Method. *Chalcogenide Letters* **2017**, *14* (7), 239–249.

(91) Bonilla, C. A. M.; Flórez, M. H. T.; Molina Velasco, D. R.; Kouznetsov, V. v. Surface Characterization of Thiol Ligands on CdTe Quantum Dots: Analysis by 1H NMR and DOSY. *New Journal of Chemistry* **2019**, *43* (22), 8452–8458. https://doi.org/10.1039/c8nj05914d.

(92) Fernández-delgado, N.; Herrera, M.; Tavabi, A. H.; Luysberg, M.; Dunin-borkowski, R. E. Applied Surface Science Structural and Chemical Characterization of CdSe-ZnS Core-Shell Quantum Dots. *Appl Surf Sci* **2018**, *457* (April), 93–97. https://doi.org/10.1016/j.apsusc.2018.06.149.

(93) Mourdikoudis, S.; Pallares, R. M.; Thanh, N. T. K. Characterization Techniques for Nanoparticles: Comparison and Complementarity upon Studying Nanoparticle Properties. *Nanoscale*. Royal Society of Chemistry July 21, 2018, pp 12871–12934. https://doi.org/10.1039/c8nr02278j.

(94) Derfus, A. M.; Chan, W. C. W.; Bhatia, S. N. Probing the Cytotoxicity of Semiconductor Quantum Dots. *Nano Lett* **2004**, *4* (1), 11–18. https://doi.org/10.1021/nl0347334.

(95) Hoshino, A.; Fujioka, K.; Oku, T.; Suga, M.; Sasaki, Y. F.; Ohta, T.; Yasuhara, M.; Suzuki, K.; Yamamoto, K. Physicochemical Properties and Cellular Toxicity of Nanocrystal Quantum Dots Depend on Their Surface Modification. *Nano Lett* **2004**, *4* (11), 2163–2169. https://doi.org/10.1021/nl048715d.

(96) Mancini, M. C.; Kairdolf, B. A.; Smith, A. M.; Nie, S. Oxidative Quenching and Degradation of Polymer-Encapsulated Quantum Dots: New Insights into the Long-Term Fate and Toxicity of Nanocrystals in Vivo. *J Am Chem Soc* **2008**, *130* (33), 10836–10837. https://doi.org/10.1021/ja8040477.

(97) Moussodia, R. O.; Balan, L.; Merlin, C.; Mustin, C.; Schneider, R. Biocompatible and Stable ZnO Quantum Dots Generated by Functionalization with Siloxane-Core PAMAM Dendrons. *J Mater Chem* **2010**, *20* (6), 1147–1155. https://doi.org/10.1039/b917629b.

(98) Oh, J. K. Surface Modification of Colloidal CdX-Based Quantum Dots for Biomedical Applications. *Journal of Materials Chemistry*. October 21, 2010, pp 8433–8445. https://doi.org/10.1039/c0jm01084g.

(99) Medintz, I. L.; Tetsuo Uyeda, H.; Goldman, E. R.; Mattoussi, H. *Quantum Dot Bioconjugates for Imaging, Labelling and Sensing*; 2005. www.nature.com/naturematerials.

(100) Dubois, F.; Mahler, B.; Dubertret, B.; Doris, E.; Mioskowski, C. A Versatile Strategy for Quantum Dot Ligand Exchange. *J Am Chem Soc* **2007**, *129* (3), 482–483. https://doi.org/10.1021/ja067742y.

(101) Alivisatos, P. The Use of Nanocrystals in Biological Detection. *Nature Biotechnology*. January 2004, pp 47–52. https://doi.org/10.1038/nbt927.

(102) Schlamp, M. C.; Peng, X.; Alivisatos, A. P. Improved Efficiencies in Light Emitting Diodes Made with CdSe(CdS) Core/Shell Type Nanocrystals and a Semiconducting Polymer. *J Appl Phys* **1997**, *82* (11), 5837–5842. https://doi.org/10.1063/1.366452.

(103) Wang, J.; Han, S.; Ke, D.; Wang, R. Semiconductor Quantum Dots Surface Modification for Potential Cancer Diagnostic and Therapeutic Applications. *Journal of Nanomaterials*. 2012. https://doi.org/10.1155/2012/129041.

(104) Green, M. The Nature of Quantum Dot Capping Ligands. *J Mater Chem* **2010**, *20* (28), 5797. https://doi.org/10.1039/c0jm00007h.

(105) Zhou, D.; Lin, M.; Chen, Z.; Sun, H.; Zhang, H.; Sun, H.; Yang, B. Simple Synthesis of Highly Luminescent Water-Soluble CdTe Quantum Dots with Controllable Surface Functionality. *Chemistry of Materials* **2011**, *23* (21), 4857–4862. https://doi.org/10.1021/cm202368w.

(106) Wang, C. L.; Xu, S. H.; Wang, Y. B.; Wang, Z. Y.; Cui, Y. P. Aqueous Synthesis of Multilayer Mn:ZnSe/Cu:ZnS Quantum Dots with White Light Emission. *J Mater Chem C Mater* **2014**, *2* (4), 660–666. https://doi.org/Doi 10.1039/C3tc31602e.

(107) Dubois, F.; Mahler, B.; Dubertret, B.; Doris, E.; Mioskowski, C. A Versatile Strategy for Quantum Dot Ligand Exchange. *J Am Chem Soc* **2007**, *129* (3), 482–483. https://doi.org/10.1021/ja067742y.

(108) Zhan, N.; Palui, G.; Mattoussi, H. Preparation of Compact Biocompatible Quantum Dots Using Multicoordinating Molecular-Scale Ligands Based on a Zwitterionic Hydrophilic Motif and Lipoic Acid Anchors. *Nat Protoc* **2015**, *10* (6), 859–874. https://doi.org/10.1038/nprot.2015.050.

(109) Colvin, V. L.; Goldstein, A. N.; Alivisatos, A. P. *Semiconductor Nanocrystals Covalently Bound to Metal Surfaces with Self-Assembled Monolayers*.

(110) Wang, Q.; Kuo, Y.; Wang, Y.; Shin, G.; Ruengruglikit, C.; Huang, Q. Luminescent Properties of Water-Soluble Denatured Bovine Serum Albumin-Coated CdTe Quantum Dots. *Journal of Physical Chemistry B* **2006**, *110* (34), 16860–16866. https://doi.org/10.1021/jp062279x.

(111) Dabbousi, B. 0; Murray, C. B.; Rubner, M. F.; Bawendi, M. G. *Langmuir-Blodgett Manipulation of Size-Selected CdSe Nanocrystallites*; 1994; Vol. 6.

(112) Berezin, M. Y.; Achilefu, S. Fluorescence Lifetime Measurements and Biological Imaging. *Chem Rev* **2010**, *110* (5), 2641–2684. https://doi.org/10.1021/cr900343z.

(113) Gu, L.; Hall, D. J.; Qin, Z.; Anglin, E.; Joo, J.; Mooney, D. J.; Howell, S. B.; Sailor, M. J. In Vivo Time-Gated Fluorescence Imaging with Biodegradable Luminescent Porous Silicon Nanoparticles. *Nat Commun* **2013**, *4*. https://doi.org/10.1038/ncomms3326.

(114) Chern, M.; Nguyen, T. T.; Mahler, A. H.; Dennis, A. M. Shell Thickness Effects on Quantum Dot Brightness and Energy Transfer. *Nanoscale* **2017**, *9* (42), 16446–16458. https://doi.org/10.1039/c7nr04296e.

(115) Dabbousi, B. O.; Mikulec, F. v; Heine, J. R.; Mattoussi, H.; Ober, R.; Jensen, K. F.; Bawendi, M. G. (CdSe) ZnS Core - Shell Quantum Dots : Synthesis and Characterization of a Size Series of Highly Luminescent Nanocrystallites. **1997**, *9463* (97), 9463–9475. https://doi.org/10.1021/jp971091y.

(116) Bozrova, S. v; Baryshnikova, M. A.; Sokolova, Z. A.; Nabiev, I. R.; Sukhanova, A. v. In Vitro Cytotoxicity of CdSe/ZnS Quantum Dots and Their Interaction with Biological Systems. *KnE Energy* **2018**, *3*, 58–63.

(117) Tian, Y.; Newton, T.; Kotov, N. A.; Guldi, D. M.; Fendler, J. H. *Coupled Composite CdS-CdSe and Core-Shell Types of (CdS)CdSe and (CdSe)CdS Nanoparticles*; Syracuse, 1995.

(118) Youn, H.-C.; Baral, S.; Fendler, J. H. *Dihexadecyl Phosphate, Vesicle-Stabilized and I n Situ Generated Mixed CdS and ZnS Semiconductor Particles. Preparation and Utilization for Photosensitized Charge Separation and Hydrogen Generation*; 1988; Vol. 92.

(119) Henglein, A.; Ploog, K.; Leland, J. K.; Bard, A. *Nucleation and Growth of CdSe on ZnS Quantum Crystallite Seeds, and Vice Versa, in Inverse Micelle Media*; 1990; Vol. 112.

(120) Danek, M.; Jensen, K. F.; Murray, C. B.; Bawendi, M. G. *Synthesis of Luminescent Thin-Film CdSe/ZnSe Quantum Dot Composites Using CdSe Quantum Dots Passivated with an Overlayer of ZnSe*; 1996.

(121) La Rosa, M.; Avellini, T.; Lincheneau, C.; Silvi, S.; Wright, I. A.; Constable, E. C.; Credi, A. An Efficient Method for the Surface Functionalization of Luminescent Quantum Dots with Lipoic Acid Based Ligands. *Eur J Inorg Chem* **2017**, *2017* (44), 5143–5151. https://doi.org/10.1002/ejic.201700781.

(122) Algar, W. R.; Krull, U. J. Luminescence and Stability of Aqueous Thioalkyl Acid Capped CdSe/ZnS Quantum Dots Correlated to Ligand Ionization. *ChemPhysChem* **2007**, *8* (4), 561–568. https://doi.org/10.1002/cphc.200600686.

(123) Zheng, H.; Mortensen, L. J.; Delouise, L. A. *Thiol Antioxidant-Functionalized CdSe/ZnS Quantum Dots: Synthesis, Characterization, Cytotoxicity*.

(124) Durán, G. M.; Plata, M. R.; Zougagh, M.; Contento, A. M.; Ríos, Á. Microwave-Assisted Synthesis of Water Soluble Thiol Capped CdSe/ZnS Quantum Dots and Its Interaction with Sulfonylurea Herbicides. *J Colloid Interface Sci* **2014**, *428*, 235–241. https://doi.org/10.1016/j.jcis.2014.04.050.

(125) Zhu, H.; Hu, M. Z.; Shao, L.; Yu, K.; Dabestani, R.; Zaman, M. B.; Liao, S. Synthesis and Optical Properties of Thiol Functionalized CdSe/ZnS (Core/Shell) Quantum Dots by Ligand Exchange. *J Nanomater* **2014**, *2014*. https://doi.org/10.1155/2014/324972.

(126) Rahman, S. A.; Ariffin, N.; Yusof, N. A.; Abdullah, J.; Mohammad, F.; Zubir, Z. A.; Aziz, N. M. A. N. A. Thiolate-Capped CdSe/ZnS Core-Shell Quantum Dots for the Sensitive Detection of Glucose. *Sensors (Switzerland)* **2017**, *17* (7). https://doi.org/10.3390/s17071537.

(127) Montaseri, H.; Adegoke, O.; Forbes, P. B. C. Development of a Thiol-Capped Core/Shell Quantum Dot Sensor for Acetaminophen. *South African Journal of Chemistry* **2019**, *72*, 108–117. https://doi.org/10.17159/0379-4350/2019/V72A14.

(128) Luan, W.; Yang, H.; Wan, Z.; Yuan, B.; Yu, X.; Tu, S. T. Mercaptopropionic Acid Capped CdSe/ZnS Quantum Dots as Fluorescence Probe for Lead(II). *Journal of Nanoparticle Research* **2012**, *14* (3). https://doi.org/10.1007/s11051-012-0762-3.

(129) Zhang, Y.; Schnoes, A. M.; Clapp, A. R. Dithiocarbamates as Capping Ligands for Water-Soluble Quantum Dots. *ACS Appl Mater Interfaces* **2010**, *2* (11), 3384–3395. https://doi.org/10.1021/am100996g.

(130) Drozd, M.; Pietrzak, M.; Kalinowska, D.; Grabowska-Jadach, I.; Malinowska, E. Glucose Dithiocarbamate Derivatives as Capping Ligands of Water-Soluble CdSeS/ZnS Quantum Dots. *Colloids Surf A Physicochem Eng Asp* **2016**, *509*, 656–665. https://doi.org/10.1016/j.colsurfa.2016.09.072.

(131) Liu, I. S.; Lo, H. H.; Chien, C. T.; Lin, Y. Y.; Chen, C. W.; Chen, Y. F.; Su, W. F.; Liou, S. C. Enhancing Photoluminescence Quenching and Photoelectric Properties of CdSe Quantum Dots with Hole Accepting Ligands. *J Mater Chem* **2008**, *18* (6), 675–682. https://doi.org/10.1039/b715253a.

(132) Frederick, M. T.; Amin, V. A.; Weiss, E. A. Optical Properties of Strongly Coupled Quantum Dot-Ligand Systems. *Journal of Physical Chemistry Letters* **2013**, *4* (4), 634–640. https://doi.org/10.1021/jz301905n.

(133) Frederick, M. T.; Amin, V. A.; Swenson, N. K.; Ho, A. Y.; Weiss, E. A. Control of Exciton Confinement in Quantum Dot-Organic Complexes through Energetic Alignment of Interfacial Orbitals. *Nano Lett* **2013**, *13* (1), 287–292. https://doi.org/10.1021/nl304098e.

(134) Zhao, H.; Rosei, F. Colloidal Quantum Dots for Solar Technologies. *Chem* **2017**, *3* (2), 229–258. https://doi.org/10.1016/j.chempr.2017.07.007.

(135) Albero, J.; Clifford, J. N.; Palomares, E. Quantum Dot Based Molecular Solar Cells. *Coord Chem Rev* **2014**, *263–264* (1), 53–64. https://doi.org/10.1016/j.ccr.2013.07.005.

(136) Rosi, N. L.; Mirkin, C. A. Nanostructures in Biodiagnostics. **2005**.

(137) Gao, X.; Yang, L.; Petros, J. A.; Marshall, F. F.; Simons, J. W.; Nie, S. In Vivo Molecular and Cellular Imaging with Quantum Dots. **2005**. https://doi.org/10.1016/j.copbio.2004.11.003.

(138) Drummond, T. G.; Hill, M. G.; Barton, J. K. Electrochemical DNA Sensors. **2003**, *21* (10), 1192–1199. https://doi.org/10.1038/nbt873.

(139) Cai, W.; Chen, X. Reviews Nanoplatforms for Targeted Molecular Imaging in Living Subjects. **2007**, No. 11, 1840–1854. https://doi.org/10.1002/smll.200700351.

(140) Burns, A.; Wiesner, U.; Burns, A. Fluorescent Core – Shell Silica Nanoparticles : Towards ‘“ Lab on a Particle ”’ Architectures for Nanobiotechnology. **2006**, 1028–1042. https://doi.org/10.1039/b600562b.

(141) Alivisatos, P. The Use of Nanocrystals in Biological Detection. **2004**, *22* (1), 47–52. https://doi.org/10.1038/nbt927.

(142) Stewart, M. E.; Anderton, C. R.; Thompson, L. B.; Maria, J.; Gray, S. K.; Rogers, J. A.; Nuzzo, R. G. Nanostructured Plasmonic Sensors. **2008**, 494–521. https://doi.org/10.1021/cr068126n.

(143) Daniel, M.; Astruc, D. Gold Nanoparticles : Assembly , Supramolecular Chemistry , Quantum-Size-Related Properties , and Applications toward Biology , Catalysis , and Nanotechnology. **2004**.

(144) Peterson, M. D.; Cass, L. C.; Harris, R. D.; Edme, K.; Sung, K.; Weiss, E. A. The Role of Ligands in Determining the Exciton Relaxation Dynamics in Semiconductor Quantum Dots. *Annu Rev Phys Chem* **2014**, *65*, 317–339. https://doi.org/10.1146/annurev-physchem-040513-103649.

(145) Anikeeva, P. O.; Halpert, J. E.; Bawendi, M. G.; Bulovic, V. Quantum Dot Light-Emitting Devices with Electroluminescence Tunable over the Entire Visible Spectrum 2009. **2009**.

(146) Michalet, X.; Weiss, S. Single-Molecule Spectroscopy and Microscopy. *C R Phys* **2002**, *3* (5), 619–644. https://doi.org/10.1016/S1631-0705(02)01343-9.

(147) Jin, W. J.; Fernández-Argüelles, M. T.; Costa-Fernández, J. M.; Pereiro, R.; Sanz-Medel, A. Photoactivated Luminescent CdSe Quantum Dots as Sensitive Cyanide Probes in Aqueous Solutions. *Chemical Communications* **2005**, No. 7, 883–885. https://doi.org/10.1039/b414858d.

(148) Chen, Y.; Rosenzweig, Z. Luminescent CdS Quantum Dots as Selective Ion Probes. *Anal Chem* **2002**, *74* (19), 5132–5138. https://doi.org/10.1021/ac0258251.

(149) Gattás-asfura, K. M.; Leblanc, R. M. Peptide-Coated CdS Quantum Dots for the Optical Detection of Copper (II) and Silver (I)†‡. *Chem* **2003**, 2684–2685.

(150) Jin, W. J.; Pereiro, R.; Sanz-medel, A. Surface-Modified CdSe Quantum Dots as Luminescent Probes for Cyanide Determination. **2004**, *522*, 1–8. https://doi.org/10.1016/j.aca.2004.06.057.

(151) Fern, M. T.; Pereiro, R.; Sanz-medel, A. Surface-Modified CdSe Quantum Dots for the Sensitive and Selective Determination of Cu (II) in Aqueous Solutions by Luminescent Measurements. **2005**, *549*, 20–25. https://doi.org/10.1016/j.aca.2005.06.013.

(152) Wu, H.; Liang, J.; Han, H. Original Paper A Novel Method for the Determination of Pb 2 1 Based on the Quenching of the Fluorescence of CdTe Quantum Dots. **2008**, 81–86. https://doi.org/10.1007/s00604-007-0801-4.

(153) Zhang, J.; Cheng, F.; Li, J.; Zhu, J.; Lu, Y.; Lou, Y.; Zhu, J.; Wu, P.; Zhao, T.; Hou, X. Semicondutor Quantum Dots-Based Metal Ion. **2014**, *2* (4), 43–64. https://doi.org/10.1039/c3nr04628a.

(154) Lee, H. L.; Dhenadhayalan, N.; Lin, K. C. Metal Ion Induced Fluorescence Resonance Energy Transfer between Crown Ether Functionalized Quantum Dots and Rhodamine B: Selectivity of K+ Ion. *RSC Adv* **2015**, *5* (7), 4926–4933. https://doi.org/10.1039/c4ra10925b.

(155) Cai, C.; Cheng, H.; Wang, Y.; Bao, H. Mercaptosuccinic Acid Modified CdTe Quantum Dots as a Selective Fluorescence Sensor for Ag+ Determination in Aqueous Solutions. *RSC Adv* **2014**, *4* (103), 59157–59163. https://doi.org/10.1039/c4ra07891h.

(156) Swarnkar, A.; Shanker, G. S.; Nag, A. Organic-Free Colloidal Semiconductor Nanocrystals as Luminescent Sensors for Metal Ions and Nitroaromatic Explosives. *Chemical Communications* **2014**, *50* (36), 4743–4746. https://doi.org/10.1039/c4cc00829d.

(157) Wu, P.; Yan, X. P. A Simple Chemical Etching Strategy to Generate "Ion-Imprinted" Sites on the Surface of Quantum Dots for Selective Fluorescence Turn-on Detecting of Metal Ions. *Chemical Communications* **2010**, *46* (37), 7046–7048. https://doi.org/10.1039/c0cc01762k.

(158) Wu, D.; Chen, Z.; Huang, G.; Liu, X. ZnSe Quantum Dots Based Fluorescence Sensors for Cu2+ Ions. *Sens Actuators A Phys* **2014**, *205*, 72–78. https://doi.org/10.1016/j.sna.2013.10.020.

(159) Bu, X.; Zhou, Y.; He, M.; Chen, Z.; Zhang, T. Bioinspired, Direct Synthesis of Aqueous CdSe Quantum Dots for High-Sensitive Copper(Ii) Ion Detection. *Dalton Transactions* **2013**, *42* (43), 15411–15420. https://doi.org/10.1039/c3dt51399h.

(160) Liang, G. X.; Liu, H. Y.; Zhang, J. R.; Zhu, J. J. Ultrasensitive Cu2+ Sensing by Near-Infrared-Emitting CdSeTe Alloyed Quantum Dots. *Talanta* **2010**, *80* (5), 2172–2176. https://doi.org/10.1016/j.talanta.2009.11.025.

(161) Sha, J.; Tong, C.; Zhang, H.; Feng, L.; Liu, B.; Lü, C. CdTe QDs Functionalized Mesoporous Silica Nanoparticles Loaded with Conjugated Polymers: A Facile Sensing Platform for Cupric (II) Ion Detection in Water through FRET. *Dyes and Pigments* **2015**, *113*, 102–109. https://doi.org/10.1016/j.dyepig.2014.07.040.

(162) Ding, Y.; Shen, S. Z.; Sun, H.; Sun, K.; Liu, F. Synthesis of L-Glutathione-Capped-ZnSe Quantum Dots for the Sensitive and Selective Determination of Copper Ion in Aqueous Solutions. *Sens Actuators B Chem* **2014**, *203*, 35–43. https://doi.org/10.1016/j.snb.2014.06.054.

(163) Zhao, X.; Du, J.; Wu, Y.; Liu, H.; Hao, X. Synthesis of Highly Luminescent POSS-Coated CdTe Quantum Dots and Their Application in Trace Cu2+ Detection. *J Mater Chem A Mater* **2013**, *1* (38), 11748–11753. https://doi.org/10.1039/c3ta12335a.

(164) Yang, P.; Zhao, Y.; Lu, Y.; Xu, Q. Z.; Xu, X. W.; Dong, L.; Yu, S. H. Phenol Formaldehyde Resin Nanoparticles Loaded with CdTe Quantum Dots: A Fluorescence Resonance Energy Transfer Probe for Optical Visual Detection of Copper(II) Ions. *ACS Nano* **2011**, *5* (3), 2147–2154. https://doi.org/10.1021/nn103352b.

(165) Liu, B.; Zeng, F.; Wu, G.; Wu, S. Nanoparticles as Scaffolds for FRET-Based Ratiometric Detection of Mercury Ions in Water with QDs as Donors. *Analyst* **2012**, *137* (16), 3717–3724. https://doi.org/10.1039/c2an35434a.

(166) Tao, H.; Liao, X.; Xu, M.; Li, S.; Zhong, F.; Yi, Z. Determination of Trace Hg2+ Ions Based on the Fluorescence Resonance Energy Transfer between Fluorescent Brightener and CdTe Quantum Dots. *J Lumin* **2014**, *146*, 376–381. https://doi.org/10.1016/j.jlumin.2013.10.005.

(167) Mu, Q.; Li, Y.; Xu, H.; Ma, Y.; Zhu, W.; Zhong, X. Quantum Dots-Based Ratiometric Fluorescence Probe for Mercuric Ions in Biological Fluids. *Talanta* **2014**, *119*, 564–571. https://doi.org/10.1016/j.talanta.2013.11.036.

(168) Li, T.; Zhou, Y.; Sun, J.; Tang, D.; Guo, S.; Ding, X. Ultrasensitive Detection of Mercury(II) Ion Using CdTe Quantum Dots in Sol-Gel-Derived Silica Spheres Coated with Calix[6]Arene as Fluorescent Probes. *Microchimica Acta* **2011**, *175* (1–2), 113–119. https://doi.org/10.1007/s00604-011-0655-7.

(169) Page, L. E.; Zhang, X.; Jawaid, A. M.; Snee, P. T. Detection of Toxic Mercury Ions Using a Ratiometric CdSe/ZnS Nanocrystal Sensor. *Chemical Communications* **2011**, *47* (27), 7773–7775. https://doi.org/10.1039/c1cc11442e.

(170) Zhu, X.; Zhao, Z.; Chi, X.; Gao, J. Facile, Sensitive, and Ratiometric Detection of Mercuric Ions Using GSH-Capped Semiconductor Quantum Dots. *Analyst* **2013**, *138* (11), 3230–3237. https://doi.org/10.1039/c3an00011g.

(171) Zhao, Q.; Rong, X.; Chen, L.; Ma, H.; Tao, G. Layer-by-Layer Self-Assembly Xylenol Orange Functionalized CdSe/CdS Quantum Dots as a Turn-on Fluorescence Lead Ion Sensor. *Talanta* **2013**, *114*, 110–116. https://doi.org/10.1016/j.talanta.2013.04.016.

(172) de Souza, G. C. S.; de Santana, É. E. A.; da Silva, P. A. B.; Freitas, D. v.; Navarro, M.; Paim, A. P. S.; Lavorante, A. F. Employment of Electrochemically Synthesized TGA-CdSe Quantum Dots for Cr3+ Determination in Vitamin Supplements. *Talanta* **2015**, *144*, 986–991. https://doi.org/10.1016/j.talanta.2015.07.054.

(173) Han, J.; Bu, X.; Zhou, D.; Zhang, H.; Yang, B. Discriminating Cr(Iii) and Cr(vi) Using Aqueous CdTe Quantum Dots with Various Surface Ligands. *RSC Adv* **2014**, *4* (62), 32946–32952. https://doi.org/10.1039/c4ra04535a.

(174) Li, S.; Chen, D.; Zheng, F.; Zhou, H.; Jiang, S.; Wu, Y. Water-Soluble and Lowly Toxic Sulphur Quantum Dots. *Adv Funct Mater* **2014**, *24* (45), 7133–7138. https://doi.org/10.1002/adfm.201402087.

(175) Ge, S.; Zhang, C.; Zhu, Y.; Yu, J.; Zhang, S. BSA Activated CdTe Quantum Dot Nanosensor for Antimony Ion Detection. *Analyst* **2010**, *135* (1), 111–115. https://doi.org/10.1039/b915622d.

(176) Mahapatra, N.; Panja, S.; Mandal, A.; Halder, M. A Single Source-Precursor Route for the One-Pot Synthesis of Highly Luminescent CdS Quantum Dots as Ultra-Sensitive and Selective Photoluminescence Sensor for Co2+ and Ni2+ Ions. *J Mater Chem C Mater* **2014**, *2* (35), 7373–7384. https://doi.org/10.1039/c4tc00887a.

(177) Völker, J.; Zhou, X.; Ma, X.; Flessau, S.; Lin, H.; Schmittel, M.; Mews, A. Semiconductor Nanocrystals with Adjustable Hole Acceptors: Tuning the Fluorescence Intensity by Metal-Ion Binding. *Angewandte Chemie - International Edition* **2010**, *49* (38), 6865–6868. https://doi.org/10.1002/anie.201001441.

(178) Xia, Y.; Wang, J.; Zhang, Y.; Song, L.; Ye, J.; Yang, G.; Tan, K. Quantum Dot Based Turn-on Fluorescent Probes for Anion Sensing. *Nanoscale* **2012**, *4* (19), 5954–5959. https://doi.org/10.1039/c2nr31809a.

(179) Chen, J.; Gao, Y. C.; Xu, Z. B.; Wu, G. H.; Chen, Y. C.; Zhu, C. Q. A Novel Fluorescent Array for Mercury (II) Ion in Aqueous Solution with Functionalized Cadmium Selenide Nanoclusters. *Anal Chim Acta* **2006**, *577* (1), 77–84. https://doi.org/10.1016/j.aca.2006.06.039.

(180) Shang, Z. bin; Wang, Y.; Jin, W. J. Triethanolamine-Capped CdSe Quantum Dots as Fluorescent Sensors for Reciprocal Recognition of Mercury (II) and Iodide in Aqueous Solution. *Talanta* **2009**, *78* (2), 364–369. https://doi.org/10.1016/j.talanta.2008.11.025.

(181) Shang, Z. bin; Hu, S.; Wang, Y.; Jin, W. J. Interaction of β-Cyclodextrin-Capped CdSe Quantum Dots with Inorganic Anions and Cations. *Luminescence* **2011**, *26* (6), 585–591. https://doi.org/10.1002/bio.1274.

(182) Li, H.; Zhang, Y.; Wang, X.; Xiong, D.; Bai, Y. Calixarene Capped Quantum Dots as Luminescent Probes for Hg2+ Ions. *Mater Lett* **2007**, *61* (7), 1474–1477. https://doi.org/10.1016/j.matlet.2006.07.064.

(183) Li, H.; Zhang, Y.; Wang, X.; Gao, Z. A Luminescent Nanosensor for Hg(II) Based on Functionalized CdSe/ZnS Quantum Dots. *Microchimica Acta* **2008**, *160* (1–2), 119–123. https://doi.org/10.1007/s00604-007-0816-x.

(184) Clever, G. H.; Kaul, C.; Carell, T. DNA-Metal Base Pairs. *Angewandte Chemie - International Edition*. 2007, pp 6226–6236. https://doi.org/10.1002/anie.200701185.

CHAPTER 2

INFLUENCE OF MERCURY IONS (Hg^{2+}) ON OPTICAL AND STRUCTURAL PROPERTIES OF QUANTUM DOTS CdSe-ZnS/OA WITH DIFFERENT SHELL THICKNESS

ABSTRACT

Quantum dots (QDs) are zero-dimensional nanocrystal materials with 1-10 nm lengths.[1] Their advantages include broad absorption spectra, narrow emission spectra, and high quantum yield.[2,3] The optical and structural properties can be adjusted by modifying the size and surface of QDs with metal ions or ligands.[4–8] These properties make their application possible in fluorescence sensing, wherein QDs such as CdSe, CdTe, and CdS are used.[9–11]

This Chapter shows the influence of S and Zn-treatment in synthesizing three CdSe-ZnS core-shell QDs on their structural and optical properties, thus QD-0.3 ML (Zn/S, 0.1/9), QD-0.9 ML (Zn/S, 0.6/2), QD-1.0 ML (Zn/S, 1.1/0.9). All the core-shell QDs were characterized by X-ray diffraction to analyze the crystallinity, high-resolution electron microscopy (HR TEM) to determine the size and crystallinity, X-ray photoelectron and FT-IR spectroscopy were used to analyze the coordination of ligands on the surface of CdSe-ZnS QDs.

The XRD patterns analysis showed three peaks at 25.5, 42.7, and 50.2 degrees, corresponding to the (111), (220), and (311) lattice planes of cubic zinc blend CdSe. The diffraction peaks of the core shell show a shift to higher reflection angle positions due to the formation of the ZnS shell. The HRTEM analysis showed particles non-aggregated with distribution sizes around 2.7 nm, 3.0 nm, and 3.2 nm. The XPS measurements showed changes in the S2p, Zn2p, and Cd3d, indicating the existence of different species of these elements on the surface of CdSe-ZnS QDs with different S and Zn-treatment used during synthesis. The FT-IR results showed the oleic acid capped CdSe-ZnS QDs; however, the wavenumber difference of carboxylate bands is increasing as [Zn] precursor concentration for core/shell samples. These $\Delta\nu$ values indicate that the carboxylate ion coordinates to metal ions of QDs surface as bidentate.[12,13]

The optical properties of QDs with different Zn:S ratios were developed using absorption, emission, and time-resolved photoluminescence. The S-excess in the CdSe-ZnS QDs (QD-0.3 ML) produces a lower QY than other QDs studied because the S acts as a hole trap that favors the non-radiative recombination and decreased photoluminescence. However, the Zn-treatment removes/eliminates the hole traps, and the photoluminescence is increased, and QY increases, as in QD-0.9 ML (QY: 0.54). This metal ion produces a passivation effect on the surface of QDs. On the other hand, when the CdSe-ZnS QDs have a thicker shell, as in QD-1.0 ML, the PL QY decreases due to the increase of Zn-treatment. The high amount of Zn in the shell produces a high shell thickness and, thus, lattice incoherence is formed, increases the strain by forming surface defects, and decreases photoluminescence.

The analysis of three CdSe-ZnS QDs (QD-0.3 ML, QD-0.9 ML, and QD-1.0 ML) as Hg^{2+} ion sensing was developed in homogeneous phase using a solution of QDs in a mixture $CHCl_3$/ethanol (1/1, v/v) and aqueous solution of Hg^{2+} using absorption, emission, and time-resolved photoluminescence. The addition of Hg^{2+} produces opposite changes in the photoluminescence of QDs. For example, in QD-0.3 ML, a quenching of fluorescence is produced due to the formation of HgSe particles on the core of QD; these HgSe particles are produced by a cation exchange reaction between Cd from core and Hg, the Ksp of HgSe is lower than CdSe, and the reaction is favored.[14] The S-excess from $(TMS)_2S$ used in the synthesis of QD produces HgS due to the high affinity from S and Hg in concordance with the HSAB theory.[15]

On the other hand, adding Hg^{2+} ions in CdSe-ZnS QDs with thicker shells (QD-0.9 ML and QD-1.0 ML) produces the opposite effect, i.e., an enhancement in the photoluminescence is produced. In these QDs, the Hg^{2+} produces HgS particles on the shell surface, forming a pseudo-shell that passivates the surface traps and improves the photoluminescence. A cation exchange reaction forms these HgS particles from Zn-to-Hg because the Ksp of HgS is lower than ZnS, and the reaction is favored.[14]

In addition, the detection limit (LOD) of Hg^{2+} ions was determined with the plots obtained in a linear range from 0.5-5.0 μM with correlation coefficients (R^2) around 0.999. The LOD for QD-0.3 ML calculated was 11.2 nM. For QDs with thicker shells (QD-0.9 ML and QD-1.0 ML), the LOD was 8.98 nM and 10.7 nM for QD-0.9 ML and QD-1.0 ML, respectively. These values of LOD are lower than other QDs reported. [16–20]

Finally, the analysis with foreign metal ions was developed with an aqueous solution of Zn^{2+}, Mn^{2+}, Cd^{2+}, Pb^{2+}, Co^{2+}, Ni^{2+}, and Hg^{2+} chloride salts and QDs in a mixture with $CHCl_3$/ethanol (1/1, v/v). This analysis showed a photoluminescence quenching with all the metal ions evaluated in QD-0.3 ML; however, the most significant quenching observed was obtained with Hg^{2+} ions due to the formation of HgSe particles on the core because the Ksp of HgSe is lower than other metal ions evaluated. While in the case of QD-0.9 ML and QD-1.0 ML, they enhance the photoluminescence due to the passivation of surface traps formed during the synthesis of QDs.

2.1 Introduction

Quantum dots (QDs) of semiconductors are nanocrystals with particle sizes between 1 and 10 nm applied in different fields, such as sensors, lasers, photovoltaics, and light-emitting diodes.[21] Particularly, II-VI semiconductors like CdSe are characterized by a broad absorption spectrum and a narrow and intense emission that could be multicolor since it depends on their size due to the quantum confinement effect, as described above. These characteristics are very appreciated for metal ion sensing applications.[22,23]

Precisely for QD-based metal ions detection, CdSe QDs have been modified with different ligands to avoid aggregation, aid stability and improve their selectivity or sensitivity. With this goal, the CdSe QDs surface has been modified with hydrophilic ligands resulting in the affectation of fluorescence intensity signal that could be quenched or enhanced as a response to metal ions.[8,11] For instance, quenching of fluorescence has been reported with L-cysteine-capped CdSe QDs to detect Pb^{2+} ions,[24] mercapto acetic acid-capped CdSe QDs have been applied in the detection of Ag^{+} ions,[25] mercaptoethanesulfonate-capped CdSe QDs to be used in the Cu^{2+} ions determination.[26] While enhancement of PL has been reported with L-cysteine-capped CdSe to detect Zn^{2+} ions.[26] Other QD types have also reported the increment of PL intensity induced by cations. For example, mercaptopropionic acid-capped CdTe QDs in the presence of Cd^{2+}, [27] mercaptoethanol-capped PbS QDs in the presence of mercapto acetic acid-capped InP QDs in the presence of Hg^{2+} ions [28] and L-cysteine capped CdS QDs in the presence of Ag^{+} ions. [29]

Mercury ions, the most potent neurotoxin in human physiology, are selected as analyte in the present investigation due to the severe environmental and public health problems in counties that use mercury in gold extraction mining. Many fluorescent-based optical sensors[30] have been applied to detect Hg^{2+} ions in real-time with high sensibility, selectivity, and signal-to-noise ratio.[31]

For QDs-based mercury ions, the interaction between analyte and nanocrystals is a process that leads to many pathways that affect photoluminescence intensity. According to the affinity of metal ions and QDs, a cation exchange could be produced by replacing cations of starting QDs with cations of analyte solution, preserving the original anion sublattice.[14] This cation exchange reaction forms small particles on the QD surface, causing non-radiative recombination of excited electrons and holes that finally quenches fluorescence.[32]

Conversely, the strategies reported in the literature literature that lead to increased fluorescence for determining cation ions are less frequent. Surface state passivation of QDs removes the traps that facilitate non-radiative recombination pathways.[33] The understanding of the trap states role is challenging. In its simplest form, a trap can be described as a stable nonbonding orbital of an undercoordinated atom. This orbital usually lies deep in the band-gap, where it can act as an electron or

hole trap. Metal ions on QDs surface can produce non-coordinative atoms and dimers,[34] indirectly affecting the number of dangling bonds and the presence of traps.[35]

In this context, the growth of a shell of semiconducting material with a larger band-gap (3.7 > 1.7 eV)[1] than CdSe, as ZnS, plays a determinant role since shell passivates the traps and defects of core,[36,37] improving their stability, [36,38] and photoluminescence.[1] [39,40,41] However, excess of shell (greater than 2.2 monolayers[42]) can cause an opposite effect in the PL of core/shell QDs, because the lattice mismatch between CdSe and ZnS is 12%, which causes a strain at interface[43]that creates non-radiative recombination sites, impairing the properties of PL.[37,44,45]

Our group has previously studied the Hg^{2+} ions detection by PL measurements using CdSe-ZnS QDs modified with two ligands of different water affinity, such as L-glutathione and oleic acid. Both QDs produced PL quenching. Since oleic acid-capped CdSe-ZnS showed good capacity to detect metal ions, we used these nanomaterials to induce PL quenching and enhancement in the present investigation. For this, the present investigation used the variation of the molar ratio of shell precursors to obtain three nanocrystals with different shell thicknesses and to induce the formation of traps that affected PL properties in different ways. We discussed the response fluorescence of QDs in terms of the shell thickness, [Zn]/[S] molar relation, surface properties, and PL decay dynamics. Surface properties are characterized by FT-IR, XPS, TEM, and HR-TEM measurements. Results show that an excess of shell precursor creates traps sites that passivate surface QDs, and protect the core from exchange cation reactions avoiding the quenching of PL in the presence of Hg^{2+} ions.

2.2 *Methodology*

2.2.1 Synthesis of CdSe-ZnS/OA QDs

CdSe core QDs were prepared via published reports.[46–48] 34.2 mg (0.25 mmol) of CdO, 0.6 mL (1.9 mmol) of oleic acid (OA), and 10 mL of 1-octadecene (ODE) were mixed into a 250 mL three-neck flask under N_2 protection. The mixture was heated at 225 °C under magnetic stirring for 90 min. In these conditions, CdO was dissolved. In another three-neck flask and under N_2 atmosphere, Se/TOP was prepared by mixing 30.5 mg (0.38 mmol) of selenium powder, 5 mL of ODE, and 0.45 mL (0.90 mmol) of tri-octyl phosphine (TOP) solution; and heated at 80 °C for 3 h. Then, 1.0 mL Se/TOP was quickly injected into CdO solution at 225 °C for CdSe nucleus growth for 3 mins, and at that moment, the temperature was adjusted to 100 °C.

After this, three Zn/S/TOP solutions were prepared by mixing 32, 160, and 320 μL (0.032 mmol (QD-0.3 ML), 0.160 mmol (QD-0.9 ML), and 0.320 mmol (QD-1.0 ML)) of $Zn(C_2H_5)_2$ 1M solution, 64 μL (0.28 mmol) of $(TMS)_2S$ and 1 mL (2 mmol) of TOP under N_2 atmosphere. This solution was added dropwise to CdSe solution under magnetic stirring, keeping N_2 atmosphere, and heated to 80 °C for 4 h. CdSe/ZnS/OA QDs were washed repeatedly with an excess of methanol to remove the excess of unbound ligands (OA and TOP). After that, the QDs were precipitated when 10 mL of cold chloroform was added at 30 °C, followed by centrifugation at 4.000 rpm for 5 min. The resulting solid was dissolved in toluene, precipitated with chloroform and acetonitrile (1:1 volumetric ratio) at 30 °C, and centrifuged at 4.000 rpm for 10 min. This purification process was repeated 3 times.[32]

2.2.2 Characterization of CdSe-ZnS/OA QDs

2.2.2.1 Structural

Panalytical X'Pert3 Pro-Multipurpose Diffractometer with CuKα radiation source (45 kV and 40 mA) was employed to measure the powder XRD patterns. The diffraction dataset cards from the Joint Committee of Powders Diffraction Standards (JCPDS) were used to compare the obtained patterns. The FT-IR spectra were taken in a Thermo Scientific Nicolet iS10 spectrometer. XPS experiments were performed with the A Centeno-XPS/ISS/UPS surface characterization platform built by SPECS (Germany), and the employed experimental parameters were previously reported.[49] CasaXPS program (Casa Software Ltd) for data analysis and the SPECS Prodigy library for RSF values were used. The High-Resolution Transmission Electron Microscopy (HR-TEM) images of the QDs were taken using a Tecnai F20 Super Twin TMP Microscope. A drop of the sample was deposited on a carbon film grid; then, the sample was dried and analyzed in the transmission microscope using 450.000 x magnification. Image-J software was used to calculate the average diameter and d-spacing [111] of QDs with HR-TEM micrographs.

2.2.2 Optical

A Varian UV-Vis-NIR spectrophotometer Cary 5000 was used to obtain the UV-Vis absorption spectra, and a HORIBA Jobin-Yvon Fluorolog-3 spectrophotometer was used for PL measurements. The PL QY (ϕ) of CdSe/ZnS/OA (dissolved in a mixture chloroform/ethanol 1/1) was calculated using Rhodamine 6 G in ethanol solution as standard (ϕ = 0.94), with excitation wavelength (λ_{ex}) at 500 nm. The quantification of PL QY and Hg^{2+} - other metal ions sensing assay are explained in detail in Chapter 6.

2.3 *Structural properties*

2.3.1 XRD analysis

Figure 12 shows the X-ray diffraction patterns of the CdSe core and CdSe-ZnS core-shell QDs. The diffraction peaks of core-shell samples are centered around 25.5, 42.7, and 50.2 degrees, corresponding to the (111), (220), and (311) lattice planes of cubic zinc blend CdSe. Compared to the CdSe pattern (JCPDS file No. JCPDS-77-2100), diffraction peaks of the core-shell show a shift to higher reflection angle positions due to the formation of the ZnS shell. This behavior is due to the smaller ZnS lattice (5.42 Å) constant compared with CdSe (6.05 Å), an indication of epitaxial growth of the shell around the core.[50,51] These results are different from other reports where the diffraction peaks were broadened with a shell thickness larger than 4 ML.[52–54] Samples prepared under a more amount of Zn (QD-0.9 ML and QD-1.0 ML) produced broader and more intense peaks but not severe crystal changes in the lattice of QDs.

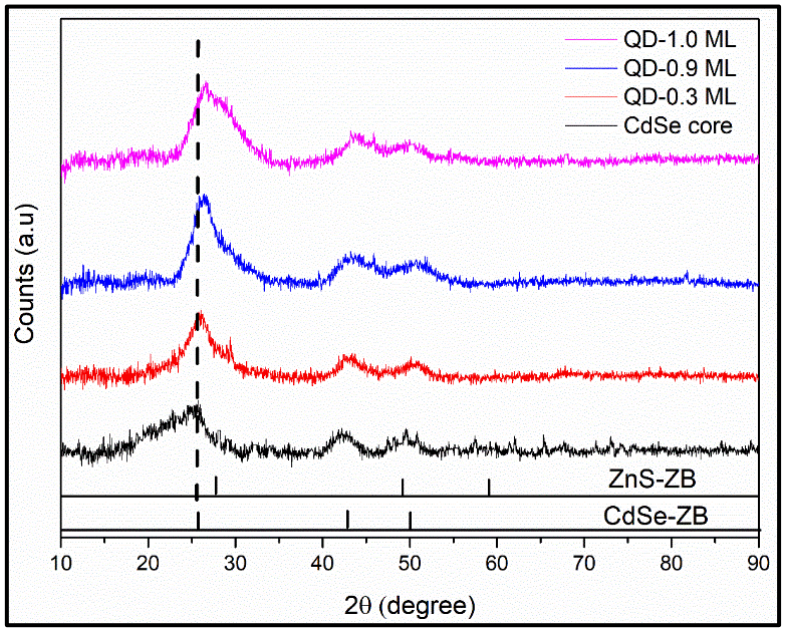

Figure 12. XRD patterns of CdSe (core) and CdSe-ZnS QDs with different shell thicknesses.

2.3.2 HR TEM analysis

The particle sizes of core-shell QDs have been determined by HRTEM (**Figure 13**). HRTEM images reveal spherical structures with good crystallinity and reasonably narrow size distributions. There is no evidence of an interface between the core and the shell, which shows epitaxial growth and demonstrates that the shell growth does not disturb the crystalline form of the core.[37]

The average diameters determined from HRTEM images are 2.7 nm, 3.2 nm, and 3.3 nm, respectively (**Table 2**), using the different Zn:S ratios (0.1/9, 0.6/2, 1.1/0.9). The corresponding ZnS monoshells (MLs) are found to be 0.3, 0.9, and 1.0, which are calculated from the core diameter of 2.5 nm (**Figure 13a**) and also obtained with the empirical equation of Peng et al.[55] (Equation 2), and with the literature value of one ZnS monoshell around CdSe core (0.70 nm).[56] As observed from the HRTEM histograms, there is an increment in size resulting from the growth of the shell (ZnS) over the core (CdSe).

The distribution size (histograms) obtained from HRTEM analysis shows the size in the CdSe core, and QD-1.0 ML is polydisperse, while QD-0.3 ML and QD-0.9 ML show a monodisperse distribution. These results correlate with the FWHM values calculated rom fluorescence spectra (**Tables 2** and **3**).

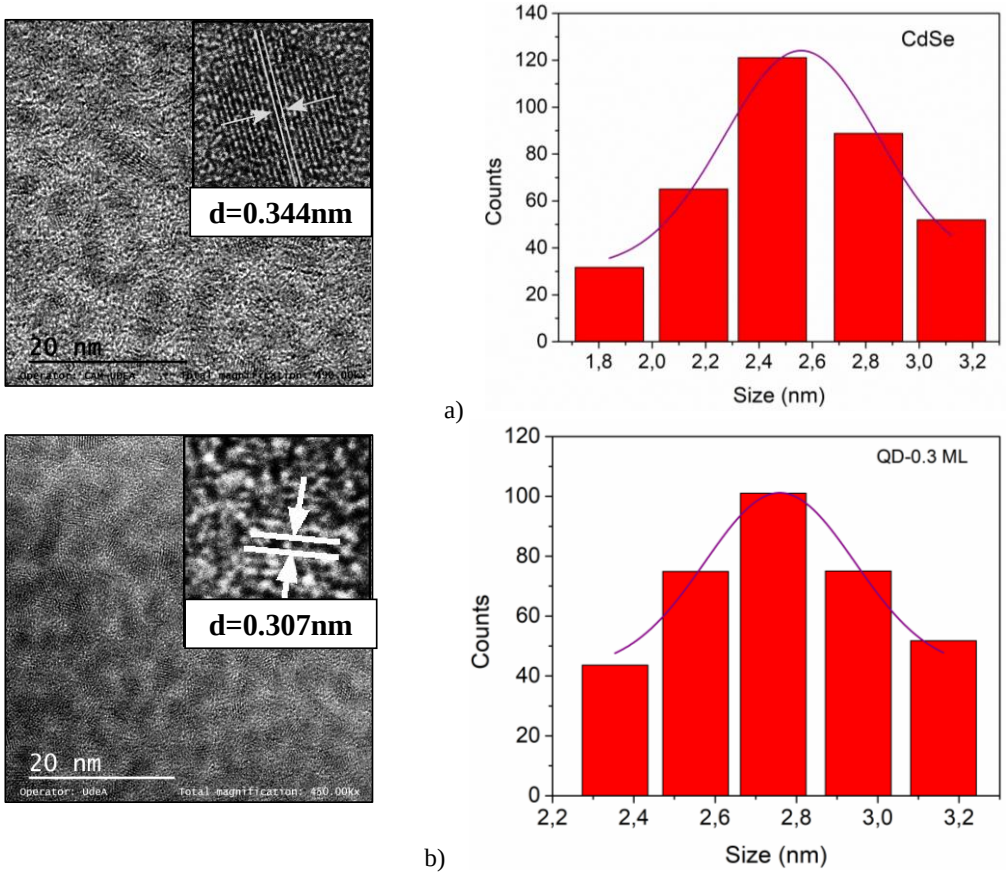

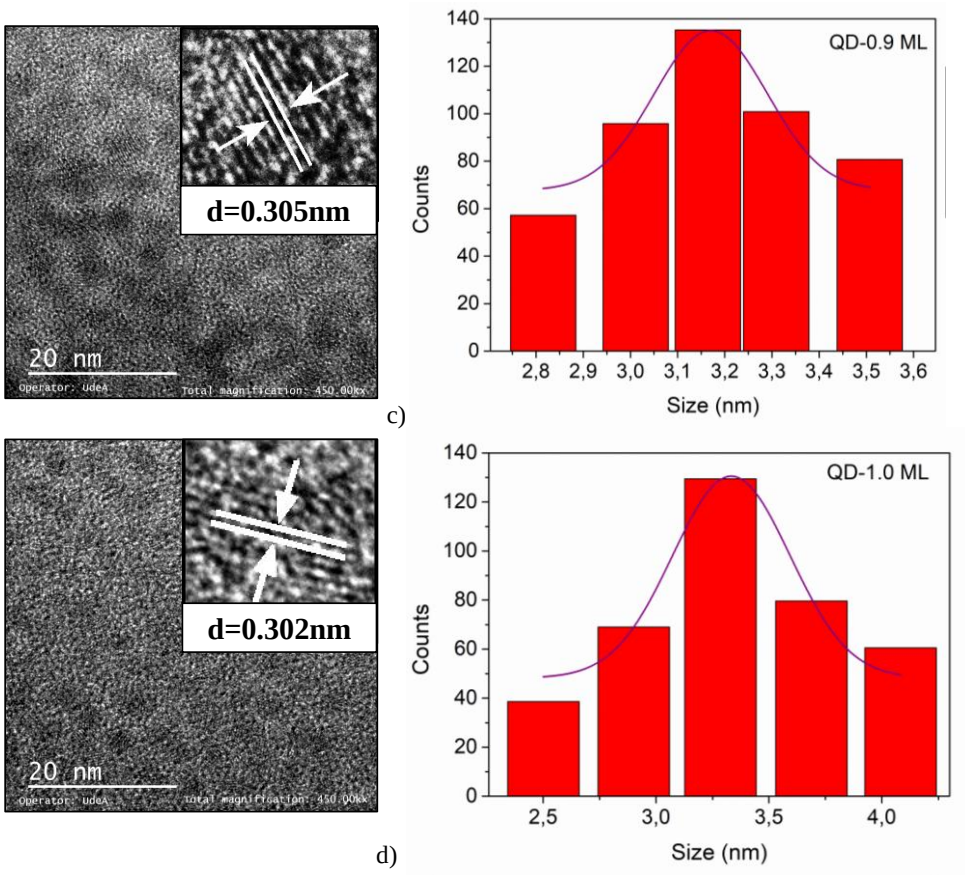

Figure 13. HR-TEM micrographs and distribution of size (histograms) of core-shell CdSe-ZnS QDs, a) CdSe; b) QD-0.30 ML; c) QD-0.90 ML; d) QD-1.00 ML.

Using ImageJ software, crystal phases of QDs are determined with the interplanar distance spacing from the Fast Fourier Transform (FFT) of selected areas in the HRTEM images (**Figure 13 (a-d)** and **Figure 65, Annexes**). The interplanar spacing (d-spacing) has been calculated as 0.307 nm for QD-0.30 ML, 0.305 nm for QD-0.9 ML, and 0.302 nm for QD-1.0 ML, which matches the lattice spacing of (111) plane of cubic ZnS (0.31 nm for Z.B. ZnS).[57] The measured d-spacing of CdSe core is 0.344 nm, indexed as CdSe [111] plane,[58] in concordance with the cubic zinc blende CdSe (JCPDS No. JCPDS-77-2100). For CdSe-ZnS core-shell QDs, 2.5 nm CdSe nanocrystals as the core was increased to 3.3 nm after overcoating 1.0 ML of ZnS shell. These results evidence the growth of the ZnS shell on the CdSe core.[56]

Table 2. The parameters of CdSe-ZnS QDs obtained with HR-TEM analysis

QDs	Zn:S Ratio	d-spacing (nm)	Size (nm)	Shell thickness (nm)	Monoshell Number
CdSe	0	0.344	2.55 ± 0.031	-	-
QD-0.30 ML	0.1/9	0.307	2.76 ± 0.022	0.21	0.30
QD-0.90 ML	0.6/2	0.305	3.17 ± 0.028	0.62	0.88
QD-1.00 ML	1.1/0.9	0.302	3.33 ± 0.069	0.78	1.11

2.3.3 FT-IR analysis

FT-IR analysis shows the effect of the Zn:S ratio on the QDs surface. **Figure 14** shows the FT-IR spectra of synthesized CdSe (core) and CdSe-ZnS (core-shell) nanoparticles. FTIR spectra in the region 2000-1000 cm^{-1} of oleic acid-capped CdSe core and CdSe-ZnS core-shell QDs compared with the oleic acid spectrum are shown in **Figure 14**. The bands for pure oleic acid are found at 1460, 1412 $cm^{-1,}$ and 1282 $cm^{-1,}$ which are associated respectively with CH_3, O-H, and C-O groups, and are observed in all QDs samples. The intense band at 1707 cm^{-1}, characteristic of the C=O bond of oleic acid, disappeared for the CdSe and CdSe/ZnS samples. It diminished and shifted to 1732 cm^{-1} for QDs with a high amount of Zn (QD-0.9 ML and QD-1.0 ML), indicating the coexistence of free oleic acid on the QDs surface. Two bands around 1534 and 1407 cm^{-1} for CdSe are attributed to carboxylate anion asymmetric and symmetric stretching (COO^-). The asymmetric band is shifted up to 1543 cm^{-1} as [Zn^{2+}] concentration increased from the synthesis process. The separation between carboxylate bands ($\Delta\nu = \nu_{asym}COO^- - \nu_{sym}COO^-$) is 127 cm^{-1} for core, which rises in the wavenumber range of 130-136 cm^{-1} as [Zn] precursor concentration increase for core/shell samples. These $\Delta\nu$ values indicate that the carboxylate ion coordinates to metal ions of QDs surface as bidentate.[12,13]

Furthermore, at 1100 and 1033 $cm^{-1,}$ two bands correspond to the $\upsilon C–P$[59,60] from TOP remaining on the QD surface. Finally, in CdSe (core) and CdSe-ZnS (core-shell), there is a band at 721 cm^{-1} for -(CH_2)n- vibration from oleic acid.[60,61] The FT-IR analysis shows the oleic acid (OA) and TOP capped on the surface of QDs.

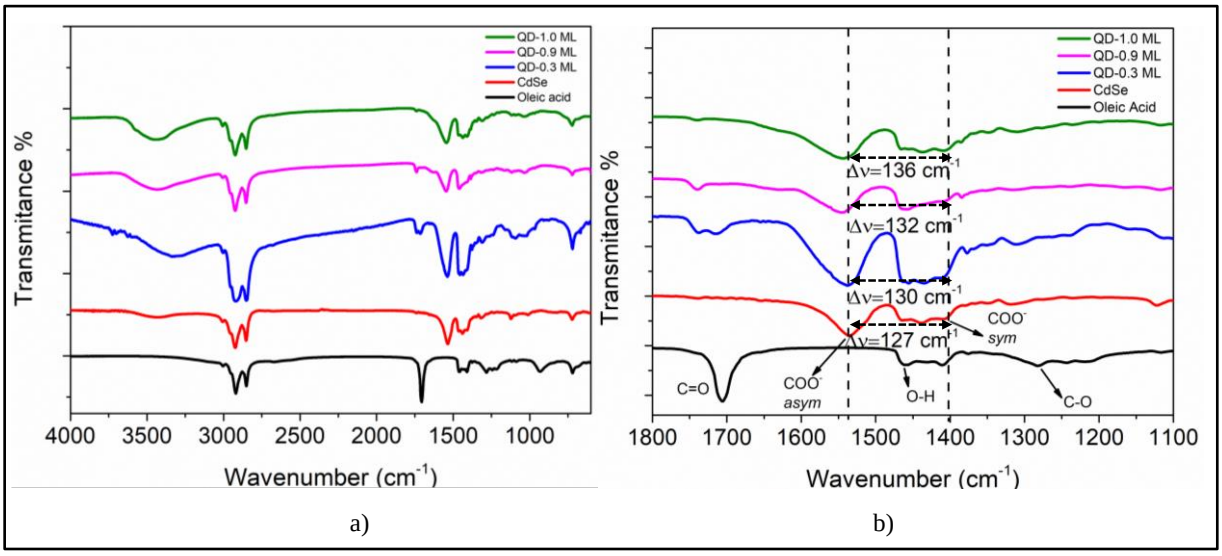

Figure 14. FT-IR spectra of synthesized CdSe core and CdSe-ZnS core-shell QDs with different shell thicknesses.

2.3.4 XPS Analysis

Figure 15 shows the high-resolution XPS spectrum of QDs samples to characterize the composition and chemical speciation of QDs surface. We compare the Cd3d and Se3d spectra from the core, Zn2p and S2p spectra of core-shell, and C1s and O1s spectra from the ligand of core and core-shell samples.

The C1s region is shown in **Figure 15A.** The C1s peak of CdSe was deconvoluted onto two components associated with 283.04 eV for C-C and C=C bonds and the peak at 288.7 eV for the COO^- of oleic acid (OA).[62,63] The C1s peak corresponded to carboxylic carbon (-COOH), found at 290 eV,[62] did not appear in the spectra, indicating the absence of free acid on the surface CdSe core QDs. For core-shell samples, 287 eV correspond with the signal of the carboxylate, and two components could be deconvoluted: at 285 eV associated with C-C (or C-H),[64] and at 284.5 eV attributed to C=C of oleic acid (OA). [65]

The O1s peak was deconvoluted onto two components attributed to C-O and C=O of the carboxylate group from oleic acid.[65] The O1s region (**Figure 15B**) of the CdSe core shows a peak at 530 eV, while the CdSe-ZnS samples show a single peak at 532.0 eV due to the different chemical environment produced by the ZnS shell; no noticeable changes between core/shell QDs samples are observed.

The Zn2p spin–orbit splitting of core/shell samples is shown in **Figure 15C**. The Zn2p peak is resolved into two splitting peaks at 1045.7 eV and 1022.6 eV, corresponding to $Zn2p_{1/2}$ and $Zn2p_{3/2}$, respectively.[66] The difference in the two peaks was $\Delta Zn2p = Zn\ 2p_{1/2} - Zn\ 2p_{3/2} = 23.02$ eV corresponding to the oxidation state 2+,[67] confirming the Zn-S bond from the shell in QD. The Zn2p spectra of the QD-0.9 ML sample is shifted to higher binding energies, and non-symmetry peaks are observed attributed to different environments of Zn^{2+} species. [68,69] These changes could occur due to the growth of a thicker ZnS shell, where Zn^{2+} is binding to S^{2-}, and the under-passivated Zn^{2+} due to the increase in Zn amount, which could be related to the amount of Zn^{2+} that affects the PLQY of QD-1.0 ML sample.

The S2p region is shown in **Figure 15D**. Two signals are shown in CdSe-ZnS QDs at 160.11 eV and 161.93 eV associated with $S2p_{3/2}$ and $S2p_{1/2,}$ respectively. These signals correspond to the S^{2-} of Zn-S bonds from the shell in QD,[70] confirming ZnS formation (shell) around the CdSe core. The S2p peak is shifted to higher binding energies for QDs with thicker ZnS shells.

The Se3d region is shown in **Figure 15E**. The peak in the CdSe core is observed at 54.1 eV, characteristic of metal selenides. [71] In CdSe-ZnS samples, the signal was deconvoluted onto a doublet. The peak at 53.1 eV is assigned to $Se3d_{5/2}$, and the peak at 54.1 eV is attributed to $Se3d_{3/2}$.[72] The Se3d peak for core/shell samples has a similar profile; no shifts are observed. In addition, the Se3d peak of SeO_2 at 58-60 eV was not observed,[71] the absence of any SeO_x as we have observed indicates that the CdSe core is partially protected by ZnS shell.[73]

Figure 15F shows the Cd3d peaks. A characteristic doublet is shown at 405.1 eV and 411.9 eV for $Cd3d_{5/2}$ and $Cd3d_{3/2,}$ respectively, confirming the oxidation state 2+ of cadmium ions. [71] The binding

energy of $Cd3d_{5/2}$ is in accord with the reported value: 405.6 eV for CdSe bulk,[71] and 405 eV for CdSe/ZnS QD.[74] Cd3d spectrum for QD-0.3 ML sample remained unchanged (compared with core), but is slightly moved to higher binding energies for QD-0.9 ML. For this sample, the doublet is deconvoluted in several components, indicating different environments of Cd^{2+} on the surface, e.g., Cd^{2+} binding to Se^{2-} and under-passivated Cd^{2+}.[75]

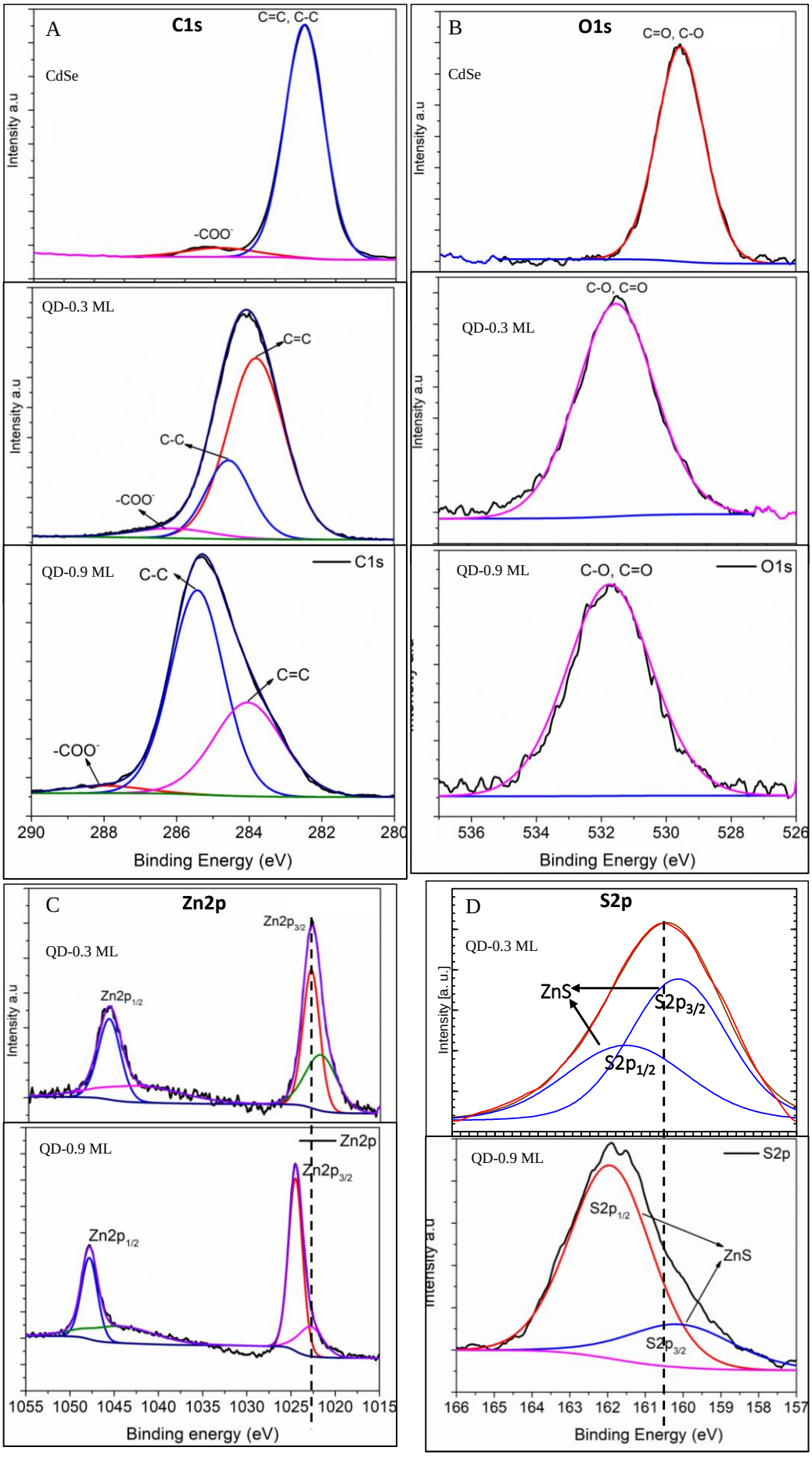
A
C1s
CdSe
C=C, C-C
-COO-
Intensity a.u
QD-0.3 ML
C=C
C-C
-COO-
QD-0.9 ML
C1s
C-C
C=C
-COO-
290 288 286 284 282 280
Binding Energy (eV)
B
O1s
CdSe
C=O, C-O
C-O, C=O
QD-0.3 ML
QD-0.9 ML
C-O, C=O
O1s
536 534 532 530 528 526
Binding Energy (eV)
C
Zn2p
QD-0.3 ML
Zn2p3/2
Zn2p1/2
QD-0.9 ML
Zn2p
1055 1050 1045 1040 1035 1030 1025 1020 1015
Binding energy (eV)
D
S2p
QD-0.3 ML
ZnS
S2p3/2
S2p1/2
Intensity [a. u.]
QD-0.9 ML
S2p
ZnS
166 165 164 163 162 161 160 159 158 157
Binding Energy (eV)

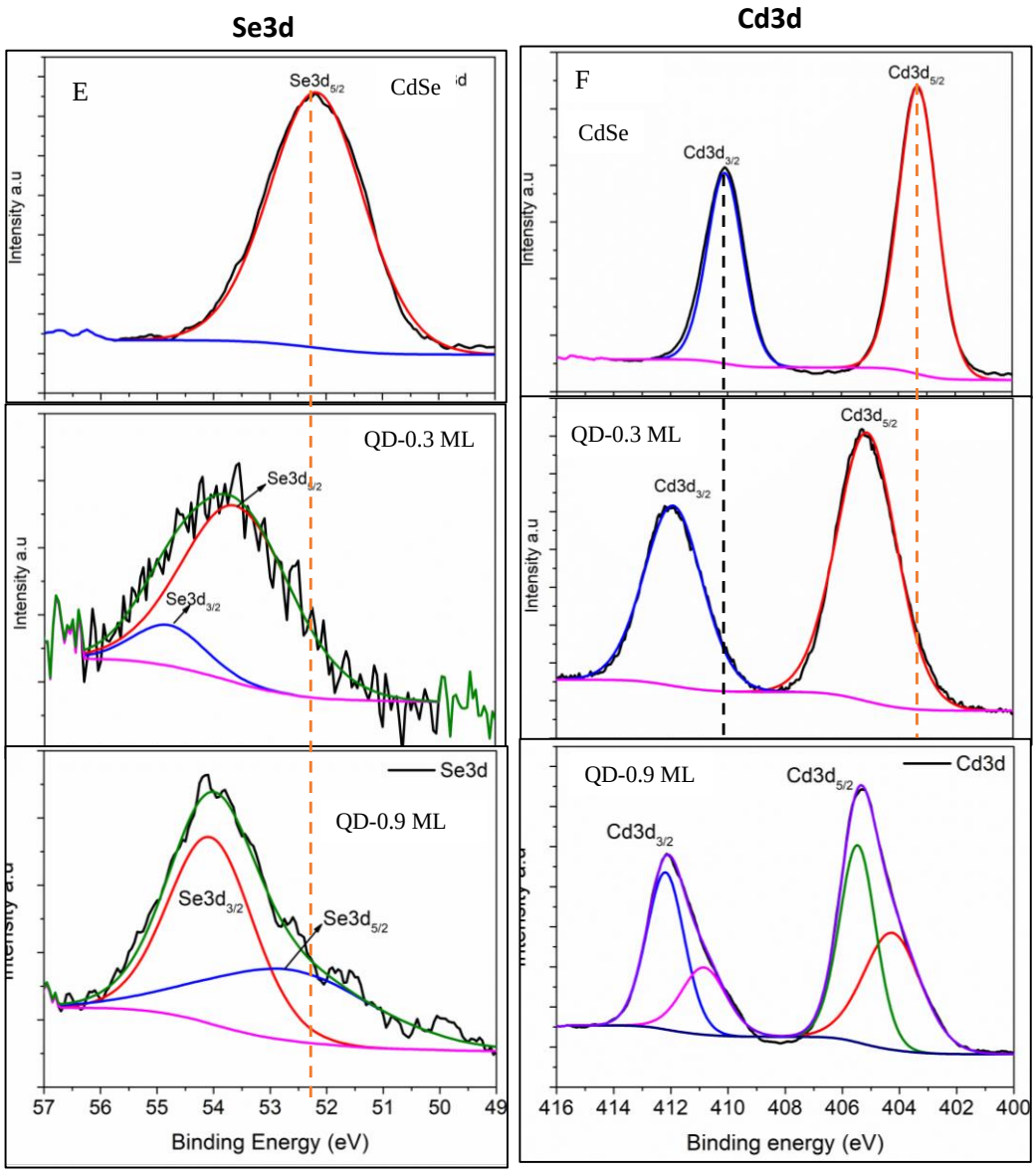

Figure 18. XPS spectra of CdSe and CdSe-ZnS-OA (QD-0.3 ML and QD-0.9 ML) core-shell QDs: A) C1s ; B) O1s ; C) Zn2p ; D) S2p ; E) Se3d and F) Cd3d.

2.4 *Optical properties*

2.4.1 Absorption and Fluorescence

Electronic absorption and emission spectra of the CdSe core and CdSe-ZnS core-shell QDs with different ZnS shell thicknesses are shown in **Figure 16** and **Table 3**. Compared with the core, CdSe-ZnS samples show the characteristic red-shift of the first exciton absorption peak and the emission maximum and enhanced PL quantum yield, confirming the growth of the ZnS shell on the core.[76,77] QD-0.9 ML has the higher PL QY (0.54), which decreased to 0.47 when one ZnS ML was formed (QD-1.0 ML).

The photoluminescence quantum yield PLQY was determined using fluorescence emission and rhodamine 6G as standard. The shell growth around the core (CdSe) improves the QY (**Table 3**). However, the lowest PL QY observed in QD-0.3 ML (0.45) is due to the surface traps produced by the excess S-precursor used in synthesis. It has been shown that treatment of core-shell QDs with S_2^-, SH^-, or H_2S produces a photoluminescence quenching [78] due to sulfide ions acting as a hole trap that delocalizes the exciton and the non-radiative recombination increase and the photoluminescence decrease.

The highest QY observed in the sample with a Zn:S ratio (0.6/2) is enough to passivate the defect states, surface traps, and non-radiative recombination sites after coating with the ZnS shell.[1,37,79] Thus, the free exciton is effectively confined, and non-radiative recombination decrease.[37] However, PL QY decreases when many monoshells of ZnS grow on the core.[80] This work shows a slight growth of ZnS (1 ML) reduced PLQY. This decrease in QY is associated with presumably excess or unpassivated Zn surface sites.[78]

In both cases, the absorption and emission spectra broaden with increasing ZnS shell (**Table 3** FWHM). The FWHM can be considered as dispersion criteria related to the nanoparticle size.[81] This value in QD-0.3 ML and QD-0.9 ML is lower than the CdSe core, confirming the monodispersed size. In contrast, in QD-1.0 ML, this value is higher than other nanoparticles, confirming a polydispersity in size, which is congruent with the distribution of size observed in the HRTEM analysis.

In addition, with the absorption wavelength of the CdSe core (518 nm), the size of the core was calculated using the Peng equation:[55]

$$D = (1.6122x10^{-9})\lambda^4 - (2.6575x10^{-6})\lambda^3 + (1.6242x10^{-3})\lambda^2 - (0.4277)\lambda + (41.57) \quad \text{Eq. 2}$$
$$= 2.53\ nm$$

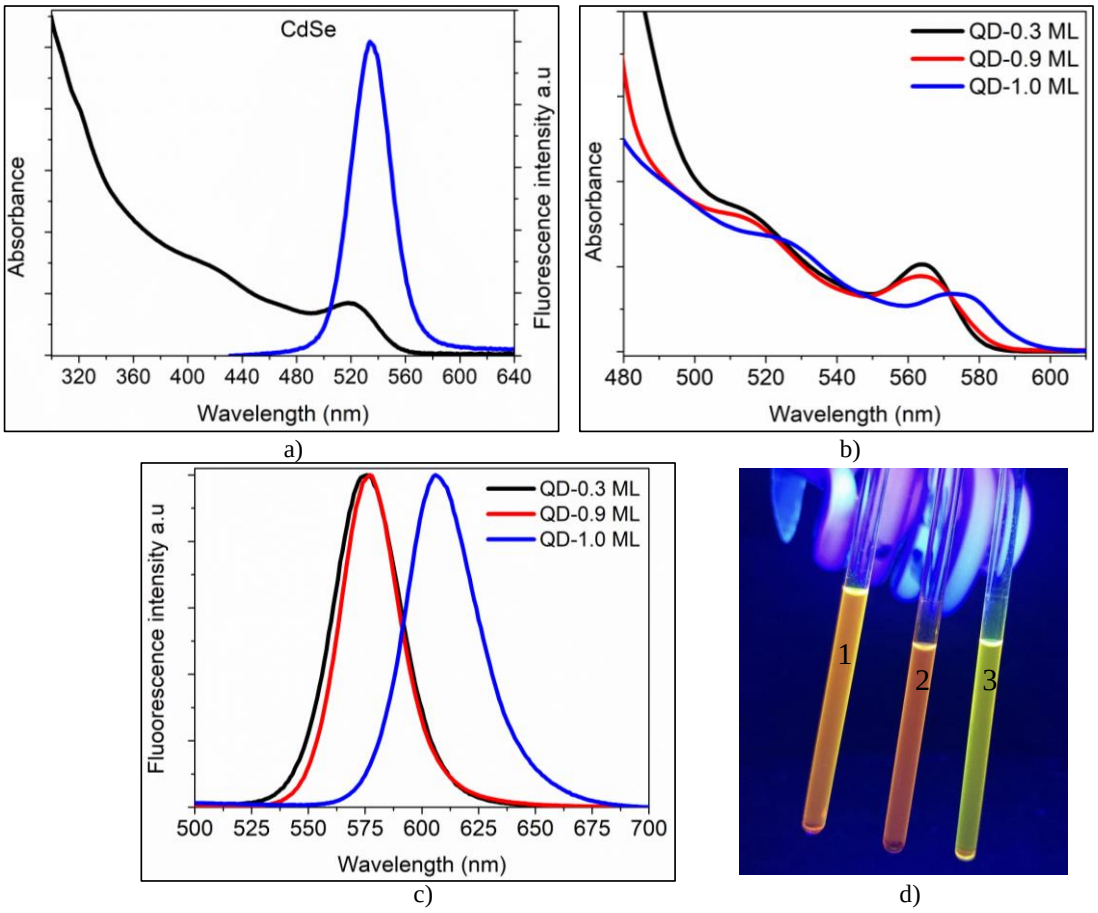

Figure 16. Absorption-emission spectra of a) CdSe core, b) absorption spectra of CdSe-ZnS QDs, c) fluorescence spectra of CdSe-ZnS QDs with a different shell thickness, d) CdSe-ZnS QDs with different shell thickness (1. QD-0.3 ML, 2. QD-0.9 ML y 3. QD-1.0 ML). λ_{exc}: 380 nm. Solvent: chloroform ($CHCl_3$).

2.4.2 Optical band-gap analysis

The optical band gap of the quantum dots was determined using Tauc's equation:

$$(\alpha hv) = B(hv - Eg)^n \qquad \text{Eq. 3}$$

Where α is the absorption coefficient, hv is the photon energy, and Eg is the optical band gap of the QD. From the above equation, an intercept was drawn to determine the band gap Eg of QDs (**Figure 17**).

The band gap obtained for the CdSe core was 2.19 eV (**Table 3**). Comparing this value with the Eg of the CdSe in bulk phase (1.74 eV), [82] shows an increase of around 0.45 eV. This result indicates the nanophase and quantized nature of the prepared CdSe core due to the quantum confinement effect.[1]

The optical band-gap of QDs (**Table 3**) is decreased with the increase of the Zn^{2+} ratio due to the ZnS shell growth of QDs.[1] The difference in size is due to the increase in shell thickness of QDs by the

increase in the amount of Zn^{2+}.[83] These results are associated with the size determined from HRTEM analysis, a decrease in band-gap is observed with increasing QD size.

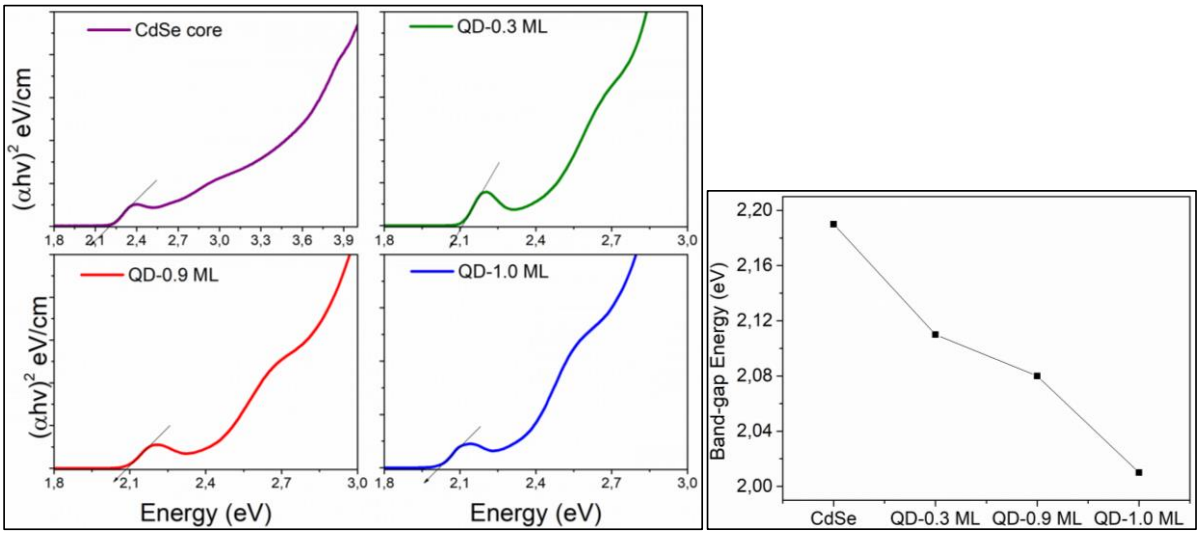

a) b)

Figure 17. a) Plot of $(\alpha hv)^2$ versus hv (eV) for CdSe-ZnS core-shell QDs with different shell thickness, b) band-gap energy (eV) as a function of the ZnS shell thickness.

The Stokes shift of CdSe-ZnS was 0.040 eV, 0.047 eV, and 0.070 eV for QD-0.30 ML, QD-0.90 ML, and QD-1.00 ML, respectively (**Table 3**). These results correlate to the Stokes shifts of the colloidal QDs type I (core semiconductors like CdSe and CdS with wide band-gap shells, such as ZnS and CdS).[84,85] The reduced Stokes shift and the increase of quantum yield in QD-0.9 ML used in synthesis could be associated with a minor formation of defects and density of surface states.[86] For the sample prepared with a high amount of Zn (QD-1.0 ML), the stokes shift value is increasing due to the formation of defect/traps states on the surface producing new non-radiative centers, decreasing the QY.[87]

Table 3. Optical properties of QDs synthesized.

QD	Zn:S ratio	ML number	Maximum wavelength absorption (nm)	Maximum wavelength emission (nm)	FWHM (nm)	Stokes shift (eV)	Quantum Yield PL-QY	Band-gap Energy (eV)
CdSe core	0	0	518	533	35	0.050	0.17	2.19
QD-0.30 ML	0.1/9	0.3	563	576	31	0.040	0.45	2.11
QD-0.90 ML	0.6/2	0.9	564	578	34	0.047	0.53	2.08
QD-1.00 ML	1.1/0.9	1.0	581	606	37	0.070	0.47	2.01

2.4.3 Photoluminescence decay analysis

Fluorescence lifetime measurements were performed to investigate the exciton recombination dynamics and the role of the Zn:S ratio. The fluorescence decay of CdSe-ZnS QDs with different shell thicknesses showed non-exponential kinetics but could be mathematically fit by multiple exponentials (Equation 4), which was subsequently used to approximate an average lifetime. This indicating multiple emitting states typically associated with quantum dots,

$$I(t) = I_0 + A_1 e^{\left(-\frac{t}{\tau_1}\right)} + A_2 e^{\left(-\frac{t}{\tau_2}\right)} A_3 e^{\left(-\frac{t}{\tau_3}\right)} + A_4 e^{\left(-\frac{t}{\tau_4}\right)} \qquad Eq.4$$

The A is amplitude associated with decays, and τ is the decay constants.[88,89] While it is not feasible attribute each of these apparent components, they will receive contributions from the characteristic lifetime of exciton relaxation and longer-lived defect luminescence.[90] Average lifetime $\langle \tau_{FL} \rangle$ is determined from the A_i and τ_i values as,[88,89] the time-resolved average of fluorescence (τ_{FL}) was calculated with this equation:

$$\langle \tau_{FL} \rangle = \sum_{i=4}^{4} A_i \, \tau_i / \sum_{i=4}^{4} A_i \qquad Eq.5$$

Figure 18 shows the luminescence measurements of CdSe-ZnS samples with different ZnS shell thicknesses. The QDs core-shell shows a longer fluorescent decay due to the influence of the shell. The

ZnS shell passivates the non-radiative trap states on the CdSe core, making the core more photostable and less affected by non-radiative recombination pathways.[39,79,91] The photoluminescence lifetime measurements are summarized in **Table 4.**

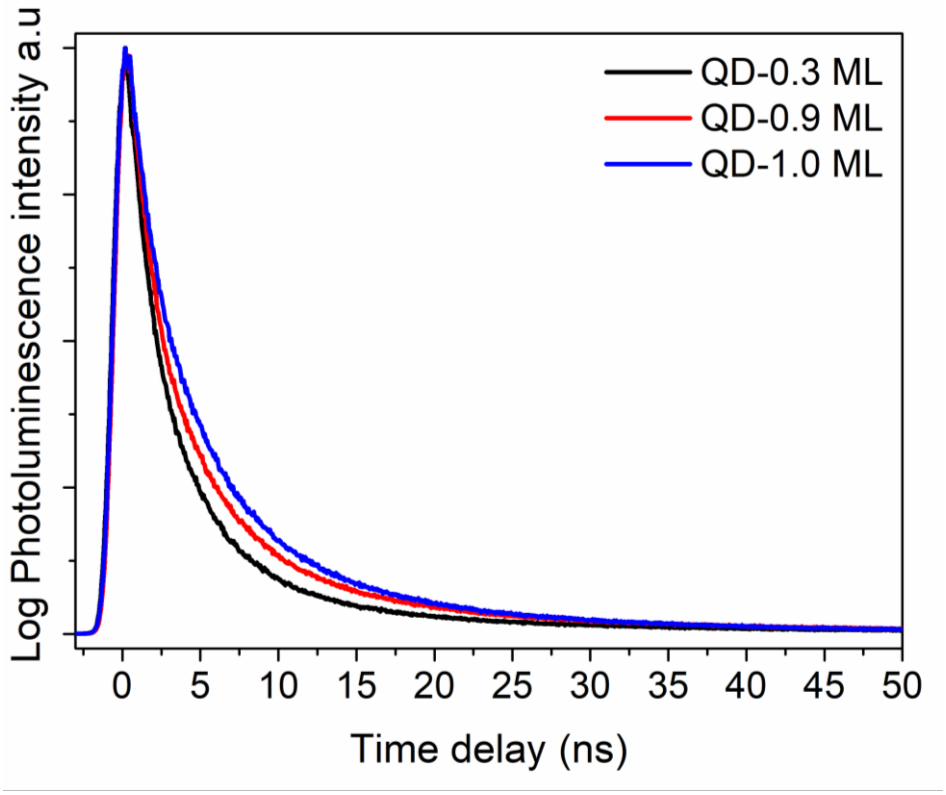

Figure 18. Photoluminescence decay curves of CdSe-ZnS core-shell QDs with different shell thickness. λ_{exc}: 540 nm. Solvent: chloroform.

Table 4. Lifetime average of CdSe-ZnS core-shell QDs

QDs	τ_{FL} *(ns)*	χ^2
QD-1.00 ML	3.29	1.49
QD-0.90 ML	4.34	1.14
QD-0.30 ML	4.82	1.05

Core-shell systems with up to two shell monoshells have shown decay lifetimes shorter[92] due to the diminution of non-radiative recombination sites obtained with shell growth.[93,94] The present results show longer lifetimes, indicating the formation of non-radiative recombination sites associated possibly with the amount of Zn precursor. The τ_{FL} in the sample with S-excess (QD-0.3 ML) is lower than other QDs samples due to the sulfide being a hole trap and quenched the photoluminescence,[78,95,96] thus producing a delocalization of exciton. The amount of Zn^{2+} used in QD-0.3 ML (Zn:S ratio, 0.1/9) would not be possible to passivate all the S-excess on the surface of the nanocrystals, resulting in relatively poor

emission. This result indicates that the S-excess used in QD-0.3 acts as a hole-trap producing an excitonic delocalization and the photoluminescence decrease.

Thus, the Zn:S ratio (0.6/2) of QD-0.9 ML produced a thicker shell that passivates the core surface defects, enhancing PLQY[94] The Zn-treatment used is enough to passivate the hole traps produced by S_2^- ion from $(TMS)_2S$ during synthesis. This thicker shell confines the exciton to improve the photoluminescence, thus increasing the QY. However, the highest Zn:S ratio (1.1/0.9) decreases PLQY by traps, presumably excess or unpassivated Zn surface sites due to non-radiative trap formation, as observed in QD-1.0 ML. These trap states could be near the conduction band (CB) acting as electron traps or near the valence band acting as hole traps (h^+).[97]

Table 4 and **Figure 19** show the τ_{FL} was increased significantly from 3.29 ns in QD-0.30 ML to $2.17x10^2$ ns in QD-1.0 ML, and τ_{FL} increased with the amount of Zn^{2+} in the shell; similarly, Li et al.[98] showed the τ_{FL} was enormously increased from 243.6 ns to 1111.7 ns in Cu_2S QDs with Zn-treatment. These results show that the amount of Zn^{2+} and S^{2-} increases the fluorescence intensity and changes the proportion of short and long lifetimes.[98] The effect of the highest amount of Zn^{2+} used (Zn:S, 1.1/0.9) can be associated with greater exciton confinement from the surrounding environment due to increased ZnS shell thickness.[99] These results suggested that excess Zn^{2+} ions on the surface of CdSe-ZnS core-shell QDs create surface traps with relatively long lifetimes.

The behavior in QD-0.3 ML is congruent with other reports. For example, Gao et al. showed that the treatment with Se-excess in CdSe QDs produces poor photoluminescence due to the appearance of trapping the holes and quenching the PL by Se^{2-} ions.[100] Morgan et al.[6] showed treatment with tributyl phosphine (TBP) in CdSe QDs produced a decrease in photoluminescence due to the TBP being a hole trap and quenched the PL, however, treatment with alkylamines passivate these hole traps and photoluminescence is regenerated.

While in QDs with greater amounts of Zn^{2+} (QD-0.9 ML and QD-1.0 ML) show an opposite behavior, in both CdSe-ZnS QDs, the lifetime increases, the Zn^{2+} acts as an electron trap and the photoluminescence increases. This situation is congruent with other reports on QDs; these reports show that impurities are associated with metals. For example, Shi et al.[90] showed that the τ_1 of Zn-treatment in PbS QDs (2.4 μs) significantly increased with free PbS (1.8 μs), indicating that the Zn-treatment improved the photoluminescence lifetime of QDs, and thus the PLQY was enhanced. Another study developed by Amar et al.[101] demonstrated the same effect in CdS QDs with a treatment of Cu, the τ_1 of Cu:CdS QDs (292.9 ns) strongly increased with CdS (8.03 ns), indicating that the Cu treatment improved the PL lifetime of QDs. Similarly, Li et al.[98] proved that the addition of Zn treatment in Cu_2S QDs increased the PL lifetimes, the τ_1 was significantly extended from 45.9 ns in Cu_2S to 215.3 ns in Zn:Cu_2S QDs and τ_2 from 361.8 ns in Cu_2S to 1274.8 ns in Zn:Cu_2S QDs.

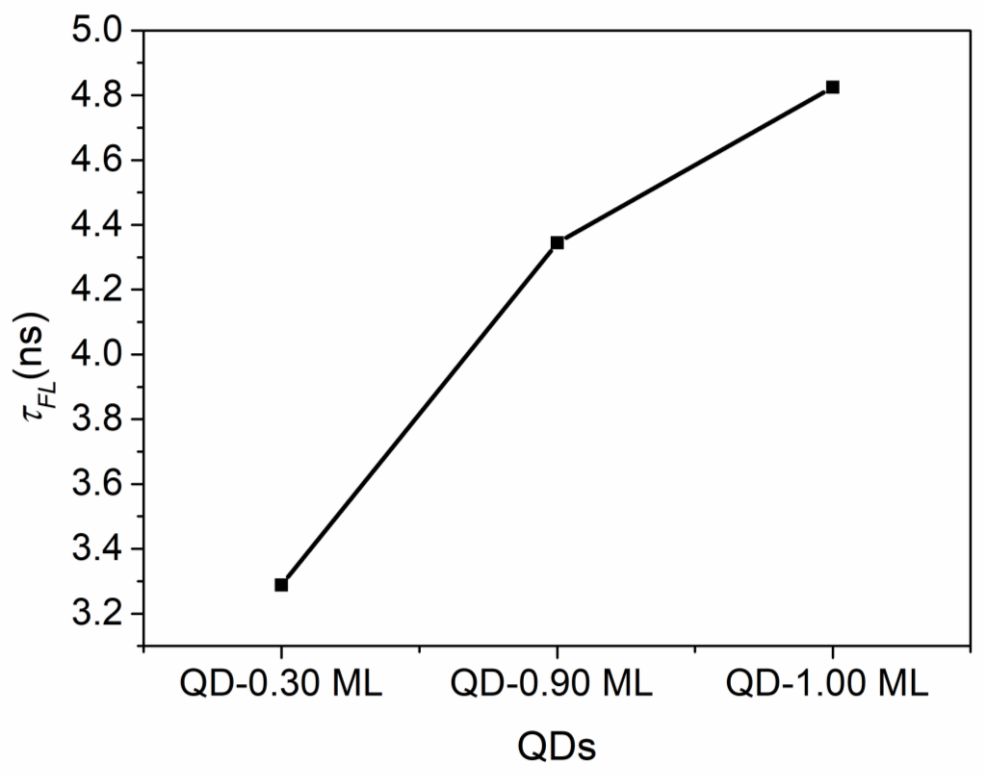

Figure 19. Correlation of shell thickness and τ_{FL} in CdSe core and CdSe-ZnS core-shell QDs.

The mechanism of the Zn^{2+} effect to increase the photoluminescence intensity of CdSe-ZnS QDs can be explained: when the valence band is excited by UV-light, the electrons of QDs are promoted from the valence band (ground state) to the conduction band (excited state). After a short stay in the excited state, the excited electrons return to the ground state to radiatively combine with the holes yielding fluorescence. In this process, there are two ways: direct transition (from the bottom of the conduction band to the top of the valence band) and indirect transition (from the surface defect state back to the ground state). These transition processes correspond to τ_1 and τ_2 lifetimes, respectively.[102]

Figure 20 shows the schematic passivation effect with the ZnS shell (*Eg*: 3.5 eV)[103,104,105,105] around CdSe (*Eg*: 2.1 eV), which leads to type-I core-shell structure, with the confinement of excitons in CdSe QDs.[106] Zn-related sites act as non-radiative recombination traps decreasing PL However, when the Zn/S ratio is the highest (1.1/0.9), new non-radiative centers are formed due to surface defects, and the QY decreases. This behavior is associated with the excess or unpassivated Zn surface sites.[78] [107,108]

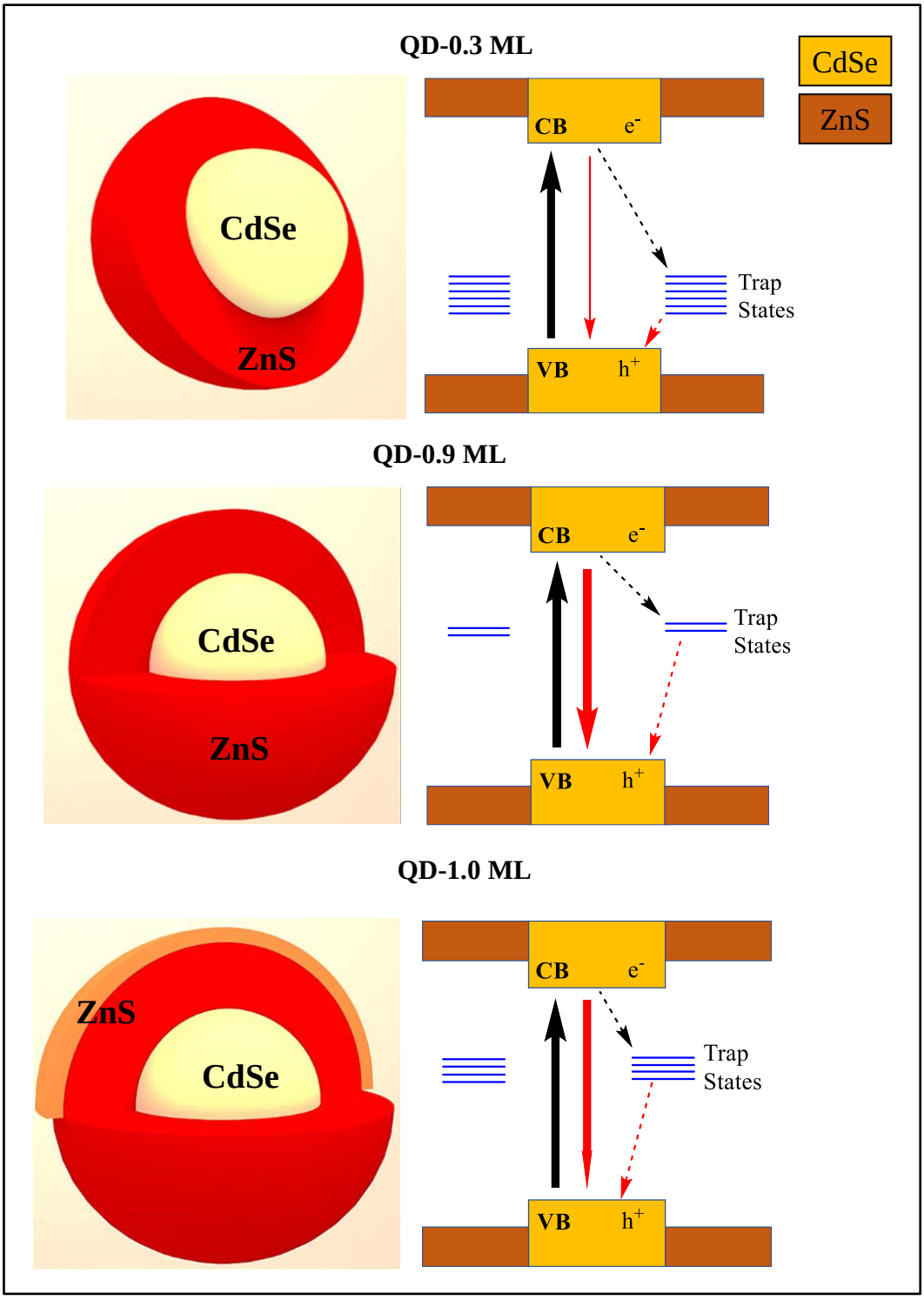

Figure 20. Photoluminescence effect produced by Zn^{2+} ratio on the shell surface in CdSe-ZnS core-shell QDs with different shell thicknesses.

2.4.4 Effect of Hg^{2+} ions on the absorption and fluorescence of CdSe-ZnS QDs with different shell thickness

2.3.4.1 Absorption and fluorescence analysis

The effect of Hg^{2+} ions on the fluorescence of CdSe-ZnS QD is shown in **Figure 21**. In the absorption spectra of CdSe-ZnS QDs with different shell thicknesses, there is an increase in the first excitonic peak, increasing the molar extinction coefficient as the Hg^{2+} concentration increases (**Figure 44 Annexes**).[55]

Adding Hg^{2+} ions produces a quantitative decrease in the fluorescence of QD-0.30 ML (quenching), and a slight red shift of the emission band is shown in QD-0.30 ML (**Figure 21**). This effect is attributed to the high affinity between Hg^{2+} and Se^{2-} from the core and S^{2-} from S-excess used during the synthesis of QD, a process that can be explained due to a Se^{2-} to Hg^{2+} cation exchange reaction (**Figure 22**), this process can be explained by the solubility constant *Ksp* HgSe (4.0×10^{-59}) is much lower than *Ksp* ZnS (2.0×10^{-22}),[14] favoring the formation of HgSe onto the QD core and HgS due the sulfide free due to the S-excess used in synthesis (Zn/S, 0.11/9), which generates new centers of non-radiative recombination, decreasing the photoluminescence of QDs.[109–113]

On the other hand, the samples with more Zn^{2+} show an increase in photoluminescence and a slight red-shift in the maximum emission wavelength with increasing Hg^{2+} concentration (QD-0.9 ML and QD-1.0 ML). In these two cases, the amount of ZnS shell is enough to remove the defect states on the surface and effectively confine the exciton (e^-/h^+ pair) to protect the CdSe core. The increase in photoluminescence is due to the formation of small HgS particles on the surface of the ZnS shell, which according to some reports in the literature, have shown an increase in photoluminescence. [114,115] This can be explained due to the Zn^{2+}-to-Hg^{2+} cation exchange to form HgS on the surface of QDs (**Figure 23**), forming a pseudo-shell around the core to confine the exciton; this cation exchange reaction is favored due to the solubility constant *Ksp* of HgS (4.0×10^{-53}) is much lower than *Ksp* of ZnS (2.0×10^{-22}).[14] This process passivates the surface defects/traps,[115] decreasing the non-radiative recombination and producing an enhancement in the emission of QDs.[1,39,79,116,117]

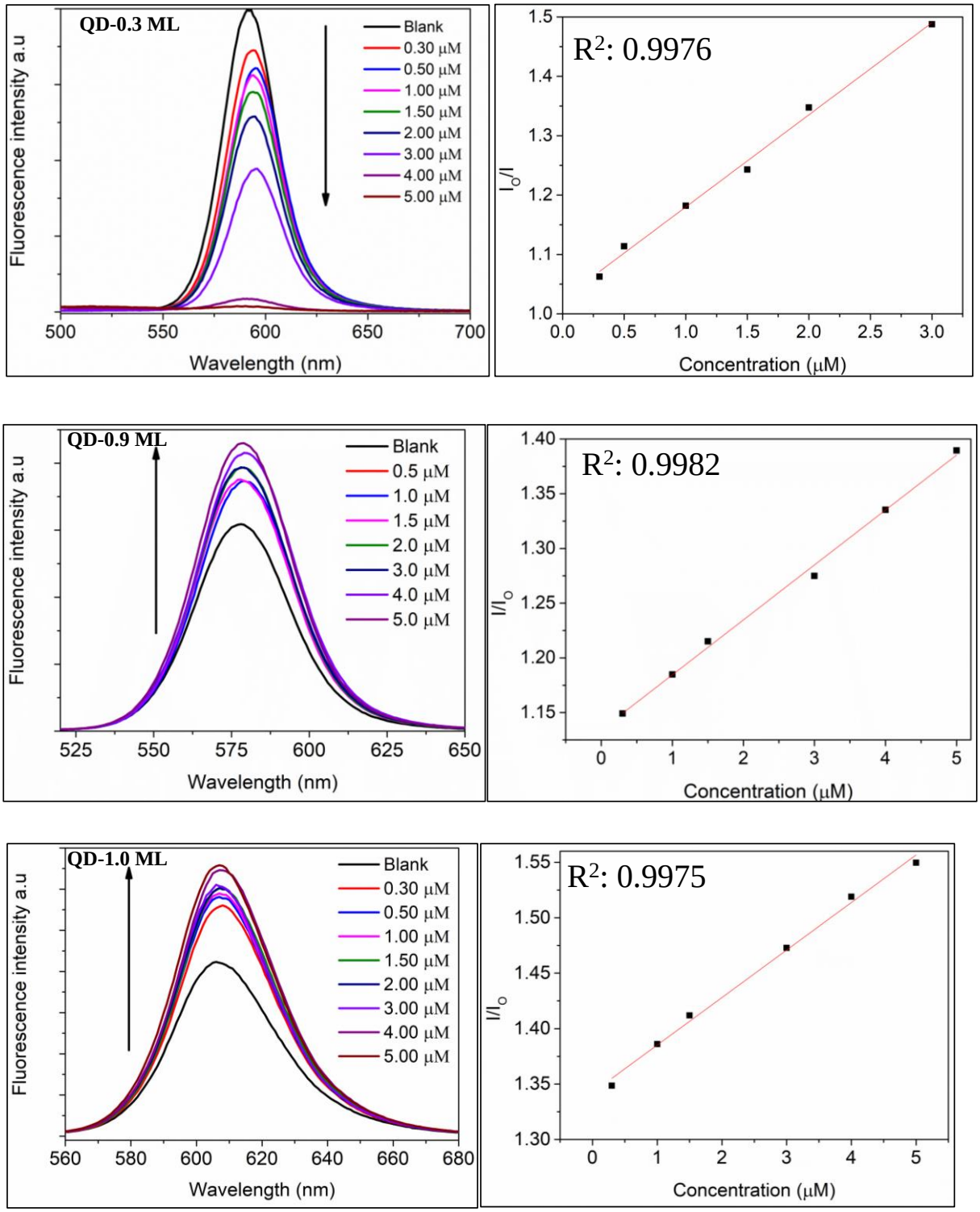

Figure 21. Emission spectra and linear plots of photoluminescence response of QD-0.3ML to QD-1.0ML as a function of Hg^{2+} concentration (0.30-3.0 μM for QD-0.3 ML respectively; 0.30-5.0 μM for QD-0.9 ML and QD-1.0 ML respectively) λ_{exc}: 380 nm. Solvent: chloroform/ethanol (1:1, v/v).

On the other hand, the fluorescence of QD-0.30 ML decreases progressively upon the addition of Hg^{2+} concentration (quenching). This behavior can be described by the Stern-Volmer equation:

$$\frac{I_O}{I} = 1 + K_{SV}[Q] \qquad Eq.6$$

Figure 21 shows a Stern-Volmer quenching curve describing I_o/I as a function of Hg^{2+} ion concentration. The linear range of the calibration curve was 0.3-3.0 × 10^{-4} M (0.3-3.0 μM Hg^{2+}) with the correlation coefficient R^2: 0.9976. The limit of detection (LOD) is calculated by the equation LOD = 3σ/*k*, where σ is the residual deviation of the regression line, and *k* is the slope of the calibration graph.[118] The LOD was found as 0.011 μM ~ 11.2 nM. For semiconductor QDs, the quenching of fluorescence is attributed to the increase of non-radiative recombination,[52] due to the action of hole trap by the S-excess precursor used in the synthesis of QD.

Figure 21 shows the fluorescence titration experiments with different concentrations of Hg^{2+} ions in QD-0.9 ML y QD-1.0 ML samples. With increasing Hg^{2+} ions concentration, the PL of QDs gradually increased, and a slight red-shift is observed (1 nm). The plots show good linearity between PL and [Hg^{2+}] ions (from 0.30 to 5.0 μM) with the correlation coefficient R^2: 0.9982 and R^2: 0.9982 for QD-0.9 ML and QD-1.0 ML respectively; the limit of detection (LOD) were calculated as 0.00898 μM~8.98 nM and 0.0107 μM~10.7 nM for QD-0.90 ML and QD-1.00 ML respectively. The detection limit calculated for Hg^{2+} with these CdSe-ZnS core-shell QDs is much lower in the three samples synthesized than other fluorescence probes (**Table 5**). Furthermore, the LOD calculated for these CdSe-ZnS QDs is lower than the acceptable LOD of inorganic Hg^{2+} in drinking water established by the World Health Organization (WHO) and the USA Environmental Protection Agency (EPA) as 30.0 nM,[119] and 10.0 nM,[120] respectively.

The fluorescence enhancement may be attributed to the previously discussed cation exchange (Zn^{2+}-to-Hg^{2+}) passivating the surface and producing new radiative recombination centers.[14] A study by Zhu et al.[114] showed that the Hg^{2+} ions on the surface of InP-MAA (mercapto acetic acid ligand) QDs produce ultrasmall particles of HgS. This situation is the same in this work; these HgS particles could passivate the defect states due to the formation of the HgS pseudo-shell, blocking/decreasing the non-radiative recombination and increasing the photoluminescence (**Figure 22**).

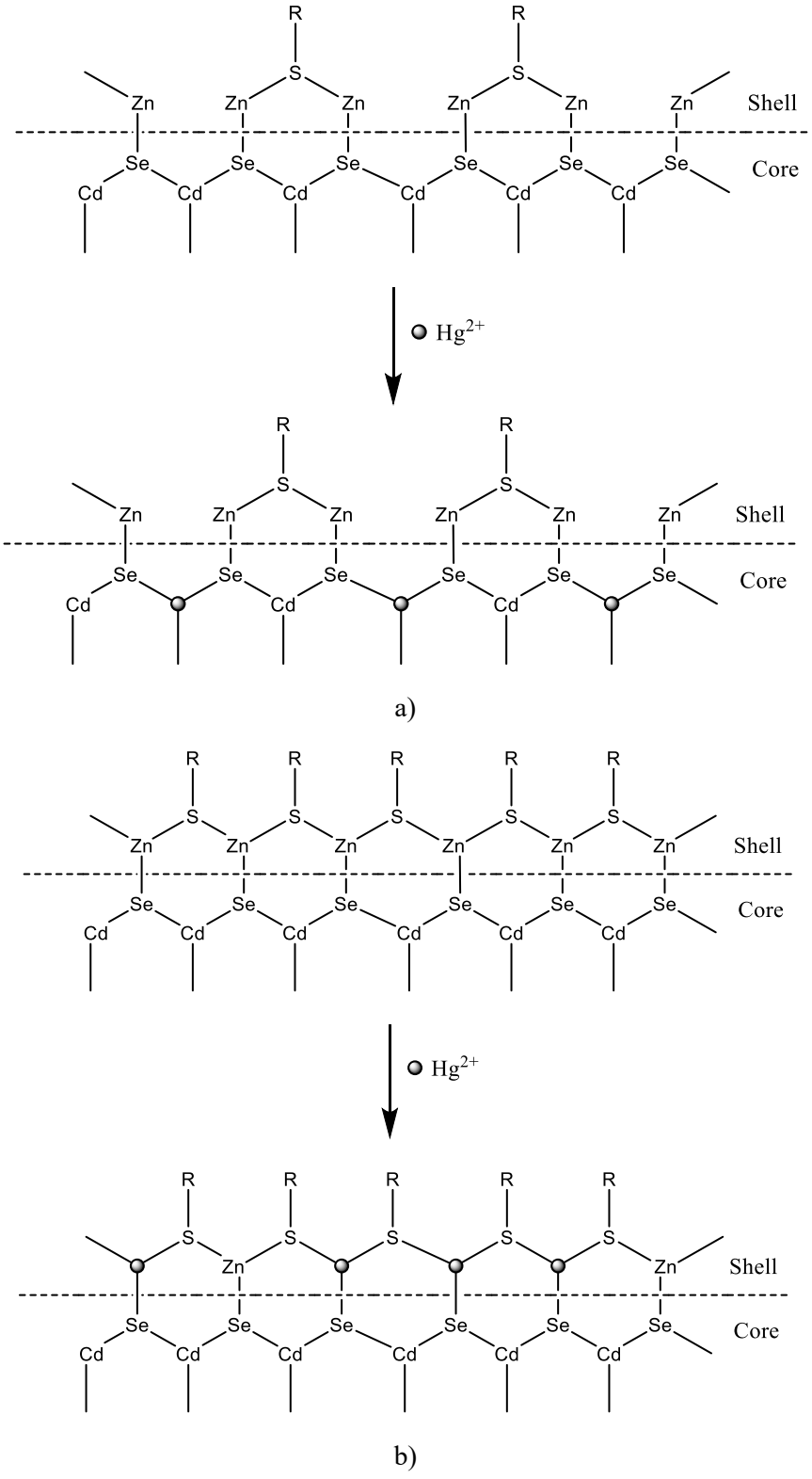

Figure 22. Schematic illustration of cation exchange reaction with Hg^{2+} ions on the surface of CdSe-ZnS QDs. a) QD-0.3 ML and b) QD-0.9 and QD-1.0 ML.

Table 5. Comparison of LOD calculated for CdSe-ZnS QDs synthesized and other QDs probes for determining Hg^{2+}.

Probes	Mechanism	LOD nM	Reference
2-mercaptoetanosulfonate capped CdTe QDs	Turn-off	95	[116]
Calixarene-CdSe/ZnS	Turn-off	15	[117]
L-carnitine-CdSe/ZnS	Turn-off	180	[118]
ZnS:Ce QDs	Turn-off	8200	[119]
Cys-CdSe: Eu	Turn-off	2000	[120]
QD-0.3 ML	Turn-off	11.2	This work
InP-MAA QDs	Turn-on	500	[109]
Rhodamine B derivative capped CdTe: Zn QDs	Turn-on	500	[121]
QD-0.9 ML	Turn-on	8.98	This work
QD-1.0 ML	Turn-on	10.7	This work

2.4.4.2 Photoluminescence decay analysis of CdSe-ZnS QDs with different shell thicknesses after interaction with Hg^{2+} ions

Time-resolved fluorescence measurements were used to evaluate the interaction between CdSe-ZnS QDs with different shell thicknesses and Hg^{2+} ions. **Figure 23** shows the fluorescence lifetime curve of free QDs (black line) and QDs with 5 μM Hg^{2+} ions (red line).

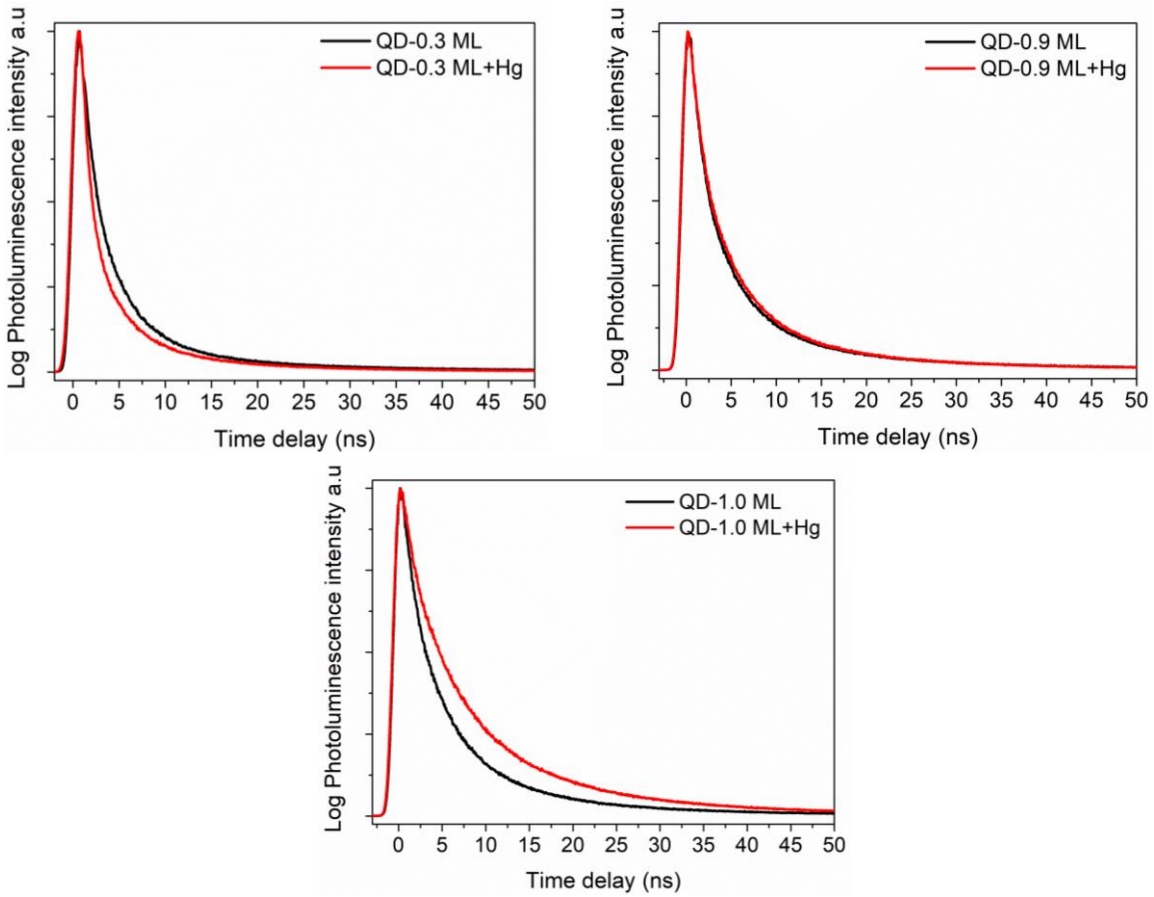

Figure 23. Decay curves of CdSe-ZnS core-shell QDs with different shell thicknesses before and after adding Hg^{2+} ions (5 µM). λ_{exc}: 540 nm. Solvent: chloroform/ethanol (1:1, v/v).

In free CdSe-ZnS core-shell QDs, the decay curve was satisfactorily fitted by 4-exponential decay kinetics, which serve to approximate an average luminescence lifetime (**Table 6**). When a 5 µM Hg^{2+} solution is added to the QD-0.30 ML solution, the fluorescence lifetime emission decreases while QD-0.9 and QD-1.0 ML increase (**Figure 24** and **Table 6**).

Table 6. Lifetime average (τ_{FL}) of CdSe-ZnS QDs with Hg^{2+}.

QDs + Hg	τ_{FL} *(ns)*	χ^2
QD-1.0 ML	2.81	1.10
QD-0.9 ML	4.43	1.12
QD-0.3 ML	5.00	1.06

After adding Hg^{2+} onto the QD-0.3 ML solution, the lifetime was decreased, while QD-0.9 ML showed a relatively constant lifetime (**Figure 24**). It has been established that a decrease in the fluorescence lifetime of QDs can be observed when an electron or hole acceptor is adsorbed onto the semiconductor

surface.[122,123] In this case, the S-excess used in synthesis (Zn/S: 0.11/9) is a hole acceptor and quenched the photoluminescence.[78,95,96] The Hg^{2+} ions produce a quenching in the photoluminescence of QD-0.3 ML due to the production of defects/trap states by forming HgSe particles onto the CdSe core, and the S-excess produces HgS particles in QD-0.3 ML by adding Hg^{2+} ions affecting the optical properties.[27,12] The behavior in emission lifetime in QD-0.3 ML (*turn-off*) mechanism is congruent with other similar systems reported (**Table 7**).

The preservation of the original lifetime for QD-0.9 ML upon adding Hg^{2+} is attributed to the protection of the ZnS shell that prevented the potential disruption from the external environments.[123] As a result, the exciton recombination of the electron-hole pair of QDs was unaffected, and a constant lifetime was observed. While in the sample with the highest amount of Zn used (QD-1.0 ML), the value in τ_{FL} is increasing due to the passivation of surface traps producing new radiative centers and increasing the photoluminescence.[1,39,79] The behavior in emission lifetime in QD-0.9 ML and QD-1.0 ML (Turn on mechanism) is congruent with other similar systems reported (**Table 7**).

In the QD-0.9 ML and QD-1.0 ML samples, the amount of Hg^{2+} can be used as a "shallow electron trap" to increase the lifetime of photogenerated electrons and holes in QDs.[125] The increasing of Hg^{2+} amount could partially remove the surface traps, increasing the probability of radiative recombination, and reducing the amount of non-radiative recombination, resulting in fluorescence enhancement, i.e., the increasing of [Hg^{2+}] passivate the traps states of CdSe-ZnS QDs; thus an increase in the photoluminescence was produced.[102]

Table 7. Comparison of τ_{FL} values of the QDs synthesized and other reported QDs with some metal transition ions.

QDs	Analyte	PL Mechanism	τ_{FL} free QDs (ns)	τ_{FL}+M^{2+} (ns)	Reference
CdTe QDs	Fe^{2+}	Turn off	28	17	[126]
MPA-capped green CdTe-CdS	Hg^{2+}	Turn off	25	6	[123]
Cu_2S QDs	Zn^{2+} (Doping)	Turn on	244	1112	[93]
CdS QDs	Cu^{2+} (Doping)	Turn on	284	3170	[127]
AgInZnS	Cd^{2+}	Turn on	262	292	[128]
QD-1.0 ML	Hg^{2+}	Turn on	3.29	2.81	This work
QD-0.9 ML	Hg^{2+}	Turn on	4.34	4.43	This work
QD-0.3 ML	Hg^{2+}	Turn off	4.82	5.00	This work

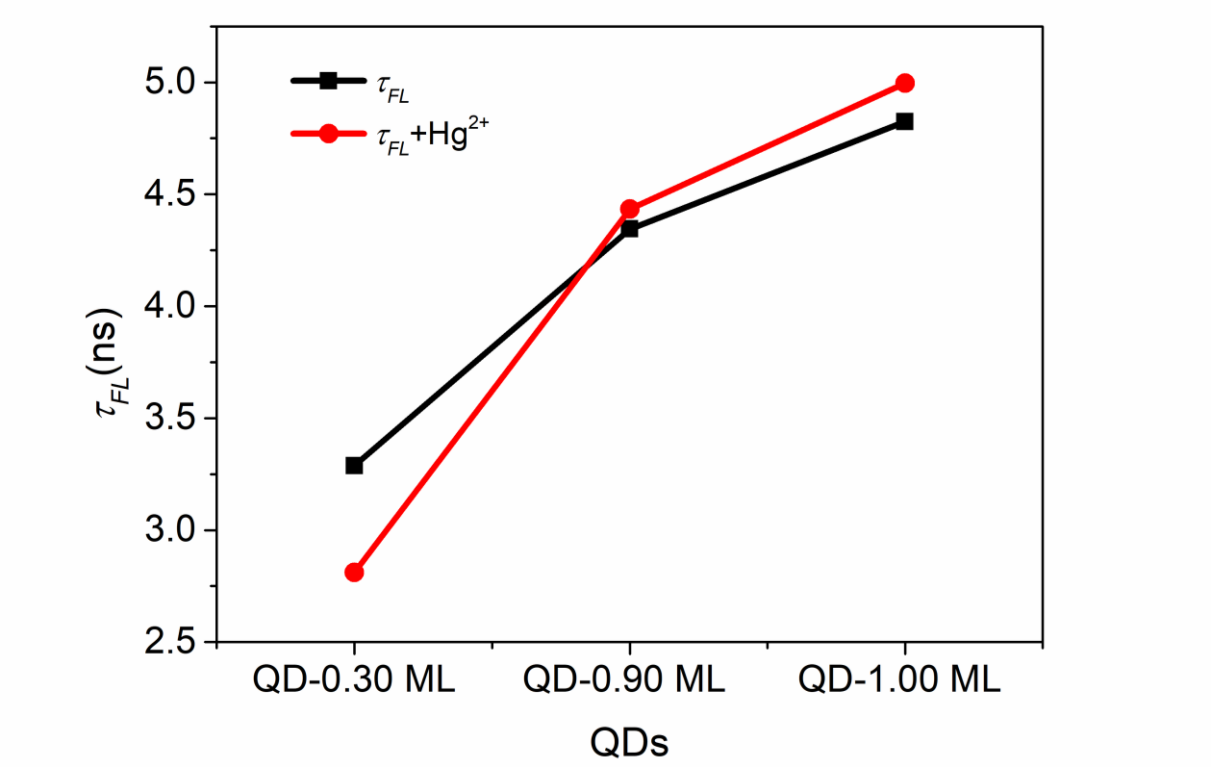

Figure 24. τ_{FL} values before and after the addition of Hg^{2+} ions.

2.4.5 Effect of metal ions on absorption and fluorescence of CdSe-ZnS QDs

This test shows the effect of some metal transition cations on the optical properties (Absorption and fluorescence) of CdSe-ZnS quantum dots (QD-0.30 ML, QD-0.90 ML, and QD-1.00 ML) and was performed using a solution of QDs in chloroform: ethanol (1:1 v/v) and aqueous solutions of metal chloride salts Co^{2+}, Mn^{2+}, Ni^{2+}, Zn^{2+}, Pb^{2+}, Cd^{2+} and Hg^{2+} in water with a concentration of 5µM.

The effect of these cations on absorption and fluorescence as a function of the amount of Zn used onto the shell of QDs (**Figure 45-46, annexes**). In QD-0.30 ML, a fluorescence quenching and a slight red shift were produced with all the cations evaluated. The Hg^{2+} cation produced the highest quenching. This behavior is due to the high affinity between Hg^{2+} with Se^{2+} and S^{2-} exposed previously.[15] This phenomenon is due to the cation exchange reaction forming HgSe on the core surface and HgS by the interaction between Hg^{2+} ions and S-excess used in the synthesis of this QD producing new non-radiative centers, which is possible due to the ZnS shell being thin (0.3 ML). It is not enough to cover all the core, leaving it exposed. This selective behavior can be explained based on the *Ksp* values of HgSe 4.0×10^{-59} is lower than other ions used, and the high affinity between Hg^{2+} and S^{2-},[15] favoring the formation of HgSe particles due to the easy access to the core by Hg^{2+} ions (**Table 8**)[15,129] and HgS particles was formed by the disponibility of sulfide ion from S-excess used in synthesis (Zn:S, 0.11/9), the quenching effect produced in this sample is a product by the formation of both particles.

In the samples with more Zn (QD-0.90 ML and QD-1.00 ML), all ions evaluated produce fluorescence *turn-on* (**Figure 25**). However, the *turn-on* effect with Hg^{2+} is higher than other cations evaluated due to the affinity of Hg^{2+} to S^{2-} favoring the cation exchange with Zn^{2+}.[14,15] In both cases, all the cations evaluated produce a surface passivation, removing some defects and surface traps, thus increasing photoluminescence. [11]

The large surface-to-volume ratio of nano-sized QDs favors the diffusion of foreign metal ions.[130] **Figure 26** shows a model according to the photoluminescence results obtained after adding Hg^{2+} ions. The evaluated transition metal ions M^{2+} can diffuse through the lattice structure of the surface and directly affect the CdSe core producing a fluorescence quenching due to the production of new surface traps that decrease the photoluminescence. At the same time, in the samples with a high amount of Zn, this property increases due to the passivation effect of these traps increasing the excitonic recombination.

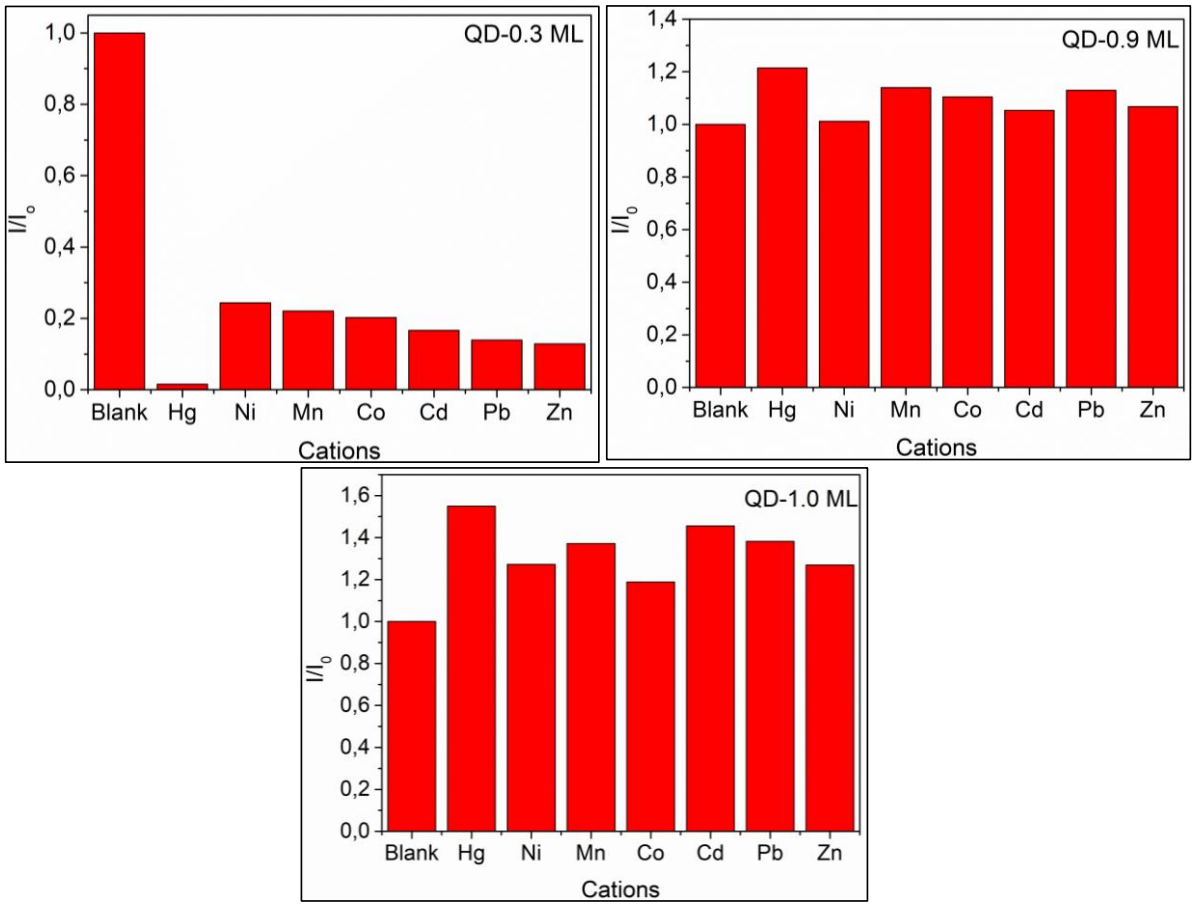

Figure 25. Relative photoluminescence response of CdSe-ZnS core-shell QDs with different shell thicknesses in the presence of Hg^{2+} and other metal transition ions evaluated.

Table 8. Solubility product constants of metal transition cations evaluated at 25 °C.[14,131]

Metal	Sulfide	Selenide
Hg^{2+}	1.6×10^{-52}	4.0×10^{-59}
Cd^{2+}	8.0×10^{-27}	4.0×10^{-35}
Zn^{2+}	1.6×10^{-24}	3.6×10^{-26}
Ni^{2+}	3.2×10^{-19}	2.0×10^{-26}
Pb^{2+}	8.0×10^{-28}	1.0×10^{-37}
Co^{2+}	4.0×10^{-21}	-
Mn^{2+}	2.5×10^{-13}	-

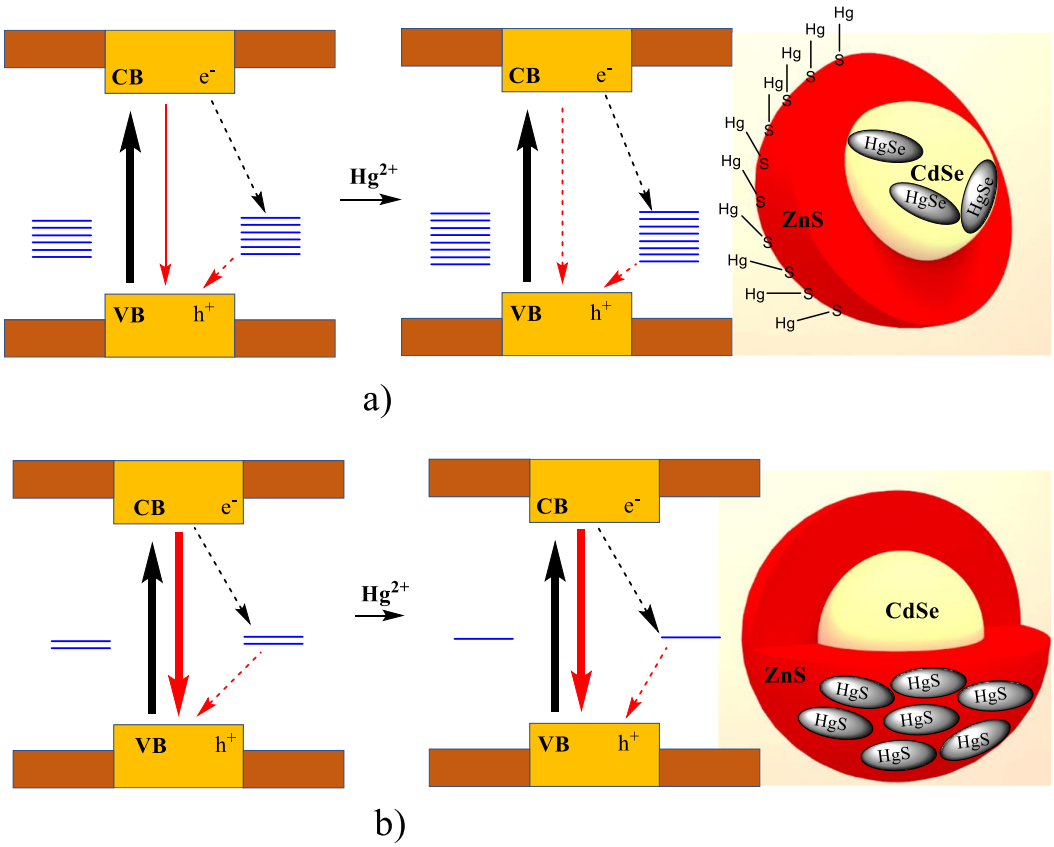

Figure 26. Photoluminescence effect on the QDs before and after the addition of cations (M^{2+} or Hg^{2+}), a) fluorescence quenching (QD-0.3 ML), and b) in the enhancement of photoluminescence (QD-0.90 ML and QD-1.00 ML).

2.5 CONCLUSIONS

Three systems of type CdSe-ZnS core-shell QDs were synthesized with different shell thicknesses (QD-0.30 ML, QD-0.90 ML, and QD-1.00 ML). These systems were characterized by optical and structural analysis (UV-Vis, PL, decay fluorescence, XRD, HRTEM, XPS, FT-IR). The shell thickness produced changes in different properties, such as size, surface, and optical properties.

The shell thicknesses increases the size in CdSe-ZnS QDs; the variation in PL QY and photoluminescence decay measurements correlate with the surface traps associated with the concentration of Zn^{2+} and S^{2-} precursors on the shell surface.

The Hg^{2+} ions sensing produces two different mechanisms on the optical properties of CdSe-ZnS core-shell QDs. In QD-0.3 ML produces a quenching of photoluminescence due to the formation of HgSe particles on the core by a cation exchange reaction and HgS particles for the interaction with S-excess precursor, while in QD-0.90 ML and QD-1.00 ML, the shell thickness is thicker, the Hg^{2+} ions produce an enhancement of fluorescence due to the passivation of traps by the formation of HgS particles on the ZnS shell surface. This mechanism is a typical cation exchange in colloidal nanoparticle systems. This situation influences the sensitivity and selectivity in Hg^{2+} ion sensing. For example, the QDs studied showed lower LOD than QDs reported with similar characteristics (CdSe-ZnS). These QDs systems are innovative and promising for application in detecting Hg^{2+} ions.

2.6 REFERENCES

(1) Vasudevan, D.; Gaddam, R. R.; Trinchi, A.; Cole, I. Core-Shell Quantum Dots: Properties and Applications. *J Alloys Compd* **2015**, No. February. https://doi.org/10.1016/j.jallcom.2015.02.102.

(2) R. W. Knoss. *Quantum Dots: Research, Technology and Applications*; 2008.

(3) Dorfs, D.; Krahne, R.; Falqui, A.; Manna, L.; Giannini, C.; Zanchet, D. *Quantum Dots: Synthesis and Characterization*; Elsevier Ltd., 2011; Vol. 1. https://doi.org/10.1016/B978-0-12-812295-2.00028-3.

(4) Asor, L.; Liu, J.; Ossia, Y.; Tripathi, D. C.; Tessler, N.; Frenkel, A. I.; Banin, U. InAs Nanocrystals with Robust P-Type Doping. *Adv Funct Mater* **2021**, *31* (6). https://doi.org/10.1002/adfm.202007456.

(5) Sahu, A.; Kang, M. S.; Kompch, A.; Notthoff, C.; Wills, A. W.; Deng, D.; Winterer, M.; Frisbie, C. D.; Norris, D. J. Electronic Impurity Doping in CdSe Nanocrystals. *Nano Lett* **2012**, *12* (5), 2587–2594. https://doi.org/10.1021/nl300880g.

(6) Morgan, D. P.; Kelley, D. F. Mechanism of Hole Trap Passivation in CdSe Quantum Dots by Alkylamines. *Journal of Physical Chemistry C* **2018**, *122* (44), 25661–25667. https://doi.org/10.1021/acs.jpcc.8b08798.

(7) Green, M. The Nature of Quantum Dot Capping Ligands. *J Mater Chem* **2010**, *20* (28), 5797. https://doi.org/10.1039/c0jm00007h.

(8) Zhou, J.; Liu, Y.; Tang, J.; Tang, W. Surface Ligands Engineering of Semiconductor Quantum Dots for Chemosensory and Biological Applications. *Biochem Pharmacol* **2017**, *20* (7), 360–376. https://doi.org/10.1016/j.mattod.2017.02.006.

(9) Malik, P.; Singh, J.; Kakkar, R. A Review on CdSe Quantum Dots in Sensing. *Advanced Materials Letters*. VBRI Press 2014, pp 612–628. https://doi.org/10.5185/amlett.2014.4562.

(10) Goicoechea, J.; Arregui, F. J.; Matias, I. R. Quantum Dots for Sensing. In *Sensors Based on Nanostructured Materials*; Springer US, 2009; pp 131–181. https://doi.org/10.1007/978-0-387-77753-5_6.

(11) Lou, Y.; Zhu, J. Metal Ions Optical Sensing by Semiconductor Quantum Dots. *J Mater Chem C Mater* **2014**, *2* (4), 585–772. https://doi.org/10.1039/c3tc31937g.

(12) Kim, K. M.; Jeon, J. H.; Kim, Y. Y.; Lee, H. K.; Park, O. O.; Wang, D. H. Effects of Ligand Exchanged CdSe Quantum Dot Interlayer for Inverted Organic Solar Cells. *Org Electron* **2015**, *25* (November), 44–49. https://doi.org/10.1016/j.orgel.2015.05.040.

(13) Premaratne, W. A. P. J.; Priyadarshana, W. M. G. I.; Gunawardena, S. H. P.; De Alwis, A. A. P. Synthesis of Nanosilica from Paddy Husk Ash and Their Surface Functionalization. *Journal of Science of the University of Kelaniya Sri Lanka* **2014**, *8* (July 2013), 33. https://doi.org/10.4038/josuk.v8i0.7238.

(14) De Trizio, L.; Manna, L. Forging Colloidal Nanostructures via Cation Exchange Reactions. *Chemical Reviews*. American Chemical Society September 28, 2016, pp 10852–10887. https://doi.org/10.1021/acs.chemrev.5b00739.

(15) Pearson, R. G.; Busch, D. H. *Hard and Soft Acids and Bases*; 1963.

(16) Li, H.; Zhang, Y.; Wang, X.; Xiong, D.; Bai, Y. Calixarene Capped Quantum Dots as Luminescent Probes for Hg2+ Ions. *Mater Lett* **2007**, *61* (7), 1474–1477. https://doi.org/10.1016/j.matlet.2006.07.064.

(17) Chu, H.; Yao, D.; Chen, J.; Yu, M.; Su, L. Double-Emission Ratiometric Fluorescent Sensors Composed of Rare-Earth-Doped ZnS Quantum Dots for Hg2+Detection. *ACS Omega* **2020**, *5* (16), 9558–9565. https://doi.org/10.1021/acsomega.0c00861.

(18) Li, H.; Zhang, Y.; Wang, X.; Gao, Z. A Luminescent Nanosensor for Hg(II) Based on Functionalized CdSe/ZnS Quantum Dots. *Microchimica Acta* **2008**, *160* (1–2), 119–123. https://doi.org/10.1007/s00604-007-0816-x.

(19) Zhang, K.; Zhang, J. M. A Fluorescent Probe for the Detection of Hg2+ Based on Rhodamine Derivative and Modified CdTe Quantum Dots. *Research on Chemical Intermediates* **2020**, *46* (2), 987–997. https://doi.org/10.1007/s11164-015-2298-5.

(20) Zhang, K.; Yu, Y.; Sun, S. Facile Synthesis L-Cysteine Capped CdS:Eu Quantum Dots and Their Hg 2+ Sensitive Properties. *Appl Surf Sci* **2013**, *276*, 333–339. https://doi.org/10.1016/j.apsusc.2013.03.093.

(21) Reiss, P.; Protière, M.; Li, L. Core/Shell Semiconductor Nanocrystals. *Small* **2009**, *5* (2), 154–168. https://doi.org/10.1002/smll.200800841.

(22) Fernández-delgado, N.; Herrera, M.; Tavabi, A. H.; Luysberg, M.; Dunin-borkowski, R. E. Applied Surface Science Structural and Chemical Characterization of CdSe-ZnS Core-Shell Quantum Dots. *Appl Surf Sci* **2018**, *457* (April), 93–97. https://doi.org/10.1016/j.apsusc.2018.06.149.

(23) Jin, L. H.; Han, C. S. Ultrasensitive and Selective Fluorimetric Detection of Copper Ions Using Thiosulfate-Involved Quantum Dots. *Anal Chem* **2014**, *86* (15), 7209–7213. https://doi.org/10.1021/ac501515f.

(24) Ren, J.; Chen, H. L.; Ren, C. L.; Sun, J. F.; Liu, Q.; Wang, M.; Chen, X. G. L-Cysteine Capped CdSe as Sensitive Sensor for Detection of Trace Lead Ion in Aqueous Solution. *Materials Research Innovations* **2010**, *14* (2), 133–137. https://doi.org/10.1179/143307510X12639910071476.

(25) Liang, J. G.; Ai, X. P.; He, Z. K.; Pang, D. W. Functionalized CdSe Quantum Clots as Selective Silver Ion Chemodosimeter. *Analyst* **2004**, *129* (7), 619–622. https://doi.org/10.1039/b317044f.

(26) Fernández-Argüelles, M. T.; Wei, J. J.; Costa-Fernández, J. M.; Pereiro, R.; Sanz-Medel, A. Surface-Modified CdSe Quantum Dots for the Sensitive and Selective Determination of Cu(II) in Aqueous Solutions by Luminescent Measurements. *Anal Chim Acta* **2005**, *549* (1–2), 20–25. https://doi.org/10.1016/j.aca.2005.06.013.

(27) Wu, P.; Yan, X. P. A Simple Chemical Etching Strategy to Generate "Ion-Imprinted" Sites on the Surface of Quantum Dots for Selective Fluorescence Turn-on Detecting of Metal Ions. *Chemical Communications* **2010**, *46* (37), 7046–7048. https://doi.org/10.1039/c0cc01762k.

(28) Pendyala, N. B.; Koteswara Rao, K. S. R. Efficient Hg and Ag Ion Detection with Luminescent PbS Quantum Dots Grown in Poly Vinyl Alcohol and Capped with Mercaptoethanol. *Colloids Surf A Physicochem Eng Asp* **2009**, *339* (1–3), 43–47. https://doi.org/10.1016/j.colsurfa.2009.01.013.

(29) Chen, J. L.; Zhu, C. Q. Functionalized Cadmium Sulfide Quantum Dots as Fluorescence Probe for Silver Ion Determination. *Anal Chim Acta* **2005**, *546* (2), 147–153. https://doi.org/10.1016/j.aca.2005.05.006.

(30) Chern, M.; Kays, J. C.; Bhuckory, S.; Dennis, A. M. Sensing with Photoluminescent Semiconductor Quantum Dots. *Methods Appl Fluoresc* **2019**, *7* (1). https://doi.org/10.1088/2050-6120/aaf6f8.

(31) Demchenko, A. P. *Introduction to Fluorescence Sensing*.

(32) Granados-Oliveros, G.; Pineros, B. S. G.; Calderon, F. G. O. CdSe/ZnS Quantum Dots Capped with Oleic Acid and L-Glutathione: Structural Properties and Application in Detection of Hg2+. *J Mol Struct* **2022**, *1254*. https://doi.org/10.1016/j.molstruc.2021.132293.

(33) Rodrigues, S. S. M.; Ribeiro, D. S. M.; Soares, J. X.; Passos, M. L. C.; Saraiva, M. L. M. F. S.; Santos, J. L. M. Application of Nanocrystalline CdTe Quantum Dots in Chemical Analysis: Implementation of Chemo-Sensing Schemes Based on Analyte-Triggered Photoluminescence Modulation. *Coordination Chemistry Reviews*. Elsevier B.V. January 1, 2017, pp 127–143. https://doi.org/10.1016/j.ccr.2016.10.001.

(34) Hartley, C. L.; Kessler, M. L.; Dempsey, J. L. Molecular-Level Insight into Semiconductor Nanocrystal Surfaces. *J Am Chem Soc* **2021**, *143* (3), 1251–1266. https://doi.org/10.1021/jacs.0c10658.

(35) Houtepen, A. J.; Hens, Z.; Owen, J. S.; Infante, I. On the Origin of Surface Traps in Colloidal II-VI Semiconductor Nanocrystals. *Chemistry of Materials* **2017**, *29* (2), 752–761. https://doi.org/10.1021/acs.chemmater.6b04648.

(36) Ren, C.; Hao, J.; Chen, H.; Wang, K.; Wu, D. Prepare Core-Multishell CdSe/ZnS Nanocrystals with Pure Color and Controlled Emission by Tri-n-Octylphosphine-Assisted Method. *Appl Surf Sci* **2015**, *353*, 480–488. https://doi.org/10.1016/j.apsusc.2015.06.149.

(37) Dabbousi, B. O.; Rodriguez-Viejo, J.; Mikulec, F. V.; Heine, J. R.; Mattoussi, H.; Ober, R.; Jensen, K. F.; Bawendi, M. G. (CdSe)ZnS Core−Shell Quantum Dots: Synthesis and Characterization of a Size Series of Highly Luminescent Nanocrystallites. *J Phys Chem B* **1997**, *101* (46), 9463–9475. https://doi.org/10.1021/jp971091y.

(38) Reiss, P.; Protière, M.; Li, L. Core/Shell Semiconductor Nanocrystals. *Small* **2009**, *5* (2), 154–168. https://doi.org/10.1002/smll.200800841.

(39) Mathew, S.; Bhardwaj, B. S.; Saran, A. D.; Radhakrishnan, P.; Nampoori, V. P. N.; Vallabhan, C. P. G.; Bellare, J. R. Effect of ZnS Shell on Optical Properties of CdSe-ZnS Core-Shell Quantum Dots. *Opt Mater (Amst)* **2015**, *39*, 46–51. https://doi.org/10.1016/j.optmat.2014.10.061.

(40) Reiss, P.; Pron, A. Highly Luminescent CdSe / ZnSe Core / Shell Nanocrystals of Low Size Dispersion. **2002**, 21–24.

(41) Vasudevan, D.; Gaddam, R. R.; Trinchi, A.; Cole, I. Core-Shell Quantum Dots: Properties and Applications. *J Alloys Compd* **2015**, No. February. https://doi.org/10.1016/j.jallcom.2015.02.102.

(42) Vinayakan, R.; Shanmugapriya, T.; Nair, P. V.; Ramamurthy, P.; Thomas, K. G. An Approach for Optimizing the Shell Thickness of Core - Shell Quantum Dots Using Photoinduced Charge Transfer. *Journal of Physical Chemistry C* **2007**, *111* (28), 10146–10149. https://doi.org/10.1021/jp072823h.

(43) Pisheh, H. S.; Gheshlaghi, N.; Ünlü, H. The Effects of Strain and Spacer Layer in CdSe/CdS/ZnS and CdSe/ZnS/CdS Core/Shell Quantum Dots. *Physica E Low Dimens Syst Nanostruct* **2017**, *85*, 334–339. https://doi.org/10.1016/j.physe.2016.07.007.

(44) Speranskaya, E. S.; Goftman, V. V.; Goryacheva, I. Y. Preparation of Water Soluble Zinc-Blende CdSe/ZnS Quantum Dots. *Nanotechnol Russ* **2013**, *8* (1–2), 129–135. https://doi.org/10.1134/S1995078013010163.

(45) Baranov, V.; Rakovich, Y. P.; Donegan, F.; Perova, S.; Moore, A.; Talapin, V.; Rogach, L.; Masumoto, Y.; Nabiev, I. Effect of ZnS Shell Thickness on the Phonon Spectra in CdSe Quantum Dots. *Phys Rev B Condens Matter Mater Phys* **2003**, *68* (16). https://doi.org/10.1103/PhysRevB.68.165306.

(46) Peng, Z. A.; Peng, X. Mechanisms of the Shape Evolution of CdSe Nanocrystals. *J Am Chem Soc* **2001**, *123* (7), 1389–1395. https://doi.org/10.1021/ja0027766.

(47) Boatman, E. M.; Lisensky, G. C.; Nordell, K. J. *A Safer, Easier, Faster Synthesis for CdSe Quantum Dot Nanocrystals*; 2005. www.JCE.DivCHED.org.

(48) Stiven Gómez-Piñeros, B.; Granados-Oliveros, G. *Fisicoquímica y Química Inorgánica*; 2015; Vol. 44.

(49) Tan, A. C. W.; Polo-Cambronell, B. J.; Provaggi, E.; Ardila-Suárez, C.; Ramirez-Caballero, G. E.; Baldovino-Medrano, V. G.; Kalaskar, D. M. Design and Development of Low Cost Polyurethane Biopolymer Based on Castor Oil and Glycerol for Biomedical Applications. *Biopolymers* **2018**, *109* (2). https://doi.org/10.1002/bip.23078.

(50) Botao Ji, S. K. I. S. S. R. U. B. ZnSe-ZnS Core-Shell Quantum Dots with Superior Optical. *Nano Lett* **2020**, *20*, 2387–2395. https://doi.org/https://dx.doi.org/10.1021/acs.nanolett.9b05020.

(51) Hien, N. T.; Vinh, N. D.; Thanh, L. D.; Do, P. V; Tuyen, V. P.; Ca, N. X.; Vinh, N. D.; Thanh, L. D.; Do, P. V; Tuyen, V. P.; Ca, N. X. Synthesis, Characterization and the Photoinduced Electron-Transfer Energetics of CdTe/CdSe Type-II Core/Shell Quantum Dots. *Journal of Luminiscence* **2019**. https://doi.org/https://doi.org/10.1016/j.jlumin.2019.116822.

(52) Xie, R.; Kolb, U.; Li, J.; Basché, T.; Mews, A. Synthesis and Characterization of Highly Luminescent CdSe-Core CdS/Zn 0.5Cd0.5S/ZnS Multishell Nanocrystals. *J Am Chem Soc* **2005**, *127* (20), 7480–7488. https://doi.org/10.1021/ja042939g.

(53) Fu, Y.; Kim, D.; Jiang, W.; Yin, W.; Ahn, T. K.; Chae, H. Excellent Stability of Thicker Shell CdSe@ZnS/ZnS Quantum Dots. *RSC Adv* **2017**, *7* (65), 40866–40872. https://doi.org/10.1039/c7ra06957j.

(54) Liu, N.; Ding, L.; Xue, H.; Ji, Y.; Ye, Y. Effect of Shell Thickness on Optical Properties of ZnSe/ZnS Quantum Dots under Solar and Laser Excitation. *Journal of Nanoparticle Research* **2022**, *24* (7). https://doi.org/10.1007/s11051-022-05503-6.

(55) Yu, W. W.; Qu, L.; Guo, W.; Peng, X. Experimental Determination of the Extinction Coefficient of CdTe, CdSe, and CdS Nanocrystals. *Chemistry of Materials* **2003**, *15* (14), 2854–2860. https://doi.org/10.1021/cm034081k.

(56) Hao, J.; Liu, H.; Miao, J.; Lu, R.; Zhou, Z.; Zhao, B.; Xie, B. A Facile Route to Synthesize CdSe / ZnS Thick-Shell Quantum Dots with Precisely Controlled Green Emission Properties : Towards QDs Based LED Applications. *Sci Rep* **2019**, No. August, 1–8. https://doi.org/10.1038/s41598-019-48469-7.

(57) György, E.; Pérez Del Pino, A.; Roqueta, J.; Ballesteros, B.; Miguel, A. S.; Maycock, C.; Oliva, A. G. Synthesis and Characterization of CdSe/ZnS Core-Shell Quantum Dots Immobilized on Solid Substrates through Laser Irradiation. *Physica Status Solidi (A) Applications and Materials Science* **2012**, *209* (11), 2201–2207. https://doi.org/10.1002/pssa.201127749.

(58) Chang, K. P.; Yeh, Y. C.; Wu, C. J.; Yen, C. C.; Wuu, D. S. Improved Characteristics of CdSe/CdS/ZnS Core-Shell Quantum Dots Using an Oleylamine-Modified Process. *Nanomaterials* **2022**, *12* (6). https://doi.org/10.3390/nano12060909.

(59) Chen, S.; Zhang, X.; Zhang, Q.; Tan, W. Trioctylphosphine as Both Solvent and Stabilizer to Synthesize CdS Nanorods. *Nanoscale Res Lett* **2009**, *4* (10), 1159–1165. https://doi.org/10.1007/s11671-009-9375-x.

(60) Guo, H.; Chen, Y.; Ping, H.; Jin, J.; Peng, D. L. Facile Synthesis of Cu and Cu@Cu-Ni Nanocubes and Nanowires in Hydrophobic Solution in the Presence of Nickel and Chloride Ions. *Nanoscale* **2013**, *5* (6), 2394–2402. https://doi.org/10.1039/c3nr33142c.

(61) Kim, K. M.; Jeon, J. H.; Kim, Y. Y.; Lee, H. K.; Park, O. O.; Wang, D. H. Effects of Ligand Exchanged CdSe Quantum Dot Interlayer for Inverted Organic Solar Cells. *Org Electron* **2015**, *25*, 44–49. https://doi.org/10.1016/j.orgel.2015.05.040.

(62) Zhang, L.; He, R.; Gu, H. C. Oleic Acid Coating on the Monodisperse Magnetite Nanoparticles. *Appl Surf Sci* **2006**, *253* (5), 2611–2617. https://doi.org/10.1016/j.apsusc.2006.05.023.

(63) Zhang, N.; Xie, J.; Varadan, V. K. *Functionalization of Carbon Nanotubes by Potassium Permanganate Assisted with Phase Transfer Catalyst*; 2002.

(64) Watts, J. F.; Wolstenholme, John. *An Introduction to Surface Analysis by XPS and AES*; J. Wiley, 2003.

(65) Briggs', D.; Beamson, G.; Plc, Z. *XPS Studies of the Oxygen Is and 2s Levels in a Wide Range of Functional Polymers*; Vol. 1883.

(66) Cingarapu, S.; Yang, Z.; Sorensen, C. M.; Klabunde, K. J. Synthesis of CdSe/ZnS and CdTe/ZnS Quantum Dots: Refined Digestive Ripening. *J Nanomater* **2012**, *2012*. https://doi.org/10.1155/2012/312087.

(67) Granada-Ramirez, D. A.; Arias-Cerón, J. S.; Gómez-Herrera, M. L.; Luna-Arias, J. P.; Pérez-González, M.; Tomás, S. A.; Rodríguez-Fragoso, P.; Mendoza-Alvarez, J. G. Effect of the Indium Myristate Precursor Concentration on the Structural, Optical, Chemical Surface, and Electronic Properties of InP Quantum Dots Passivated with ZnS. *Journal of Materials Science: Materials in Electronics* **2019**, *30* (5), 4885–4894. https://doi.org/10.1007/s10854-019-00783-6.

(68) Zhang, D.; Du, C.; Chen, J.; Shi, Q.; Wang, Q.; Li, S.; Wang, W.; Yan, X.; Fan, Q. Improvement of Structural and Optical Properties of ZnAl2O4:Cr3+ Ceramics with Surface Modification by Using Various Concentrations of Zinc Acetate. *J Solgel Sci Technol* **2018**, *88* (2), 422–429. https://doi.org/10.1007/s10971-018-4820-x.

(69) Tshabalala, K. G.; Cho, S. H.; Park, J. K.; Pitale, S. S.; Nagpure, I. M.; Kroon, R. E.; Swart, H. C.; Ntwaeaborwa, O. M. Luminescent Properties and X-Ray Photoelectron Spectroscopy Study of ZnAl2O4:Ce3+,Tb3+ Phosphor. *J Alloys Compd* **2011**, *509* (41), 10115–10120. https://doi.org/10.1016/j.jallcom.2011.08.054.

(70) Gopannagari, M.; Kumar, D. P.; Park, H.; Kim, E. H.; Bhavani, P.; Reddy, D. A.; Kim, T. K. Influence of Surface-Functionalized Multi-Walled Carbon Nanotubes on CdS Nanohybrids for Effective Photocatalytic Hydrogen Production. *Appl Catal B* **2018**, *236*, 294–303. https://doi.org/10.1016/j.apcatb.2018.05.009.

(71) Bowen Katari, J. E.; Colvin, V. L.; Alivisatos, A. P. *X-Ray Photoelectron Spectroscopy of CdSe Nanocrystals with Applications to Studies of the Nanocrystal Surface*; 1994; Vol. 98.

(72) Canava, B.; Vigneron, J.; Etcheberry, A.; Guillemoles, J. F.; Lincot, D. *High Resolution XPS Studies of Se Chemistry of a Cu(In, Ga)Se 2 Surface*.

(73) Parani, S.; Tsolekile, N.; Pandian, K.; Oluwafemi, O. S. Thiolated Selenium as a New Precursor for the Aqueous Synthesis of CdSe/CdS Core/Shell Quantum Dots. *Journal of Materials Science: Materials in Electronics* **2017**, *28* (15), 11151–11162. https://doi.org/10.1007/s10854-017-6902-x.

(74) Pechstedt, K.; Whittle, T.; Baumberg, J.; Melvin, T. Photoluminescence of Colloidal CdSe/ZnS Quantum Dots: The Critical Effect of Water Molecules. *Journal of Physical Chemistry C* **2010**, *114* (28), 12069–12077. https://doi.org/10.1021/jp100415k.

(75) Vale, B. R. C.; Mourão, R. S.; Bettini, J.; Sousa, J. C. L.; Ferrari, J. L.; Reiss, P.; Aldakov, D.; Schiavon, M. A. Ligand Induced Switching of the Band Alignment in Aqueous Synthesized CdTe/CdS Core/Shell Nanocrystals. *Sci Rep* **2019**, *9* (1). https://doi.org/10.1038/s41598-019-44787-y.

(76) Gómez-Pineros, B. S.; Granados-Oliveros, G. Synthesis and Characterization of Optic Properties of CdSe and CdSe/ZnS Quantum Dots. *Revista Colombiana de Quimica* **2018**, *47* (1). https://doi.org/10.15446/rev.colomb.quim.v47n1.61067.

(77) Granados-Oliveros, G.; Pineros, B. S. G.; Calderon, F. G. O. CdSe/ZnS Quantum Dots Capped with Oleic Acid and L-Glutathione: Structural Properties and Application in Detection of Hg2+. *J Mol Struct* **2022**, *1254*, 132293. https://doi.org/10.1016/J.MOLSTRUC.2021.132293.

(78) Pu, C.; Peng, X. To Battle Surface Traps on CdSe/CdS Core/Shell Nanocrystals: Shell Isolation versus Surface Treatment. *J Am Chem Soc* **2016**, *138* (26), 8134–8142. https://doi.org/10.1021/jacs.6b02909.

(79) Rajapaksha, R. D.; Ranasinghe, M. I. The Shell Thickness and Surface Passivation Dependence of Fluorescence Decay Kinetics in CdSe/ZnS Core-Shell and CdSe Core Colloidal Quantum Dots. *J Lumin* **2017**, *192*, 860–866. https://doi.org/10.1016/j.jlumin.2017.08.024.

(80) Rajapaksha, R. D.; Ranasinghe, M. I. The Shell Thickness and Surface Passivation Dependence of Fluorescence Decay Kinetics in CdSe/ZnS Core-Shell and CdSe Core Colloidal Quantum Dots. *J Lumin* **2017**, *192*, 860–866. https://doi.org/10.1016/J.JLUMIN.2017.08.024.

(81) Talapin, D. V; Rogach, A. L.; Kornowski, A.; Haase, M.; Weller, H. Highly Luminescent Monodisperse CdSe and CdSe / ZnS Nanocrystals Synthesized in a Hexadecylamine − Trioctylphosphine Oxide − Trioctylphospine Mixture. *Nano Lett* **2001**, *1* (4), 207–211. https://doi.org/10.1021/nl0155126.

(82) Park, J.; Lee, K. H.; Galloway, J. F.; Searson, P. C. Synthesis of Cadmium Selenide Quantum Dots from a Non-Coordinating Solvent: Growth Kinetics and Particle Size Distribution. *Journal of Physical Chemistry C* **2008**, *112* (46), 17849–17854. https://doi.org/10.1021/jp803746b.

(83) Aplop, F.; Johan, M. R. Synthesis of Zn Doped CdSe Quantum Dots via Inverse Micelle Technique. *Materials Science Forum* **2015**, *807*, 115–121. https://doi.org/10.4028/www.scientific.net/MSF.807.115.

(84) AbouElhamd, A. R.; Al-Sallal, K. A.; Hassan, A. Review of Core/Shell Quantum Dots Technology Integrated into Building's Glazing. *Energies (Basel)* **2019**, *12* (6). https://doi.org/10.3390/en12061058.

(85) Dos Santos, J. A. L.; Baum, F.; Kohlrausch, E. C.; Tavares, F. C.; Pretto, T.; Dos Santos, F. P.; Leite Santos, J. F.; Khan, S.; Leite Santos, M. J. 3-Mercaptopropionic, 4-Mercaptobenzoic, and Oleic Acid-Capped CdSe Quantum Dots: Interparticle Distance, Anchoring Groups, and Surface Passivation. *J Nanomater* **2019**, *2019*. https://doi.org/10.1155/2019/2796746.

(86) Alvarenga, S.; Ponce, H.; González Oliva, I.; Rudamas, C. Changes on the Stokes Shift in Large CdSe Colloidal Quantum Dots by a Ligand Exchange. In *Proceedings of the 2nd International Conference of Theoretical and Applied Nanoscience and Nanotechnology (TANN'18)*; Avestia Publishing, 2018. https://doi.org/10.11159/tann18.140.

(87) Yang, Y.; Chen, O.; Angerhofer, A.; Cao, Y. C. Radial-Position-Controlled Doping of CdS/ZnS Core/Shell Nanocrystals: Surface Effects and Position-Dependent Properties. *Chemistry - A European Journal* **2009**, *15* (13), 3186–3197. https://doi.org/10.1002/chem.200802295.

(88) Verma, S.; Kaniyankandy, S.; Ghosh, H. N. Charge Separation by Indirect Bandgap Transitions in CdS/ZnSe Type-II Core/Shell Quantum Dots. *Journal of Physical Chemistry C* **2013**, *117* (21), 10901–10908. https://doi.org/10.1021/jp400014j.

(89) Jiang, Z. J.; Kelley, D. F. Hot and Relaxed Electron Transfer from the CdSe Core and Core/Shell Nanorods. *Journal of Physical Chemistry C* **2011**, *115* (11), 4594–4602. https://doi.org/10.1021/jp112424z.

(90) Shi, X.; Chen, S.; Luo, M. Y.; Huang, B.; Zhang, G.; Cui, R.; Zhang, M. Zn-Doping Enhances the Photoluminescence and Stability of PbS Quantum Dots for in Vivo High-Resolution Imaging in the NIR-II Window. *Nano Res* **2020**, *13* (8), 2239–2245. https://doi.org/10.1007/s12274-020-2843-4.

(91) Sambur, J. B.; Parkinson, B. A. CdSe/ZnS Core/Shell Quantum Dot Sensitization of Low Index Tio2 Single Crystal Surfaces. *J Am Chem Soc* **2010**, *132* (7), 2130–2131. https://doi.org/10.1021/ja9098577.

(92) Li, J.; Zheng, H.; Zheng, Z.; Rong, H.; Zeng, Z.; Zeng, H. Synthesis of CdSe and CdSe/ZnS Quantum Dots with Tunable Crystal Structure and Photoluminescent Properties. *Nanomaterials 2022, Vol. 12, Page 2969* **2022**, *12* (17), 2969. https://doi.org/10.3390/NANO12172969.

(93) La Rosa, M.; Denisov, S. A.; Jonusauskas, G.; McClenaghan, N. D.; Credi, A. Designed Long-Lived Emission from CdSe Quantum Dots through Reversible Electronic Energy Transfer with a Surface-Bound Chromophore. *Angewandte Chemie International Edition* **2018**, *57* (12), 3104–3107. https://doi.org/10.1002/ANIE.201712403.

(94) Kempken, B.; Dzhagan, V.; Zahn, D. R. T.; Alcocer, M. J. P.; Kriegel, I.; Scotognella, F.; Parisi, J.; Kolny-Olesiak, J. Synthesis, Optical Properties, and Photochemical Activity of Zinc-Indium-Sulfide Nanoplates. *RSC Adv* **2015**, *5* (109), 89577–89585. https://doi.org/10.1039/C5RA20570K.

(95) Frederick, M. T.; Weiss, E. A. Relaxation of Exciton Confinement in CdSe Quantum Dots by Modification with a Conjugated Dithiocarbamate Ligand. *ACS Nano* **2010**, *4* (6), 3195–3200. https://doi.org/10.1021/nn1007435.

(96) Jin, S.; Harris, R. D.; Lau, B.; Aruda, K. O.; Amin, V. A.; Weiss, E. A. Enhanced Rate of Radiative Decay in Cdse Quantum Dots upon Adsorption of an Exciton-Delocalizing Ligand. *Nano Lett* **2014**, *14* (9), 5323–5328. https://doi.org/10.1021/nl5023699.

(97) Du Fossé, I.; Ten Brinck, S.; Infante, I.; Houtepen, A. J. Role of Surface Reduction in the Formation of Traps in N-Doped II-VI Semiconductor Nanocrystals: How to Charge without Reducing the Surface. *Chemistry of Materials* **2019**, *31* (12), 4575–4583. https://doi.org/10.1021/ACS.CHEMMATER.9B01395/ASSET/IMAGES/LARGE/CM-2019-013956_0004.JPEG.

(98) Li, S. L.; Jiang, P.; Hua, S.; Jiang, F. L.; Liu, Y. Near-Infrared Zn-Doped Cu2S Quantum Dots: An Ultrasmall Theranostic Agent for Tumor Cell Imaging and Chemodynamic Therapy. *Nanoscale* **2021**, *13* (6), 3673–3685. https://doi.org/10.1039/d0nr07537j.

(99) Mahler, B.; Spinicelli, P.; Buil, S.; Quelin, X.; Hermier, J. P.; Dubertret, B. Towards Non-Blinking Colloidal Quantum Dots. *Nat Mater* **2008**, *7* (8), 659–664. https://doi.org/10.1038/nmat2222.

(100) Gao, Y.; Peng, X. Photogenerated Excitons in Plain Core CdSe Nanocrystals with Unity Radiative Decay in Single Channel: The Effects of Surface and Ligands. *J Am Chem Soc* **2015**, *137* (12), 4230–4235. https://doi.org/10.1021/jacs.5b01314.

(101) Yadav, A. N.; Kumar, P.; Singh, K. Femtosecond Photoluminescence Up-Conversion Spectroscopy in Cu Doped CdS Quantum Dots. *Mater Lett* **2021**, *297*. https://doi.org/10.1016/j.matlet.2021.129925.

(102) De Trizio, L.; Prato, M.; Genovese, A.; Casu, A.; Povia, M.; Simonutti, R.; Alcocer, M. J. P.; D'Andrea, C.; Tassone, F.; Manna, L. Strongly Fluorescent Quaternary Cu-In-Zn-S Nanocrystals Prepared from Cu

1-XInS 2 Nanocrystals by Partial Cation Exchange. *Chemistry of Materials* **2012**, *24* (12), 2400–2406. https://doi.org/10.1021/cm301211e.

(103) Wang, H.; Song, D.; Zhou, Y.; Liu, J.; Zhu, A.; Long, F. Fluorescence Enhancement of CdSe/ZnS Quantum Dots Induced by Mercury Ions and Its Applications to the on-Site Sensitive Detection of Mercury Ions. *Microchimica Acta* **2021**, *188* (6), 1–9. https://doi.org/10.1007/S00604-021-04871-5/METRICS.

(104) De Trizio, L.; Manna, L. Forging Colloidal Nanostructures via Cation Exchange Reactions. *Chemical Reviews*. American Chemical Society September 28, 2016, pp 10852–10887. https://doi.org/10.1021/acs.chemrev.5b00739.

(105) Knowles, K. E.; Hartstein, K. H.; Kilburn, T. B.; Marchioro, A.; Nelson, H. D.; Whitham, P. J.; Gamelin, D. R. Luminescent Colloidal Semiconductor Nanocrystals Containing Copper: Synthesis, Photophysics, and Applications. *Chem Rev* **2016**, *116* (18), 10820–10851. https://doi.org/10.1021/ACS.CHEMREV.6B00048/ASSET/IMAGES/MEDIUM/CR-2016-00048H_0029.GIF.

(106) Dabbousi, B. O.; Rodriguez-Viejo, J.; Mikulec, F. V.; Heine, J. R.; Mattoussi, H.; Ober, R.; Jensen, K. F.; Bawendi, M. G. (CdSe)ZnS Core-Shell Quantum Dots: Synthesis and Characterization of a Size Series of Highly Luminescent Nanocrystallites. *Journal of Physical Chemistry B* **1997**, *101* (46), 9463–9475. https://doi.org/10.1021/jp971091y.

(107) Chen, X.; Lou, Y.; Samia, A. C.; Burda, C. Coherency Strain Effects on the Optical Response of Core/Shell Heteronanostructures. *Nano Lett* **2003**, *3* (6), 799–803. https://doi.org/10.1021/nl034243b.

(108) Smith, A. M.; Mohs, A. M.; Nie, S. Tuning the Optical and Electronic Properties of Colloidal Nanocrystals by Lattice Strain. *Nat Nanotechnol* **2009**, *4* (1), 56–63. https://doi.org/10.1038/nnano.2008.360.

(109) Pendyala, N. B.; Koteswara Rao, K. S. R. Efficient Hg and Ag Ion Detection with Luminescent PbS Quantum Dots Grown in Poly Vinyl Alcohol and Capped with Mercaptoethanol. *Colloids Surf A Physicochem Eng Asp* **2009**, *339* (1–3), 43–47. https://doi.org/10.1016/j.colsurfa.2009.01.013.

(110) Jaiswal, A.; Ghsoh, S. S.; Chattopadhyay, A. Quantum Dot Impregnated-Chitosan Film for Heavy Metal Ion Sensing and Removal. *Langmuir* **2012**, *28* (44), 15687–15696. https://doi.org/10.1021/la3027573.

(111) Vázquez-González, M.; Carrillo-Carrion, C. Analytical Strategies Based on Quantum Dots for Heavy Metal Ions Detection. *J Biomed Opt* **2014**, *19* (10), 101503. https://doi.org/10.1117/1.jbo.19.10.101503.

(112) Zhu, X.; Zhao, Z.; Chi, X.; Gao, J. Facile, Sensitive, and Ratiometric Detection of Mercuric Ions Using GSH-Capped Semiconductor Quantum Dots. *Analyst* **2013**, *138* (11), 3230–3237. https://doi.org/10.1039/c3an00011g.

(113) Liang, J. G.; Ai, X. P.; He, Z. K.; Pang, D. W. Functionalized CdSe Quantum Clots as Selective Silver Ion Chemodosimeter. *Analyst* **2004**, *129* (7), 619–622. https://doi.org/10.1039/b317044f.

(114) Zhu, C.; Li, L.; Fang, F.; Chen, J.; Wu, Y. Functional InP Nanocrystals as Novel Near-Infrared Fluorescent Sensors for Mercury Ions. *Chem Lett* **2005**, *34* (7), 898–899. https://doi.org/10.1246/cl.2005.898.

(115) Wang, H.; Song, D.; Zhou, Y.; Liu, J.; Zhu, A.; Long, F. Fluorescence Enhancement of CdSe/ZnS Quantum Dots Induced by Mercury Ions and Its Applications to the on-Site Sensitive Detection of Mercury Ions. https://doi.org/10.1007/s00604-021-04871-5/Published.

(116) Chern, M.; Nguyen, T. T.; Mahler, A. H.; Dennis, A. M. Shell Thickness Effects on Quantum Dot Brightness and Energy Transfer. *Nanoscale* **2017**, *9* (42), 16446–16458. https://doi.org/10.1039/c7nr04296e.

(117) Moore, D. E.; Patel, K. Q-CdS Photoluminescence Activation on Zn2+ and Cd2+ Salt Introduction. *Langmuir* **2001**, *17* (8), 2541–2544. https://doi.org/10.1021/la001416t.

(118) Shrivastava, A.; Gupta, V. Methods for the Determination of Limit of Detection and Limit of Quantitation of the Analytical Methods. *Chronicles of Young Scientists* **2011**, *2* (1), 21. https://doi.org/10.4103/2229-5186.79345.

(119) World Health Organization. *Guidelines for Drinking-Water Quality.*; World Health Organization, 2011.

(120) *U.S. EPA National Primary Drinking Water Regulations*.

(121) Paim, A. P. S.; Rodrigues, S. S. M.; Ribeiro, D. S. M.; De Souza, G. C. S.; Santos, J. L. M.; Araújo, A. N.; Amorim, C. G.; Teixeira-Neto, É.; Da Silva, V. L.; Montenegro, M. C. B. S. M. Fluorescence Probe for Mercury(II) Based on the Aqueous Synthesis of CdTe Quantum Dots Stabilized with 2-Mercaptoethanesulfonate. *New Journal of Chemistry* **2017**, *41* (9), 3265–3272. https://doi.org/10.1039/c6nj04032b.

(122) Kamat, P. V. *Photochemistry on Nonreactive and Reactive (Semiconductor) Surfaces*; 1993; Vol. 93.

(123) Mu, Q.; Li, Y.; Xu, H.; Ma, Y.; Zhu, W.; Zhong, X. Quantum Dots-Based Ratiometric Fluorescence Probe for Mercuric Ions in Biological Fluids. *Talanta* **2014**, *119*, 564–571. https://doi.org/10.1016/j.talanta.2013.11.036.

(124) Bear, J. C.; Hollingsworth, N.; Roffey, A.; Mcnaughter, P. D.; Mayes, A. G.; Macdonald, T. J.; Nann, T.; Ng, W. H.; Kenyon, A. J.; Hogarth, G.; Parkin, I. P. Doping Group IIB Metal Ions into Quantum Dot Shells via the One-Pot Decomposition of Metal-Dithiocarbamates. *Adv Opt Mater* **2015**, *3* (5), 704–712. https://doi.org/10.1002/adom.201400570.

(125) Wang, P.; Gao, Y.; Li, P.; Zhang, X.; Niu, H.; Zheng, Z. Doping Zn2+ in CuS Nanoflowers into Chemically Homogeneous Zn0.49Cu0.50S1.01 Superlattice Crystal Structure as High-Efficiency n-Type Photoelectric Semiconductors. *ACS Appl Mater Interfaces* **2016**, *8* (24), 15820–15827. https://doi.org/10.1021/acsami.6b04378.

(126) Hao, L.; Chen, X.; Liu, D.; Bian, Y.; Zhao, W.; Tang, K.; Zhang, R.; Zheng, Y.; Gu, S. Charge Transfer Dynamics of the CdTe Quantum Dots Fluorescence Quenching Induced by Ferrous (II) Ions. *Appl Phys Lett* **2020**, *116* (1). https://doi.org/10.1063/1.5129473.

(127) Yadav, A. N.; Kumar, P.; Singh, K. Femtosecond Photoluminescence Up-Conversion Spectroscopy in Cu Doped CdS Quantum Dots. *Mater Lett* **2021**, *297*. https://doi.org/10.1016/j.matlet.2021.129925.

(128) Liu, Y.; Tang, X.; Deng, M.; Zhu, T.; Edman, L.; Wang, J. Hydrophilic AgInZnS Quantum Dots as a Fluorescent Turn-on Probe for Cd^{2+} Detection. *J Alloys Compd* **2021**, *864*. https://doi.org/10.1016/j.jallcom.2020.158109.

(129) De Trizio, L.; Manna, L. Forging Colloidal Nanostructures via Cation Exchange Reactions. *Chemical Reviews*. American Chemical Society September 28, 2016, pp 10852–10887. https://doi.org/10.1021/acs.chemrev.5b00739.

(130) Wu, P.; Zhao, T.; Wang, S.; Hou, X. Semicondutor Quantum Dots-Based Metal Ion Probes. *Nanoscale* **2014**, *6* (1), 43–64. https://doi.org/10.1039/c3nr04628a.

(131) Prudnikau, A.; Artemyev, M.; Molinari, M.; Troyon, M.; Sukhanova, A.; Nabiev, I.; Baranov, A. V.; Cherevkov, S. A.; Fedorov, A. V. Chemical Substitution of Cd Ions by Hg in CdSe Nanorods and Nanodots: Spectroscopic and Structural Examination. *Mater Sci Eng B Solid State Mater Adv Technol* **2012**, *177* (10), 744–749. https://doi.org/10.1016/j.mseb.2011.12.038.

CHAPTER 3

EFFECT OF MERCURY IONS (Hg^{2+}) ON OPTICAL AND STRUCTURAL PROPERTIES OF CdSe/ZnS QUANTUM DOTS WITH SURFACE DITHIOCARBAMATE LIGANDS

ABSTRACT

The versatility in the surface of QDs is an excellent property because different ligands can coordinate to the surface and modify the structural and optical properties and their application.[1] The ligands capped on the surface of QDs can improve the physical properties, such as solubility in aqueous media, and affect their photoluminescence.[1]

The capping ligands can introduce favorable or unfavorable energy levels in the QDs and affect the photoluminescence. For example, the thiolated ligands generally act as hole traps due to the HOMO levels from the ligand being near the valence band (VB); when the QD is photoexcited, the ligand trapping the hole photogenerated and a delocalization of exciton is produced favoring the formation of new nonradiative centers and the photoluminescence is quenched.[2–4]

This Chapter shows the influence of two surface ligands on the structural and optical properties of CdSe-ZnS QD (QD-0.9 ML): 1) an aromatic dithiocarbamate (DTC) and 2) an aromatic dye ligand (Dye) capped to the surface of this QD. The QD-0.9 ML was selected because this QD has the highest QY calculated (Chapter 2). Both ligands were capped to the QD with a ligand exchange process, using a saturated solution of ligands (DTC and Dye) in methanol and a solution of QD in hexane at 60°C for 1 h (QD/DTC, 1/3). The ligand exchange produced a redshift in the maximum absorption and emission bands of new QDs: QDTC and QDTCDye.

The effect of two ligands on the structural properties of QDs was analyzed using different techniques, such as XRD to determine the crystallinity, HRTEM to calculate the size and crystallinity, and XPS and FT-IR to study the coordination of ligands on the surface of QD. The XRD patterns do not show significant changes in the diffraction peaks of QD; the crystallinity is maintained after the ligand exchange process. The HRTEM analysis showed an increase in the size of QDs from 3.2 nm to 3.4 nm and 3.7 nm for QDTC and QDTCDye, respectively. There are no significant changes in the d-spacing factor. The crystallinity is conserved, confirming the XRD analysis. The FT-IR analysis showed the coordination of DTC by the CSS^- group due to the band at 1000 cm^{-1} disappearing and the Dye ligand being coordinated by both carboxylates in their structure because the band at 1707 cm^{-1} corresponding to the C=O bonds of the carboxylic acids is not observed confirming the capping. XPS measurements showed new peaks in C1s and O1s due to the apparition of new bonds such as C-N and C-OH. Furthermore, in Zn2p and Cd3d, the peaks were deconvoluted in several components, indicating the presence of different species of Zn and Cd coordinated with the capped ligands. The structural characterization showed the coordination of ligands on the surface of QDs.

Consequently, the effect of capped ligands on QDs and their optical properties, such as absorption, emission, and time-resolved photoluminescence, were studied. The coordination of DTC ligands

produces a quenching of fluorescence. The HOMO orbital of DTC is overlapped with the orbital from the valence band (VB), trapping the photogenerated hole, delocalizing the excitonic recombination and photoluminescence decrease. The DTC ligand is a hole trap affecting the photoluminescence properties of QD, such as QY. However, the Dye ligand produces a slight improvement in this optical property, and the photoluminescence increases with the coordination of the Dye ligand, passivating the hole trap action produced by DTC ligand. The QY improves with the coordination of the Dye ligand.

The Hg^{2+} ion sensing analysis was developed using a solution of QDTC and QDTCDye in ethanol as solvent and aqueous solutions of Hg^{2+} ions from 0.5-5.0 μM. The absorption and emission changes were analyzed with UV-Vis, fluorescence, and time-resolved photoluminescence spectroscopies. Adding Hg^{2+} ions to the QDTC and QDTCDye increases their emission due to the formation of HgS particles on the ZnS shell of QDs passivating the traps produced by the DTC ligand. These HgS particles are produced on the ZnS surface due to the cation exchange reaction because the Ksp of HgS is lower than the Ksp of ZnS, favoring this reaction.[5] The behavior of QDTCDye with the addition of different concentrations of Hg^{2+} ions is ratiometric. The detection limit (LOD) of QDTC and QDTCDye was determined using fluorescence intensity response as a function of different concentrations of Hg^{2+} ions. The LOD was calculated as 3.7 nM and 4.4 nm for QDTC and QDTCDye, respectively. These LOD obtained are lower than other similar QDs systems compared and the values reported by WHO and EPA institutions.

Finally, the analysis with other transition metal ions was developed with the same form explained in Chapter 2. All the transition metal ions evaluated enhance the photoluminescence in QDTC and QDTCDye. However, Hg^{2+} produces the highest increase in fluorescence intensity in QDTC. Photoluminescence enhancement indicates the passivation of traps on the surface of QD. The enhancement phenomenon, sensitivity (low LOD), and selectivity demonstrated that these materials are promising to apply in Hg^{2+} ions sensing.

3.1 Introduction

The QDs have interesting characteristics, such as a high surface/volume ratio, i.e., a high population of atoms on the surface,[6] which can bind many molecules.[1] Consequently, it is possible to modify organic ligands on the surface, which can be attached to the surface by chemisorption or by simple physical adsorption on the surface.[6] The ligands attached to the surface can improve the solubility in aqueous media and increase or decrease their photoluminescence properties. Thus the ligands can facilitate application depending on the study objective.

The properties of QDs are related to the quantum confinement effect when the size is smaller than the Bohr radius.[7–9] In addition, the confinement energy level of QDs can be finely tuned by ligand exchange. In some cases the capping ligands can introduce unfavorable HOMO-LUMO levels that affect the fluorescence emission; [10] these delocalized molecular orbitals can reduce excitons quantum confinement energy level.[11–14]

The interaction of ligands with the surface of QDs depends on ligand and quantum dot surface structure. Ligands can bind to the surface of QDs in different geometries.[15] This binding geometry can produce different electronic properties of QDs.[15–17] There is a bond classification described by Green;[18] the ligands can be classified as L-type, X-type, and Z-type. L-type ligands are two-electron donors (Lewis bases) and form dative covalent bonds with neutral surface metal sites, such as amines, phosphines, and thiols. X-type one electron-donor can bind covalently with inorganic ions, for example, anions. Finally, Z-type ligands are two-electron acceptors (Lewis acids), which is equivalent to MX_n, M= metal; these ligands can bind to neutral surface sites; some examples of Z-type ligands include lead chloride and cadmium stearate or cations (M^{n+}) in general, that terminate the semiconductor lattice and coordinates *n* X-type ligand.[15] These features are significant and can affect the optoelectronic properties of QDs.

The fluorescence QY is also strongly affected by the nature of the ligands used; for example, QDs synthesized with TOPO/TOP mixtures had lower QYs (<0.20), while the QDs synthesized with HDA/TOP/TOPO had a high value in QY (around 0.80).[19] The photoluminescence QY can be strongly quenched or enhanced depending on the ligand type. For example, the alkyl-amines can increase the photoluminescence,[20] while the thiols or dithiocarbamate groups can decrease this optical property.[2,14,21,22]

The ligand exchange process is the most used to obtain QDs with different ligands and a wide variety of applications; this process consists of substituting native ligands on QDs (OA, TOP) with other ligands. A condition for ligand exchange to function efficiently, the incoming ligand must have a higher chemical affinity to the surface of the QDs than the ligand to be exchanged. The partial or complete exchange usually requires an excess of the incoming ligand [23] to favor the equilibrium adsorption of the incoming ligand on the surface of the QDs and the desorption of the ligand to be exchanged. The exchange reaction

occurs rapidly at room temperature or with moderate heating below 100 °C. The ligand exchange reaction must be followed using different analytical techniques to determine the appropriate conditions, such as NMR, UV-Vis, photoluminescence, and FT-IR.

A frequent negative consequence of ligand exchange is a substantial reduction in the photoluminescence of QDs; some reports have shown photoluminescence quenching due to ligand coordination.[24] This situation is due to the formation of surface trap states,[25,26] and in the case of some molecules, such as thiols, it is due to hole trapping of the valence band of QDs by the ligand.[27]

This Chapter explains the effect of two ligands on the structural and optical properties, 1) phenyl-dithiocarbamate ligand (DTC) capped to CdSe-ZnS QDs and 2) phenyl-dithiocarbamate (DTC) and Dye ligand capped to CdSe-ZnS QDs and the effect of Hg^{2+} ions on these functionalized QDs. In this Chapter, the synthesis of the ligand exchange used is described, and the structural and optical properties of these functionalized QD are discussed based on XRD, FT-IR, XPS, HR-TEM, UV-Vis, photoluminescence spectroscopy (fluorescence and lifetime measurements) analysis before and after the addition of Hg^{2+} ions (Z-type ligand). These methods reveal that the ligand exchange is affecting the structural (for example, the size is increasing) and optical properties (QY and photoluminescence are decreasing) due to the hole traps produced by the DTC ligand. Furthermore, as the Dye ligand, $Hg^{2+,}$ and metal ions are passivating the surface traps (HgS particles formed on the surface) produced by the DTC ligand due to the improved photoluminescence properties.

3.2 Methodology

3.2.1 Ligand exchange reaction

The DTC and Dye ligands were synthesized in multi-step syntheses, explained in Chapter 6. A solution of QDs (5mg) in 2 mL of hexane and mixed with DTC and Dye (15 mg, respectively) in 2 mL MeOH was stirred at 60 °C for 1 h. The UV-vis and FL spectra were recorded for 4h to determine the ideal time of the ligand exchange. After this time, the reaction mixture was cooled to room temperature, a precipitate was formed, and the solution was centrifuged and washed with methanol (three times) to remove the excess unbound ligands (DTC and Dye). The sample was dried overnight before use in the following steps.

3.2.2 Characterization

3.2.2.1 Structural

Panalytical X'Pert3 Pro-Multipurpose Diffractometer with CuKα radiation source (45 kV and 40 mA) was employed to measure the powder XRD patterns. The diffraction dataset cards from the Joint Committee of Powders Diffraction Standards (JCPDS) were used to compare the obtained patterns. The FT-IR spectra were taken in a Thermo Scientific Nicolet iS10 spectrometer. XPS experiments were performed with the A Centeno-XPS/ISS/UPS surface characterization platform built by SPECS (Germany), and the employed experimental parameters were previously reported.[28] CasaXPS program (Casa Software Ltd) for data analysis and the SPECS Prodigy library for RSF values were used. The High-Resolution Transmission Electron Microscopy (HR-TEM) images of the QDs were taken using a Tecnai F20 Super Twin TMP Microscope. A drop of the sample was deposited on a carbon film grid; then, the sample was dried and analyzed in the transmission microscope using 450.000 x magnification. Image-J software was used to calculate the average diameter and d-spacing [111] of QDs with HR-TEM micrographs.

3.2.2.2 Optical

A Varian UV-Vis-NIR spectrophotometer Cary 5000 was used to obtain the UV-Vis absorption spectra and a HORIBA Jobin-Yvon Fluorolog-3 spectrophotometer was used for PL measurements. The PL QY (ϕ) of QDTC and QDTCDye (dissolved in ethanol) was calculated using Rhodamine 6 G in ethanol solution as standard (ϕ = 0.94), with excitation wavelength (λ_{ex}) at 500 nm. The quantification of PL QY and Hg^{2+} - other metal ions sensing assay are explained in detail in Chapter 6.

3.3 QD ligand exchange with DTC and Dye ligands

Figure 27a-b shows the QDs-Ligands systems studied. The DTC ligands can displace the native hydrophobic ligands (OA and TOP) from the QD surface during the ligand exchange process.[29,30] The synthesis of DTC was synthesized with carbon disulfide (CS_2), triethylamine (base), and amine precursor (aromatic amine previously prepared (**Figure 42 Chapter 6**) dissolved in tetrahydrofuran (THF) as solvent at room temperature. [31] DTC ligands were formed immediately after the reaction with CS_2, triethylamine, and amine precursor, and the mixture was left for 12 hours to complete the reaction.

The Dye ligand was prepared via a multi-step synthesis (**Figure 43 Chapter 6**). The reaction progress of both ligands was monitored via ^{1}H-NMR. DTC shows a characteristic UV absorption peak at 273 nm and an emission band at 364 nm, while the Dye ligand has two absorption bands at 260 nm and 281 nm and an emission band at 524 nm, as shown in **Figure 27c**. These values correspond with the characteristic of the π-π* electronic transition in the aromatic compounds.[32]

The ligand exchange was performed using the CdSe-ZnS core-shell QDs with the highest quantum yield (QD-0.9 ML, QY= 0.54) with two ligands: an aryl dithiocarbamate (QDTC) and an aromatic dye (QDTCDye) (**Figure 27a-b**). The ligand exchange reaction was developed using a solution of DTC and Dye in methanol and QDs in hexane (1:1) as a solvent mixture, heating at 60 °C. The reaction was followed using UV-Vis and fluorescence each hour for 5 h (**Figure 27d-e)**. After the optimization of reaction conditions, i.e., 1 hour is enough time to obtain the ligand exchange successfully, the reaction was cooled at room temperature, and a precipitate was formed. The sample was washed with methanol three times and centrifuged to remove the excess free DTC and Dye ligands.

The bidentate coordination of dithiocarbamates to metal ions results in a bathochromic shift of the band corresponding to the π-π* transition in the aromatic ring compared to the same band in the corresponding carbodithioic acid.[33] In the case of QDTC, in the first hour, we observed a red-shift in absorption spectra from 564 nm to 570 nm and emission spectra from 578 nm to 590 nm; this red-shift was constant for 5 h. In QDTCDye, a red-shift was observed from 564 nm to 572 nm, and a new absorption band appeared at 434 nm; this band is from the Dye (λ_{abs} = 436 nm), and fluorescence emission shows a red-shift also from 578 nm to 590 nm. Furthermore, a new emission band appeared at 520 nm. The appearance of a red-shifted absorption band and a new band in absorption and emission spectra is an indication that the ligands bind to the surface of QD.[34–36]

Furthermore, monitoring the ligand exchange reaction in QDTC shows a red-shift and quenching of the fluorescence intensity (**Figure 27d**) of the new nanomaterial formed as a function of reaction time. This quenching mechanism can be produced through different non-radiative pathways, such as electron/hole transfer from the QD to the DTC ligand.[2,37] In addition, aryl-dithiocarbamate ligand (DTC), containing an aromatic ring adjacent to the anchor group, can efficiently quench the photoluminescence of QDs.[29]

QDTCDye fluorescence of QD is successively quenched, and the Dye fluorescence increased (**Figure 27e**), indicating a possible energy transfer in the QD-Dye system.[38] A ligand exchange between DTC and Dye could be associated with the partial passivation of hole traps by Dye ligand due to the carboxylate ion has more affinity to the Zn^{2+} from shell than DTC (HSAB Theory) [5] and the coordination is favored, i.e., the Dye ligand is replacement of DTC ligand in some sites to improve the luminescence of QD, this is a signal of complex formation with the Zn^{2+} ions of the surface.[38]

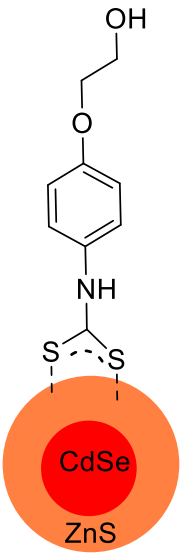

a)

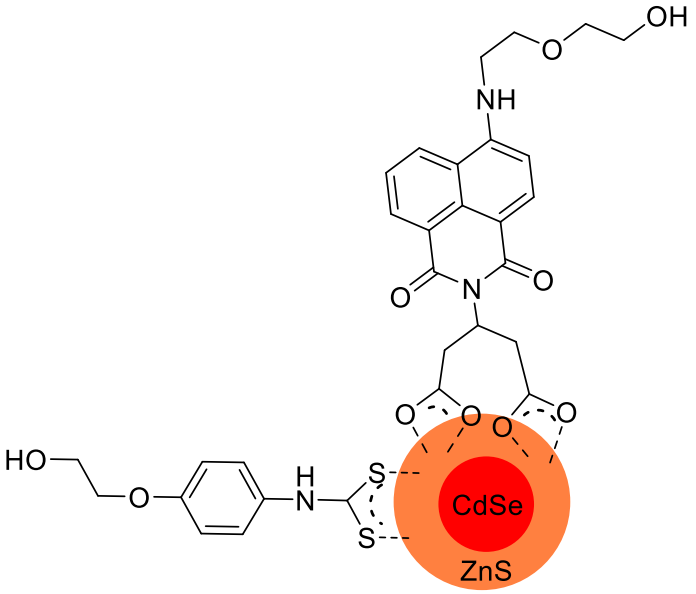

b)

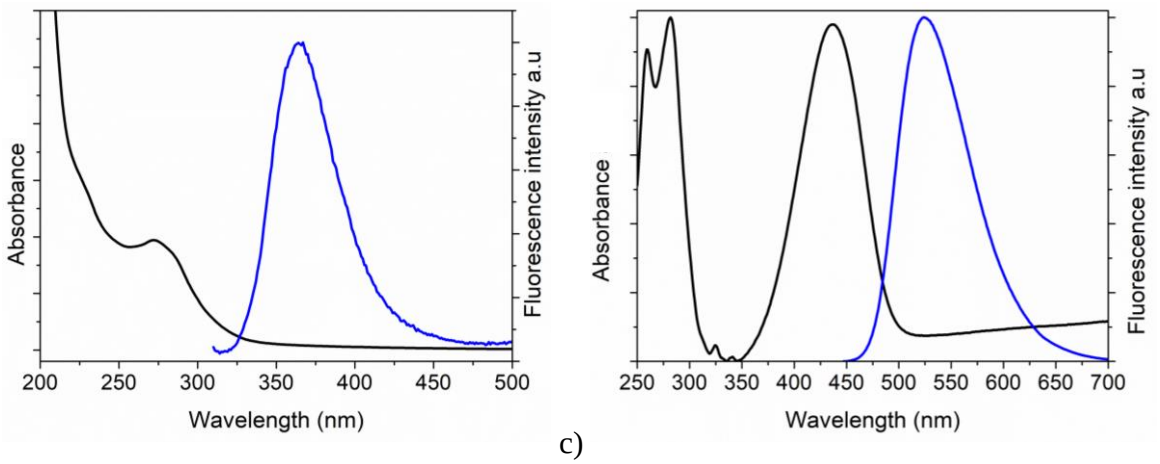

c)

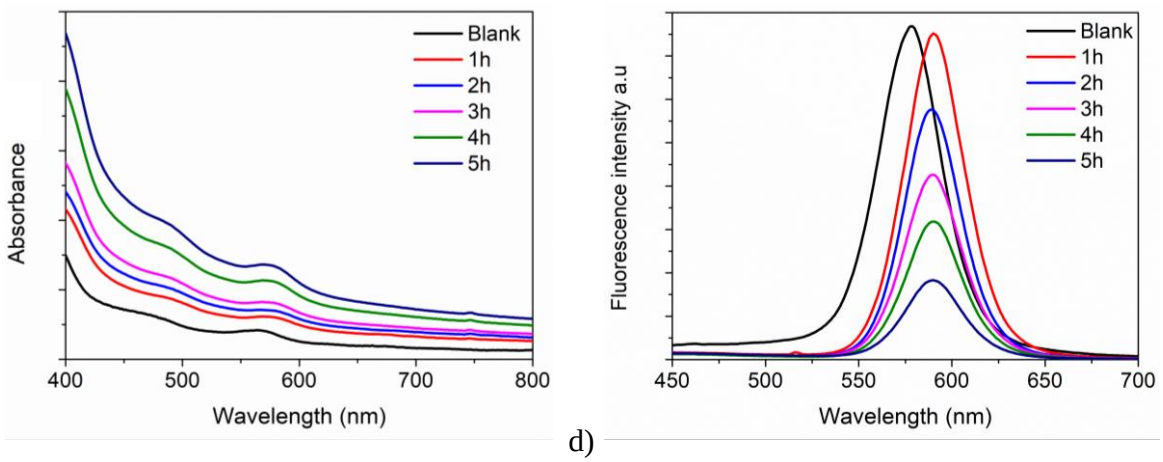

d)

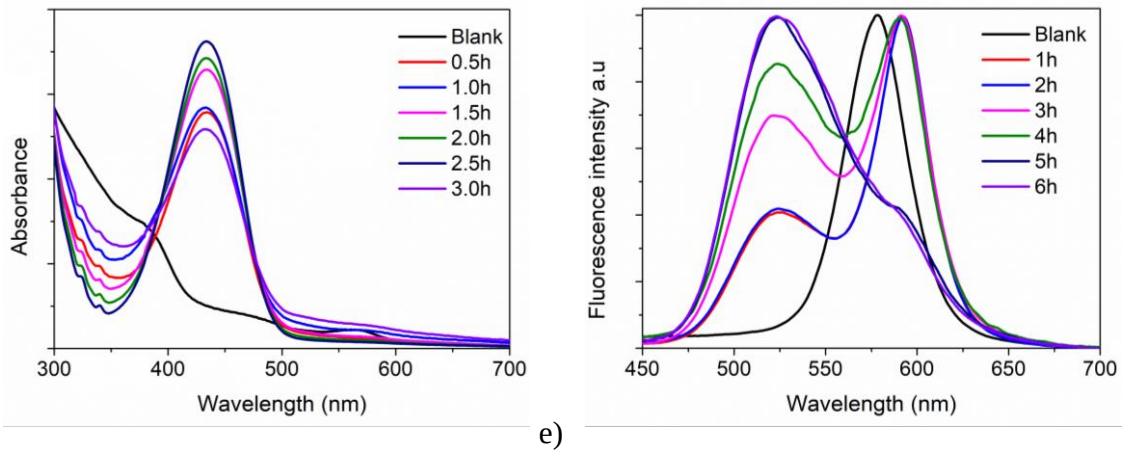

e)

Figure 27. QDs-Ligands systems a) QDTC; b) QDTCDye. Absorption and fluorescence spectra of c) DTC and Dye ligand ; d) QDTC, and e) QDTCDye as a function of time during the ligand exchange process. Solvent: ethanol. λ_{exc}: 436 nm, 270 nm, 380 nm for Dye, DTC, QDTC, and QDTCDye respectively.

3.4 Structural properties

To investigate the effect of ligand exchange with DTC and Dye on the surface of QD-0.9 ML, particle size and crystallinity, XRD patterns, FT-IR, XPS and HR-TEM image analyses were performed.

3.4.1 XRD analysis

Figure 28 shows the XRD profiles of QD-0.9 ML, QDDTC, and QDTCDye. All XRD patterns have (111), (220), and (311) peaks corresponding with the cubic zinc blende structure of the bulk CdSe (JCPDS file No. 88-2346). After the ligand exchange process, the relative intensity of each peak did not change significantly, suggesting that the crystallinity is unaffected by the ligand exchange process.

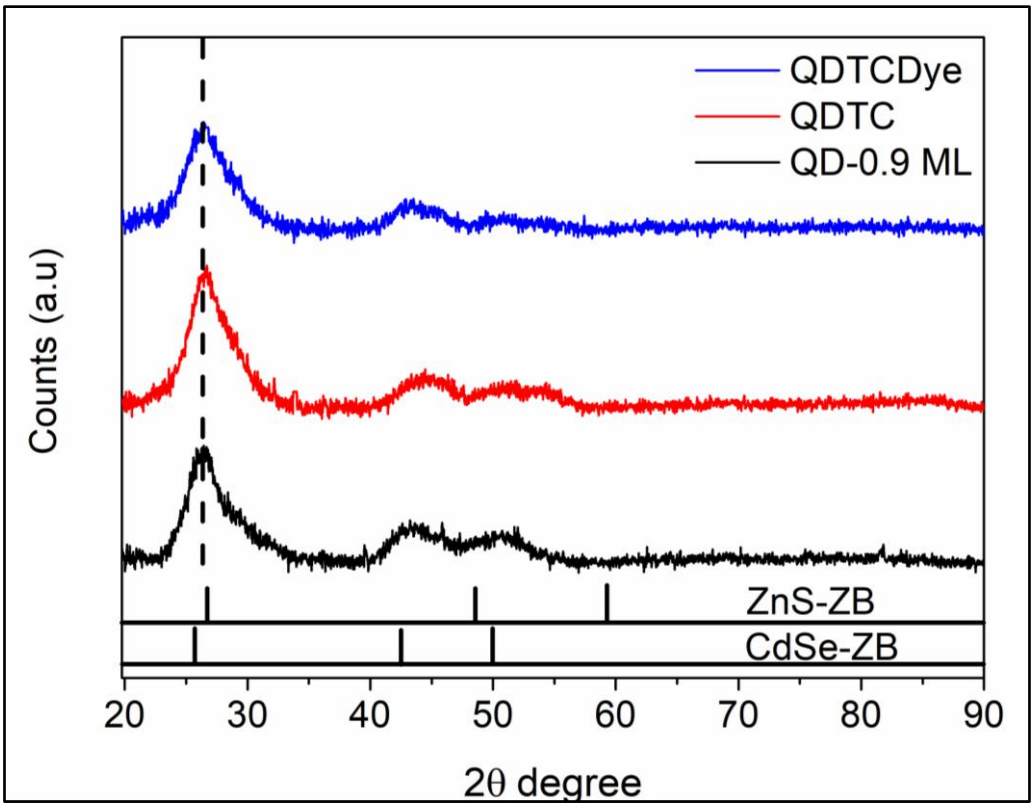

Figure 28. XRD patterns of QD-0.9 ML, QDTC, and QDTCDye.

3.4.2 HRTEM analysis

The particle size of QDs was determined with the HRTEM micrographs (**Figure 29**). The size of QDTC and QDTCDye were not considerably affected by the capping process, QDTC: 3.4±0.0018 nm and QDTCDye: approximately 3.6±0.0024 nm. These micrographs show monodisperse and non-aggregated QDs; the structural lattice is preserved during the ligand exchange reaction.

The interplanar distances (d-spacing) were calculated using FFT with ImageJ software (**Figure 65, Annexes**). The d-spacing values are 0.311 nm (QDTC) and 0.303 nm (QDTCDye). These values can be indexed to the [111] lattice plane reflection of the ZnS (zinc blende) cubic (JCPDS 05-0566) phase.[39] These results confirm crystallinity is not affected during the ligand exchange process.

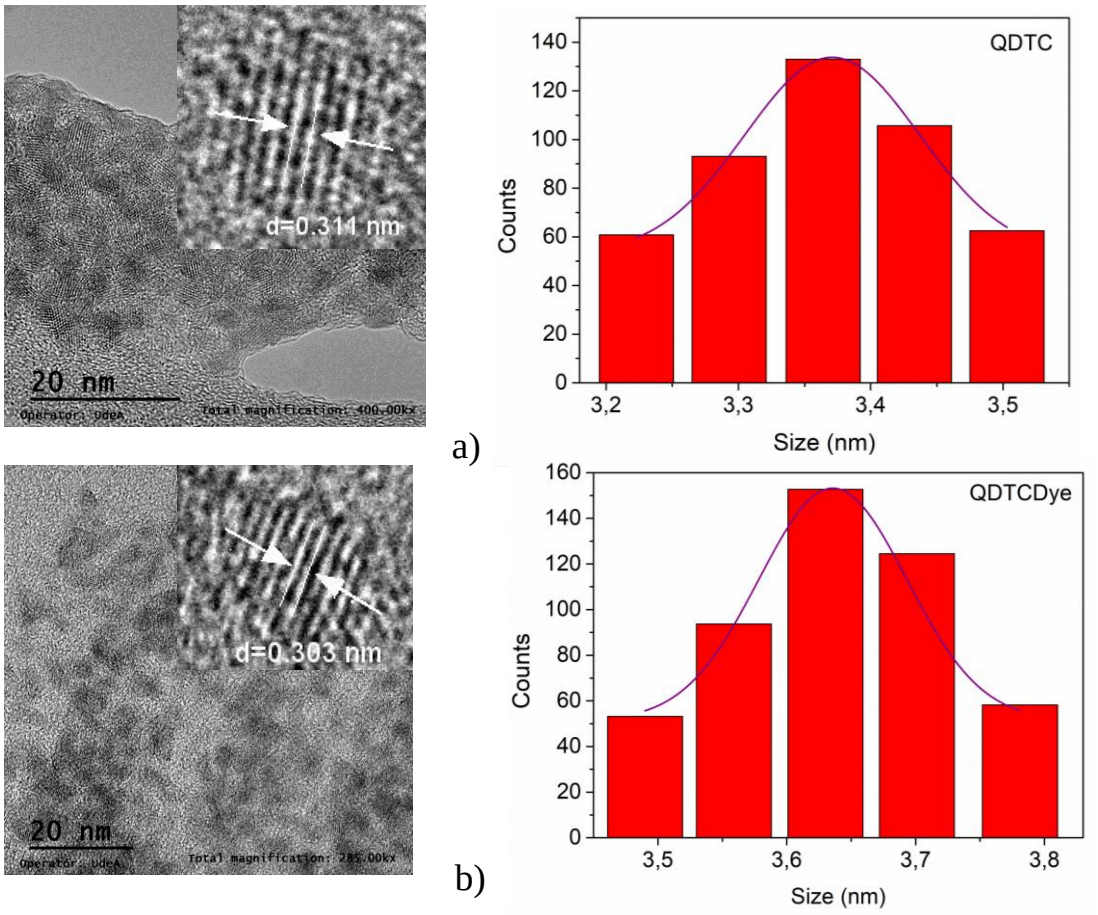

Figure 29. HRTEM measurements, micrographs, and histograms size of a) QDTC and b) QDTCDye.

3.4.3 FT-IR analysis

DTC and Dye ligand-capped CdSe-ZnS QDs were examined by recording their 4000-600 cm^{-1} FTIR spectra. Since the DTC ligands have two sulfur atoms to bind to the surface of the CdSe-ZnS QDs, the DTC group can bind in a bidentate or a monodentate coordination mode.

Figure 30 shows the FT-IR spectra of the dithiocarbamate DTC and Dye before and after the ligand exchange with QD-0.9 ML. **Figure 30a** shows the DTC and QD. The broad peak at 3404 cm^{-1} was assigned to the N-H stretching vibration.[40] The weak bands at 2920 and 2868 cm^{-1} were the characteristic peaks of the C-H and -CH_2- groups, respectively. The band at 1604 cm^{-1} may be assigned to the vibration of C=C of the aromatic ring. The strong band around 1512 cm^{-1} corresponds to the stretching of C-N of NCS_2. The band at 1010 cm^{-1} corresponds to the C-S vibration stretching. [41]

Comparing the FT-IR spectra after ligand exchange (QDTC), it can be seen that new peaks are present, which correspond to stretching vibrations C=C in aromatic compounds at 1608 cm^{-1}, C-N bonds at 1512 cm^{-1}; however, the bands at 1010 cm^{-1} assigned to the C-S stretching vibration are absent. These results indicate the coordination of DTC ligand to the surface of QD. [42,43]

Ligand exchange involving QD-0.9 ML, Dye, and DTC to form QDTCDye is shown in **Figure 30b**. The free dye spectrum shows the bands at 3363 cm^{-1} corresponding to N-H stretching for a secondary amine. A broad band at 2929 cm^{-1} corresponds to the -OH stretching in carboxylic acids, a strong band at 1707 cm^{-1} (stretching C=O) of the carboxylic acid, two strong bands at 1645 and 1585 cm^{-1} corresponding to the stretching of C=C bonds in aromatic compounds, a band at 1238 cm^{-1} for the C-O stretching in alkyl-aryl ethers, the band at 1105 cm^{-1} is associated to C-O in alkyl-alkyl ether in the chain, a band at 1050 cm^{-1} for the group C-O stretching in primary alcohol, and finally a strong band at 765 cm^{-1} corresponding to the C-H bond in aromatic compounds.

In the QDTCDye case, the spectra show two bands at 2925 cm^{-1} (asymmetric νCH_2) and 2851 cm^{-1} (symmetric νCH_2) from the alkyl chains in Dye and DTC. The band at 1707 cm^{-1} corresponding to the C=O bonds of the carboxylic acids is not observed, confirming the capping. In addition, two bands from the carboxylate ion are found between 1540 cm^{-1} (asymmetric stretching) and 1460 cm^{-1} (symmetric stretching), the separation between both bands indicate a bidentate coordination, confirming the capping. The band at 1240 cm^{-1} indicates C-O stretching vibration in acetates. The band at 1010 cm^{-1} is absent, confirming the DTC capped on the QD surface, indicating a successful ligand exchange.

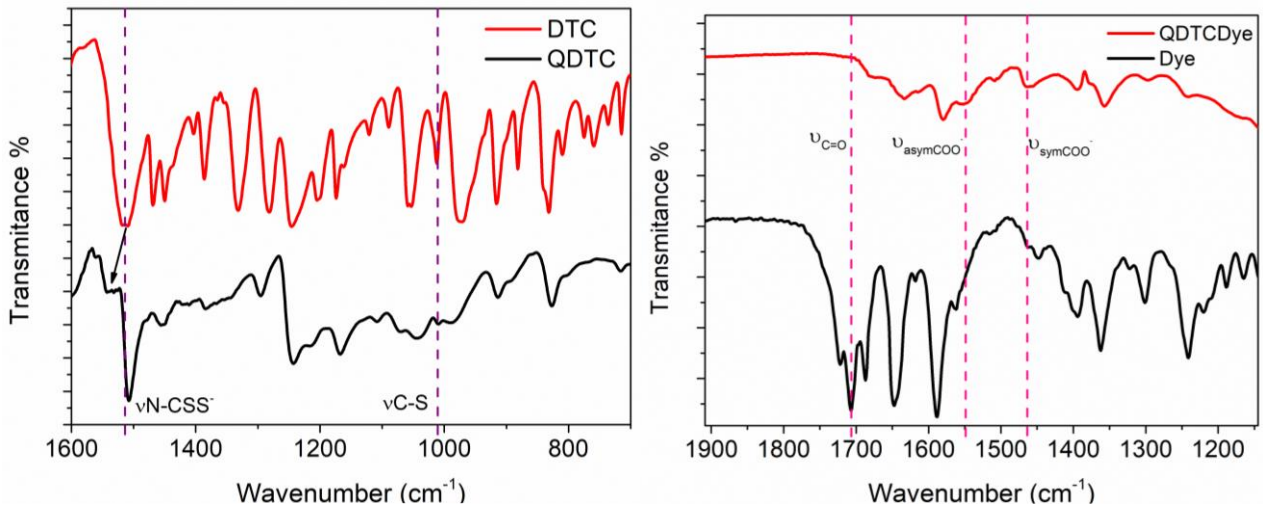

a) b)

Figure 30. FT-IR spectra of a) QDTC and b) QDTCDye.

3.4.4 XPS analysis

High-resolution XPS spectra were used to study the surface chemistry of DTC ligand-capped CdSe-ZnS QDs (**Figure 31**). The C1s peak (**Figure 31A**) of QDTC was deconvoluted into three components associated with the C-N bond from dithiocarbamate ligand (DTC) at 286.58 eV,[44,45] C-C bond at 284. eV from alkyl chain in the ligand structure and C=C bond from the aromatic ring at 283.18 eV.[46–49] However, the C1s spectra of QDTCDye (**Figure 31A**) also was deconvoluted into three components associated with C-N at 285.81 eV,[44,45,50] C-C bond at 284.02 eV from alkyl chain in the ligand structure and C=C bond from the aromatic ring at 282.72 eV.[46–49] The binding energy of these bonds shows a slight shift to lower binding energies due to the surrounding environment on the surface created by both ligands (DTC and Dye).

The O1s peak (**Figure 31B**) of QDTC was deconvoluted onto two components of hydroxyl group -CH_2-OH from DTC at 533.07 eV [51] and the signal at 531.19 eV attributed to the C-O bond. The DTC is capped on the surface of QD. Similarly, the O1s peak in QDTCDye (**Figure 31B**) was deconvoluted into two components at 530.44 eV associated with the C=O bond and 531.74 eV of the carboxylate bond (C-O) from the dye ligand.[51–54] DTC and Dye ligand is capped on the surface of QD.

The Cd3d peaks (**Figure 31C**) in QDTC and QDTC show a characteristic doublet at 405.50 eV and 412.23 eV for $Cd3d_{5/2}$ and $Cd3d_{3/2}$, respectively. [52] However, both QD systems show shoulders at low energies observed for Cd $3d_{5/2}$ and $Cd3d_{3/2}$ appearing at 403.9 eV and 410.5 eV, respectively, which is possible to associate with the beam damage of the QD surface, indicating their lower stability under such X-ray irradiation.[55] In addition, the exact interpretation of Cd $3d_{5/2}$ peaks in similar materials is complicated because the signals of CdS, CdO, and other cadmium species are generally poorly resolved.[55] The peak at 399.65 corresponds to the N1s of the C-N bond from the DTC ligand.[47,56] This implies their surface states are different between them.

Figure 31D shows the Se3d asymmetric broad peak that can be fit in two components at 53.92 eV and 52.73 eV for $Se3d_{5/2}$ and $Se3d_{3/2}$, respectively.[57] It Is possible to observe the signal of Se3d due to the shell being fragile and not covering all the core.

The Zn2ps spin-orbit splitting is shown in **Figure 31E**. These spectra show two signals at 1024.21 eV and 1047.23 eV for $Zn2p_{3/2}$ and $Zn2p_{1/2}$, respectively.[58] These binding energy values are not affected by the ligand exchange. The difference in the two peaks was $\Delta Zn2p = Zn\ 2p_{1/2} - Zn\ 2p_{3/2} = 23.02$ eV corresponding to the oxidation state 2+,[59] confirming the Zn–S bond from the shell in QD. After ligand exchange, the binding energy reveals a slight shift from 1023.4 to 1021.1 eV and from 1046.2 to 1041.4 eV for $Zn2p_{3/2}$ and $Zn2p_{1/2}$ lines, respectively, indicating that the environment of Zn^{2+} at the surface was changed after surface modification.[60]

Finally, the S2p peak (**Figure 31F**) showed a noisy signal which was deconvoluted into two components at 161.34 eV ($S2p_{1/2}$) associated with the S^{2-} of the C-S bond from DTC ligand,[61] the $S2p_{3/2}$ corresponds to 152.63 eV due to the lower binding energy of -C=S bond from DTC ligand,[46,62] the S2p do not show significant energy binding shifts between QDTC and QDTCDye systems.

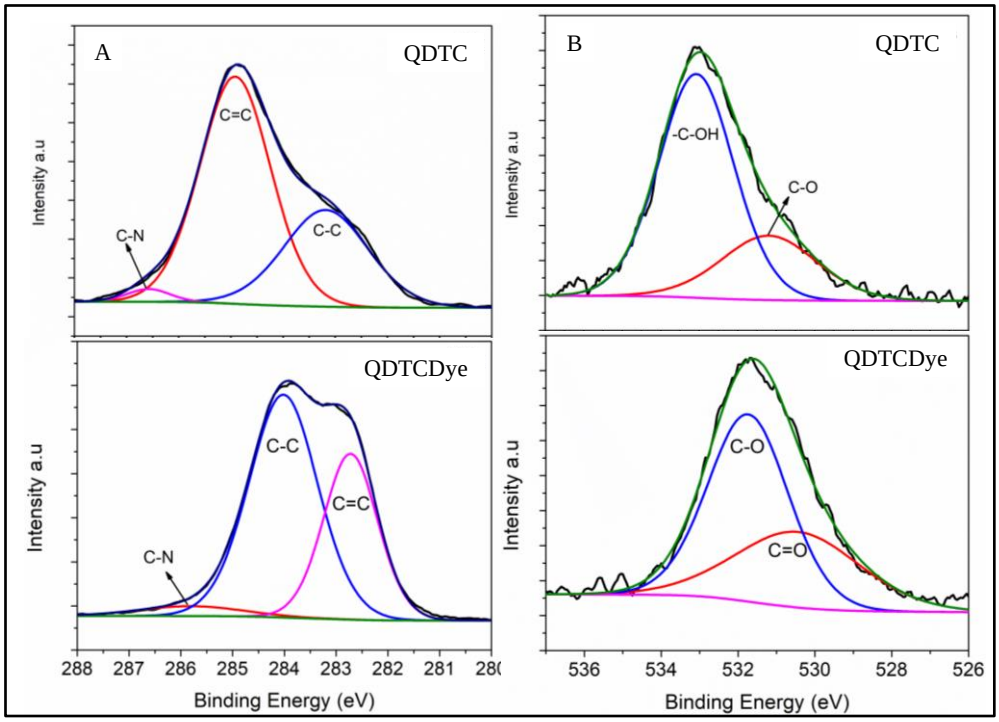

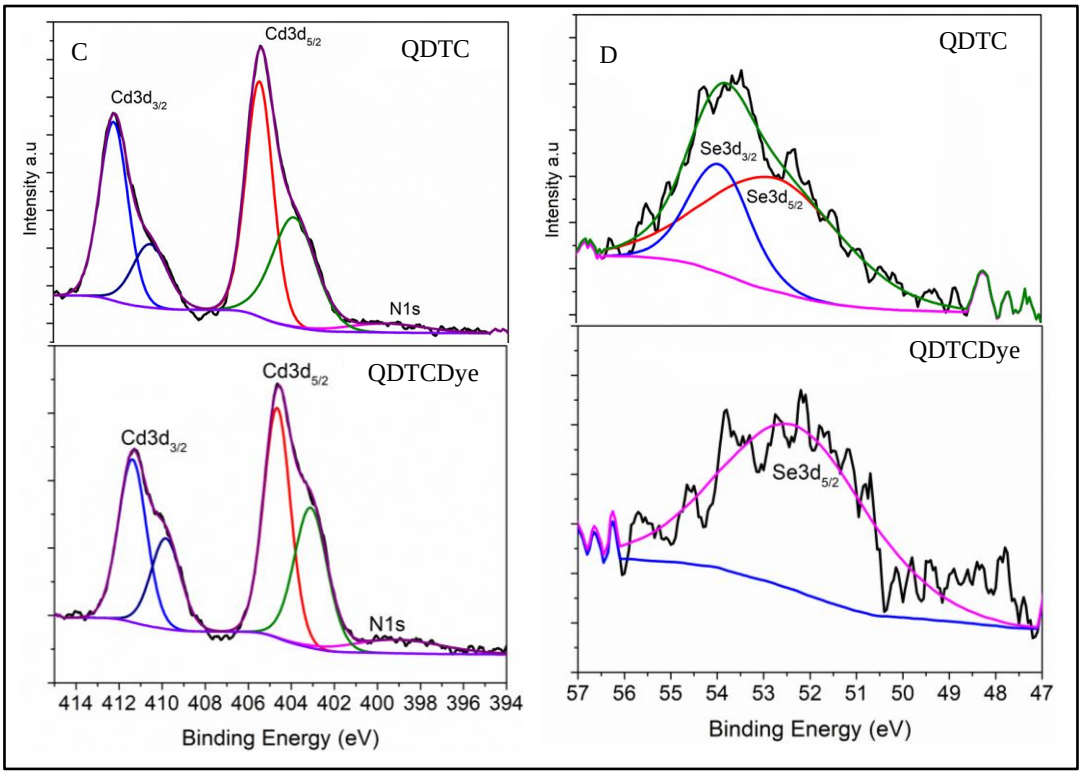

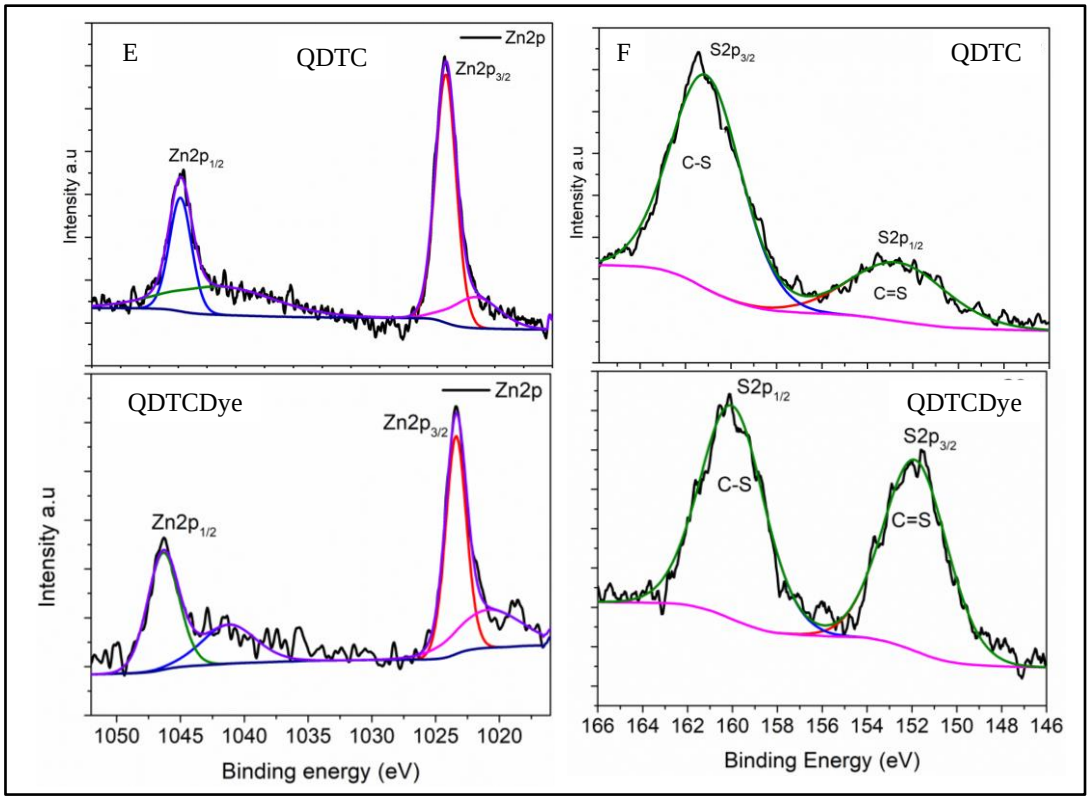

Figure 31. XPS spectra of QDTC and QDTCDye QDs, a) C1s ; b) O1s ; c) Se3d ; d) Cd3d+N1s ; e) Zn2p and f) S2p.

3.5 Optical properties

3.5.1 Absorption and fluorescence analysis

The absorption and fluorescence spectra of QDs after ligand exchange (QDTC and QDTCDye) are shown in **Figure 32**. A red-shift was observed on the QDTC and QDTC-Dye conjugates concerning QD-0.9 ML. QDTC-Dye shows a second absorption peak at 434 nm attributed to the Dye ligand. Fluorescence spectra show a red-shift at 590 nm and 520-590 nm for QDTC and QDTC-Dye, respectively. The exciton (e^-/h^+ pair) delocalizes to the DTC ligand region.[14,63] The delocalized molecular orbital characteristics of the phenyl group of DTC ligand widen the area where electrons and holes can move.[64] Some studies have shown that the HOMO orbital of DTC is near-resonant with that of the QD. Both orbitals have correct symmetry to exchange electron density (DTC is a π-donor, and the photoexcited QD is a π-acceptor),[2,3] thus both orbital are overlapped (HOMO orbital from DTC and valence band (VB) from QD),[2] this behavior produces an exciton-delocalization and an energetic stabilization of the first few excited states of the QD is produced,[2,3] and a the bathochromic shift is shown.

The full width at half maximum (FWHM) of fluorescence peaks maintained the same in (QD-0.9 ML is 34 nm and 35 nm for QDTC and QDTC-Dye). This property was not affected by the ligand exchange process.

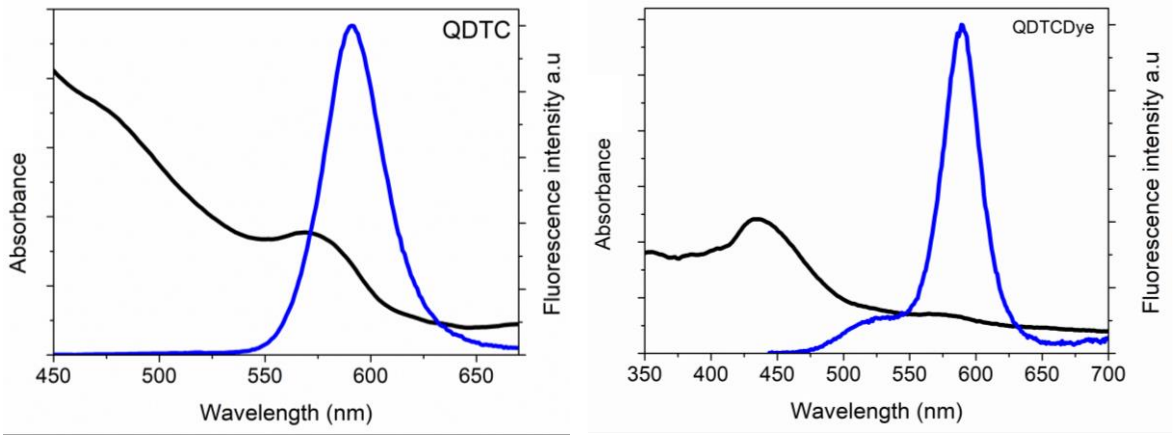

Figure 32. Absorption (λ_{max} *abs* red line) and emission (λ_{max} *ems* blue line) spectra of QDTC and QDTCDye. Solvent: ethanol. λ_{exc}: 380 nm.

3.5.2 Optical bandgap analysis

QDTC and QDTCDye have a smaller bandgap energy than QD-0.9 ML (QD precursor) (**Figure 33** and **Table 7**) due to the increase of size during the ligand exchange process (quantum confinement effect).[11,66,67] This increase is congruent with the size calculated from HRTEM analysis. Furthermore, this decrease of the band gap of QDs may be due to the stabilization of the excitonic state by the delocalization of the excitonic hole (h^+) onto new available interfacial states formed with the coordination of DTC ligands to Cd^{2+}, Pb^{2+} or in this case Zn^{2+} ions on the surface of QDs.[2,3,68]

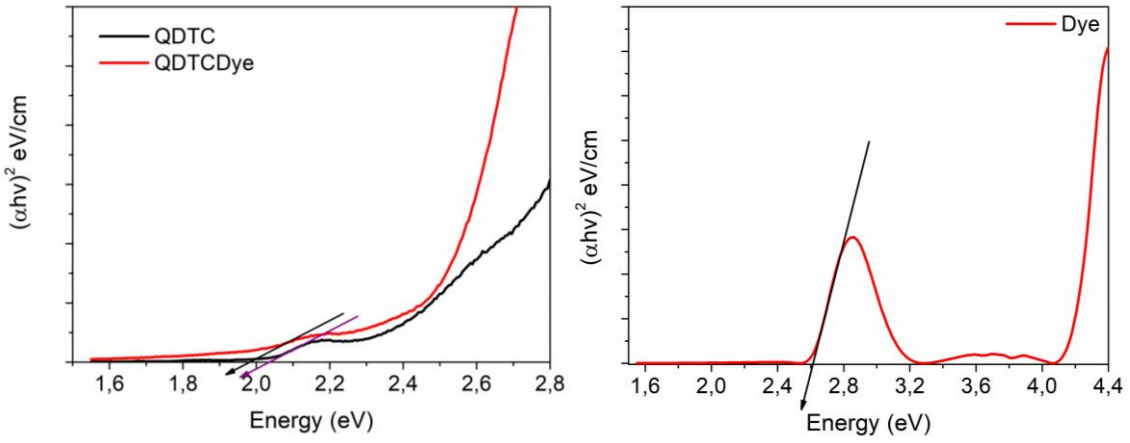

Figure 33. Tauc plot for QDs-L: QDTC, QDTCDye, and Dye.

The QY of QDs after the surface ligand exchange process showed a significant decrease, from QD-0.9 ML shows a QY= 0.53 (53%), QDTC and QDTCDye shows QY=0.06 (6 %) and QY= 0.11 (11%), respectively (**Table 9**). The low QY is correlated with the excess of DTC used during ligand exchange (QD/DTC: 1/3), in this case, the DTC ligand is a hole trap, and the excess of DTC ligand produces an exciton delocalization and favors the nonradiative recombination and the photoluminescence decreases.[2,4,14] It has been shown that treatment of core-shell QDs with S_2^-, SH^-, or H_2S produces a photoluminescence quenching,[69] because these species act as a hole trap as DTC ligand. However, the Dye ligand acts as an electron donor and improves the photoluminescence.[70]

In addition, the Stokes shift was 0.047 eV, 0.030 eV, and 0.040 eV for QD-0.9 ML, QDTC, and QDTCDye, respectively. Some works reported the reduction of the Stokes shift and presented better surface passivation.[71,72] The improved surface passivation of CdSe-ZnS QDs can be explained using the HSAB theory.[73] As Cd^{2+} and Zn^{2+} from the CdSe and ZnS are soft acids and the oleic acid is a hard base, there is a weak bond on the QD surface. After ligand exchange, the hard-soft Zn^{2+} is combined with the soft base DTC ligand, leading to a stronger interaction and better passivation.

Table 9. Optical properties of QD-0.9 ML, Dye, and QDs after ligand exchange (QDTC, QDTCDye).

QDs	Maximum absorption wavelength (nm)	Maximum emission wavelength (nm)	FWHM (nm)	Stokes shift (eV)	Quantum Yield PL-QY	Bandgap Energy (eV)
QD-0.9 ML	564	578	34	0.047	0.53	2.08
Dye	436	524	77	0.480	0.31	2.60
QDTC	570	590	35	0.030	0.06	2.01
QDTCDye	434-572	520-590	35	0.040	0.11	1.94

3.5.3 Photoluminescence decay analysis

The interaction between CdSe-ZnS QDs and ligands (DTC and Dye) was monitored by emission decay using at 560 nm laser pulse as the excitation source. The emission intensity recorded at the emission maximum (**Figure 34**) exhibited nonexponential decay kinetics previously explained in Chapter 2.

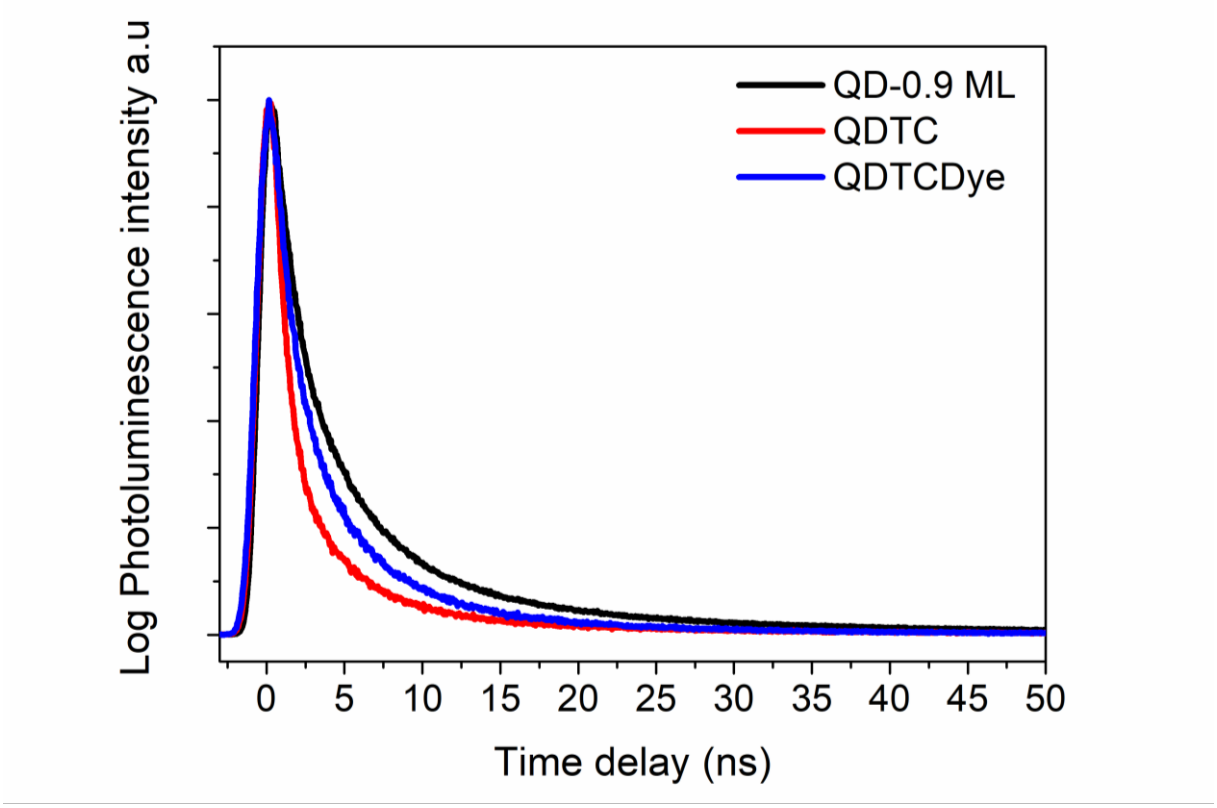

Figure 34. Comparison of free QD, QDTC, and QDTCDye photoluminescence decay curves. λ_{exc}: 560 nm. Solvent: chloroform: ethanol (1:1) for QD-1.00 ML and ethanol for QDTC, and QDTCDye.

The QDTC sample showed the most significant photoluminescence quenching effect due to the excess ligand used during the ligand exchange reaction (QD/DTC: 1/3). The HOMO orbital of the DTC ligand is near to the valence band of QD (VB), thus can act as an effective quencher of CdSe-ZnS QDs emission intercepting the hole produced in the valence band (VB) of QDs after excitation, i.e., interrupting the radiative recombination as shown in Equation 6 and 7.[4]

$$CdSe\text{-}ZnS + h\nu \rightarrow CdSe\text{-}ZnS\ (h^+ + e^-) \quad (6)$$

$$CdSe\text{-}ZnS\ (h^+ + e^-) + DTC \rightarrow CdSe\text{-}ZnS + DTC^+ \quad (7)$$

When the photon is absorbed by the CdSe-ZnS QDs, an excited electron-hole pair exciton is formed (Equation (6)). The photogenerated hole in the QDs will transfer to the DTC ligand (Equation (7)). The electron will be located in the QDs zone and the hole in the DTC zone (**Figure 35**). When the hole is trapped on the DTC ligand, radiative recombination of the exciton is not developed, resulting in a strongly reduced photoluminescence intensity.[4]

Similarly, the bi-exponential decay of QDTC and QDTCDye can be explained based on the formation of trap states.[74–76] Surface defects give rise to trap states that lie within the bandgap and complicate the

emission process. The exciton emission from the conduction band (CB) to the valence band (VB) contributes to the fastest lifetime decay.[4]

The lifetime average (τ_{FL}) in QDTC ligands showed a significant decrease (**Table 10**) due to the holes were transferred from CdSe-ZnS QDs to DTC ligand,[4] while a short increase with Dye ligand was observed (**Table 10**). The decay kinetics analysis in the QDTC shows a depopulation in the valence band (h^+ capture) as a function of time (**Table 10**) due to the excess of ligand used during ligand exchange (QD/DTC: 1/3). However, the Dye ligand improves the photoluminescence decay in QDTC (**Table 10**). A ligand exchange reaction could be associated with the enhancement in PL in QDTCDye, the Dye ligand replace the DTC ligands in some sites due to the high affinity between carboxylate ions from Dye and Zn^{2+} from ZnS shell (HSAB Theory).[73] Improved photoluminescence,[70] indicates the Dye ligand is partially removed or eliminates the trap states (hole traps) on the surface QDs produced by the DTC ligand.

To compare the emission and the average lifetimes (τ_{FL}), QDTC and QDTCDye were determined with the equation previously exposed in Chapter 2. The results are summarized in **Table 10**. The decreased photoluminescence intensity and emission lifetime indicate the DTC ligand interaction with CdSe-ZnS QDs resulting in charge transfer quenching.[4] DTC ligand acts as hole traps near the valence band (VB) in QD, delocalizing the exciton and producing new nonradiative recombination centers.[2,42,77] These results are congruent with the lowest QY observed in **Table 9**.

Furthermore, some reports have shown that sulfide compounds such as thiol and dithiocarbamate ligands produce a decrease in photoluminescence. Liu and co-workers,[4] showed the reduction in the photoluminescence decay (τ_{FL} (ns)) decrease with the functional group in the structure of three aromatic thiol compounds capped CdSe quantum dots (**Table 10**). Xu et al.[78] used a dithiocarbamate from proline-capped CdSe-ZnS core-shell QDs; the proline-DTC ligand produced a reduction in the photoluminescence and emission lifetime (τ_{FL} (ns)) from 20.56 ns to 5.41 ns (**Table 10**). The reduction in the emission lifetime of these reports and this work show that the thiols and DTC ligands capped QDs results in charge transfer quenching.

Table 10. Lifetime average of QDTC and QDTCDye.

QDs	τ_{FL} (ns)	χ^2
QD-0.9 ML	4.34	1.14
QDTCDye	2.25	1.28
QDTC	1.43	1.58
***α*-toluene thiol**	11.5 [4]	
thiophenol	5.8 [4]	
proline-DTC	5.4 [78]	
***p*-hydroxythiophenol**	3.4 [4]	

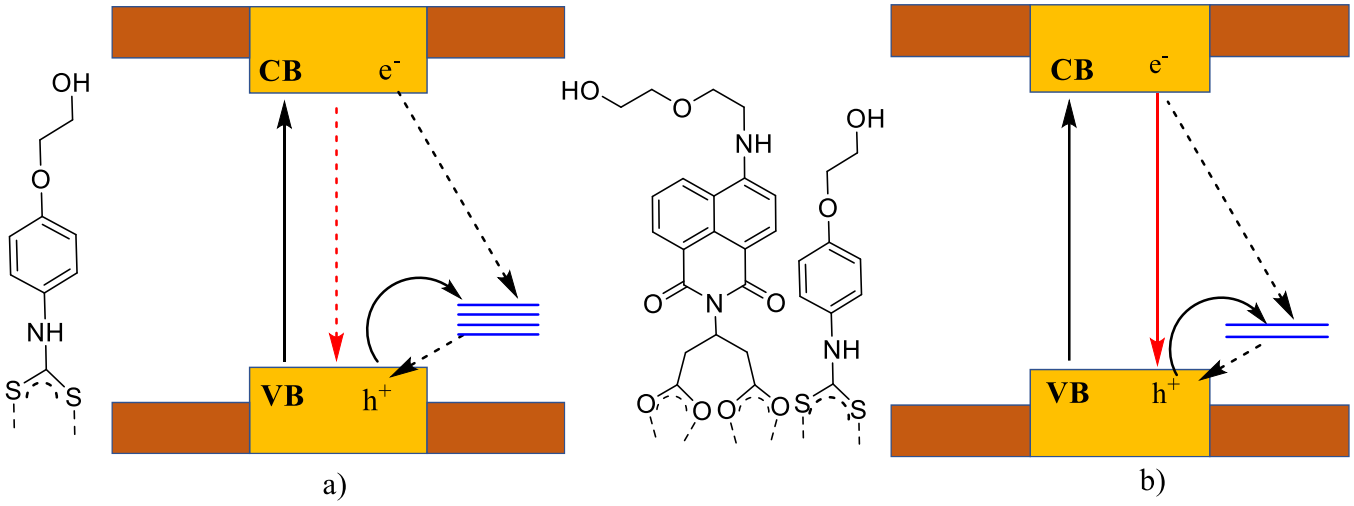

Figure 35. Mechanisms of QDs to surface attached ligands, a) QDTC and b) QDTCDye.[79]

3.5.4 Effect of different Hg^{2+} concentrations on the absorption and emission spectra of QDs after the ligand exchange process

3.5.4.1 Absorption and emission analysis

To better understand the effects of Hg^{2+} ions on the optical properties, UV-Vis and fluorescence spectroscopy in the absence and presence of Hg^{2+} were systematically carried out and investigated.

1. **Dye**

Figure 36 shows the emission spectra of free Dye ligands after the interaction with different concentrations of Hg^{2+} (1.0 - 5.0 µM). The absorption spectra show an increase in the absorption maximum at 436 nm as a function of the increased concentration of Hg^{2+} ions (**Figure 62 Annexes**). The fluorescence spectra (**Figure 36**) show a quenching in the maximum emission band with a slight red-shift from 523 nm to 525 nm with an increasing concentration of Hg^{2+} ions. However, this quenching is very low, approximately ~13 %, with the highest concentration of quencher (5µM Hg^{2+}) due to the low affinity of CO_2^- (carboxylate) from Dye with the Hg^{2+}; the HSAB theory can explain this behavior, the oxygen is a hard base, and Hg^{2+} is a soft acid, and the coordination between them is not favored.[73] However, oxygen can give electrons to complete the *d*-orbitals unfilled of Hg^{2+}, producing a linkage that interrupts the electronic communication of the molecule (electronic delocalization of the π-electrons in the aromatic system), producing a decrease in the fluorescence intensity. Furthermore, the transition metals can act as quenchers, thus producing fluorescence quenching due to the heavy atom effect.[32,80–84]

The quenching process can be explained by a Stern-Volmer plot explained previously in Chapter 2, this plot shows good linearity, and the linear range used is from 1.0-5.0 × 10^{-4} M (1.0-5.0 μM Hg^{2+}), with the correlation coefficient R^2: 0.9972, as shown in **Figure 36**.

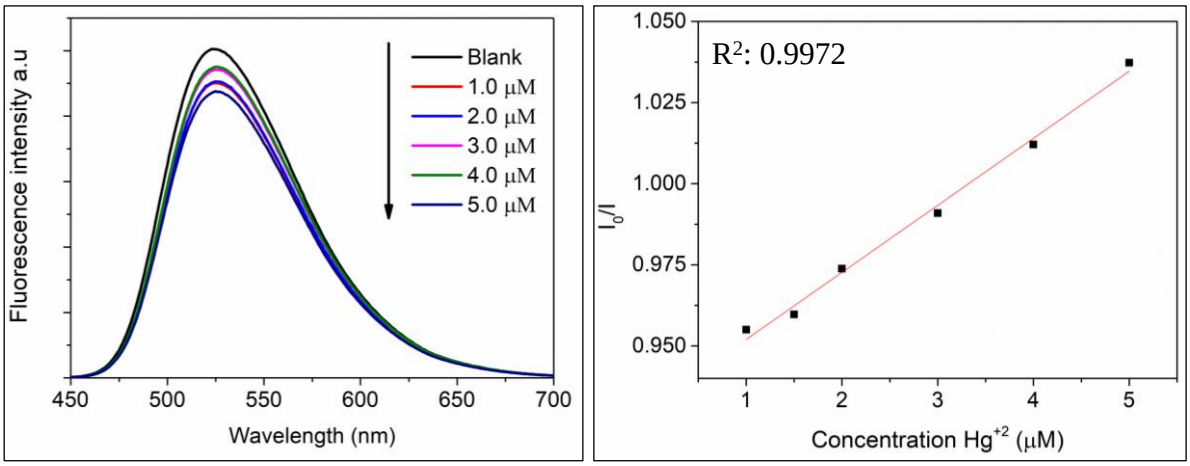

Figure 36. Emission spectra and linear plot of photoluminescence response of Dye as a function of Hg^{2+}. λ_{exc}: 436 nm. Solvent: ethanol.

2. QDTC

Figure 37 shows the emission spectra of the QDTC (120 ppm) exposed to an aqueous solution containing different concentrations of Hg^{2+} ions (0.5-5.0 μM) performed at an excitation wavelength of 380 nm, while emission wavelength was observed in the range 400-700 nm. The absorption band (**Figure 63 Annexes**) shows a progressive red shift with increasing concentrations of Hg^{2+}.

The emission intensity at 590 nm was turned on gradually in the emission spectra, with a slight red shift from 590 to 593 nm. This result shows that the increase in Hg^{2+} concentration induces a fluorescence enhancement. Hg^{2+} ions are passivating the surface, i.e., removal/elimination of trap states, and produce an enhancement of fluorescence, decreasing the nonradiative recombination. Furthermore, when the Hg^{2+} ions interact with the QDTC system, the DTC ligand does not desorb from the surface to form a complex with this cation. As in another study with a lineal DTC capped onto CdSe-ZnS, the ligand formed a complex with Hg^{2+} producing the inverse process (quenching).[65]

The exciton-delocalization into the ligand shell is facilitated by the CS_2 group[85] binding to the Zn^{2+} on the ZnS shell of CdSe-ZnS QDs, which allows for strong spatial coupling of the orbitals of the ligand to orbitals of the QDs.[2] This is indicative that the coordination between the surface of QDs and DTC ligand is strong, and it is not easy to remove the ligand from the surface due to the high affinity between S and Hg.[73]

Therefore, Hg^{2+} ions produce a cation exchange reaction with the Zn^{2+} from the ZnS shell to form HgS particles and incorporate it onto the lattice because the *Ksp* HgS is lower than *Ksp* ZnS; thus, the reaction is favored.[5] Similarly, Wang et al.[86] demonstrated this behavior in detecting Hg^{2+} ions with a nanoprobe of CdSe-ZnS QDs. In this case, an enhancement of fluorescence is produced, as in this work. In the same way, Zhu et al.[87] showed that the Hg^{2+} ions on the surface of InP-MAA (mercapto acetic acid ligand) QDs produce ultrasmall particles of HgS, these particles could be passivating/blocking the hole traps produced by DTC ligand producing new exciton recombination centers increasing the fluorescence.

This situation has been studied, for example, the treatment of the CdSe QDs with cadmium acetate increases the fluorescence intensity of the sample by a factor of two, presumably by passivating any undercoordinated selenium ions on the QD surface and thereby decreasing the number of sites for nonradiative trapping of the hole.[88] In a similar case, Spanhel and co-workers showed this effect, in which they added Cd^{2+} ions in basic medium to CdS QDs, and thus the system's emission increased.[89] Chen and Rosenzweig used CdS QDs functionalized with L-cysteine to detect Zn^{2+} ions, showing a similar result.[90] Chen and co-workers used this same QD system to detect Ag^{+} ions; this system is based on the high affinity of the thiol group of L-cysteine to some cations.[91] Both works are based on forming a complex with the amino acid and, in turn, binding to the surface of the QD, forming an active state that produces an increase in fluorescence.

Finally, the titration with Hg^{2+} shows an enhancement in the photoluminescence and good linearity; the lineal range used: 0.5-5.0 × 10^{-4} M (0.5-5.0 µM Hg^{2+}) with the correlation coefficient R^2: 0.9995 as shown in **Figure 37**.

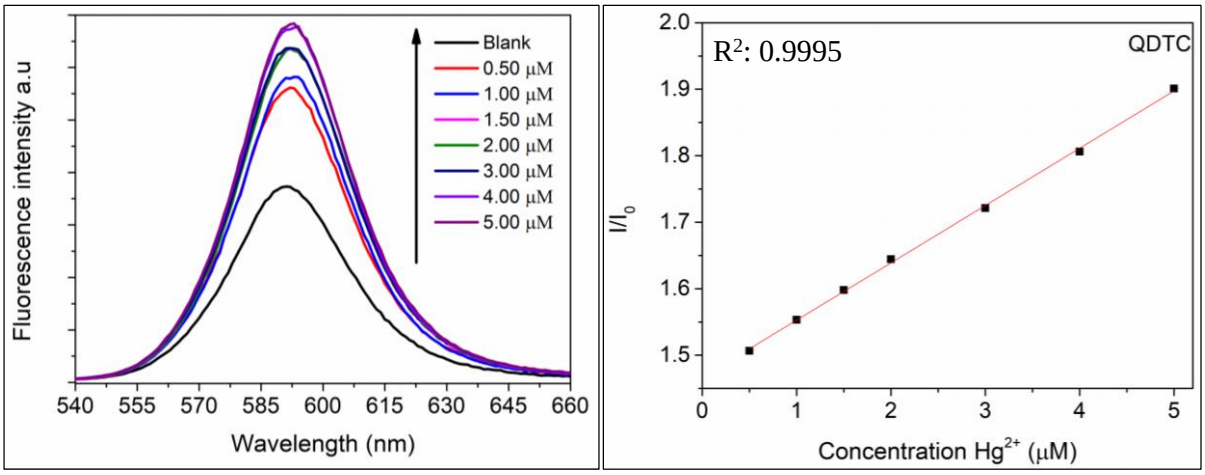

Figure 37. Emission spectra and linear plot of photoluminescence response of QDTC as a function of Hg^{2+}. λ_{exc}: 380 nm. Solvent: ethanol.

3. QDTCDye

The fluorescence turn-on and ratiometric detection were confirmed by monitoring the fluorescence responses of the two emission bands of the dual-emitting probe of Hg^{2+}. The effects of Hg^{2+} on the emission of QDTCDye are shown in **Figure 38**. The maximum absorption band (**Figure 63 Annexes**) increases progressively with increasing concentrations of Hg^{2+}, maintaining the same behavior in the emission band maximum.

In the fluorescence spectra (**Figure 38**), the QDTCDye (120 ppm) presents two emission bands, one band at 520 nm from the Dye and a second band at lower energy (590 nm) from QD. With an increasing concentration of Hg^{2+}, the emission intensity at 590 nm was turned on gradually due to switching off.[37] The results show that the increase of Hg^{2+} to the probe solution induces a remarkable fluorescence enhancement at 590 nm. In contrast, the emission intensity at 520 nm almost remains unchanged mainly (increasing slightly). The emission intensity ratio, I_{520}/I_{590}, gradually increased with the concentration of Hg^{2+}. When Hg^{2+} was added up to 5 μM, about 4.2-fold ratiometric fluorescence enhancement was observed.

In this case, the behavior is similar to QDTC; there is no evidence of desorption in both ligands bound to the QD: Dye and DTC. As the ligand is not desorbed from the surface, the Hg^{2+} ions may form bonds with the S^{2-} of the ZnS shell of the QD by cation exchange reaction, thus forming tiny HgS particles, taking onto account its high affinity with S^{2-} (*Ksp* and Pearson acid-base theory).[5] Thus, these particles fall onto the band gap, enhancing radiative recombination and increasing fluorescence as a function of Hg^{2+} concentration. The ultra-small particles of HgS cannot quench QDs; these particles form a pseudo-shell to confine the exciton and improve the photoluminescence; the Dye ligand plays a dual role as the component of a ratiometrically reporting chromophore and replace the DTC ligands in somes sites to remove hole traps (DTC ligand) and produce new radiative centers in the QD.[70,92]

The Dye is improving electronic communication in the QDTCDye system. Dye is a ligand with many π-electrons due to its aromaticity, which may benefit the optical properties of the overall system. In conclusion, the Hg^{2+} partially removes the trap states (hole traps) produced by the DTC ligand and favors the production of new radiative recombination centers to increase photoluminescence.

The titration with Hg^{2+} ions (I_{520}/I_{590}) showed a linear relationship with the Hg^{2+} concentration from 0.5-5.0 × 10^{-4} M (0.5-5.0 μM) with the correlation coefficient R^2: 0.9992, as shown in **Figure 38**.

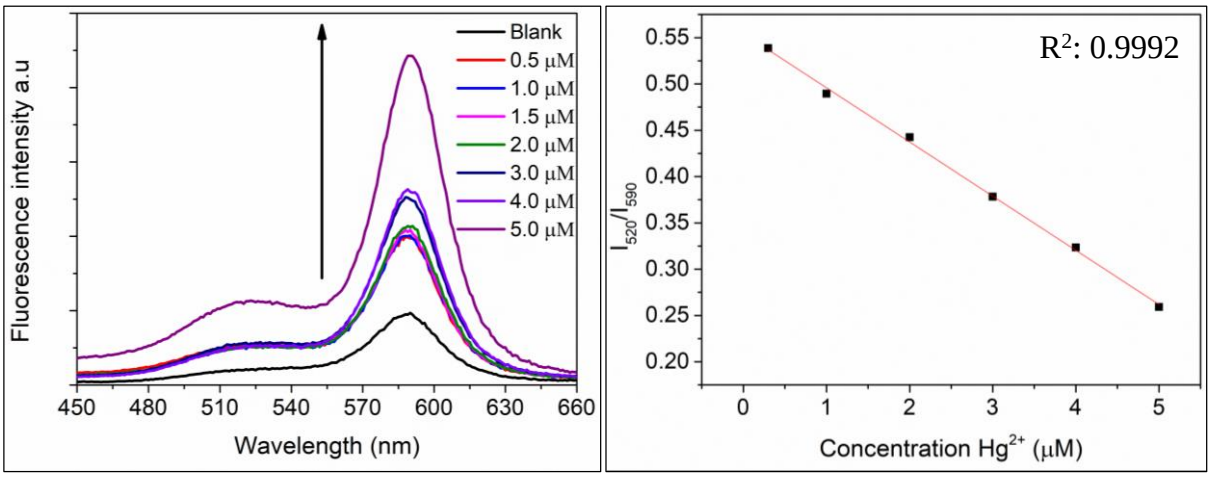

Figure 38. Emission spectra and linear plot of relative photoluminescence response of QDTCDye as a function of Hg^{2+}. λ_{exc}: 380 nm. Solvent: ethanol.

Finally, the limit of detection (LOD) was calculated with the parameters obtained from linear regression shown in **Figures 36-38**. The limit of detection was calculated as 0.00106 μM ~ 1.06 nM, 0.00371 μM ~ 3.71 nM, and 0.0044 μM ~4.4 nM. The detection limit of this ratiometric fluorescence QDs probe for Hg^{2+} is comparable with the QDs-based dual-emission nanoprobe (5.6 nM).[93] The detection limit calculated for Hg^{2+} is much lower than those of other fluorescence probes (**Table 11**).

Furthermore, the LOD calculated for these ligands capped CdSe-ZnS QDs is lower than the acceptable LOD of inorganic Hg^{2+} in drinking water established by the World Health Organization (WHO) and the USA Environmental Protection Agency (EPA) as 30.0 nM,[94] and 10.0 nM,[95] respectively. The low LOD is an excellent feature for applying these promising nanomaterials in mercury ion sensing.

Table 11. Comparison of the main characteristics of the selected fluorescence ratiometric probes for determining Hg^{2+}.

Probes	Mechanism	LOD (nM)	Reference
MAA capped CdS	Turn-off	4.2	[96]
L-Cysteine-capped CdSe	Turn-off	6.0	[97]
Dye	Turn-off	1.06	This work
Mn-doped ZnSe QDs	Turn-on	10	[98]
InP-MAA QDs	Turn-on	500	[87]
QDTC	Turn-on	3.71	This work
RhB-CdSe/ZnS QDs	Ratiometric	395	[92]
CdTe/CdS-chitosan	Ratiometric	5.6	[93]

RhB-CdTe QDs/SiO_2	Ratiometric	260	[99]
C-dots/GDTC-CdSe/ZnS QDs	Ratiometric	100	[100]
QDTCDye	Ratiometric	4.4	This work

3.5.4.2 Photoluminescence decay analysis of QDTC and QDTCDye after interaction with Hg^{2+} ions

The decay kinetics measurements are shown in **Figure 39**. The compounds treated with Hg^{2+} were adjusted: Dye was fitted to a monoexponential function, while QDTC and QDTCDye were to a tri-exponential function. In the case of Dye ligand with Hg^{2+} the τ_{FL} value decreased concerning the free Dye (**Table 12**). This behavior is due to the low affinity between carboxylate ions and Hg^{2+}, oxygen is a hard base, and Hg^{2+} is a soft acid. The coordination between them will not be favored.[73]

On the other hand, the emission lifetime in QDTC and QDTCDye show similar behavior (**Figure 39**). The effect of Hg^{2+} ions increases the τ_{FL} (**Table 12**) due to the passivation of the trap states in the QD surface, which decreases the contribution of nonradiative decay to the overall observed excited state lifetime.[101]

Table 12. Parameters obtained from fitting of fluorescence decay curves of samples (Dye, QDTC and QDTCDye before and after Hg^{2+}.

QDs+ Hg	τ_{FL} *free* (ns)	τ_{FL} + *Hg* (ns)	χ^2
Dye	9.1	9.0	1.10
QD-0.9 ML	4.34	4.43	1.63
QDTCDye	2.25	3.34	1.76
QDTC	1.43	2.51	1.27

DTC ligand is a hole acceptor (hole trap) that affects the optical properties due to the exciton delocalization. However, when the Hg^{2+} ions interact with QDTC and QDTCDye, the decay measurements showed an increase in the τ_{FL} (**Table 12**) due to the passivation trap states in the QDs. Jin and co-workers showed a similar result in treating CdSe QDs in dichloromethane with phenyl dithiocarbamate (DTC), reducing the photoluminescence quantum yield by 95%. Still, subsequently, the treatment with Cd^{2+} not only restored the initial quantum yield but enhanced it.[101]

This behavior is congruent with other reports (**Table 13**). For example, Xu et al.[78] probed a treatment with Zn^{2+} ions on the emission lifetime of dithiocarbamate from proline and di-2-picolylamine (DPA) capped CdSe-ZnS core-shell QDs. This treatment with Zn^{2+} ions increases the emission lifetime (τ_{FL} (ns)) from 5 ns to 14 ns. In addition, Gui et al.[102] demonstrated the effect of Cd^{2+} ions on the emission

lifetime of thioglycolic acid (TGA) capped-CdTe QDs, Cd^{2+} ions produce an increase in the emission lifetime (τ_{FL} (ns)) from 28 ns to 36 ns.

The increased average emission lifetime τ_{FL} and slight spectra redshift was ascribed to forming HgS particles on the ZnS shell of QDs by an exchange cation reaction Hg-to-Zn,[5] thus a pseudo-shell of HgS particles was created to confine the exciton. This pseudo-shell of HgS particles suppressed the nonradiative recombination pathway, significantly enhancing photoluminescence.[78] The formation of these particles probably modulates the hole-accepting ability of DTC. As a result, the exciton recombination of QDs is restored, the photoluminescence is recovered, and an increased emission lifetime is observed.[102]

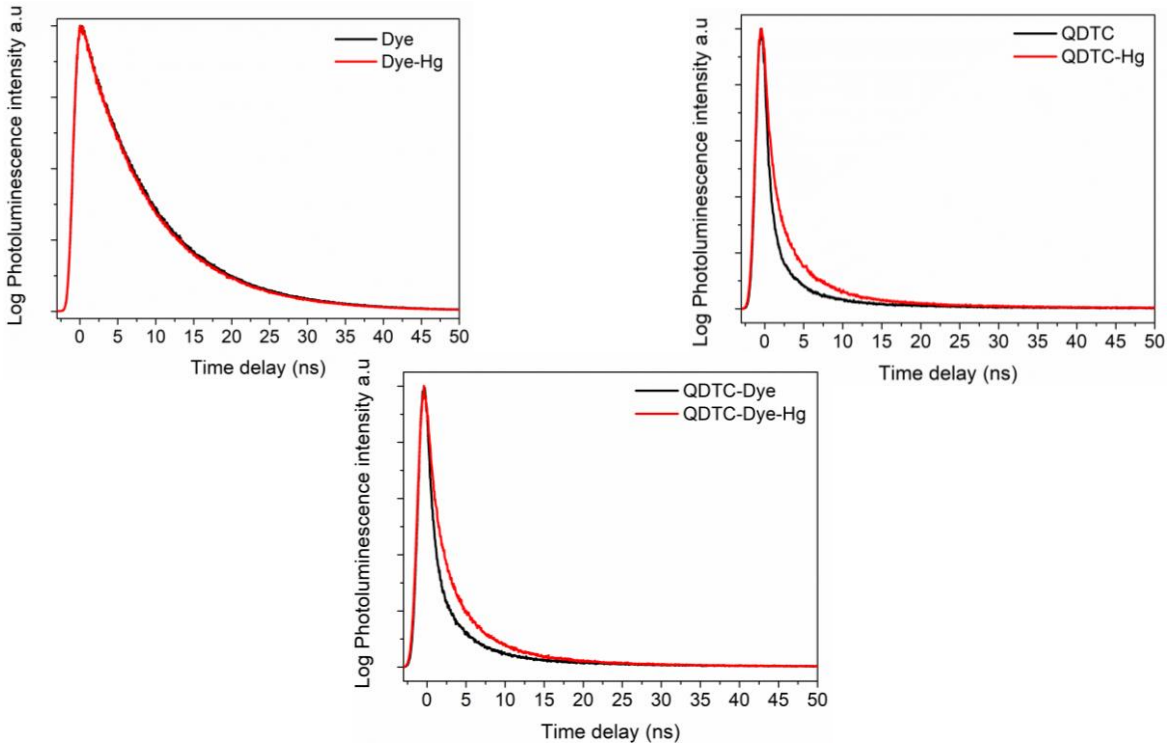

Figure 39. Time-resolved PL curves of Dye, QDTC, and QDTCDye. λ_{exc}: 560 nm. Solvent: ethanol.

Table 13. Comparison of τ_{FL} values of the selected QDs with metal transition ions.

QDs	Analyte	τ_{FL} (ns)	τ_{FL} + M^{2+}(ns)	Reference
MPA-capped red CdTe-CdS	Hg^{2+}	29	30	[103]
DPA-P-DTC-QDs	Zn^{2+}	5	14	[78]
CdTe-TGA QDs	Cd^{2+}	28	36	[102]
QD-0.9 ML	Hg^{2+}	4.34	4.43	This work
QDTCDye	Hg^{2+}	2.25	3.34	This work
QDTC	Hg^{2+}	1.43	2.51	This work

3.5.5 Effect of metal ions on the absorption and emission of the QDs after ligand exchange

The effect of cations on the absorption and fluorescence of Dye, QDTC, and QDTCDye was developed using a concentration of 120 ppm with the chloride salts of transition metal ions: Zn^{2+}, Mn^{2+}, Pb^{2+}, Cd^{2+}, Co^{2+}, Hg^{2+}, Ni^{2+}, at the concentration of 5 μM. **Figure 40** presents the results of the interaction of Dye and cations. The absorption spectra showed an increase in the absorption band with the addition of metal ions (**Figure 64, annexes**). In emission spectra, all the cations evaluated produce a quenching of the fluorescence. Hg^{2+} shows the highest quenching of fluorescence. This behavior is due to the low affinity between carboxylates from Dye with the cations.[73]

In the case of QDTC, the results are summarized in **Figure 40.** The absorption spectra show a substantial increase in the absorption band with Cd^{2+} and a strong decrease with Hg^{2+} (**Figure 64, annexes**). In the fluorescence spectra, Hg^{2+} shows a significant enhancement of fluorescence intensity with a slight red shift (from 590 to 592 nm). This effect can be due to the high affinity between Hg^{2+} to the $S^{2-}$from shell (ZnS) of QD,[34,73] This effect can include cation exchange reaction from Zn^{2+} in the surface and Hg^{2+} to form HgS, passivating the hole traps produced by the DTC ligand to the QD, and thus increase the radiative recombination to improves the fluorescence intensity. In addition, the substantial red-shift, presented by cations-type soft acids like Hg^{2+} and intermediate acids like Zn^{2+}, Cd^{2+}, and Pb^{2+}, can act as weak or hard acids.[73] In this case, the Hg^{2+} shows the highest enhancement in fluorescence intensity, confirming the high affinity to QDTC due to the S^{2-} present in the DTC ligand and ZnS shell on the surface of QDs. On the other hand, a slight red-shift at 591 nm is shown with Co^{2+} and Mn^{2+} ions, while a similar red-shift is produced at 592 nm with Zn^{2+}, Pb^{2+}, Cd^{2+}, and Ni^{2+} ions.

Finally, in QDTCDye, the results are shown in **Figure 40**. In the absorption spectra, Hg^{2+} is the only ion that shows a substantial increase in the absorption band **(Figure 64, annexes**). A similar effect is shown in the emission spectra (**Figure 40**). The Hg^{2+} ions show an increase in the fluorescence of the two emission bands. This behavior generated the lowest value in I_0/I (**Figure 40**). However, all cations enhance the fluorescence intensity of the emission band at 590 nm, and the emission band at 521 nm does not show a significant change. All the cations may produce a cation exchange reaction with the Zn^{2+} present in the surface of QDs, i.e., a similar behavior of Hg^{2+} ions.[5]

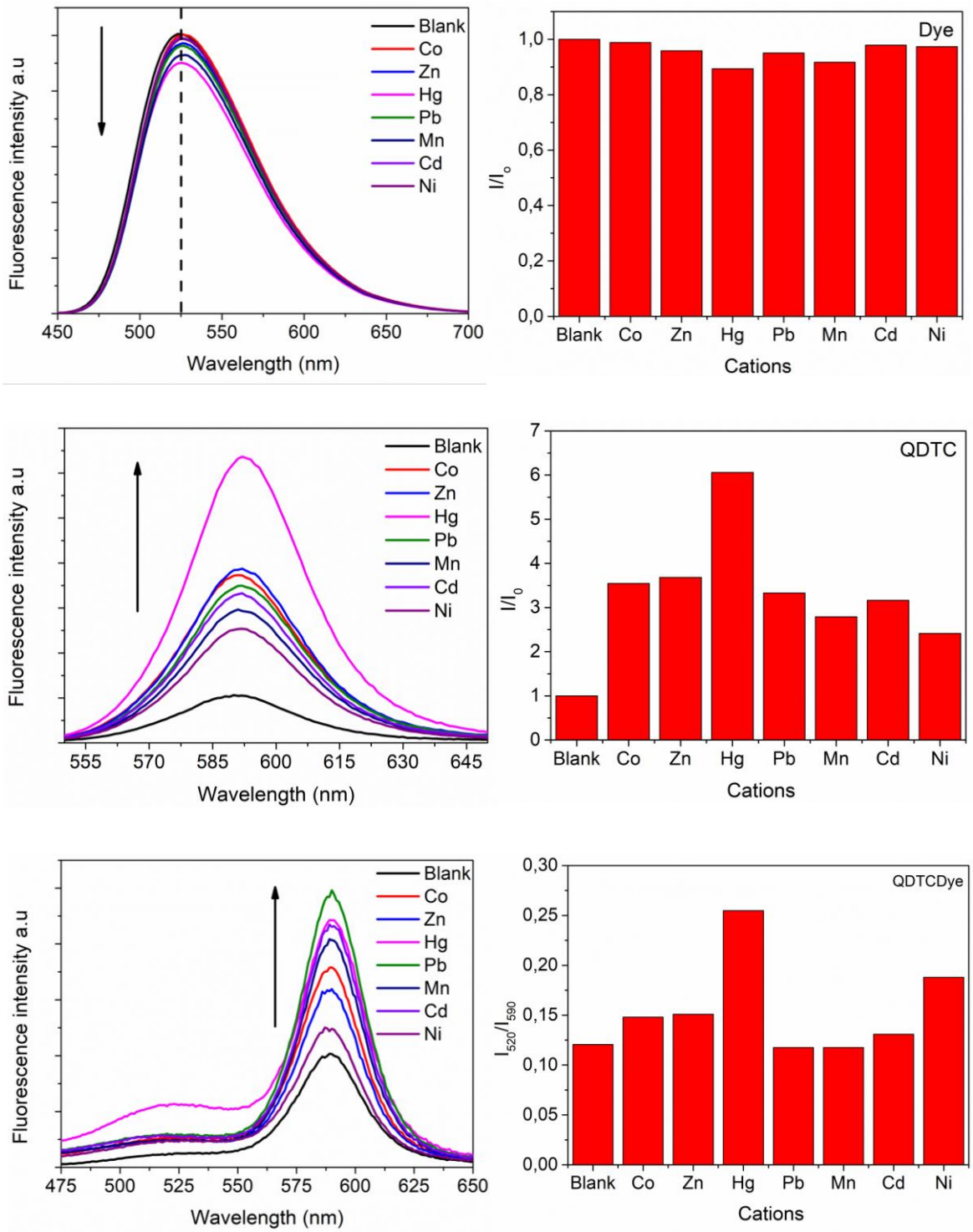

Figure 40. Relative photoluminescence response of Dye, QDTC, and QDTCDye in the presence of Hg^{2+} and other metal transition ions evaluated.

The DTC ligands act as hole traps on the surface of the QDs, producing a delocalization of exciton (e^- /h^+ pair) and decreasing the optical properties and photoluminescence. However, the fluorescence

enhancement and redshift of the fluorescence emission band of QDTC and QDTCDye observed after the addition of Hg^{2+} and metal ions can be explained due to the passivation of these hole traps produced by DTC ligands capped on the surface of QDs;[104] the Hg^{2+} ions are binding with the S^{2-} from the shell of CdSe-ZnS QDs taking onto an account that the formation of HgS is more favored (Ksp_{HgS}:4.0×10^{-53}) than ZnS (Ksp_{ZnS}: 2.0×10^{-22}).[105] The small particles of HgS formed on the surface are effectively blocking the nonradiative recombination at traps sites on the surface of the functionalized QDs improving the photoluminescence emission (**Figure 41**).[86,87,104,106,107]

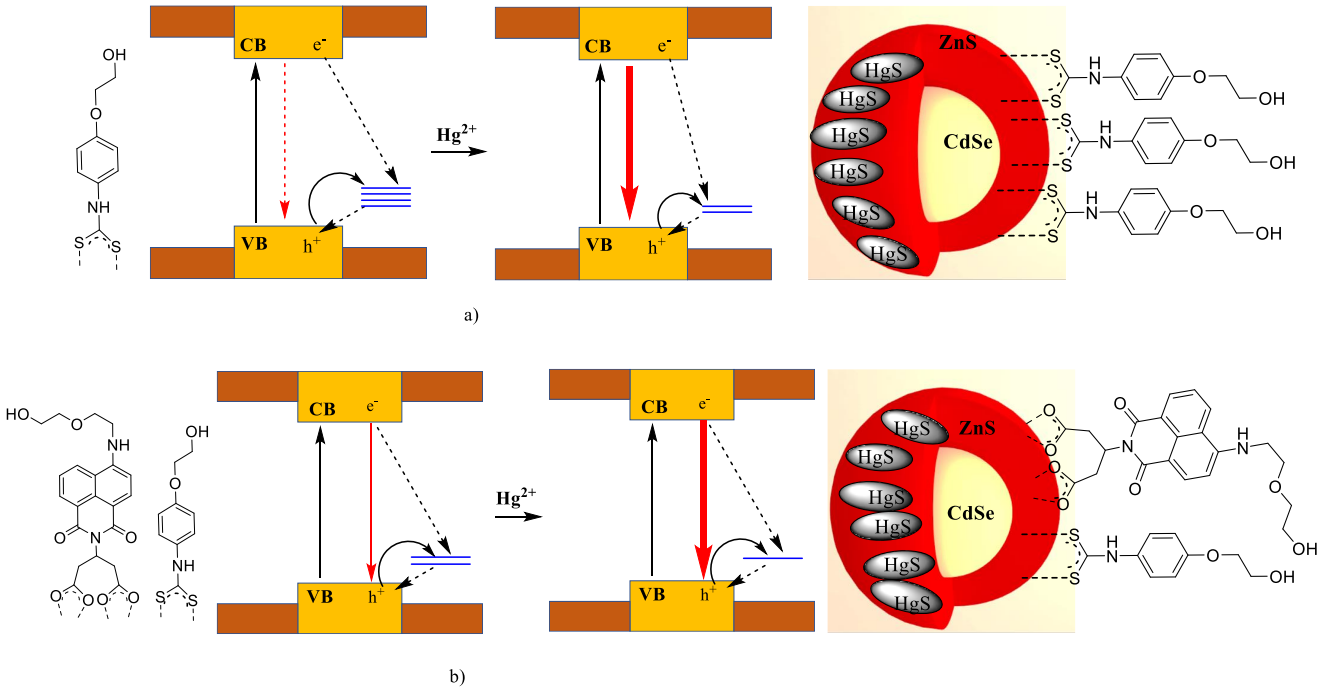

Figure 41. Photoluminescence effect on the shell surface before and after adding cations (M^{2+}, Hg^{2+}), a) QDTC, and b) QDTCDye.

3.6 CONCLUSIONS

The coordination of DTC and Dye ligands on the QD surface did not significantly affect the crystal structure. The size of QDs calculated by HR-TEM showed a slight increase due to the exchange ligand process.

The optical properties of CdSe-ZnS QDs, such as QY, are strongly affected by the coordination of dithiocarbamate ligand (DTC) due to this ligand acting as hole traps. These trap states producing delocalization of exciton favor the nonradiative recombination, and the emission is quenched. The Dye ligand replace some DTC ligands and reduce the hole traps to produce a partial regeneration of exciton recombination and fluorescence increase.

In the analysis of Hg^{2+} ions sensing, an improvement in the photoluminescence is produced due to partially removing the trap states formed by the DTC ligand by the formation of ultrasmall particles of HgS on the surface as a pseudo-shell. QDTC shows a higher affinity to Hg^{2+} ions than other cations evaluated; both cases (QDTC and QDTCDye) show higher LOD than QD-0.9 ML and other QDs reported. This behavior can be attributed to the partial passivation of hole traps formed by the effect of Hg^{2+} ions. Furthermore, it is possible that the population of both ligands (DTC and Dye) on the QDTCDye is higher than QDTC, and free sites on ZnS are not available to form HgS particles, affecting the selectivity to Hg^{2+} ions in QDTCDye.

3.7 REFERENCES

(1) Zhou, J.; Liu, Y.; Tang, J.; Tang, W. Surface Ligands Engineering of Semiconductor Quantum Dots for Chemosensory and Biological Applications. *Biochem Pharmacol* **2017**, *20* (7), 360–376. https://doi.org/10.1016/j.mattod.2017.02.006.

(2) Frederick, M. T.; Weiss, E. A. Relaxation of Exciton Confinement in CdSe Quantum Dots by Modification with a Conjugated Dithiocarbamate Ligand. *ACS Nano* **2010**, *4* (6), 3195–3200. https://doi.org/10.1021/nn1007435.

(3) Frederick, M. T.; Amin, V. A.; Cass, L. C.; Weiss, E. A. A Molecule to Detect and Perturb the Confinement of Charge Carriers in Quantum Dots. *Nano Lett* **2011**, *11* (12), 5455–5460. https://doi.org/10.1021/nl203222m.

(4) Liu, I. S.; Lo, H. H.; Chien, C. T.; Lin, Y. Y.; Chen, C. W.; Chen, Y. F.; Su, W. F.; Liou, S. C. Enhancing Photoluminescence Quenching and Photoelectric Properties of CdSe Quantum Dots with Hole Accepting Ligands. *J Mater Chem* **2008**, *18* (6), 675–682. https://doi.org/10.1039/b715253a.

(5) De Trizio, L.; Manna, L. Forging Colloidal Nanostructures via Cation Exchange Reactions. *Chemical Reviews*. American Chemical Society September 28, 2016, pp 10852–10887. https://doi.org/10.1021/acs.chemrev.5b00739.

(6) Vasudevan, D.; Gaddam, R. R.; Trinchi, A.; Cole, I. Core-Shell Quantum Dots: Properties and Applications. *J Alloys Compd* **2015**, No. February. https://doi.org/10.1016/j.jallcom.2015.02.102.

(7) R. W. Knoss. *Quantum Dots: Research, Technology and Applications*; 2008.

(8) Gidwani, B.; Sahu, V.; Shukla, S. S.; Pandey, R.; Joshi, V.; Jain, V. K.; Vyas, A. Quantum Dots: Prospectives, Toxicity, Advances and Applications. *Journal of Drug Delivery Science and Technology*. Editions de Sante February 1, 2021. https://doi.org/10.1016/j.jddst.2020.102308.

(9) Dorfs, D.; Krahne, R.; Falqui, A.; Manna, L.; Giannini, C.; Zanchet, D. *Quantum Dots: Synthesis and Characterization*; Elsevier Ltd., 2011; Vol. 1. https://doi.org/10.1016/B978-0-12-812295-2.00028-3.

(10) Zhang, Y.; Schnoes, A. M.; Clapp, A. R. Dithiocarbamates as Capping Ligands for Water-Soluble Quantum Dots. *ACS Appl Mater Interfaces* **2010**, *2* (11), 3384–3395. https://doi.org/10.1021/am100996g.

(11) Reshma, V. G.; Mohanan, P. v. Quantum Dots: Applications and Safety Consequences. *Journal of Luminescence*. Elsevier B.V. January 1, 2019, pp 287–298. https://doi.org/10.1016/j.jlumin.2018.09.015.

(12) Giansante, C. Surface Chemistry Control of Colloidal Quantum Dot Band Gap. *Journal of Physical Chemistry C* **2018**, *122* (31), 18110–18116. https://doi.org/10.1021/acs.jpcc.8b05124.

(13) Knowles, K. E.; Tice, D. B.; McArthur, E. A.; Solomon, G. C.; Weiss, E. A. Chemical Control of the Photoluminescence of CdSe Quantum Dot-Organic Complexes with a Series of Para-Substituted Aniline Ligands. *J Am Chem Soc* **2010**, *132* (3), 1041–1050. https://doi.org/10.1021/ja907253s.

(14) Frederick, M. T.; Amin, V. A.; Weiss, E. A. Optical Properties of Strongly Coupled Quantum Dot-Ligand Systems. *Journal of Physical Chemistry Letters* **2013**, *4* (4), 634–640. https://doi.org/10.1021/jz301905n.

(15) Hartley, C. L.; Kessler, M. L.; Dempsey, J. L. Molecular-Level Insight into Semiconductor Nanocrystal Surfaces. *J Am Chem Soc* **2021**, *143* (3), 1251–1266. https://doi.org/10.1021/jacs.0c10658.

(16) Peterson, M. D.; Jensen, S. C.; Weinberg, D. J.; Weiss, E. A. Mechanisms for Adsorption of Methyl Viologen on Cds Quantum Dots. *ACS Nano* **2014**, *8* (3), 2826–2837. https://doi.org/10.1021/nn406651a.

(17) Jeong, S.; Achermann, M.; Nanda, J.; Ivanov, S.; Klimov, V. I.; Hollingsworth, J. A. Effect of the Thiol-Thiolate Equilibrium on the Photophysical Properties of Aqueous CdSe/ZnS Nanocrystal Quantum Dots. *J Am Chem Soc* **2005**, *127* (29), 10126–10127. https://doi.org/10.1021/ja042591p.

(18) Green, M. The Nature of Quantum Dot Capping Ligands. *J Mater Chem* **2010**, *20* (28), 5797. https://doi.org/10.1039/c0jm00007h.

(19) de Mello Donegá, C.; Hickey, S. G.; Wuister, S. F.; Vanmaekelbergh, D.; Meijerink, A. Single-Step Synthesis to Control the Photoluminescence Quantum Yield and Size Dispersion of CdSe Nanocrystals. *Journal of Physical Chemistry B* **2003**, *107* (2), 489–496. https://doi.org/10.1021/jp027160c.

(20) de Mello Donegá, C.; Hickey, S. G.; Wuister, S. F.; Vanmaekelbergh, D.; Meijerink, A. Single-Step Synthesis to Control the Photoluminescence Quantum Yield and Size Dispersion of CdSe Nanocrystals. *Journal of Physical Chemistry B* **2003**, *107* (2), 489–496. https://doi.org/10.1021/jp027160c.

(21) Bullen, C.; Mulvaney, P. The Effects of Chemisorption on the Luminescence of CdSe Quantum Dots. *Langmuir* **2006**, *22* (7), 3007–3013. https://doi.org/10.1021/la051898e.

(22) Munro, A. M.; Plante, I. J. la; Ng, M. S.; Ginger, D. S. Quantitative Study of the Effects of Surface Ligand Concentration on CdSe Nanocrystal Photoluminescence. *Journal of Physical Chemistry C* **2007**, *111* (17), 6220–6227. https://doi.org/10.1021/jp068733e.

(23) Bodnarchuk, M. I.; Kovalenko, M. v. Engineering Colloidal Quantum Dots: Synthesis, Surface Chemistry, and Self-Assembly. In *Colloidal Quantum Dot Optoelectronics and Photovoltaics*; Cambridge University Press, 2010; Vol. 9780521198264, pp 1–29. https://doi.org/10.1017/CBO9781139022750.002.

(24) Tohgha, U.; Varga, K.; Balaz, M. Achiral CdSe Quantum Dots Exhibit Optical Activity in the Visible Region upon Post-Synthetic Ligand Exchange with D- or L-Cysteine. *Chemical Communications* **2013**, *49* (18), 1844–1846. https://doi.org/10.1039/c3cc37987f.

(25) Baker, D. R.; Kamat, P. V. Tuning the Emission of CdSe Quantum Dots by Controlled Trap Enhancement. *Langmuir* **2010**, *26* (13), 11272–11276. https://doi.org/10.1021/la100580g.

(26) Liang, Y.; Thorne, J. E.; Parkinson, B. A. Controlling the Electronic Coupling between CdSe Quantum Dots and Thiol Capping Ligands via PH and Ligand Selection. *Langmuir* **2012**, *28* (30), 11072–11077. https://doi.org/10.1021/la301237p.

(27) Wuister, S. F.; De Mello Donegá, C.; Meijerink, A. Influence of Thiol Capping on the Exciton Luminescence and Decay Kinetics of CdTe and CdSe Quantum Dots. *Journal of Physical Chemistry B* **2004**, *108* (45), 17393–17397. https://doi.org/10.1021/jp047078c.

(28) Tan, A. C. W.; Polo-Cambronell, B. J.; Provaggi, E.; Ardila-Suárez, C.; Ramirez-Caballero, G. E.; Baldovino-Medrano, V. G.; Kalaskar, D. M. Design and Development of Low Cost Polyurethane Biopolymer Based on Castor Oil and Glycerol for Biomedical Applications. *Biopolymers* **2018**, *109* (2). https://doi.org/10.1002/bip.23078.

(29) Querner, C.; Reiss, P.; Bleuse, J.; Pron, A. Chelating Ligands for Nanocrystals' Surface Functionalization. *J Am Chem Soc* **2004**, *126* (37), 11574–11582. https://doi.org/10.1021/ja047882c.

(30) Querner, C.; Benedetto, A.; Demadrille, R.; Rannou, P.; Reiss, P. Carbodithioate-Containing Oligo- and Polythiophenes for Nanocrystals' Surface Functionalization. *Chemistry of Materials* **2006**, *18* (20), 4817–4826. https://doi.org/10.1021/cm061105p.

(31) Murru, S.; Ghosh, H.; Sahoo, S. K.; Patel, B. K. Intra- and Intermodular C-S Bond Formation Using a Single Catalytic System: First Direct Access to Arylthiobenzothiazoles. *Org Lett* **2009**, *11* (19), 4254–4257. https://doi.org/10.1021/ol9017535.

(32) Lakowicz, J. R. *Principles of Fluorescence Spectroscopy*; 2006. https://doi.org/10.1007/978-0-387-46312-4.

(33) Furlani, C. and L. M. L. Complexes of Dithiocarboxylic Acids. *Inorg Chem* **1968**, *7* (8), 1586–1592.

(34) Dubois, F.; Mahler, B.; Dubertret, B.; Doris, E.; Mioskowski, C. A Versatile Strategy for Quantum Dot Ligand Exchange. *J Am Chem Soc* **2007**, *129* (3), 482–483. https://doi.org/10.1021/ja067742y.

(35) Alvarenga, S.; Ponce, H.; González Oliva, I.; Rudamas, C. Changes on the Stokes Shift in Large CdSe Colloidal Quantum Dots by a Ligand Exchange. In *Proceedings of the 2nd International Conference of Theoretical and Applied Nanoscience and Nanotechnology (TANN'18)*; Avestia Publishing, 2018. https://doi.org/10.11159/tann18.140.

(36) Zhu, H.; Hu, M. Z.; Shao, L.; Yu, K.; Dabestani, R.; Zaman, M. B.; Liao, S. Synthesis and Optical Properties of Thiol Functionalized CdSe/ZnS (Core/Shell) Quantum Dots by Ligand Exchange. *J Nanomater* **2014**, *2014*. https://doi.org/10.1155/2014/324972.

(37) Zhang, K.; Yu, T.; Liu, F.; Sun, M.; Yu, H.; Liu, B.; Zhang, Z.; Jiang, H.; Wang, S. Selective Fluorescence Turn-on and Ratiometric Detection of Organophosphate Using Dual-Emitting Mn-Doped ZnS Nanocrystal Probe. *Anal Chem* **2014**, *86* (23), 11727–11733. https://doi.org/10.1021/ac503134r.

(38) Ren, T.; Mandal, P. K.; Erker, W.; Liu, Z.; Aviasevich, Y.; Puhl, L.; Mullen, K.; Basché, T. A Simple and Versatile Route to Stable Quantum Dot-Dye Hybrids in Nonaqueous and Aqueous Solutions. *J Am Chem Soc* **2008**, *130* (51), 17242–17243. https://doi.org/10.1021/ja8073962.

(39) György, E.; Pérez Del Pino, A.; Roqueta, J.; Ballesteros, B.; Miguel, A. S.; Maycock, C.; Oliva, A. G. Synthesis and Characterization of CdSe/ZnS Core-Shell Quantum Dots Immobilized on Solid Substrates through Laser Irradiation. *Physica Status Solidi (A) Applications and Materials Science* **2012**, *209* (11), 2201–2207. https://doi.org/10.1002/pssa.201127749.

(40) Akintola, O. S.; Saleh, T. A.; Khaled, M. M.; al Hamouz, O. C. S. Removal of Mercury (II) via a Novel Series of Cross-Linked Polydithiocarbamates. *J Taiwan Inst Chem Eng* **2016**, *60*, 602–616. https://doi.org/10.1016/j.jtice.2015.10.039.

(41) Drozd, M.; Pietrzak, M.; Kalinowska, D.; Grabowska-Jadach, I.; Malinowska, E. Glucose Dithiocarbamate Derivatives as Capping Ligands of Water-Soluble CdSeS/ZnS Quantum Dots. *Colloids Surf A Physicochem Eng Asp* **2016**, *509*, 656–665. https://doi.org/10.1016/j.colsurfa.2016.09.072.

(42) Tan, Y.; Jin, S.; Hamers, R. J. Photostability of CdSe Quantum Dots Functionalized with Aromatic Dithiocarbamate Ligands. **2013**.

(43) Casas, S.; Sanchez, August.; Bravo, J.; GARCiA-FONTAN, S.; Castellano, E. E.; Jones, M. M. *Cadmium Coordination Chemistry Related to Chelate Therapy**; 1989; Vol. 158.

(44) Zhang, L.; He, R.; Gu, H. C. Oleic Acid Coating on the Monodisperse Magnetite Nanoparticles. *Appl Surf Sci* **2006**, *253* (5), 2611–2617. https://doi.org/10.1016/j.apsusc.2006.05.023.

(45) Permatasari, F. A.; Aimon, A. H.; Iskandar, F.; Ogi, T.; Okuyama, K. Role of C-N Configurations in the Photoluminescence of Graphene Quantum Dots Synthesized by a Hydrothermal Route. *Sci Rep* **2016**, *6*. https://doi.org/10.1038/srep21042.

(46) Zhang, W.; Zhong, Y.; Tan, M.; Tang, N.; Yu, K. *Molecules Synthesis and Structure of Bis(Dibutyldithiocarbamate)Zinc(II): Zn 2 [(n-Bu) 2 NCSS] 4*; 2003; Vol. 8. http://www.mdpi.org/.

(47) Scharf, T. W.; Ott, R. D.; Yang, D.; Barnard, J. A. Structural and Tribological Characterization of Protective Amorphous Diamond-like Carbon and Amorphous CNx Overcoats for next Generation Hard Disks. *J Appl Phys* **1999**, *85* (6), 3142–3154. https://doi.org/10.1063/1.369654.

(48) Gong, P.; Hou, K.; Ye, X.; Ma, L.; Wang, J.; Yang, S. Synthesis of Highly Luminescent Fluorinated Graphene Quantum Dots with Tunable Fluorine Coverage and Size. *Mater Lett* **2015**, *143*, 112–115. https://doi.org/10.1016/j.matlet.2014.12.058.

(49) Ju, J.; Zhang, R.; He, S.; Chen, W. Nitrogen-Doped Graphene Quantum Dots-Based Fluorescent Probe for the Sensitive Turn-on Detection of Glutathione and Its Cellular Imaging. *RSC Adv* **2014**, *4* (94), 52583–52589. https://doi.org/10.1039/c4ra10601f.

(50) Artemenko, A.; Shchukarev, A.; Štenclová, P.; Wagberg, T.; Segervald, J.; Jia, X.; Kromka, A. Reference XPS Spectra of Amino Acids. In *IOP Conference Series: Materials Science and Engineering*; IOP Publishing Ltd, 2021; Vol. 1050. https://doi.org/10.1088/1757-899X/1050/1/012001.

(51) Artemenko, A.; Shchukarev, A.; Štenclová, P.; Wagberg, T.; Segervald, J.; Jia, X.; Kromka, A. Reference XPS Spectra of Amino Acids. In *IOP Conference Series: Materials Science and Engineering*; IOP Publishing Ltd, 2021; Vol. 1050. https://doi.org/10.1088/1757-899X/1050/1/012001.

(52) Bowen Katari, J. E.; Colvin, V. L.; Alivisatos, A. P. *X-Ray Photoelectron Spectroscopy of CdSe Nanocrystals with Applications to Studies of the Nanocrystal Surface*; 1994; Vol. 98.

(53) Bastidas, J. M.; Cano, E.; Torres, C. L. An XPS Study of Copper Corrosion Originated by Formic Acid Vapour at 40% and 80% Relative Humidity. *Materials and Corrosion* **2001**, *52*, 667–676. https://doi.org/10.1002/1521-4176(200109)52:9<667::AID-MACO667>3.0.CO;2-H.

(54) Bagaria, H. G.; Ada, E. T.; Shamsuzzoha, M.; Nikles, D. E.; Johnson, D. T. Understanding Mercapto Ligand Exchange on the Surface of FePt Nanoparticles. *Langmuir* **2006**, *22* (18), 7732–7737. https://doi.org/10.1021/la0601399.

(55) Vale, B. R. C.; Mourão, R. S.; Bettini, J.; Sousa, J. C. L.; Ferrari, J. L.; Reiss, P.; Aldakov, D.; Schiavon, M. A. Ligand Induced Switching of the Band Alignment in Aqueous Synthesized CdTe/CdS Core/Shell Nanocrystals. *Sci Rep* **2019**, *9* (1). https://doi.org/10.1038/s41598-019-44787-y.

(56) Riedo, E.; Comin, F.; Chevrier, J.; Schmithusen, F.; Decossas, S.; Sancrotti, M. *Structural Properties and Surface Morphology of Laser-Deposited Amorphous Carbon and Carbon Nitride Films*; 2000; Vol. 125. www.elsevier.nl/locate/surfcoat.

(57) Canava, B.; Vigneron, J.; Etcheberry, A.; Guillemoles, J. F.; Lincot, D. *High Resolution XPS Studies of Se Chemistry of a Cu(In, Ga)Se 2 Surface*.

(58) Cingarapu, S.; Yang, Z.; Sorensen, C. M.; Klabunde, K. J. Synthesis of CdSe/ZnS and CdTe/ZnS Quantum Dots: Refined Digestive Ripening. *J Nanomater* **2012**, *2012*. https://doi.org/10.1155/2012/312087.

(59) Granada-Ramirez, D. A.; Arias-Cerón, J. S.; Gómez-Herrera, M. L.; Luna-Arias, J. P.; Pérez-González, M.; Tomás, S. A.; Rodríguez-Fragoso, P.; Mendoza-Alvarez, J. G. Effect of the Indium Myristate Precursor Concentration on the Structural, Optical, Chemical Surface, and Electronic Properties of InP Quantum Dots Passivated with ZnS. *Journal of Materials Science: Materials in Electronics* **2019**, *30* (5), 4885–4894. https://doi.org/10.1007/s10854-019-00783-6.

(60) Tshabalala, K. G.; Cho, S. H.; Park, J. K.; Pitale, S. S.; Nagpure, I. M.; Kroon, R. E.; Swart, H. C.; Ntwaeaborwa, O. M. Luminescent Properties and X-Ray Photoelectron Spectroscopy Study of ZnAl2O4:Ce3+,Tb3+ Phosphor. *J Alloys Compd* **2011**, *509* (41), 10115–10120. https://doi.org/10.1016/j.jallcom.2011.08.054.

(61) Gopannagari, M.; Kumar, D. P.; Park, H.; Kim, E. H.; Bhavani, P.; Reddy, D. A.; Kim, T. K. Influence of Surface-Functionalized Multi-Walled Carbon Nanotubes on CdS Nanohybrids for Effective Photocatalytic Hydrogen Production. *Appl Catal B* **2018**, *236*, 294–303. https://doi.org/10.1016/j.apcatb.2018.05.009.

(62) Wang, J.; Zhou, X.; Ma, H.; Tao, G. Diethyldithiocarbamate Functionalized CdSe/CdS Quantum Dots as a Fluorescent Probe for Copper Ion Detection. *Spectrochim Acta A Mol Biomol Spectrosc* **2011**, *81* (1), 178–183. https://doi.org/10.1016/j.saa.2011.05.098.

(63) Kim, J. S.; Lee, C. W.; Han, K. Y. Energy Level Tuning of InP/ZnS Nanocrystals by Electronically Delocalized Dithiocarbamate Derivatives. *Mater Today Commun* **2019**, *18*, 149–152. https://doi.org/10.1016/j.mtcomm.2018.12.002.

(64) Yoo, J. Y.; Park, S. A.; Jung, W. H.; Lee, C. W.; Kim, J. S.; Kim, J. G.; Chin, B. D. Effect of Dithiocarbamate Chelate Ligands on the Optical Properties of InP/ZnS Quantum Dots and Their Display Devices. *Mater Chem Phys* **2020**, *253*. https://doi.org/10.1016/j.matchemphys.2020.123415.

(65) Yuan, C.; Zhang, K.; Zhang, Z.; Wang, S. Highly Selective and Sensitive Detection of Mercuric Ion Based on a Visual Fluorescence Method. *Anal Chem* **2012**, *84* (22), 9792–9801. https://doi.org/10.1021/ac302822c.

(66) Onyia, A. I.; Ikeri, H. I.; Nwobodo, A. N. Theoretical Study of the Quantum Confinement Effects on Quantum Dots Using Particle in a Box Model. *Journal of Ovonic Research* **2018**, *14* (1), 49–54.

(67) Malgras, V.; Nattestad, A.; Kim, J. H.; Dou, S. X.; Yamauchi, Y. Understanding Chemically Processed Solar Cells Based on Quantum Dots. *Science and Technology of Advanced Materials*. Taylor and Francis Ltd. January 1, 2017, pp 334–350. https://doi.org/10.1080/14686996.2017.1317219.

(68) Frederick, M. T.; Amin, V. A.; Swenson, N. K.; Ho, A. Y.; Weiss, E. A. Control of Exciton Confinement in Quantum Dot-Organic Complexes through Energetic Alignment of Interfacial Orbitals. *Nano Lett* **2013**, *13* (1), 287–292. https://doi.org/10.1021/nl304098e.

(69) Pu, C.; Peng, X. To Battle Surface Traps on CdSe/CdS Core/Shell Nanocrystals: Shell Isolation versus Surface Treatment. *J Am Chem Soc* **2016**, *138* (26), 8134–8142. https://doi.org/10.1021/jacs.6b02909.

(70) Ren, T.; Mandal, P. K.; Erker, W.; Liu, Z.; Aviasevich, Y.; Puhl, L.; Mullen, K.; Basché, T. A Simple and Versatile Route to Stable Quantum Dot-Dye Hybrids in Nonaqueous and Aqueous Solutions. *J Am Chem Soc* **2008**, *130* (51), 17242–17243. https://doi.org/10.1021/ja8073962.

(71) Rogach, A. L.; Franzl, T.; Klar, T. A.; Feldmann, J.; Gaponik, N.; Lesnyak, V.; Shavel, A.; Eychmüller, A.; Rakovich, Y. P.; Donegan, J. F. Aqueous Synthesis of Thiol-Capped CdTe Nanocrystals: State-of-the-Art. *Journal of Physical Chemistry C* **2007**, *111* (40), 14628–14637. https://doi.org/10.1021/jp072463y.

(72) Silva, F. O.; Carvalho, M. S.; Mendonça, R.; Macedo, W. A.; Balzuweit, K.; Reiss, P.; Schiavon, M. A. Effect of Surface Ligands on the Optical Properties of Aqueous Soluble CdTe Quantum Dots. *Nanoscale Res Lett* **2012**, *7* (1). https://doi.org/10.1186/1556-276x-7-536.

(73) Pearson, R. G. *Hard and Soft Acids and Bases*; ACADEMIC PRESS, INC., 1890; Vol. 5. https://doi.org/10.1016/B978-0-12-395706-1.50007-8.

(74) Bawendi, M. G.; Carroll, P. J.; Wilson, W. L.; Brus, L. E. Luminescence Properties of CdSe Quantum Crystallites: Resonance between Interior and Surface Localized States. *J Chem Phys* **1992**, *96* (2), 946–954. https://doi.org/10.1063/1.462114.

(75) Underwood, D. F.; Kippeny, T.; Rosenthal, S. J. Ultrafast Carrier Dynamics in CdSe Nanocrystals Determined by Femtosecond Fluorescence Upconversion Spectroscopy. *Journal of Physical Chemistry B* **2001**, *105* (2), 436–443. https://doi.org/10.1021/jp003088b.

(76) Kloepfer, J. A.; Bradforth, S. E.; Nadeau, J. L. Photophysical Properties of Biologically Compatible CdSe Quantum Dot Structures. *Journal of Physical Chemistry B* **2005**, *109* (20), 9996–10003. https://doi.org/10.1021/jp044581g.

(77) Kaniyankandy, S.; Verma, S. Role of Core-Shell Formation in Exciton Confinement Relaxation in Dithiocarbamate-Capped CdSe QDs. *Journal of Physical Chemistry Letters* **2017**, *8* (14), 3228–3233. https://doi.org/10.1021/acs.jpclett.7b01259.

(78) Xu, H.; Wang, Z.; Li, Y.; Ma, S.; Hu, P.; Zhong, X. A Quantum Dot-Based "off-on" Fluorescent Probe for Biological Detection of Zinc Ions. *Analyst* **2013**, *138* (7), 2181–2191. https://doi.org/10.1039/c3an36742h.

(79) Azpiroz, J. M.; Angelis, F. de. Ligand Induced Spectral Changes in CdSe Quantum Dots. **2015**. https://doi.org/10.1021/acsami.5b05418.

(80) Wang, B.; Anslyn, E. v. *Chemosensors: Principles, Strategies, and Applications*; 2011. https://doi.org/10.1002/9781118019580.

(81) Chemosensors, F.; Recognition, M.; Series, A. C. S. S.; Society, A. C. Fluorescent Chemosensors for Ion and Molecule Recognition. **1993**.

(82) Prodi, L.; Bolletta, F.; Montalti, M.; Zaccheroni, N. Luminescent Chemosensors for Transition Metal Ions. *Coord Chem Rev* **2000**, *205* (1), 59–83. https://doi.org/10.1016/S0010-8545(00)00242-3.

(83) Jeong, Y.; Yoon, J. Recent Progress on Fluorescent Chemosensors for Metal Ions. *Inorganica Chim Acta* **2012**, *381* (1), 2–14. https://doi.org/10.1016/j.ica.2011.09.011.

(84) Formica, M.; Fusi, V.; Giorgi, L.; Micheloni, M. New Fluorescent Chemosensors for Metal Ions in Solution. *Coord Chem Rev* **2012**, *256* (1–2), 170–192. https://doi.org/10.1016/j.ccr.2011.09.010.

(85) Erenburg, S. B.; Bausk, N. V; Zemskova, S. M.; Mazalov, L. N. *Spatial Structure of Transition Metal Complexes in Solution Determined by EXAFS Spectroscopy*; 2000; Vol. 448.

(86) Wang, H.; Song, D.; Zhou, Y.; Liu, J.; Zhu, A.; Long, F. Fluorescence Enhancement of CdSe/ZnS Quantum Dots Induced by Mercury Ions and Its Applications to the on-Site Sensitive Detection of Mercury Ions. https://doi.org/10.1007/s00604-021-04871-5/Published.

(87) Zhu, C.; Li, L.; Fang, F.; Chen, J.; Wu, Y. Functional InP Nanocrystals as Novel Near-Infrared Fluorescent Sensors for Mercury Ions. *Chem Lett* **2005**, *34* (7), 898–899. https://doi.org/10.1246/cl.2005.898.

(88) Wang, C. W.; Moffitt, M. G. Surface-Tunable Photoluminescence from Block Copolymer-Stabilized Cadmium Sulfide Quantum Dots. *Langmuir* **2004**, *20* (26), 11784–11796. https://doi.org/10.1021/la048390g.

(89) Spanhel, L.; Haase, M.; Weller, H.; Henglein, A. Photochemistry of Colloidal Semiconductors. 20. Surface Modification and Stability of Strong Luminescing CdS Particles. *J Am Chem Soc* **1987**, *109* (19), 5649–5655. https://doi.org/10.1021/ja00253a015.

(90) Chen, Y.; Rosenzweig, Z. Luminescent CdS Quantum Dots as Selective Ion Probes. *Anal Chem* **2002**, *74* (19), 5132–5138. https://doi.org/10.1021/ac0258251.

(91) Chen, J. L.; Zhu, C. Q. Functionalized Cadmium Sulfide Quantum Dots as Fluorescence Probe for Silver Ion Determination. *Anal Chim Acta* **2005**, *546* (2), 147–153. https://doi.org/10.1016/j.aca.2005.05.006.

(92) Page, L. E.; Zhang, X.; Jawaid, A. M.; Snee, P. T. Detection of Toxic Mercury Ions Using a Ratiometric CdSe/ZnS Nanocrystal Sensor. *Chemical Communications* **2011**, *47* (27), 7773–7775. https://doi.org/10.1039/c1cc11442e.

(93) Sun, X.; Liu, B.; Xu, Y. Dual-Emission Quantum Dots Nanocomposites Bearing an Internal Standard and Visual Detection for Hg2+. *Analyst* **2012**, *137* (5), 1125–1129. https://doi.org/10.1039/c2an16026a.

(94) World Health Organization. *Guidelines for Drinking-Water Quality.*; World Health Organization, 2011.

(95) *U.S. EPA National Primary Drinking Water Regulations*.

(96) Koneswaran, M.; Narayanaswamy, R. CdS/ZnS Core-Shell Quantum Dots Capped with Mercaptoacetic Acid as Fluorescent Probes for Hg(II) Ions. *Microchimica Acta* **2012**, *178* (1–2), 171–178. https://doi.org/10.1007/s00604-012-0819-0.

(97) Cai, Z. X.; Yang, H.; Zhang, Y.; Yan, X. P. Preparation, Characterization and Evaluation of Water-Soluble l-Cysteine-Capped-CdS Nanoparticles as Fluorescence Probe for Detection of Hg(II) in Aqueous Solution. *Anal Chim Acta* **2006**, *559* (2), 234–239. https://doi.org/10.1016/j.aca.2005.11.061.

(98) Zhou, Z. Q.; Yan, R.; Zhao, J.; Yang, L. Y.; Chen, J. L.; Hu, Y. J.; Jiang, F. L.; Liu, Y. Highly Selective and Sensitive Detection of Hg2+ Based on Fluorescence Enhancement of Mn-Doped ZnSe QDs by Hg2+-Mn2+ Replacement. *Sens Actuators B Chem* **2018**, *254*, 8–15. https://doi.org/10.1016/j.snb.2017.07.033.

(99) Liu, B.; Zeng, F.; Wu, G.; Wu, S. Nanoparticles as Scaffolds for FRET-Based Ratiometric Detection of Mercury Ions in Water with QDs as Donors. *Analyst* **2012**, *137* (16), 3717–3724. https://doi.org/10.1039/c2an35434a.

(100) Cao, B.; Yuan, C.; Liu, B.; Jiang, C.; Guan, G.; Han, M. Y. Ratiometric Fluorescence Detection of Mercuric Ion Based on the Nanohybrid of Fluorescence Carbon Dots and Quantum Dots. *Anal Chim Acta* **2013**, *786*, 146–152. https://doi.org/10.1016/j.aca.2013.05.015.

(101) Jin, S.; Harris, R. D.; Lau, B.; Aruda, K. O.; Amin, V. A.; Weiss, E. A. Enhanced Rate of Radiative Decay in Cdse Quantum Dots upon Adsorption of an Exciton-Delocalizing Ligand. *Nano Lett* **2014**, *14* (9), 5323–5328. https://doi.org/10.1021/nl5023699.

(102) Gui, R.; An, X.; Huang, W. An Improved Method for Ratiometric Fluorescence Detection of PH and Cd2+ Using Fluorescein Isothiocyanate-Quantum Dots Conjugates. *Anal Chim Acta* **2013**, *767* (1), 134–140. https://doi.org/10.1016/j.aca.2013.01.006.

(103) Mu, Q.; Li, Y.; Xu, H.; Ma, Y.; Zhu, W.; Zhong, X. Quantum Dots-Based Ratiometric Fluorescence Probe for Mercuric Ions in Biological Fluids. *Talanta* **2014**, *119*, 564–571. https://doi.org/10.1016/j.talanta.2013.11.036.

(104) Chen, J. L.; Zhu, C. Q. Functionalized Cadmium Sulfide Quantum Dots as Fluorescence Probe for Silver Ion Determination. *Anal Chim Acta* **2005**, *546* (2), 147–153. https://doi.org/10.1016/j.aca.2005.05.006.

(105) Granados-Oliveros, G.; Pineros, B. S. G.; Calderon, F. G. O. CdSe/ZnS Quantum Dots Capped with Oleic Acid and L-Glutathione: Structural Properties and Application in Detection of Hg2+. *J Mol Struct* **2022**, *1254*. https://doi.org/10.1016/j.molstruc.2021.132293.

(106) Chen, Y.; Rosenzweig, Z. Luminescent CdS Quantum Dots as Selective Ion Probes. *Anal Chem* **2002**, *74* (19), 5132–5138. https://doi.org/10.1021/ac0258251.

(107) Chen, J.; Zheng, A. F.; Gao, Y.; He, C.; Wu, G.; Chen, Y.; Kai, X.; Zhu, C. Functionalized CdS Quantum Dots-Based Luminescence Probe for Detection of Heavy and Transition Metal Ions in Aqueous Solution. *Spectrochim Acta A Mol Biomol Spectrosc* **2008**, *69* (3), 1044–1052. https://doi.org/10.1016/j.saa.2007.06.021.

CHAPTER 4

FINAL CONCLUSION AND PERSPECTIVES

The main objective of this thesis was to study the effect of mercury ions on the optical properties of CdSe-ZnS QDs with aromatic dithiocarbamate ligands. In this goal, the surface of CdSe-ZnS was modified with two ligands: an aryl dithiocarbamate and a dye ligand; the structural and optical properties were studied before and after adding mercury ions in different concentrations.

The results of structural analysis (size and shell thickness) and optical properties such as QY and photoluminescence decay kinetics analysis showed that the increase of [S] and [Zn^{2+}] precursor on the surface of CdSe-ZnS QDs produces surface traps, these traps are correlated with the concentration of precursors used during the synthesis of CdSe-ZnS QDs.

The coordination of ligands showed different behavior; the DTC ligand produces a quenching of PL while the Dye ligand produces a slight improvement of PL. The concentration of DTC ligands produces hole traps on the surface, decreasing the PL. However, the Dye ligand partially passivates these traps, improving the PL.

The analysis with different concentrations of mercury (Hg^{2+}) showed different mechanisms in the CdSe-ZnS core-shell and QD-Ligands (DTC and Dye); in QD-0.3 ML, a fluorescence quenching was produced due to the S-excess used, while an enhancement of fluorescence was observed in QD-0.9 ML, QD-1.0 ML, QDTC, and QDTCDye due the formation of HgS particles (pseudo shell) on the ZnS shell by cation exchange reaction decreasing the non-radiative recombination and improved the photoluminescence.

The CdSe-ZnS core-shell QDs showed a high LOD but poor selectivity in the Hg^{2+} and other cations analyzed. However, QDTC shows higher selectivity to Hg^{2+} ions than other cations evaluated and low LOD compared to similar nanomaterials. These results showed nanomaterials are innovative and promising in Hg^{2+} ion sensing.

PERSPECTIVES

The analysis with Hg^{2+} ions produce a quenching (QD-0.3 ML) and fluorescence enhancement in the rest of QDs. The low limit of detection (LOD) calculated for these nanomaterials is promising to use in environment analysis in the future.

The analysis and interaction between QDs and Hg^{2+} ions produce HgSe and HgS particles, these particles are semiconductors; the QDs not only detect Hg^{2+} ions, these nanomaterials can remove the Hg^{2+} from water and forming these particles on the surface of QDs. This phenomenon are very intereseting and promising due to can be used as a type of environment remediation with more studies in the future.

The low limit of detection (LOD) and selectivity shown in some QDs studied, such as QDTC, is enough to use in countries with high concentrations of mercury (Hg^{2+}) in their location affected.

The toxicology studies are necessary to use the QDs as mercury (Hg^{2+}) fluorescent sensors in the water.

The use of sulfur ligands, such as thiols and dithiocarbamates capped onto the surface of QDs produce different optical phenomenons in the QDs, and influence the selectivity and sensitivity in the interaction with Hg^{2+} ions, this is very promising to use as a sensor for mercury ions (Hg^{2+}).

CHAPTER 5

EXPERIMENTAL SECTION

6.1 Solvents

Commercially available products purchased from Sigma Aldrich, Alfa Aesar, and Fluka were used as received unless otherwise stated. Solvents of technical grade. Some reactions, like quantum dots and ligands, were performed under a nitrogen atmosphere using standard techniques. Dimethylsulfoxide ExtraDry 99.8% (DMSO) and toluene ExtraDry 99.9% were purchased from Acros Organics and stored over molecular sieves. Absolute ethanol (99.8%) and anhydrous methanol (99.8%) were purchased from Sigma Aldrich. Deuterated solvents for NMR analysis were bought from Sigma-Aldrich and Euriso-top. Deionized water was purified over an ion exchange column and a membrane filter of 0.45 μm (Micron Separation, Inc.). Solvents for spectroscopy without the addition of stabilizing agents or other absorbing material were employed as received.

6.2 Thin layer chromatography, silica, and alumina columns

Thin layer chromatography was performed on silica gel 60 F254 and alumina sheets on aluminum produced by Merck. Spots on the TLC plate were observed under UV light (254 nm / 365 nm), while an appropriate staining agent was employed for non-absorbing compounds. Column chromatography for separating organic compounds was performed using silica gel from Merck with a particle size of 40 – 63 μm (230 – 400 mesh). Organic crude compounds for separation were dissolved in a minimum amount of silica and solvent, concentrated and deposited on top of the column, and subsequently eluted.

6.3 Nuclear magnetic resonance spectroscopy (NMR)

^{1}H and ^{13}C-NMR spectra were recorded at 300 MHz at 295 K on a Bruker Avance 300 (^{1}H: 300 MHz, ^{13}C: 75 MHz) spectrometer. Chemical shifts are reported in ppm (δ) and are referenced to the NMR solvent residual peaks ($CDCl_3$, $(CD_3)_2SO$, D_2O) residual peak. Abbreviations are s = singlet, d = doublet, t = triplet, q = quartet, qu – quintet, dd = doublet of doublets, dt = doublet of triplets, and m = multiplet. The coupling constants (J) are reported in Hertz (Hz).

6.4 Mass spectrometry

Mass spectrometry was performed by the “Centre d’Etude Structurale et d’Analyse des Molecules Organique” (CESAMO) at the University of Bordeaux, on a QStar Elite mass spectrometer (Applied Biosystems). HR-MS were performed on an instrument equipped with an ESI source, and spectra were recorded in positive mode. The electrospray needle was maintained at 5000 V and operated at room temperature. Samples were injected through a 20 μL sample loop into a 4500 μL/min methanol flow from the LC pump. ESI-MS experiments were performed on an ion trap spectrometer equipped with an electrospray ion source (ESI), and spectra were recorded in positive mode.

6.5 Electronic absorption (UV-Vis) and fluorescence Spectroscopy

Electronic absorption spectra were measured on a Varian UV-Vis-NIR spectrophotometer Cary 5000. The wavelengths observed ranged from 250 – 700 nm. Sample solutions were measured in matched quartz cells with a path length of 10 mm. Before each measurement, a pure solvent baseline was recorded and subtracted from the measured spectra. Fluorescence emission spectra were measured on a HORIBA Jobin-Yvon Fluorolog-3 equipped with a xenon lamp (450 W), with Hamamatsu and R928P photomultiplier (PMT) detection. Quartz cells of 10 mm length were employed to study optically dilute samples with fluorescence emission measured at a right angle concerning the excitation beam. Time-correlated single photon counting was performed with a monochromatic pulsed light source (nanoLED 370 nm and 456 nm; 1.2 ns FWHM) on a Fluorolog-3 spectrofluorometer.

6.6 Fluorescence quantum yield

Fluorescence quantum yields were determined by comparison with an optically dilute fluorescence standard of known quantum yield according to the Parker method[1] in quartz cells. The fluorescence quantum yield of the sample solution (Φ) was then calculated using Equation 8 where Φ_R is the fluorescence quantum yield of the reference, I am the integral of the fluorescence emission of the sample solution, I_R is the integral of the fluorescence emission of the reference, A is the absorption at the excitation wavelength, and η is the refractive index of the solvent used. An optically dilute solution of rhodamine 6G in ethanol (Φ = 0.95) for QDs and coumarin 153 in ethanol (Φ = 0.38) for the Dye were used as the standard at λ_{ex} = 500 nm and 425 nm, respectively, slit : 3 (excitation) and 2 (emission), integration time: 0.3 s.[1,2]

Equation 8 $$QY = QY_R \left(\frac{I_S}{I_R}\right) x \left(\frac{A_R}{A_S}\right) x \left(\frac{\eta_S}{\eta_R}\right)^2$$

6.8 Optical change induced by Hg^{2+}

6.8.1 UV-Vis and Fluorescence Analysis

The Effect of Hg^{2+} ions on the fluorescence of CdSe/ZnS QDs functionalized by oleic acid, dithiocarbamate (DTC), and Dye was studied at different concentrations of Hg^{2+} ions, as described below. 100 µL of Hg^{2+} ions aqueous solution (0.15 µM - 5.0 µM) was added to 3000 µL of an ethanolic solution containing CdSe/ZnS, CdSe/ZnS/DTC and CdSe/ZnS/DTC-Dye QDs (240, 120 and 120 ppm, respectively). The mixtures containing Hg^{2+} and QDs systems were stirred at room temperature, and then electronic absorption spectra were recorded in a range between 250-700 nm, and PL spectra were measured using a λ_{exc} = 380 nm, slit : 3 (excitation) and 2 (emission), integration time: 0.3 s.

6.8.2 Effect with other cations

The changes in electronic absorption and fluorescence intensity originated from several metal ions (Mn^{2+}, Co^{2+}, Pb^{2+}, Ni^{2+}, Ba^{2+}, Cd^{2+}, and Zn^{2+}) and were determined with experimental conditions similar to the detection of Hg^{2+}. In a typical experiment, 100 μL of an aqueous solution of metal salt (5.0 μM) was added to 3000 μL of an ethanolic solution of CdSe/ZnSe/DTC and CdSe/ZnSe/DTC-Dye (120 and 120 ppm, respectively). In the case of CdSe/ZnS/OA QDs, 100 μL of metal salt in aqueous solution (5.0 μM) were dispersed into 3000 μL of CdSe/ZnS/OA dissolved in a mixture $CHCl_3$/EtOH 1:1 (240 ppm). The mixtures containing cations and QDs systems were stirred at room temperature, and then electronic absorption spectra were recorded in a range between 250-700 nm, and PL spectra were measured using a λ_{exc} = 390 nm, slit : 3 (excitation) and 2 (emission), integration time: 0.3 s.

6. 9 FT-IR spectroscopy

Infrared spectra of functionalized ligands and quantum dots were recorded with a Thermo Nicolet Nexus 670 FTIR spectrometer at a resolution of 4 cm^{-1} using a KBr pellet, adding 50 scans.

6. 9 X-ray diffraction (XRD) analysis

Panalytical X'Pert3 Pro-Multipurpose Diffractometer with CuKα radiation source (45 kV and 40 mA) was employed to measure the powder XRD patterns. The diffraction dataset cards from the Joint Committee of Powders Diffraction Standards (JCPDS) were used to compare the obtained patterns.

6.10 High-Resolution Transmission Emission Microscopy (HR-TEM)

The High-Resolution Transmission Electron Microscopy (HR-TEM) images of the QDs were taken using a Tecnai F20 Super Twin TMP Microscope, Field emission source, resolution of 0.1 nm at 200 Kv, maximum magnification at TEM 1.0 MX, GATAN US 1000XP-P camera. EDX Oxford Instruments XMAX detector. STEM Analysis - FISCHIONE Instruments Model M3000 FP5360/22 HAADF Detector 120/200 kV. The samples were dispersed in chloroform using an ultrasonic bath. After, a drop was deposited on a carbon film grid; then, the sample was dried and analyzed in the transmission microscope using 450.000 x magnification. Image-J software was used to calculate the average diameter and d-spacing [111] of QDs with HR-TEM micrographs.

The shell thickness parameter is the value obtained of the difference between the size of QDs core-shell (CdSe-ZnS) and size core (CdSe) from HRTEM analysis.

$$Shell\ thickness = Size\ CdSe/ZnS\ QDs - Size\ CdSe\ core\ QDs$$

(Equation 8)

The monolayer number (ML) was calculated as the ratio value between the experimental shell thickness parameter and ZnS zinc-blende theoric monolayer size (0. 70 nm).[3]

$$Monolayer\ number\ (ML) = \frac{shell\ thickness\ experimental}{0.70\ nm}$$ (Equation 9)

6.11 X-ray Photoelectron Spectroscopy (XPS)

The XPS experiments were recorded using the XPS / ISS / UPS- ACenteno surface characterization platform built by SPECS (Germany). The platform is equipped with a PHOIBOS 150 2D-DLD energy analyzer. A monochromatized Al Kα X-ray source (FOCUS 500) operated at 100 W was used for the measurements. The pass energy of the hemispherical analyzer was set at 100 eV for general spectra and 20 eV for high-resolution spectra. The samples were mounted on copper conductive tape in stainless steel metal sample holders for analysis and provided by the manufacturer SPECS. These sample holders are electrically connected to the spectrometer. CasaXPS program (Casa Software Ltd) for data analysis and the SPECS Prodigy library for RSF values were used.

6.12 Time-resolved luminescence

TRPL measurements were carried out using a Horiba Fluorolog Time-Correlated Single Photon Counter (TCSPC) system, using a 635 nm laser diode as the pump emitting pulses with 60 ps width and peak powers of 300 mW. Emission was measured with a Hamamatsu infrared detector. Measurements were performed at room temperature.

6.13 Synthesis

6.13.1 Quantum dots CdSe/ZnS/OA

CdSe core QDs were prepared via published reports.[4–6] 34.2 mg (0.25 mmol) of CdO, 0.6 mL (1.9 mmol) of oleic acid (OA), and 10 mL of 1-octadecene (ODE) were mixed into a 250 mL three-neck flask under N_2 protection. The mixture was heated at 225 °C under magnetic stirring for 90 min. In these conditions, CdO was dissolved. In another three-neck flask and under N_2 atmosphere, Se/TOP was prepared by mixing 30.5 mg (0.38 mmol) of selenium powder, 5 mL of ODE, and 0.45 mL (0.90 mmol) of tri-n-octyl phosphine (TOP) solution; and heated at 80 °C for 3 h. Then, 1.0 mL Se/TOP was quickly injected

into CdO solution at 225 °C for CdSe nucleus growth for 3 mins, and at that moment, the temperature was adjusted to 100 °C.

After this, three Zn/S/TOP solutions were prepared by mixing 32, 160, and 320 μL (0.188, 0.940, and 1.88 mmol) of $Zn(C_2H_5)_2$ solution, 64 μL (0.28 mmol) of $(TMS)_2S$ and 1 mL (2 mmol) of TOP under N_2 atmosphere. This solution was added dropwise to CdSe solution under magnetic stirring, keeping N_2 atmosphere, and heated to 80 °C for 4 h. CdSe/ZnS/OA QDs were washed with an excess of methanol many times to remove the excess of unbound ligands (OA and TOP). After that, the QDs were precipitated when 10 mL of cold chloroform was added at 30 °C, followed by centrifugation at 4,000 rpm for 5 min. The resulting solid was dissolved in toluene, precipitated with chloroform and acetonitrile (1:1 volumetric ratio) at 30 °C, and centrifuged at 4000 rpm for 10 min. This purification process was repeated 3 times.[7]

6.13.2 Ligands

6.13.2.1 Dithiocarbamate

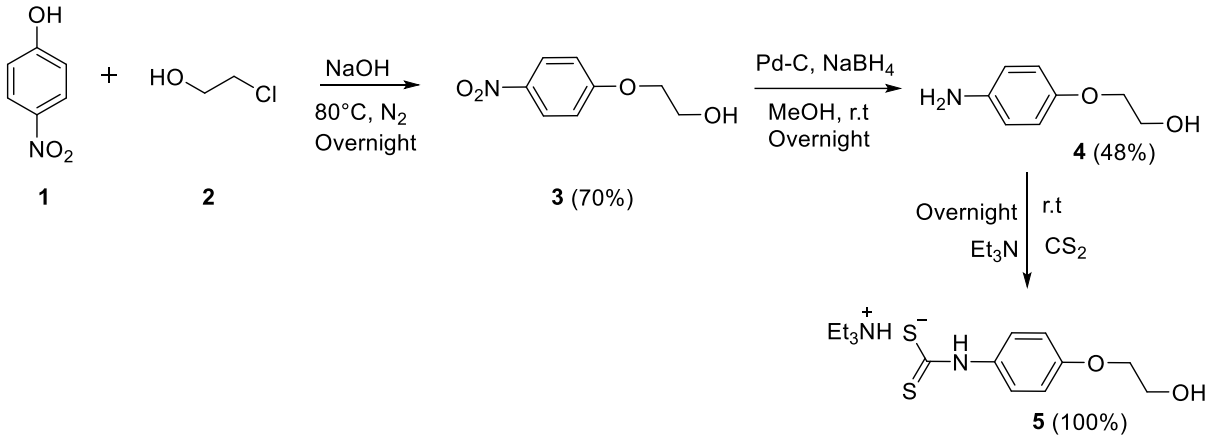

Figure 42. General synthesis route of dithiocarbamate (DTC).

2-(4-Nitrophenoxy)ethanol

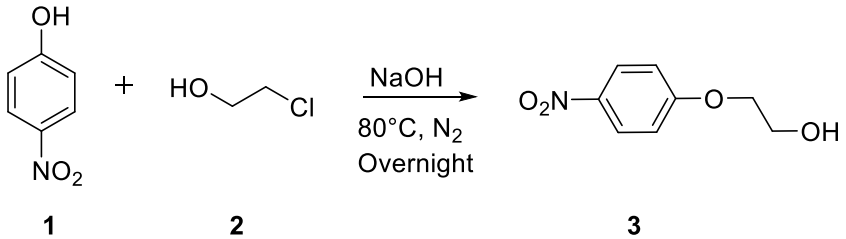

p-Nitrophenol **1** (3 g, 2.158 mmol) was added to a solution of 2-chloroethanol **2** (2.90 mL, 43.16 mmol) and NaOH (1.73 g, 43.16 mmol) in H_2O (10 mL). The mixture was refluxed overnight at 80 °C under a

nitrogen atmosphere, cooled to room temperature, diluted with H_2O, and extracted with ethyl acetate (EtOAc) several times (~5 times). The organic phases were washed sequentially with saturated aqueous NaCl, dried over anhydrous Na_2SO_4, and evaporated to dryness under reduced pressure to obtain the crude compound. The crude compound was purified by silica chromatography using a mixture of $CHCl_3$:EtOAc (50:50 to 0:100, v/v) as eluent, followed by TLC to obtain compound **3** as a white solid. Yield: 70 %. ^{1}H NMR ($CDCl_3$, 300 MHz) δ 1.95 (bs, 1H, -CH_2OH), 4.05 (t, J=5.4 Hz, 2H, -CH_2OH), 4.20 (t, 2H, -CH_2OAr), 7.02 (d, J=9.2 Hz, 2H, Ar-H), 8.23 (d, J=9.4 Hz, 2H, Ar-H). The analysis is in agreement with the literature data.[8]

2-(4-aminophenoxy) ethanol

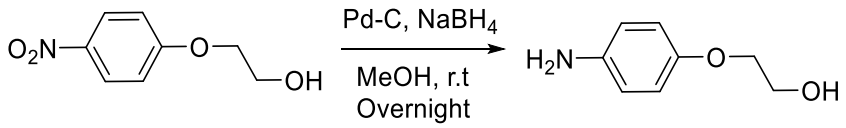

3 **4**

A solution of Sodium borohydride (1.087g, 9.58 mmol) in methanol was added to a mixture of **3** (1.468 g, 28.74 mmol) and 10% palladium on carbon (0.244g) in methanol (20 mL). The mixture was stirred in an ice-water bath overnight. After that, the solid was removed by filtration over celite, and the solvent was removed by rotatory evaporation. The crude product was purified by silica chromatography using CH_2Cl_2:EtOAc (50:50 – 0:100 v/v) as eluent followed by TLC. Yield: 48%. ^{1}H NMR ($CDCl_3$, 300 MHz), δ 3.94 (dd, J=5.0 Hz, 2H, -CH_2O-), 4.03 (dd, J=5.4 Hz, 2H, -CH_2OAr), 6.50 (m, 2H, Ar-H), 6.65 (m, 2H, Ar-H). The analysis is in agreement with the literature data.[9]

Triethylammonium (4-(2-hydroxyethoxy) phenyl)carbamodithioate

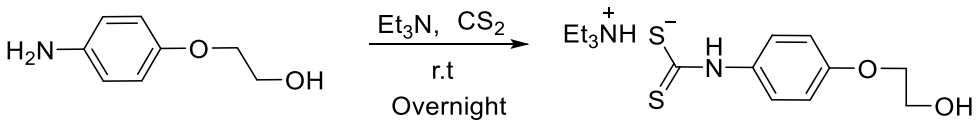

4 **5**

An excess of triethylamine (1 mL) and carbon disulfide (1 mL) was sequentially added to a solution of 2-(4-aminophenoxy) ethanol **4** (10 mmol) in THF (10 mL).[10] The reaction mixture was stirred overnight at room temperature. The mixture was centrifugated and washed with diethyl ether three times. The final compound was dried overnight. Yield: 100%. ^{1}H NMR (D_2O, 300 MHz), δ 1.17 (t, 9H, -CH_3 x 3), 3.10 (quartet, -H, -CH_2- x 2), 3.83 (t, 2H, -CH_2-OH), 4.06 (t, 2H, -CH_2-), 6.95 (d, 2H, Ar-H), 7.17 (d, 2H, -Ar-H). ^{13}C NMR (D_2O, 300 MHz), δ 8.28, 60.07, 69.43, 114.93, 127.60, 134.42, 156.66, 213.73. HRMS (ESI): m/z calculated for $C_9H_{10}NO_2S_2$: 228.01584, found: 228.01589.

6.13.2.2 Dye

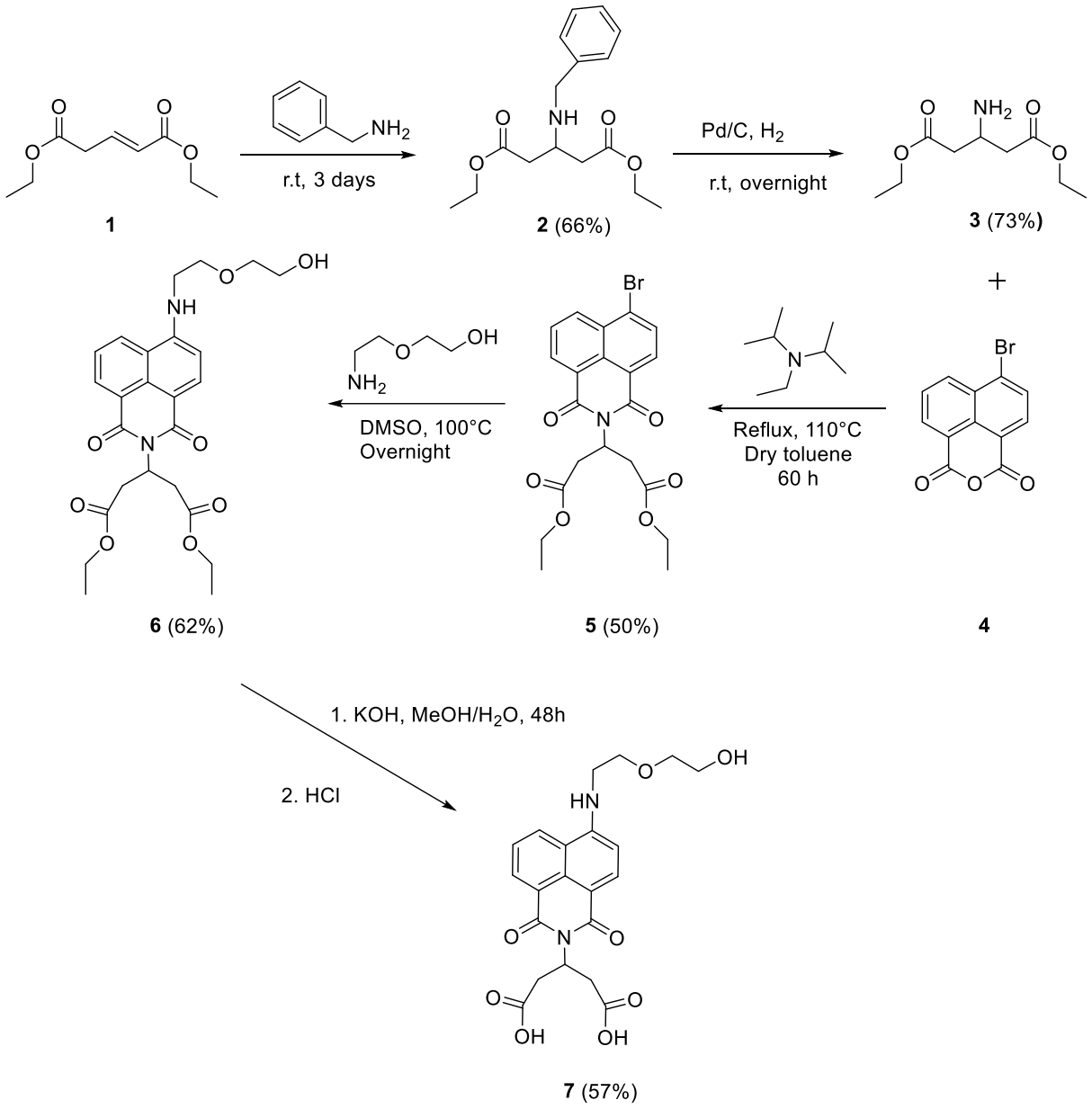

Figure 43. General synthesis route of Dye ligand.

Diethyl 3-(benzylamino)pentanedioate

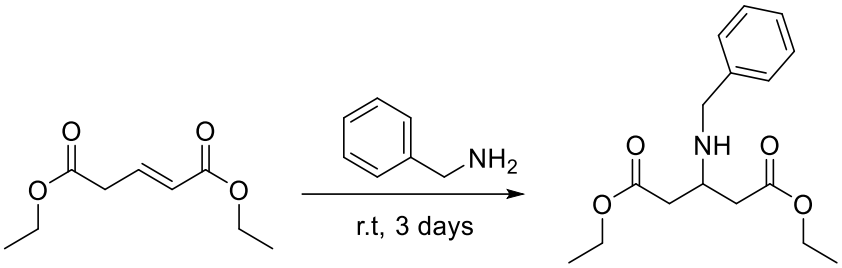

1 **2**

A solution of benzylamine (0.7 mL, 6.40 mmol) in methanol (10 mL) was stirred at room temperature for three days in the presence of diethyl gluconate (1.0 mL, 3.60 mmol).[11] The reaction mixture was then concentrated under reduced pressure, and the resulting crude material was purified by chromatography on silica gel (EtOAc/hexane 1:3) to afford **2** as a colorless oil (1.58 g, yield 66%). ^{1}H NMR (300 MHz, $CDCl_3$): δ 1.27 (t, 6H -CH_3 x 2), 1.96 (s, 1H; NH), 2.56-2.58 (d, 4H, J=6.26 Hz -CH_2=O), 3.47 (q, 1H, -CH-), 3.82 (s, 2H, -CH_2-Ar), 4.15 (quartet, 4H, -CH_2-O- x 2), 7.23-7.31 (m, 5H, Ar-H). ^{13}C NMR (300 MHz, $CDCl_3$), δ 14.13, 38.73, 49.87, 51.61, 60.48, 126.99, 128.22, 140.09, 171.79, 172.26. HRMS (ESI): m/z calculated for $C_{16}H_{23}NO_4^+$: 294.16998, found: 294.16945.

Diethyl 3-aminopentanedioate

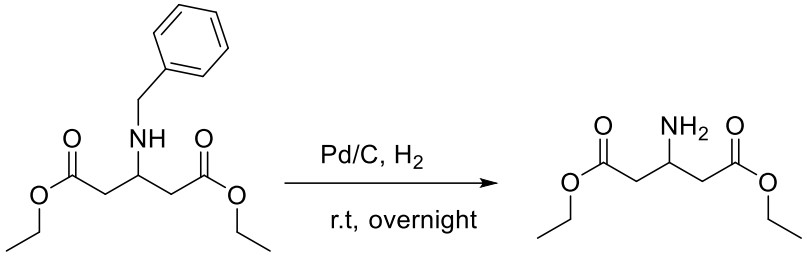

2 **3**

Compound **2** (1.58 g 0.75 mmol) was dissolved in methanol (4 mL) and reduced under H_2 atmosphere for 6 h in the presence of 10% Pd/C (26 mg). The reaction mixture was then filtered on Celite and concentrated under reduced pressure.[11] Compound **3** was obtained as a colorless oil without additional purification (1.16 g, yield 73%). ^{1}H NMR (300 MHz, $CDCl_3$): δ 1.26 (t, 6H -CH_3 x 2), 2.28-2.47 (m, 4H), 3.55 (m, 1H, -CH-), 3.63 (s, 4H, -CH_2- x 2), 4.05-4.12 (quartet, 2H, -NH_2). ^{13}C NMR (300 MHz, $CDCl_3$), δ 14.13, 41.39, 41.64, 45.72, 51.58, 60.46, 171.74, 172.18. HRMS (ESI): m/z calculated for $C_{16}H_{23}NO_4^+$: 294.16998, found: 294.16945.

Diethyl 3-(6-bromo-1,3-dioxo-1H-benzo[de]isoquinolin-2(3H)-yl)pentanedioate

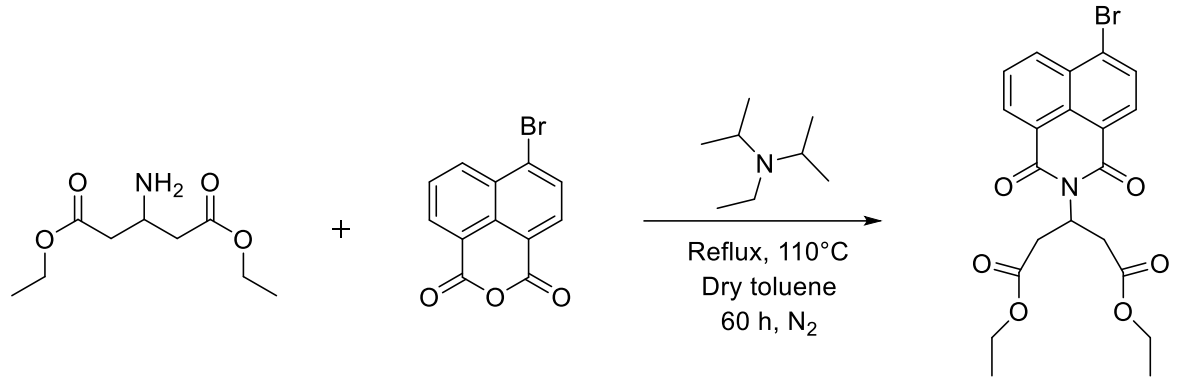

3 **4** **5**

4-Bromo-1,8-naphthalic anhydride (1.58g, 7.76 mmol) and diethyl 3-aminopentanedioate (1.16 g, 5.70 mmol) are dissolved in 50 mL of dry toluene and kept under N_2, diisopropylethylamine (3.22 ml, 18.81 mmol) is added under N_2, and the resulting mixture is heated at 110°C for 60 hours. The solution is filtered while hot and evaporated to dryness. The crude product is purified by chromatography on alumina using a mixture of hexane: ethyl acetate (8:2, v/v), followed by TLC, the fractions obtained are combined and concentrated to obtain a yellow-orange oil which dries to give a solid (1.66 g, yield 50%).

^{1}H NMR (300 MHz, $CDCl_3$) : δ 1.15 (t, 6H -CH_3 x 2), 3.02 (d, 1H, J=6.22 Hz), 3.08 (d, 1H, J=6.17 Hz), 3.27 (d, 1H, J=8.55 Hz), 3.33 (d, 1H, J=8.57 Hz), 4.08 (q, 4H, J=7.09 Hz), 6.04 (m, 1H), 7.86 (t, 1H, J=7.31 Hz), 8.06 (d, 1H, J=7.86 Hz), 8.43 (d, 1H, J=7.89 Hz), 8.59 (d, 1H, J=8.53 Hz), 8.67 (d, 1H, J=7.34 Hz). ^{13}C NMR (300 MHz, $CDCl_3$), δ 14.06, 36.38, 36.64, 46.00, 51.81, 60.65, 122.22, 123.09, 128.11, 129.17, 130.30, 130.60, 131.11, 131.50, 132.29, 133.29, 163.88, 170.74, 171.26. HRMS (ESI): m/z calculated for $C_{21}H_{21}NO_6Br$: 462.0557, found: 462.0545.

Diethyl 3-(6-((2-(2-hydroxyethoxy)ethyl)amino)-1,3-dioxo-1H-benzo[de]isoquinolin-2(3H)-yl)pentanedioate

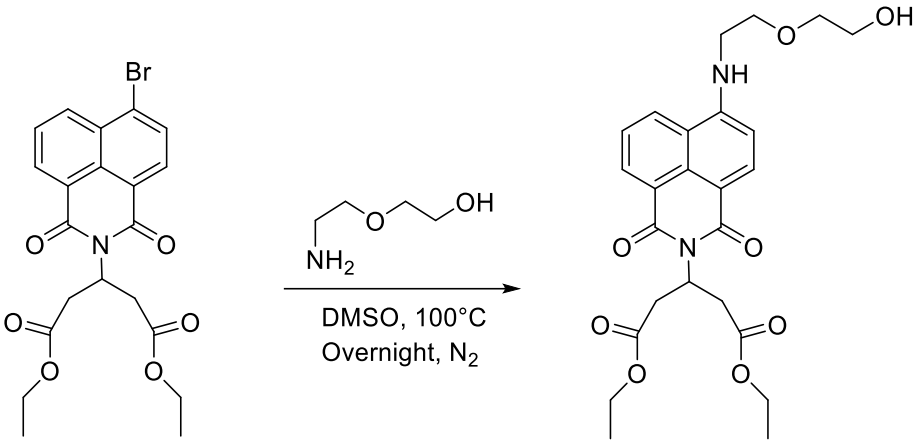

6 **7**

The diester (1.40 g, 3.02 mmol) is dissolved in 15 mL DMSO. 2-(2-aminoethoxy) ethanol (3 mL, 30.2 mmol) is added under N_2, and the solution is heated at 100°C overnight. After cooling down, the solution is poured into water and extracted many times (around 6 times) with ethyl acetate. The organic phases are combined and washed 3 times with a solution of NaCl saturated. The organic phase is dried over Na_2SO_4 anhydrous and concentrated. The crude product is purified by silica chromatography using EtOAc as eluent, followed by TLC, and concentrated to obtain a yellow oil (0.87 g, yield 62.1%).

^{1}H NMR (300 MHz, $CDCl_3$) : δ 1.13 (t, 6H -CH_3 x 2), 3.03 (d, 1H), 3.08 (d, 1H), 3.26 (d, 1H, J=8.27 Hz), 3.31 (d, 1H, J=8.31 Hz), 3.49 (q, 2H, J=5.14 Hz), 3.49 (m, 5H), 6.03 (ddd, 1H, J=6.25 Hz), 6.13 (t, 1H, J=7.13 Hz), 6.51 (d, 1H, J=8.50 Hz), 7.28 (t, 1H, J=7.31 Hz), 7.98 (dd, 1H, J=8.53 Hz), 8.31 (m, 2H). ^{13}C NMR (300 MHz, $CDCl_3$), δ 14.15, 36.70, 36.95, 43.28, 45.52, 51.78, 60.62, 61.71, 68.67, 72.41, 104.07, 109.71, 119.98, 122.42, 124.21, 126.57, 129.71, 149.79, 164.35, 164.93, 171.33, 171.84. HRMS (ESI): m/z calculated for $C_{25}H_{29}NO_8^-$: 485.1929, found: 485.1924.

3-(6-((2-(2-hydroxyethoxy) ethyl) amino)-1,3-dioxo-1H-benzo[de]isoquinolin-2(3H)-yl)pentanedioic acid

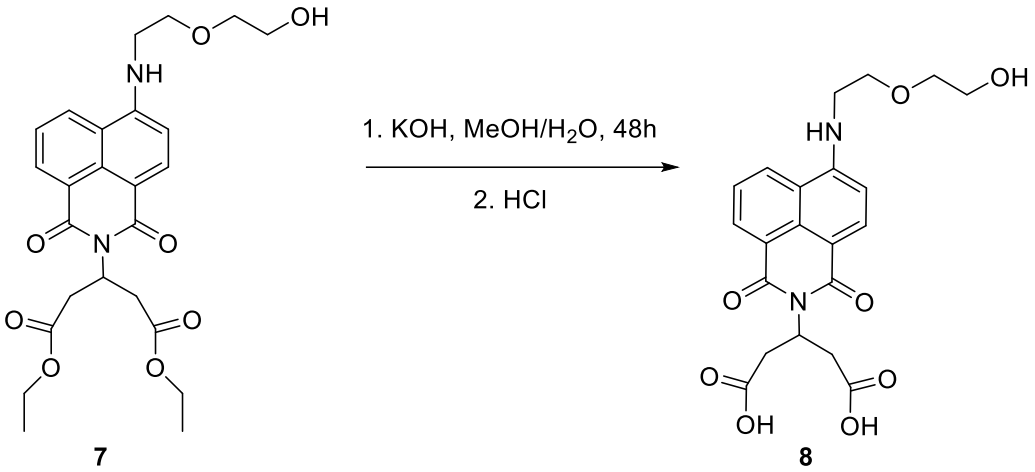

Diester (0.87 g, 1.78 mmol) is dissolved in MeOH (15 mL), 3 mL of an aqueous solution of KOH is added (10 eq), and the resulting solution is stirred for 48 h at room temperature. After evaporation of MeOH, water is added (10 mL), and the solution is acidified to pH: 1 with HCl 4M. The compound is extracted (around 6 times) with EtOAc, dried over Na_2SO_4 anhydrous, and concentrated. The compound was obtained as a yellow solid (0.50 g, yield 57.4%).

^{1}H NMR (300 MHz, DMSO d_6) : δ 2.86 (dd, 2H, J=6.64 Hz), 3.06 (dd, 1H, J=8.15 Hz), 3.33 (s, 2H), 3.59 (t, 2H, J=5.49 Hz), 3.73 (t, 2H, J=5.67 Hz), 4.63 (s, 1H), 5.82 (q, 1H, J=7.37 Hz), 6.84 (d, 1H, J=8.68 Hz), 7.69 (t, 1H, J=7.85 Hz), 7.75 (t, 1H, J=5.46 Hz), 8.25 (d, 1H, J=8.47 Hz), 8.42 (d, 1H, J=7.31 Hz), 8.69 (d, 1H, J=8.45 Hz), 12.15 (s, 1H). ^{13}C NMR (300 MHz, DMSO d_6), δ 37.12, 43.16, 45.54, 60.71, 68.57, 72.78, 104.30, 120.46, 124.73, 128.98, 130.03, 150.95, 172.67. HRMS (ESI): m/z calculated for $C_{21}H_{21}N_2O_8^-$: 429.1303, found: 485.1300.

6.13.3 Ligand Exchange

A solution of QDs (5mg) in 2mL of hexane and mixed with DTC and Dye (15 mg respectively) in 2mL MeOH was stirred at 60°C for 1 h. The UV-vis and FL spectra were recorded for 4h to determine the ideal time of the ligand exchange. After this time, the reaction mixture was cooled at room temperature, a precipitate was formed, and the solution was centrifuged and washed with methanol (three times) to remove the excess unbound ligands (DTC and Dye). The sample was dried overnight to use in the following steps.

REFERENCES

(1) Yu, W. W.; Qu, L.; Guo, W.; Peng, X. Experimental Determination of the Extinction Coefficient of CdTe, CdSe, and CdS Nanocrystals. *Chemistry of Materials* **2003**, *15* (14), 2854–2860. https://doi.org/10.1021/cm034081k.

(2) Brouwer, A. M. Standards for Photoluminescence Quantum Yield Measurements in Solution (IUPAC Technical Report). *Pure and Applied Chemistry*. 2011, pp 2213–2228. https://doi.org/10.1351/PAC-REP-10-09-31.

(3) Hao, J.; Liu, H.; Miao, J.; Lu, R.; Zhou, Z.; Zhao, B.; Xie, B.; Cheng, J.; Wang, K.; Delville, M. H. A Facile Route to Synthesize CdSe/ZnS Thick-Shell Quantum Dots with Precisely Controlled Green Emission Properties: Towards QDs Based LED Applications. *Sci Rep* **2019**, *9* (1). https://doi.org/10.1038/s41598-019-48469-7.

(4) Peng, Z. A.; Peng, X. Mechanisms of the Shape Evolution of CdSe Nanocrystals. *J Am Chem Soc* **2001**, *123* (7), 1389–1395. https://doi.org/10.1021/ja0027766.

(5) Boatman, E. M.; Lisensky, G. C.; Nordell, K. J. *A Safer, Easier, Faster Synthesis for CdSe Quantum Dot Nanocrystals*; 2005. www.JCE.DivCHED.org.

(6) Stiven Gómez-Piñeros, B.; Granados-Oliveros, G. *Fisicoquímica y Química Inorgánica*; 2015; Vol. 44.

(7) Granados-Oliveros, G.; Pineros, B. S. G.; Calderon, F. G. O. CdSe/ZnS Quantum Dots Capped with Oleic Acid and L-Glutathione: Structural Properties and Application in Detection of Hg2+. *J Mol Struct* **2022**, *1254*. https://doi.org/10.1016/j.molstruc.2021.132293.

(8) Luo, G.; Chen, M.; Lyu, W.; Zhao, R.; Xu, Q.; You, Q.; Xiang, H. Design, Synthesis, Biological Evaluation and Molecular Docking Studies of Novel 3-Aryl-4-Anilino-2H-Chromen-2-One Derivatives Targeting ERα as Anti-Breast Cancer Agents. *Bioorg Med Chem Lett* **2017**, *27* (12), 2668–2673. https://doi.org/10.1016/j.bmcl.2017.04.029.

(9) Qiu, X. P.; Korchagina, E. v.; Rolland, J.; Winnik, F. M. Synthesis of a Poly(N-Isopropylacrylamide) Charm Bracelet Decorated with a Photomobile α-Cyclodextrin Charm. *Polym Chem* **2014**, *5* (11), 3656–3665. https://doi.org/10.1039/c3py01776a.

(10) Murru, S.; Ghosh, H.; Sahoo, S. K.; Patel, B. K. Intra- and Intermodular C-S Bond Formation Using a Single Catalytic System: First Direct Access to Arylthiobenzothiazoles. *Org Lett* **2009**, *11* (19), 4254–4257. https://doi.org/10.1021/ol9017535.

(11) Song, X. P.; Bouillon, C.; Lescrinier, E.; Herdewijn, P. Iminodipropionic Acid as the Leaving Group for DNA Polymerization by HIV-1 Reverse Transcriptase. *ChemBioChem* **2011**, *12* (12), 1868–1880. https://doi.org/10.1002/cbic.201100160.

ANNEXES

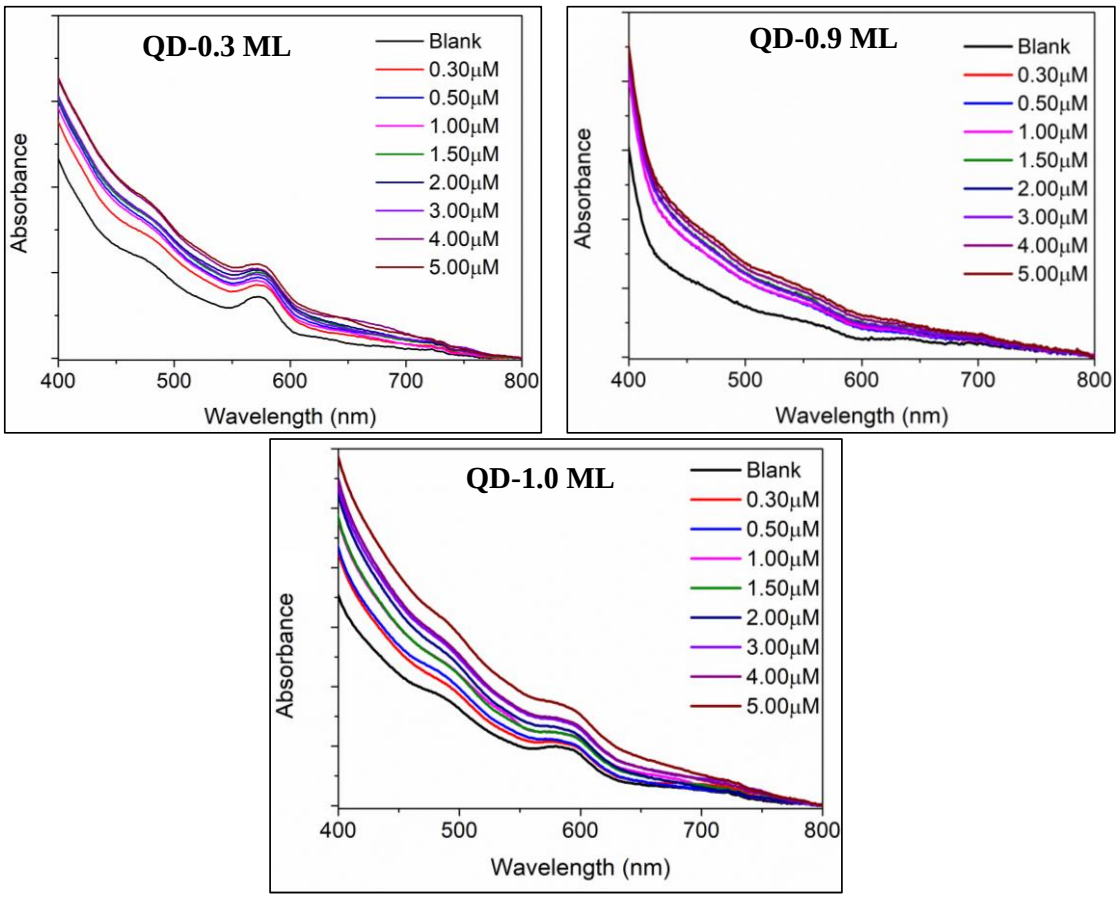

Figure 44. Absorption spectra of CdSe-ZnS QDs with different [Hg^{2+}]. a) QD-0.3 ML ; b) QD-0.9 ML and QD-1.0 ML.

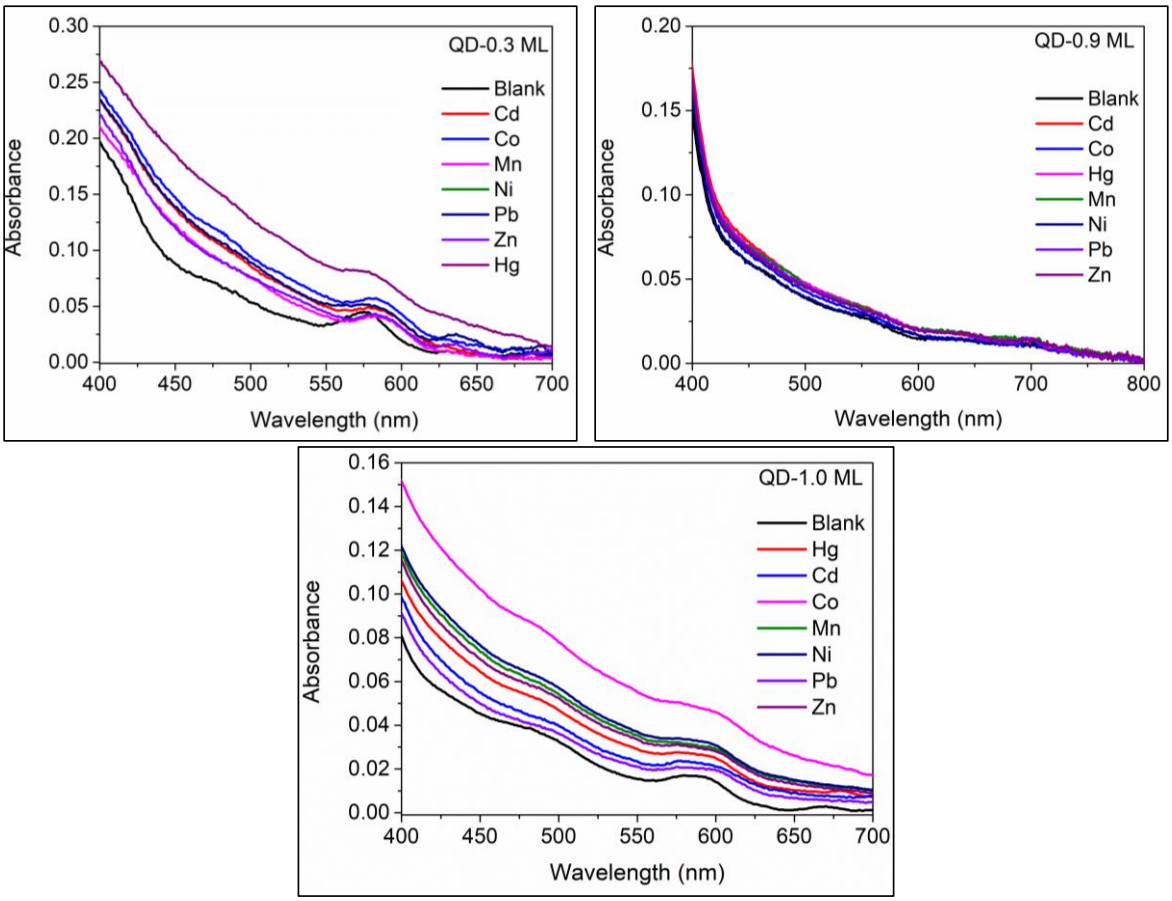

Figure 45. Absorption spectra of QDs core-shell with different cations evaluated at 5µM.

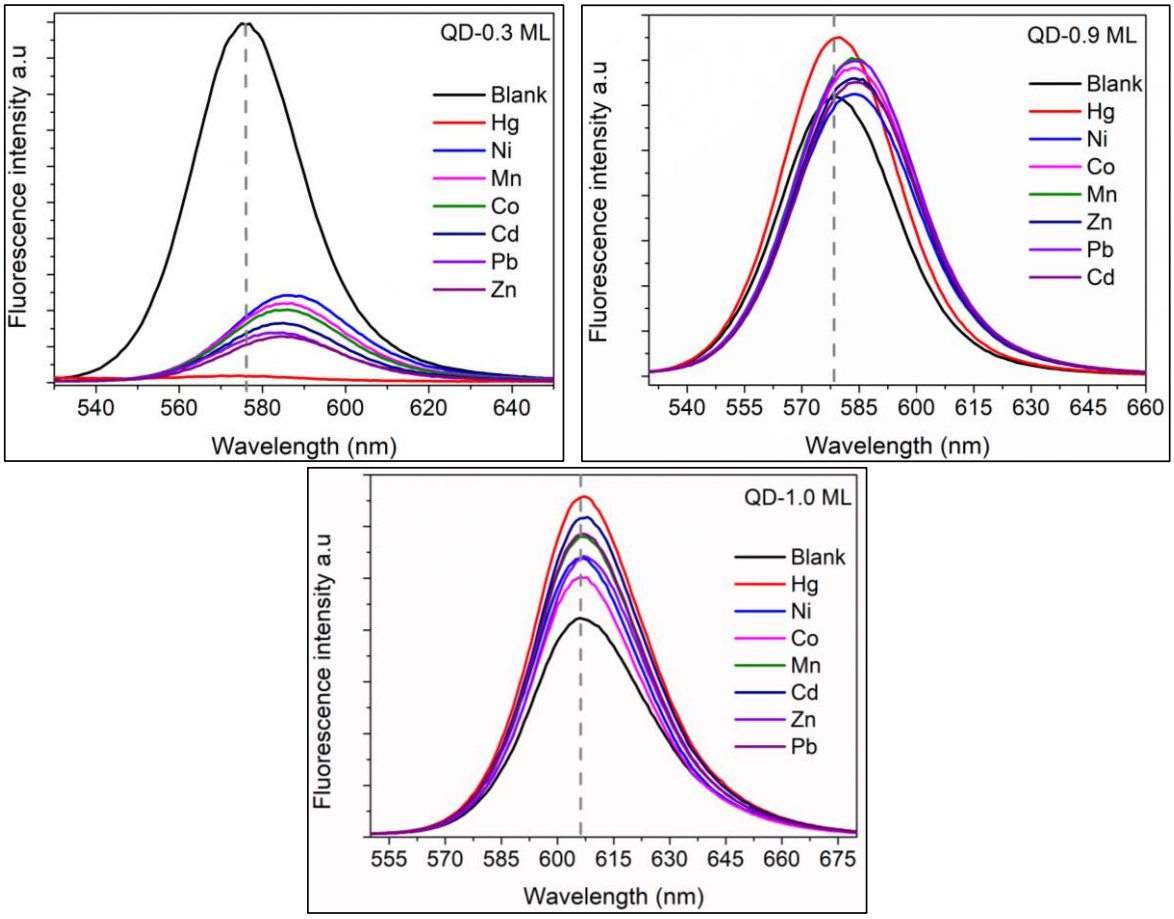

Figure 46. Fluorescence spectra of QDs core-shell with different cations evaluated at 5µM.

Nuclear Magnetic Resonance (^{1}H and ^{13}C) spectra of synthesized compounds

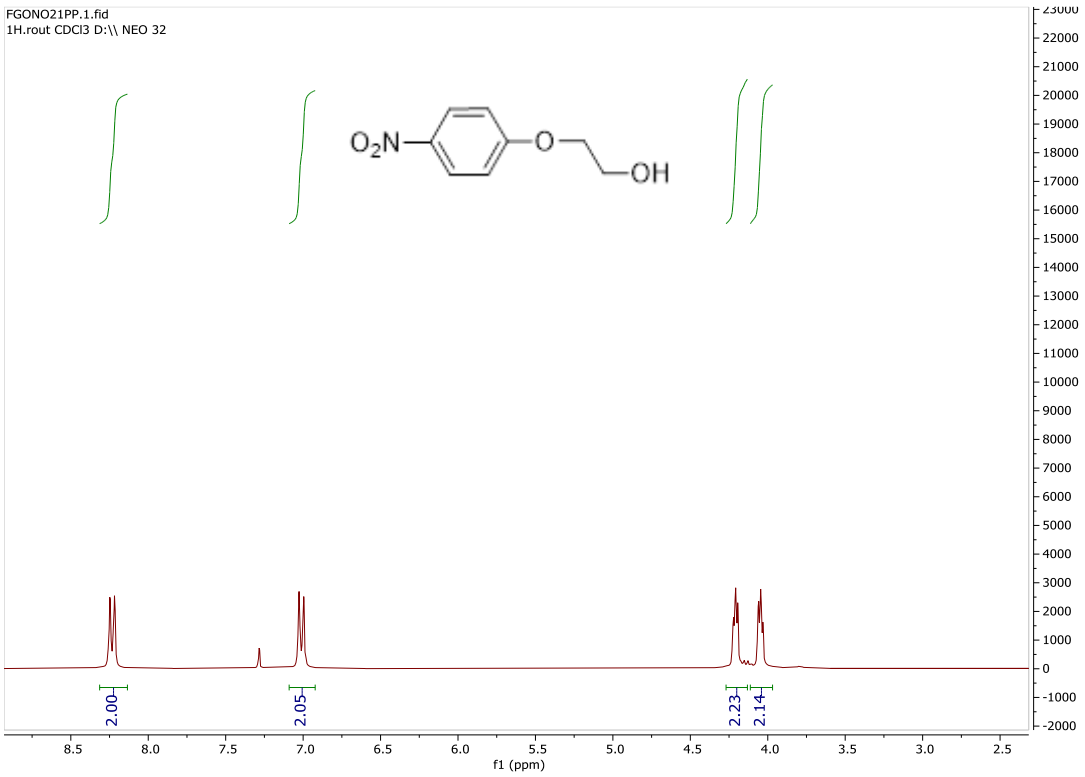

a)

Figure 47. 300 MHz ^{1}H-NMR spectra of 2-(4-Nitrophenoxy) ethanol in $CDCl_3$ at 298 K.

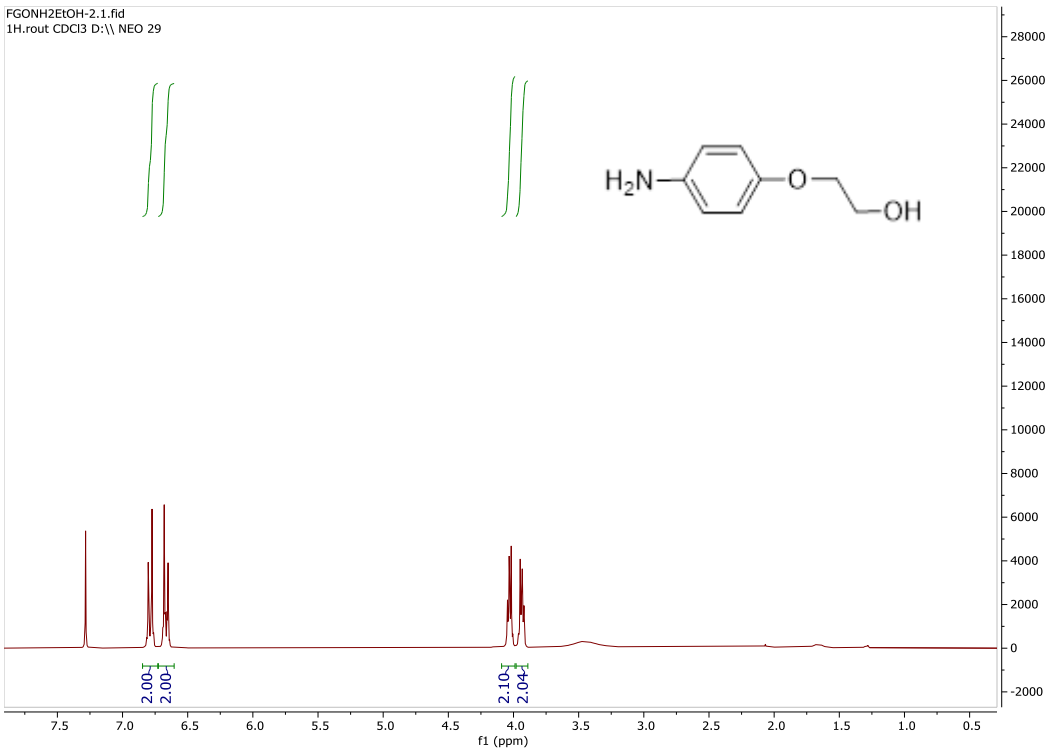

Figure 48. 300 MHz ^{1}H-NMR spectra of 2-(4-aminophenoxy) ethanol in $CDCl_3$ at 298 K.

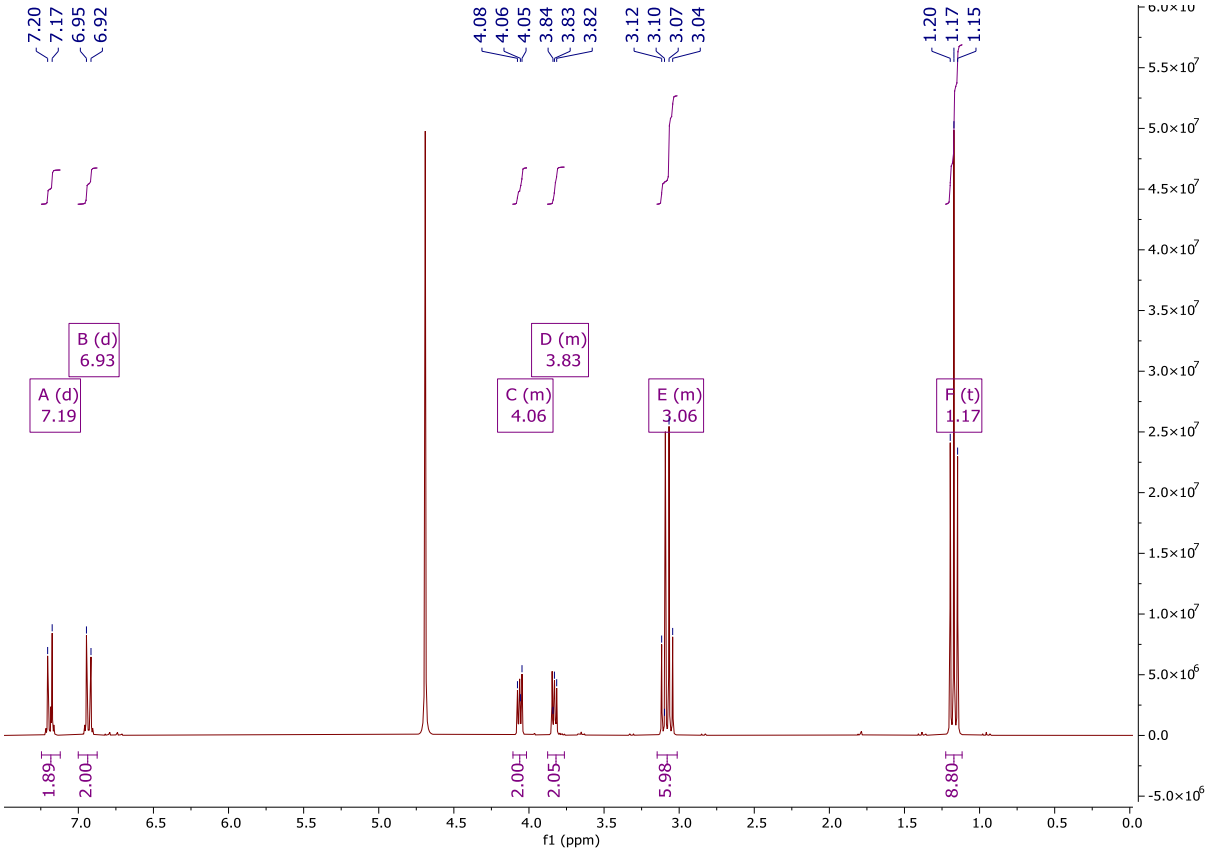

Figure 49. 300 MHz ^{1}H-NMR spectra of triethylammonium (4-(2-hydroxyethoxy) phenyl)carbamodithioate in D_2O at 298 K.

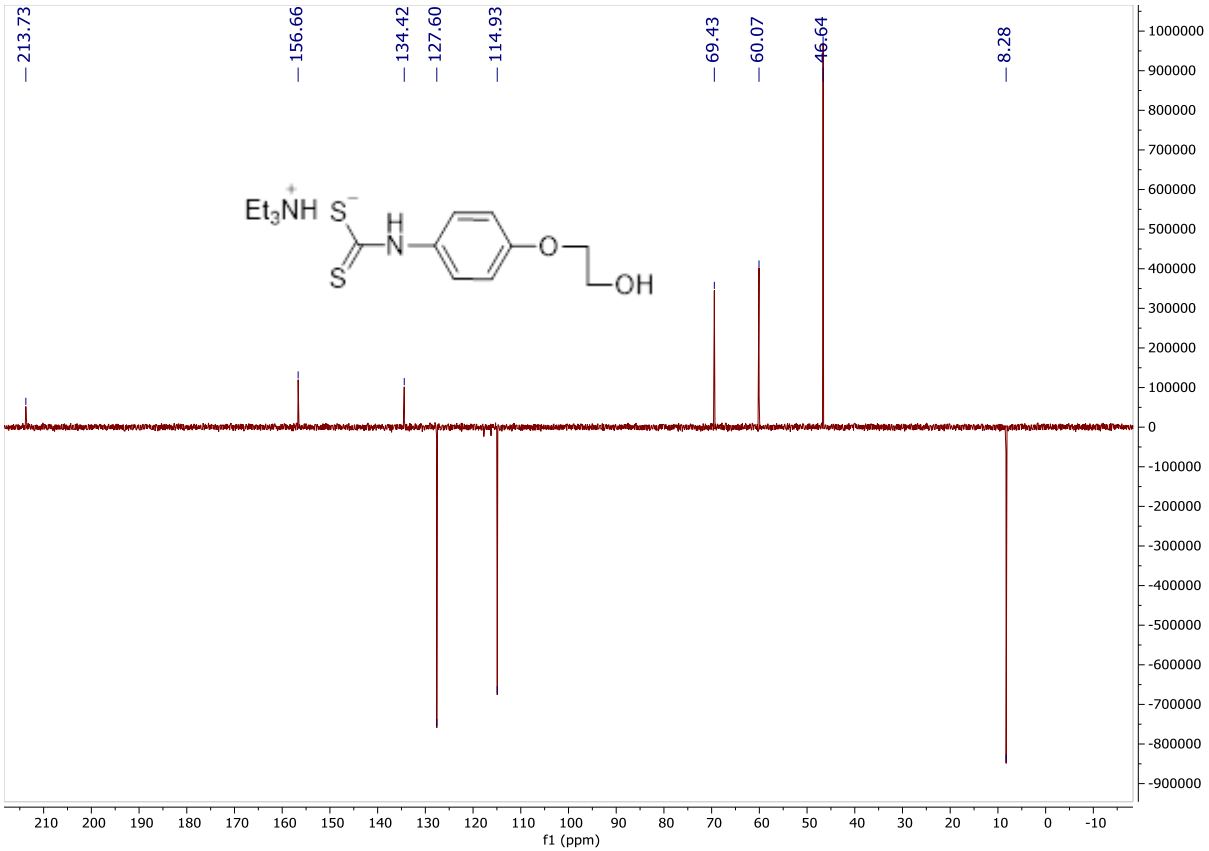

Figure 50. 300 MHz ^{13}C-NMR J-MOD spectra of triethylammonium (4-(2-hydroxyethoxy) phenyl)carbamodithioate in D_2O at 298 K.

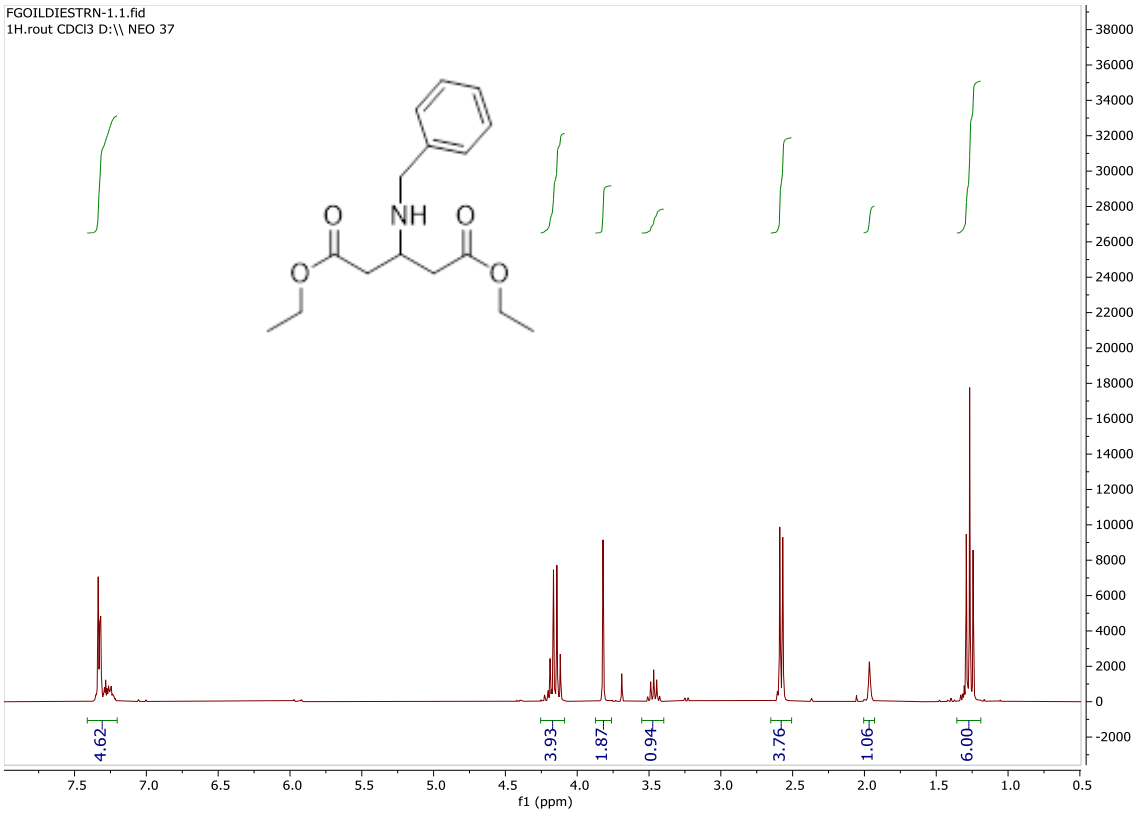

Figure 51. 300 MHz ^{1}H-NMR spectra of diethyl 3-(benzylamino)pentanedioate in $CDCl_3$ at 298 K.

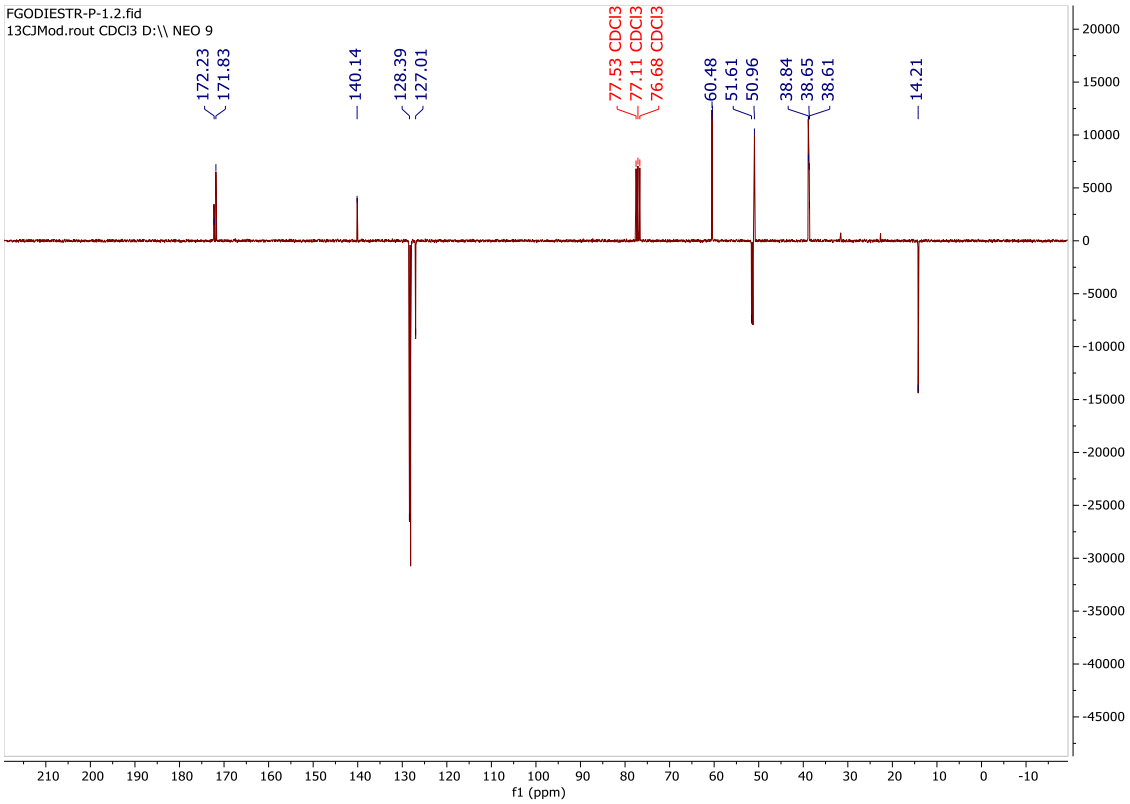

Figure 52. 300 MHz ^{13}C-NMR J-MOD spectra of diethyl 3-(benzylamino)pentanedioate in $CDCl_3$ at 298 K.

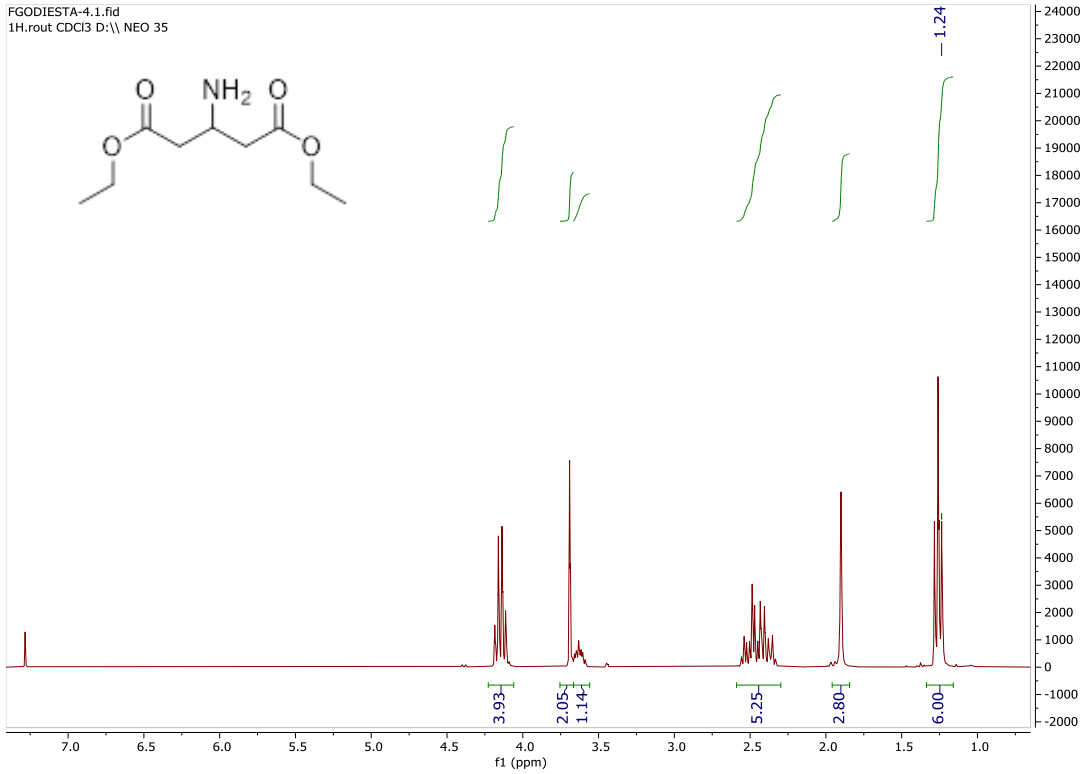

Figure 53. 300 MHz ^{1}H-NMR spectra of **d**iethyl 3-aminopentanedioate in $CDCl_3$ at 298 K.

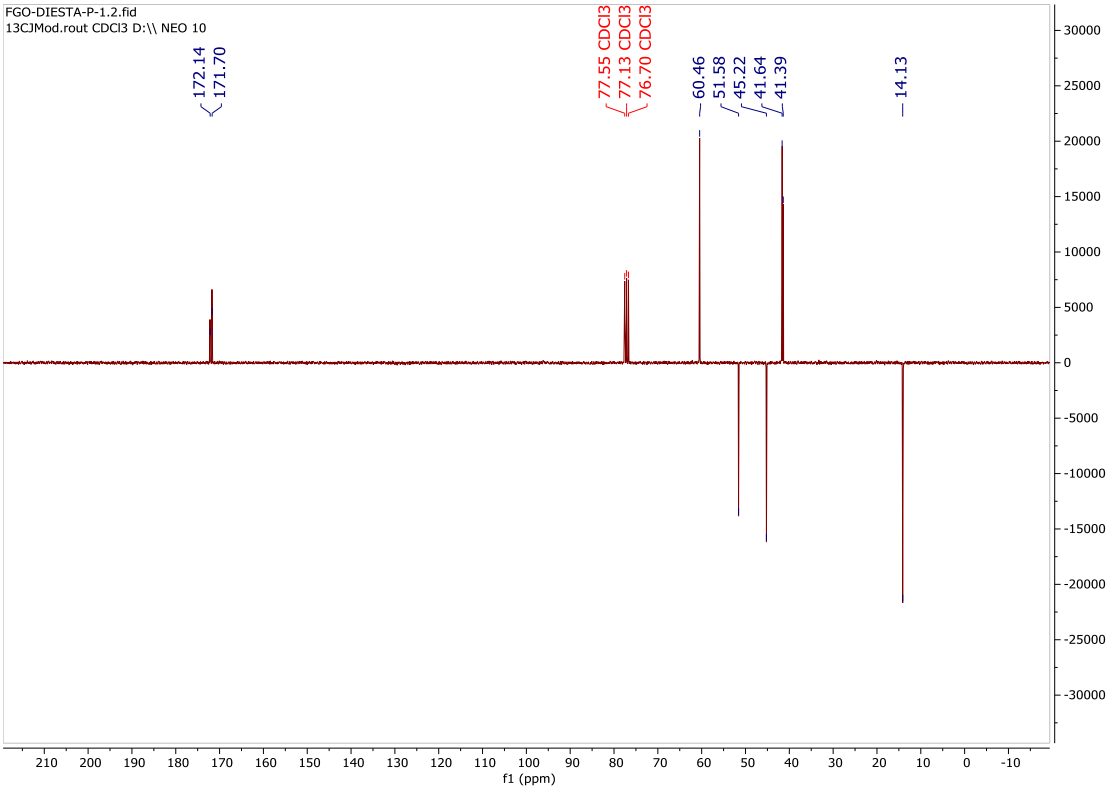

Figure 54. 300 MHz ^{13}C-NMR J-MOD spectra of **d**iethyl 3-aminopentanedioate in $CDCl_3$ at 298 K.

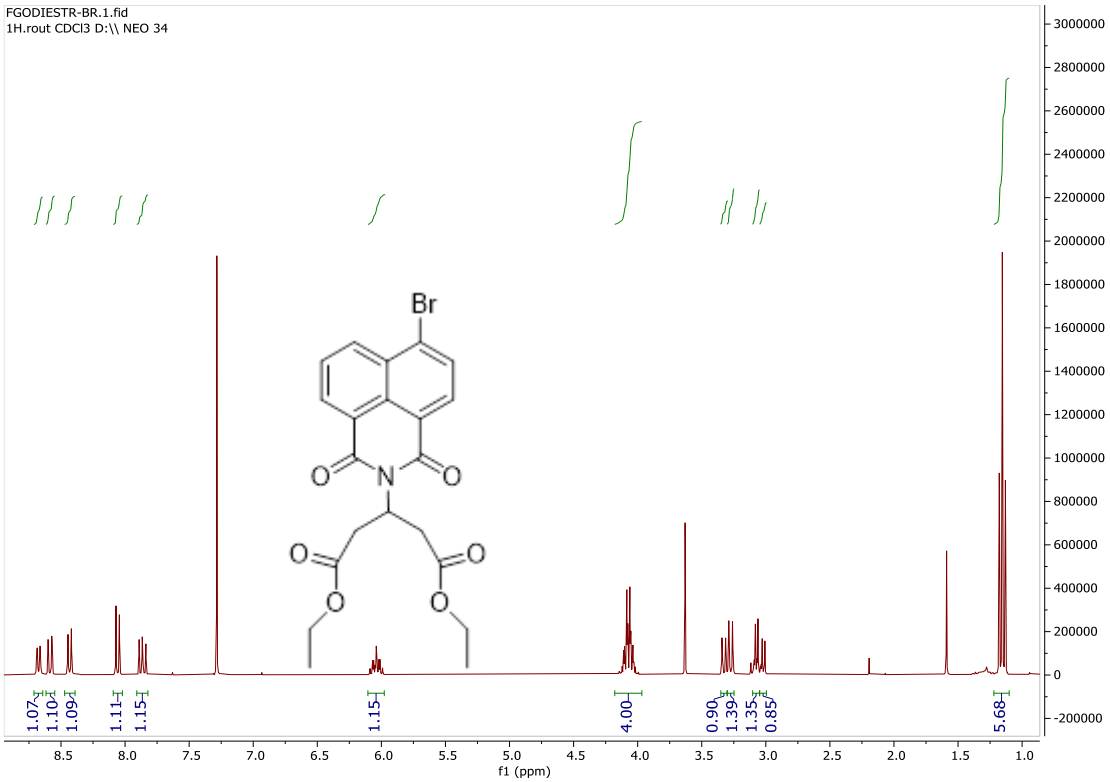

Figure 55. 300 MHz ^{1}H-NMR spectra of diethyl 3-(6-bromo-1,3-dioxo-1H-benzo[de]isoquinolin-2(3H)-yl)pentanedioate in $CDCl_3$ at 298 K.

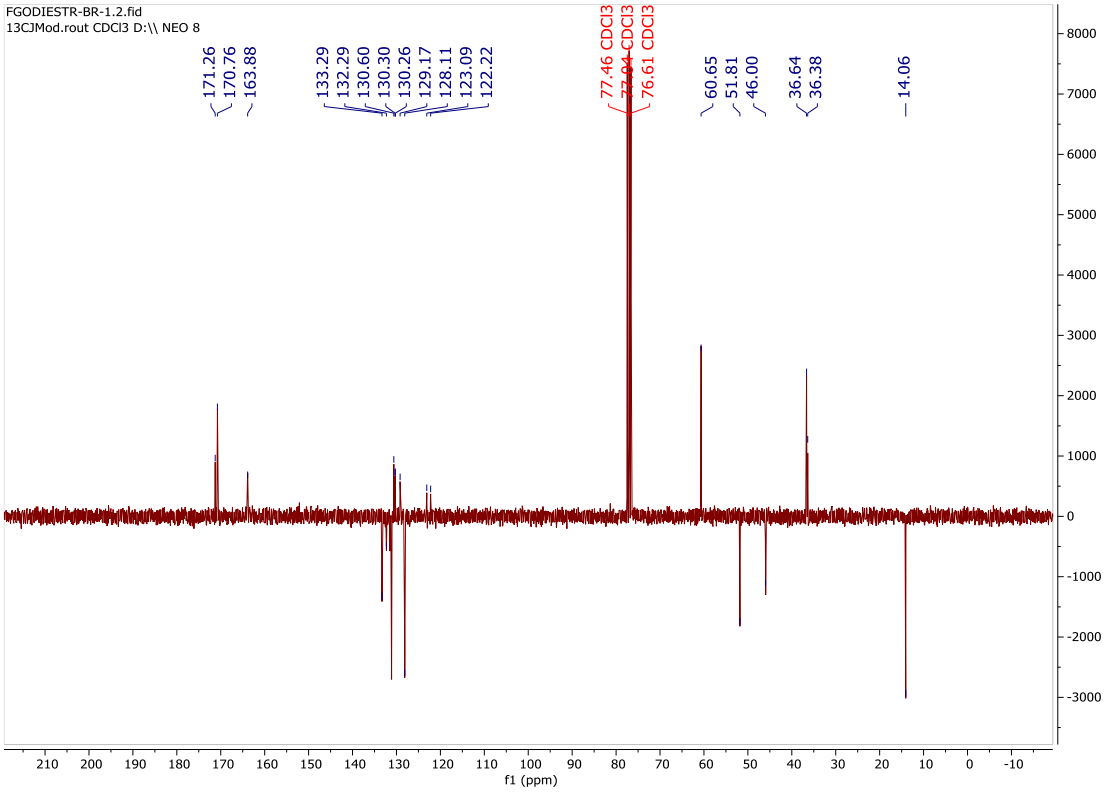

Figure 56. 300 MHz ^{13}C-NMR J-MOD spectra of diethyl 3-(6-bromo-1,3-dioxo-1H-benzo[de]isoquinolin-2(3H)-yl)pentanedioate in $CDCl_3$ at 298 K.

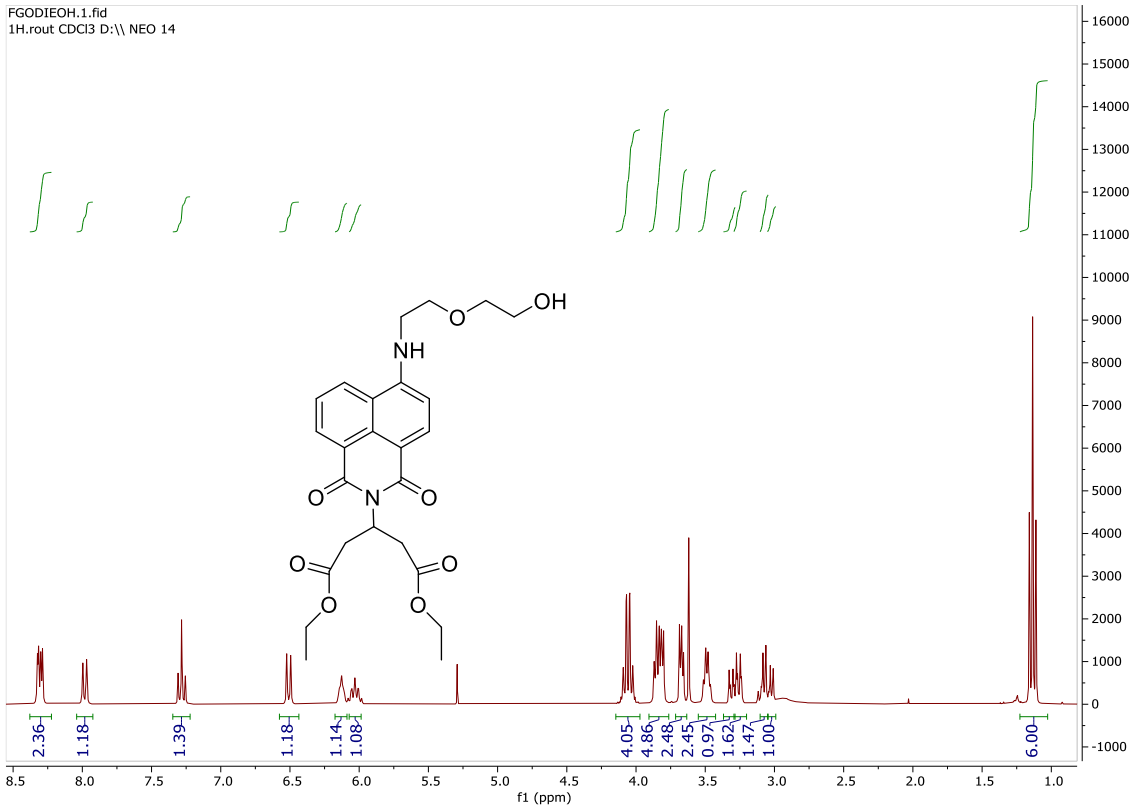

Figure 57. 300 MHz ^{1}H-NMR spectra of Diethyl 3-(6-((2-(2-hydroxyethoxy)ethyl)amino)-1,3-dioxo-1H-benzo[de]isoquinolin-2(3H)-yl)pentanedioate in $CDCl_3$ at 298 K.

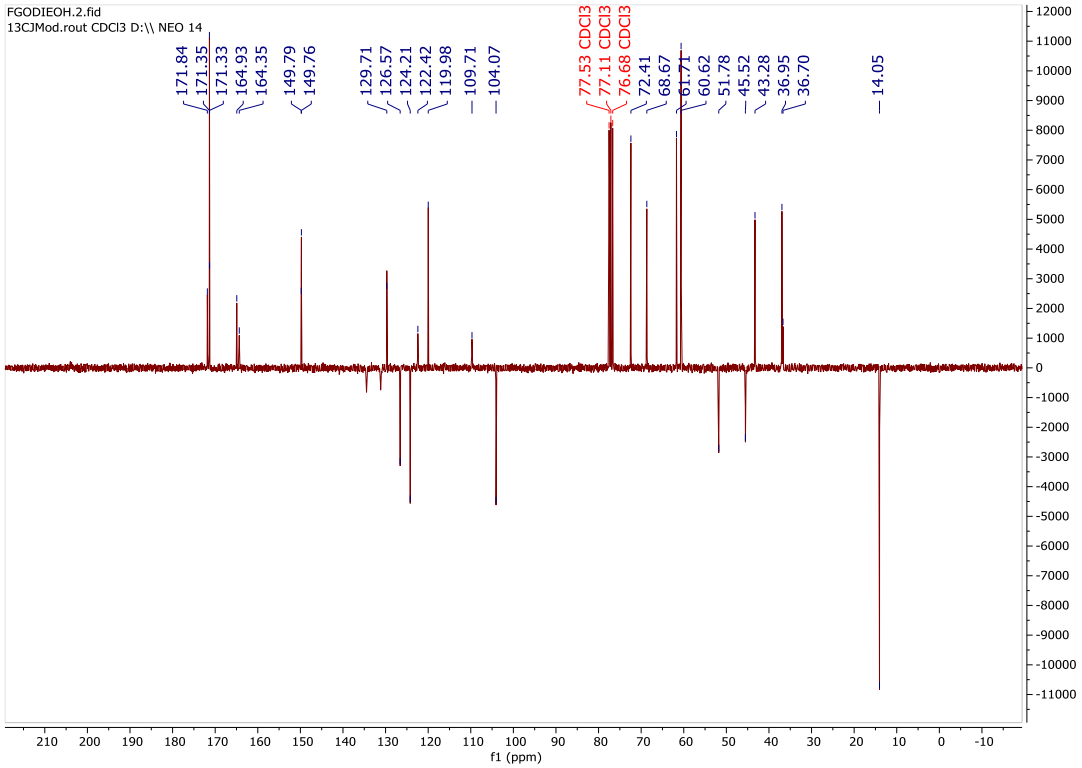

Figure 58. 300 MHz ^{13}C-NMR J-MOD spectra of **d**iethyl 3-(6-((2-(2-hydroxyethoxy)ethyl)amino)-1,3-dioxo-1H-benzo[de]isoquinolin-2(3H)-yl)pentanedioate in $CDCl_3$ at 298 K.

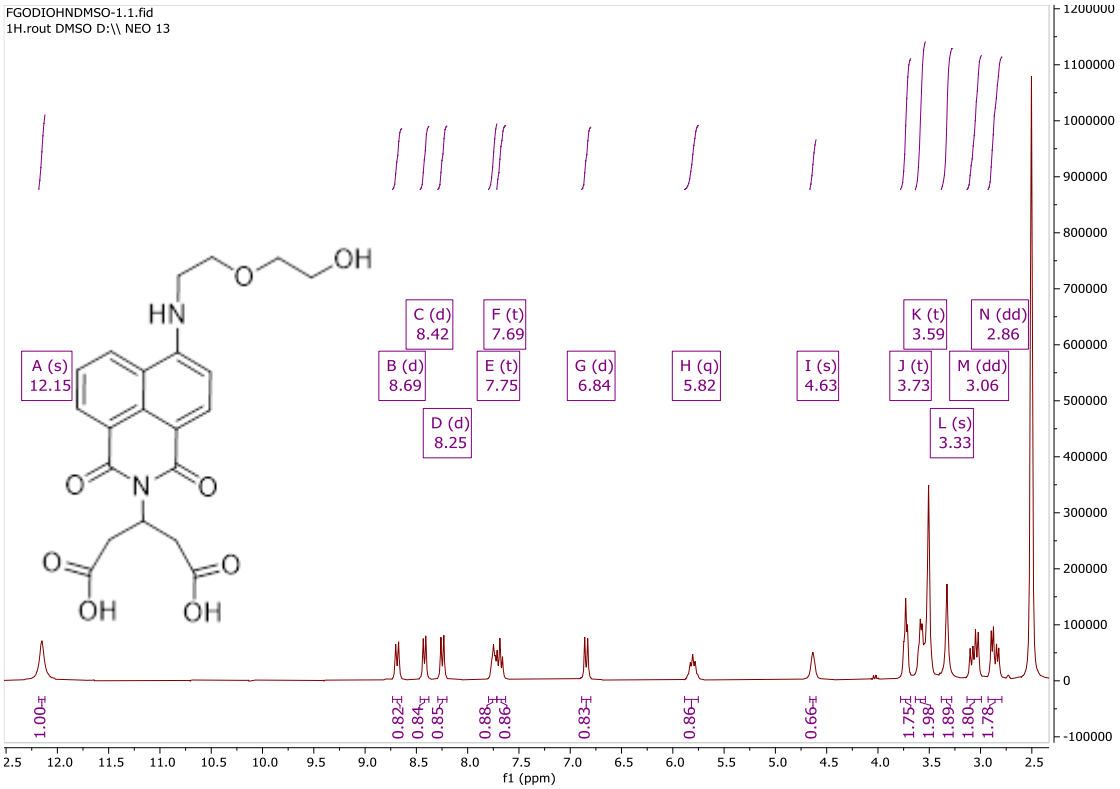

Figure 59. 300 MHz ^{1}H-NMR spectra of 3-(6-((2-(2-hydroxyethoxy) ethyl) amino)-1,3-dioxo-1H-benzo[de]isoquinolin-2(3H)-yl)pentanedioic acid in DMSO-d_6 at 298 K.

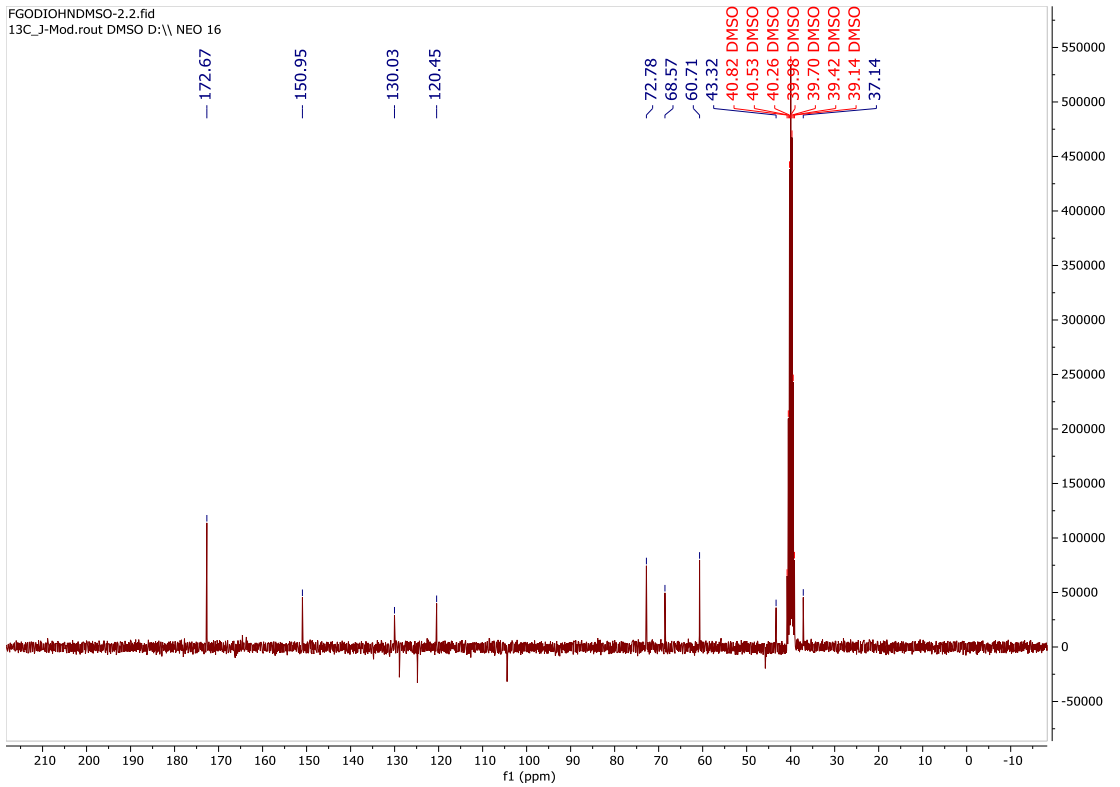

Figure 60. 300 MHz ^{13}C-NMR J-MOD spectra of 3-(6-((2-(2-hydroxyethoxy) ethyl) amino)-1,3-dioxo-1H-benzo[de]isoquinolin-2(3H)-yl)pentanedioic acid in DMSO-d_6 at 298 K.

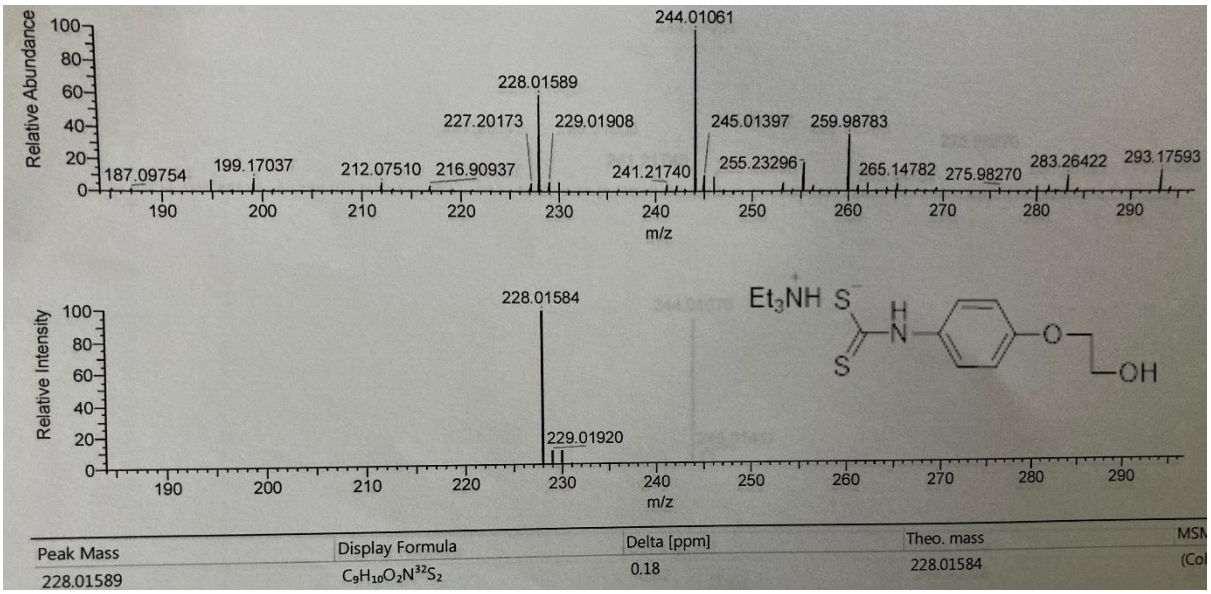

Figure 61. ESI mass spectrum of triethylammonium (4-(2-hydroxyethoxy) phenyl) carbamodithioate in methanol.

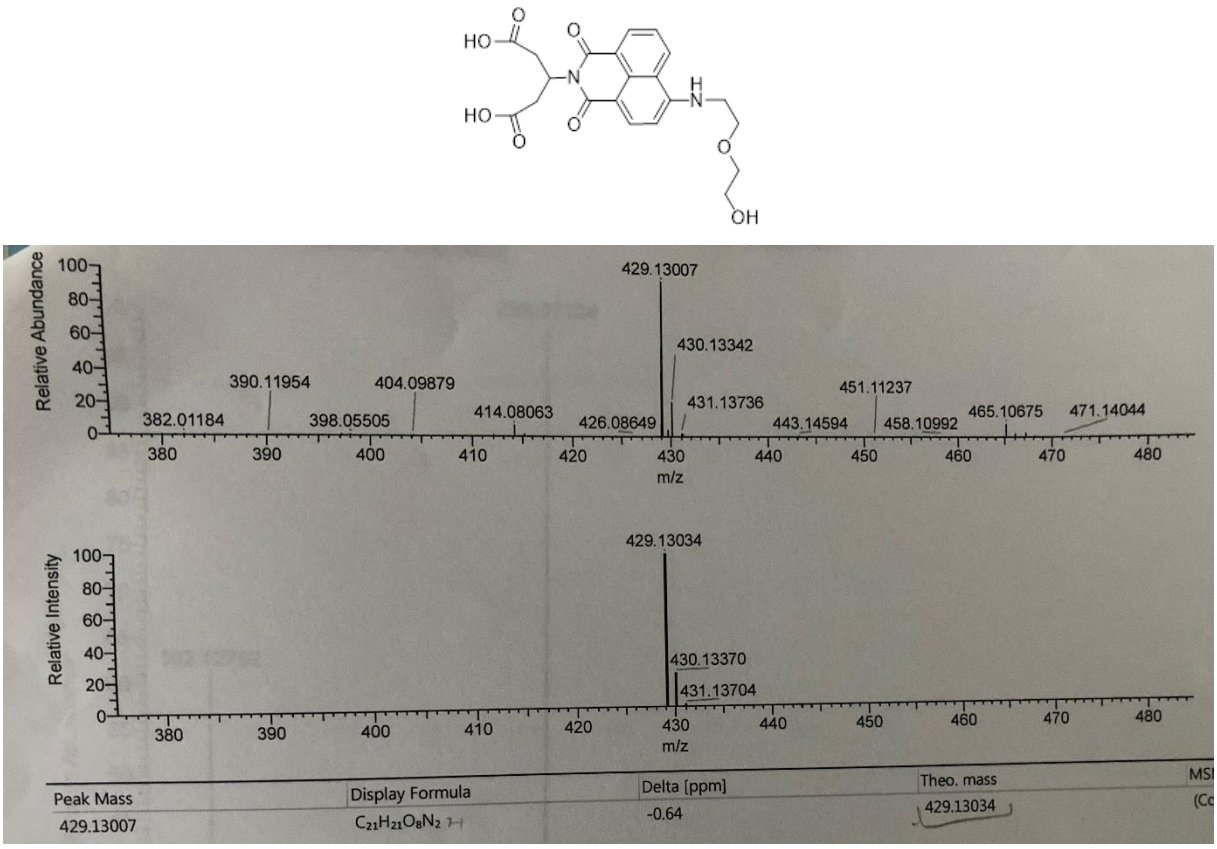

Figure 62. ESI mass spectrum of 3-(6-((2-(2-hydroxyethoxy) ethyl) amino)-1,3-dioxo-1H-benzo[de]isoquinolin-2(3H)-yl)pentanedioic acid in methanol.

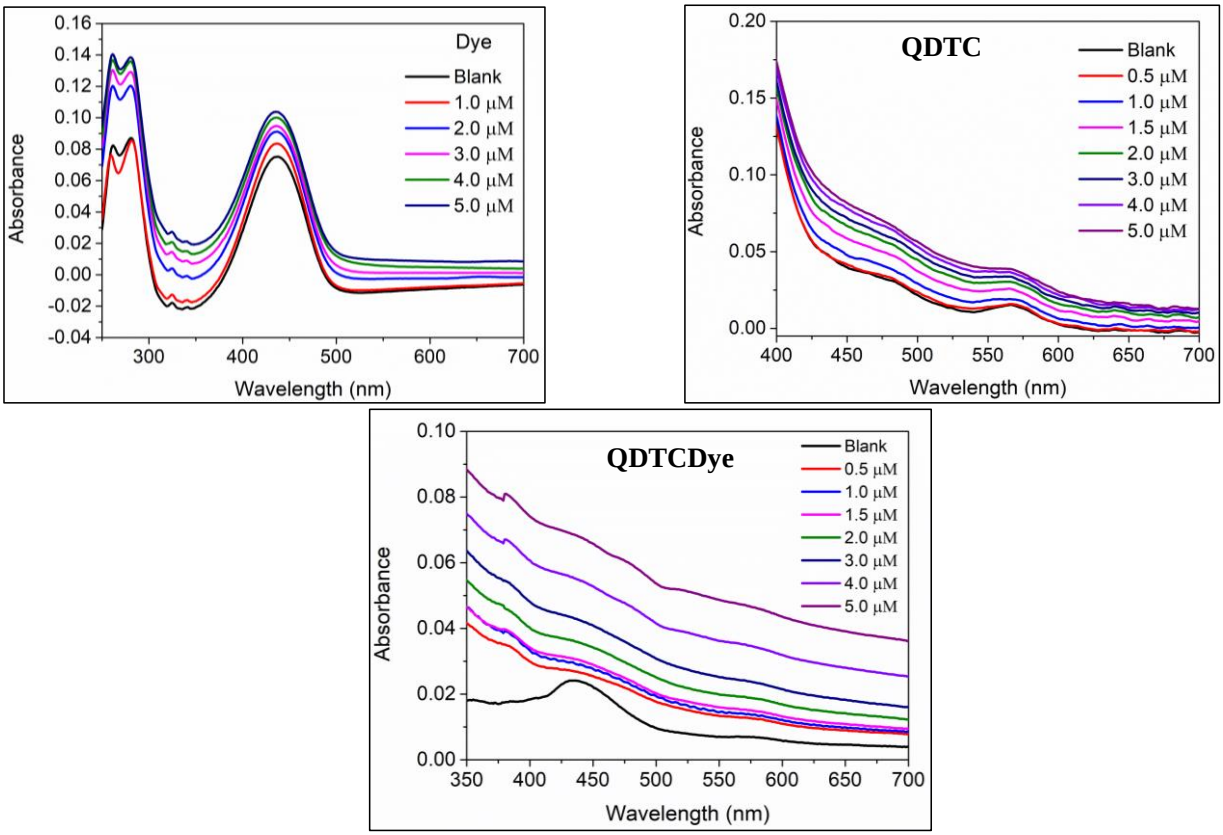

Figure 63. Absorption spectra of Dye, QDTC, and QDTCDye after the interaction with different concentrations of Hg^{2+} ions.

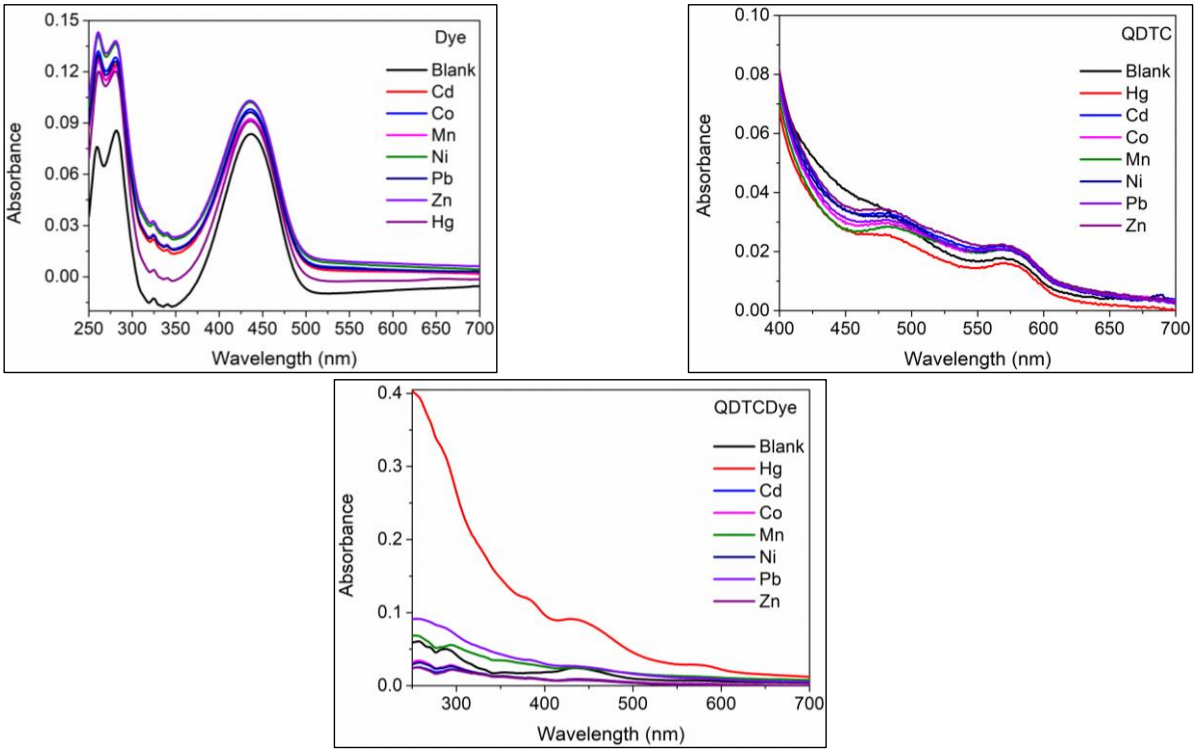

Figure 64. Absorption spectra of Dye, QDTC, and QDTCDye with different cations evaluated at 5µM.

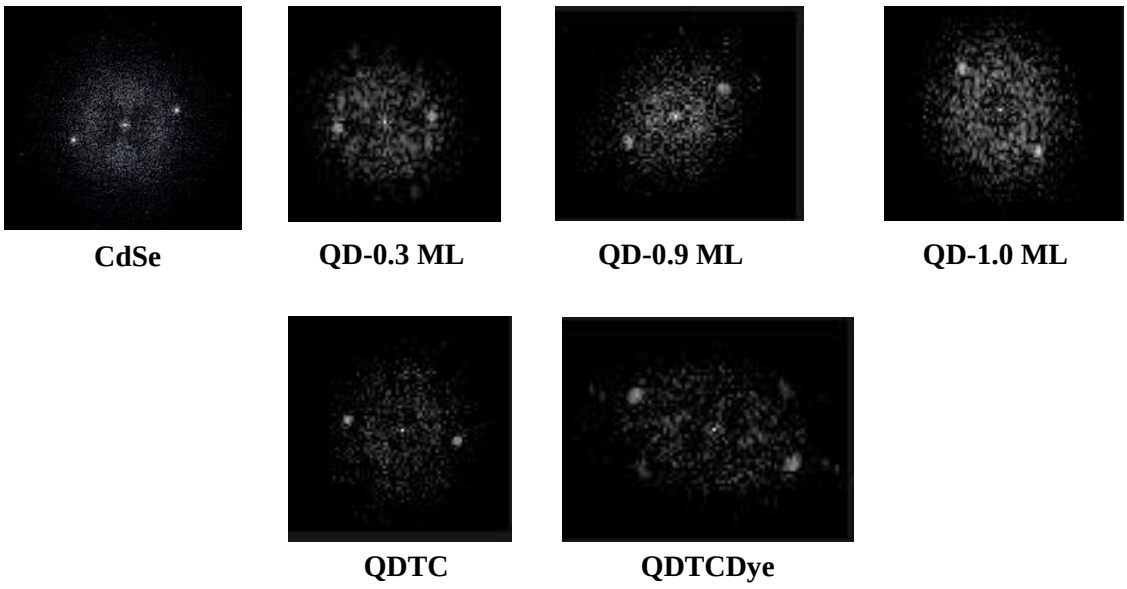

Figure 65. FFT images from CdSe, CdSe-ZnS corecore-shell and QD-L (QDTC and QDTCDye).